Tracing the Evolutionary History of the SLC_1 Gene Family

Dissertation

zur

Erlangung der naturwissenschaftlichen Doktorwürde

(Dr. sc. nat.)

vorgelegt der

Mathematisch-naturwissenschaftlichen Fakultät

der

Universität Zürich

von

André Lehnherr

aus

Uetikon am See ZH und Spiez BE

Promotionskommission

Prof. Dr. Stephan C.F. Neuhauss (Vorsitz)

Dr. Matthias Gesemann

Prof. Dr. Christian von Mering

Prof. Dr. Andreas Wagner

Zürich, 2018

"I like fools' experiments, I am always making them."

Charles Darwin

Summary

Most vertebrates are highly visual animals and are therefore depending on proper functioning of their visual system. The retina at the back of the eye is the light sensing organ of vertebrates. Light has to pass through three nuclear and two plexiform layers before it hits the visual pigments in the photoreceptor outer segments. An intracellular signaling cascade leads to closure of unselective cation channels which in turn leads to hyperpolarization of the cell.

Vertical signaling in the retina is mainly glutamatergic, which means that glutamate is the main neurotransmitter in vertebrate retinae. Postsynaptic glutamate receptors sense glutamate and act accordingly. Therefore, glutamate concentrations in synaptic clefts need to be tightly regulated to ensure proper signal transmission and to prevent cells from excitotoxicity. Excitatory amino acid transporters (EAATs) are secondary active glutamate transporters, which transport glutamate against its electrochemical gradient into cells. Besides fulfilling important glutamate transport, EAATs show an anion conductance that is thermodynamically uncoupled from glutamate transport thus EAATs can act as glutamate gated anion channels. Anion conductances vary between different EAAT subtypes. Consequently, some EAAT sub-types can act directly on signal transmission by altering the cell's membrane potential.

EAATs that are mainly expressed in glia cells are thought to fulfill a major part of glutamate re-uptake and are therefore high capacity glutamate transporters. EAAT1 and EAAT2 are expressed in glia cells in the brain. In the retina of lower vertebrates EAAT2 is expressed in Müller glia cells whereas EAAT1 is expressed in bipolar cells. Surprisingly, expression patterns changed in mice where Müller glia cells express EAAT1 and EAAT2 is expressed by bipolar cells. Zebrafish retained two paralogs of each, EAAT1 and EAAT2, after teleost-specific round of whole genome duplication. In Chapter 2 we describe expression patterns as well as biophysical properties for EAAT1 and EAAT2 orthologs from representative species of all major vertebrate classes. Distinct differences in expression for the zebrafish EAAT1 and EAAT2 orthologs indicate sub-functionalizations. Differences in biophysical properties further support this indication. Mice EAAT1 and EAAT2 orthologs show very similar biophysical properties, raising the question why a change in expression patterns happened.

In Chapter 3 we focus on the sub-functionalization of the two zebrafish EAAT2 paralogs. EAAT2a is mainly expressed in Müller glia cells whereas EAAT2b shows expression mainly in photoreceptors. Morpholino-mediated gene knockdown of EAAT2a but not of EAAT2b leads to excess of glutamate in the photoreceptor synapse. EAAT2b shows a high anion conductance and is therefore capable of brining photoreceptors back to hyperpolarization after a light stimulus, thus leading to enhanced temporal resolution.

EAAT5, EAAT6 and EAAT7 are almost exclusively expressed in neuronal cells in the retina. While all examined EAAT5 orthologs show expression in photoreceptors and bipolar cells, EAAT6 is expressed in photoreceptors of zebrafish and Xenopus, whereas in chicken bipolar cells express EAAT6. In all examined species that still possess an EAAT7 ortholog, it is expressed in bipolar cells. In Chapter 4 we investigate the biophysical properties of EAAT7 orthologs for the first time and can clearly classify it as a glutamate-gated anion channel. The loss of EAAT6 and EAAT7 in the course of mammalian evolution goes along with the loss of two opsin genes that are responsible for the perception of green and UV/violet light. We hypothesize that the loss of these opsin genes resulted in subsequent simplification in the signaling processing machinery leading ultimately to the loss of EAAT6 and EAAT7 in placental mammals.

Zusammenfassung

Für die meisten Wirbeltiere ist das visuelle System der primäre Sinn. Daher sind sie davon abhängig, dass das Visuelle System einwandfrei funktioniert. Die Retina liegt im hintersten Teil des Auges und ist das Lichtsinnesorgan. Licht fällt durch drei Zell- und zwei Plexiformschichten auf das Sehpigment in den äusseren Segmenten der Photorezeptoren. Über eine intrazelluläre Signaltransduktionskaskade werden durch das Licht nichtselektive Kationenkanäle geschlossen, was wiederum zur Hyperpolarisierung der Photorezeptoren führt.

In vertikaler Richtung geschieht die Reizweiterleitung in der Retina durch Glutamat als Neurotransmitter. Daher ist Glutamat der wichtigste Neurotransmitter in der Retina der Wirbeltiere. Postsynaptische Zellen besitzen Glutamatrezeptoren und reagieren entsprechend auf ein Glutamat-Signal. Die Glutamatkonzentration wird im synaptischen Spalt genauestens reguliert, um eine korrekte Reizweiterleitung zu bewerkstelligen und um die postsynaptischen Zellen vor Exzitotoxizität zu schützen. Excitatory Amino Acid Transporter (EAAT) sind sekundär aktive Glutamattransporter, welche Glutamat entgegen dem elektro-chemischen Gradienten in die Zelle transportieren. Neben dem wichtigen Glutamattransport besitzen die EAATs auch eine vom Glutamattransport thermodynamisch unabhängige Anionen-Leitfähigkeit und können auf diese Weise als Glutamat abhängige Anionenkanäle funktionieren. Die Anionen-Leitfähigkeit variiert zwischen verschiedenen EAAT Subtypen. Folglich können einige EAAT Subtypen über die Anionen-Leitfähigkeit direkt Zellen hyperpolarisieren und dadurch die synaptische Transmission direkt beeinflussen.

Die wiederaufnahmen von Glutamat aus dem synaptischen Spalt wird hauptsächlich von EAATs übernommen, welche auf Gliazellen exprimiert sind. EAAT1 und EAAT2 werden von Gliazellen im Hirn exprimiert. In der Retina von tieferen Wirbeltieren wird EAAT2 von Müller Gliazellen exprimiert, wohingegen EAAT1 von Bipolar Zellen exprimiert wird. Überaschenderweise haben wir herausgefunden, dass in Mäusen und anderen Säugetieren sich das Expressionsmuster geändert hat und EAAT1 in Müller Gliazellen und EAAT2 in Bipolar Zellen exprimiert wird. Zebrafische haben auf Grund der Teleost-spezifischen zusätzlichen Runde einer Genomduplizierung je zwei Paraloge von EAAT1 und EAAT2. In Kapitel 2 beschreiben wir die Expressionsmuster und biophysikalische Eigenschaften von EAAT1 und EAAT2 von repräsentativen Spezies der verschiedenen grossen Wirbeltierklassen. Unterschiede im Expressionsmuster für die verschieden Zebrafish EAAT1 und EAAT2 Paraloge deuten auf Subfunktionalisierung hin und Unterschiede in den biophysikalischen Eigenschaften der Transporter unterstützen diese Vermutung weiter. Die EAAT1 und EAAT2 Orthologe von Mäusen zeigen sehr ähnliche Eigenschaften, was wiederum die Frage aufwirft, warum sich die Expressionsmuster geändert haben. Wir vermuten, dass beide Gene erhalten blieben um eine bessere Kontrolle über die Dosis der Transporter zu haben. Dies ist vor allem wichtig in Zellen, welche beide Transporter gleichzeitig exprimieren.

Kapitel 3 widmet sich der Subfunktionalisierung der beiden EAAT2 Paralogen der Zebrafische. EAAT2a ist hauptsächlich in Müller Gliazellen exprimiert, während Photorezeptoren hauptsächlich EAAT2b exprimieren. Mittels Herunterregulierung der beiden Gene konnten wir zeigen, dass das Fehlen von EAAT2a, aber nicht jenes von EAAT2b, zu einer erhöhten Glutamat Konzentration in der Photorezeptorsynapse führt. EAAT2b besitzt eine hohe Anionen-Leitfähigkeit und kann dadurch Photorezeptoren zurück in den hyperpolarisierten Zustand bringen. Dieser Mechanismus erhöht die zeitliche Auflösung der Lichtwahrnehmung.

EAAT5, EAAT6 und EAAT7 werden fast ausschliesslich von neuronalen Zellen in der Retina exprimiert. Während EAAT5 in allen untersuchten Spezies von Bipolar Zellen und Mül-

ler Gliazellen exprimiert wird, exprimieren Photorezeptoren von Zebrafischen und Xenopus auch EAAT6. In Hühnern wird EAAT6 hingegen von Bipolarzellen exprimiert. EAAT7 wird von allen Spezies, welche ein EAAT7 Gen besitzen, von Bipolarzellen exprimiert. In Kapitel 4 widmen wir uns der erstmaligen Beschreibung der biophysikalischen Eigenschaften von EAAT7 Orthologen und können es als Glutamat abhängigen Anionenkanal klassifizieren. Der Verlust von EAAT6 und EAAT7 im Laufe der Evolution der Säugetiere geht einher mit dem Verlust von zwei Opsin Genen, die für grüne und UV-violette Farbwahrnehmung verantwortlich waren. Wir vermuten, dass der Verlust der beiden Opsin Gene in einer Vereinfachung der Signalprozesse resultiert und im Zuge dieser Vereinfachung EAAT6 und EAAT7 in höheren Säugetieren verloren ging.

Table of Contents

Chapter 1

General Introduction

1.1. Vertebrate genome evolution and organismal complexity

Duplications of genes or even whole genomes have been associated with evolutionary innovations and organismal complexity. At the base of the vertebrate lineage, two rounds of whole genome duplications took place around 550 – 500 million years ago (mya) (Figure 1). Compared to other chordate groups, vertebrates show more complex and diverse organs and body plans which is assumed to be a consequence of the genome duplications (for review see (Stellwag 2004; Crow, Wagner 2006; Glasauer, Neuhauss 2014)). The teleost fish lineage underwent an additional round of whole genome duplication. About 23'000 teleost species have been described today, populating highly diverse habitat such as salt and fresh water, deep sea or shallow rivers. Although there are some exceptions of species-poor teleost groups, the teleost-specific whole genome duplication played a crucial role in species diversity and richness of the teleost lineage (Crow, Wagner 2006).

But just simply duplicating a gene would not lead to increased complexity. After a duplication event, one copy of a duplicated gene is released from selective pressure and may subsequently accumulate mutations in regulatory regions as well as in protein-coding sequences. In most cases such mutations will ultimately lead to disrupted gene function and so-called non-functionalization. It is evident that non-functionalization will most likely not increase complexity or harbor evolutionary innovations. Another possible scenario is sub-functionalization of the duplicated genes. In this case the two copies split ancestral gene functions. The third possible outcome after a gene duplication is called neo-functionalization, a process in which one duplicated gene accumulates mutations that lead to a new gene function (Stellwag 2004; Glasauer, Neuhauss 2014). Neo- and sub-functionalizations clearly provide the potential to increase complexity and evolutionary innovations.

One example for evolutionary innovation and increased complexity is the innovation of the retina at the base of the vertebrate lineage. Although lower vertebrate classes such as the cephalochordates and tunicates possess light sensing organelles that allow them to react to a light stimulus, only vertebrates possess the ability of image-forming light-sensing or what we would generally claim as vision. Duplications of genes that are involved in phototransduction allowed ancestral vertebrates to evolve a much more complex light-sensing organ that can process more information about the stimuli like direction of the light, color or movement (Lamb et al. 2007; Lamb 2013).

Vertebrate clades and species are highly diverse, covering a huge variety of habitats. It is therefore not surprising that adaptations in the visual system are common. For example nocturnal vertebrates or species that live underground show the tendency to lose the ability to sense certain wave-lengths of light that they only rarely would encounter. This is due to the loss of opsin genes, which are part of the visual pigments and are tuned to react to specific wavelengths of light (Bowmaker 2008).

Such adaptations according to the specific needs of a species will lead to further adaptations in the processing machinery. Vertical signaling in the retina is mainly depending on the excitatory neurotransmitter glutamate. In the synapse, glutamate-concentrations need to be tightly controlled in order to shape and terminate signals. This is mainly achieved by Excitatory Amino Acid Transporters (EAATs) that belong the Solute Carrier Family 1 (SLC1) gene family (Kanai, Hediger 2004). EAATs have been shown to be expressed in the retina (Arriza et al. 1997; Eliasof et al. 1998). During vertebrate evolution several EAAT gene loss and duplication events took place (Gesemann et al. 2010).

In this thesis we take advantage of the conserved anatomical structure of the vertebrate retina to localize EAAT expression in selected species of the main higher vertebrate clades and compare consequences of duplication and loss events. In order to trace changes in biophysical properties of the genes, electrophysiological examination of different EAAT homologs from the representative species was performed.

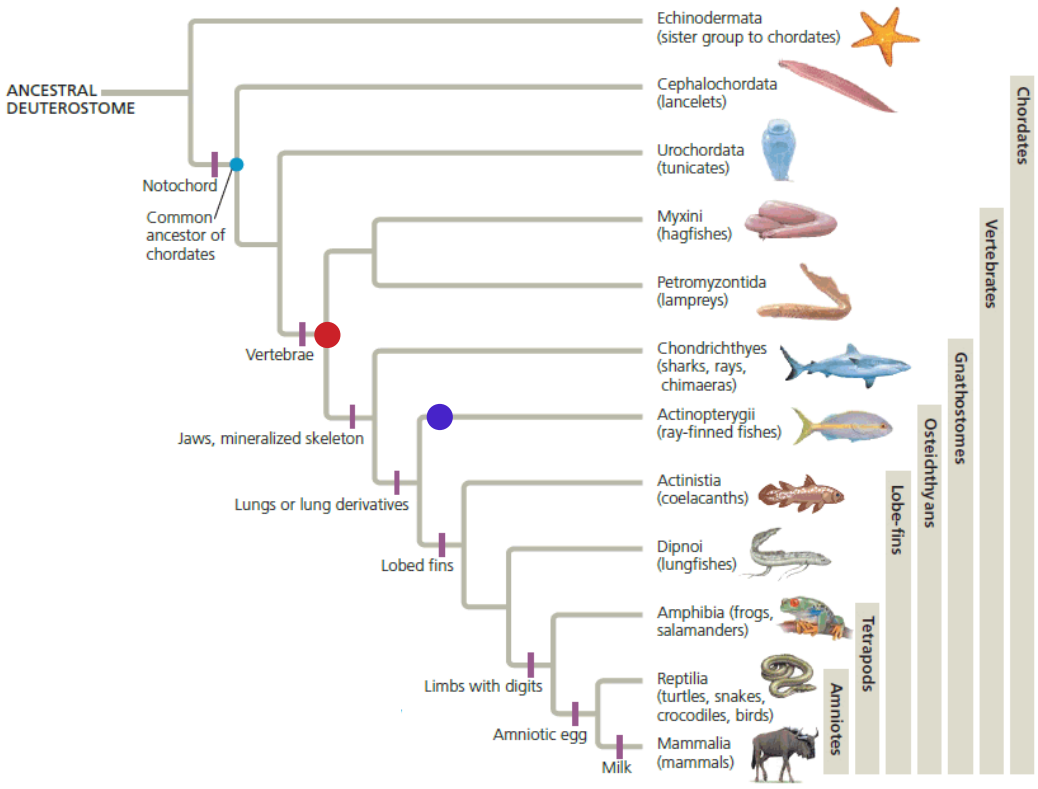

Figure 1: Schematic representation of chordate phylogeny showing major classes and defining evolutionary inventions.
Chordates split from other deuterostome around 700 mya. The split of vertebrates from chordates dates back around 500-550 mya. Most basal vertebrates are hagfishes and lampreys that together form the clade of Cyclostomata and are the only extant Agnatha group. Two rounds of whole genome duplications took place before the split of the Cyclostomata from the Gnathostomata lineage (indicated by red circle). The Actinopterygii underwent an additional round of whole genome duplication 320-350 mya (blue circle). Adapted from (Campbell, Reece 2015).

1.2. Evolution of the vertebrate retina

1.2.1. The vertebrate retina

Most vertebrates are highly visual animals and thus depend on fast and accurate processing of visual information. The retina is the neuronal structure at the back of the eye that is sensing and processing visual input and ultimately sending the processed information to destinct target sites in the brain. The retina consists of three nuclear layers and two plexiform layers (Figure 2). The outer nuclear layer (ONL) harbors the light sensing cone and rod photoreceptor cells. In the inner nuclear layer (INL) the cell bodies of horizontal cells, bipolar cells, Müller glia cells and amacrine cells are located, and the ganglion cell layer (GCL) contains ganglion cells.

Light has to pass through all these cell and plexiform layers and hits the visual pigment at the very back of the retina in the outer segments of the photoreceptors. Two different types of photoreceptors can be found in most vertebrate retinae. Cones are sensitive for different wavelengths of light and mediate color vision. Rods typically have only one absorption maximum but are highly sensitive to light and are used for scotopic vision.

Photoreceptors form synapses with bipolar cells and horizontal cells, a kind of modulatory interneuron important for contrast vision and color opponency, in the outer plexiform layer (OPL). Bipolar cells project to the inner plexiform layer (IPL) where they form synapses with ganglion cells and amacrine cells, that, similar to horizontal cells, are modulatory interneurons with diverse function that are described later in this chapter.

The INL further harbors the cell bodies of Müller glia cells. Müller glia cells support neurons in the retina by taking up neurotransmitters released by neuronal cells and supplying them with metabolites.

Ganglion cells, located in the GCL, are the last cells in the retina that get the processed visual information and their axons reach distinct target sites in the brain. In lower vertebrates such as zebrafish, retinal ganglion cells axons reach numerous projection fields. However, most of them project directly to the optic tectum (Robles et al. 2014). In mammals, retinal ganglion cells project to the lateral geniculate nucleus where the visual information is relayed to the visual

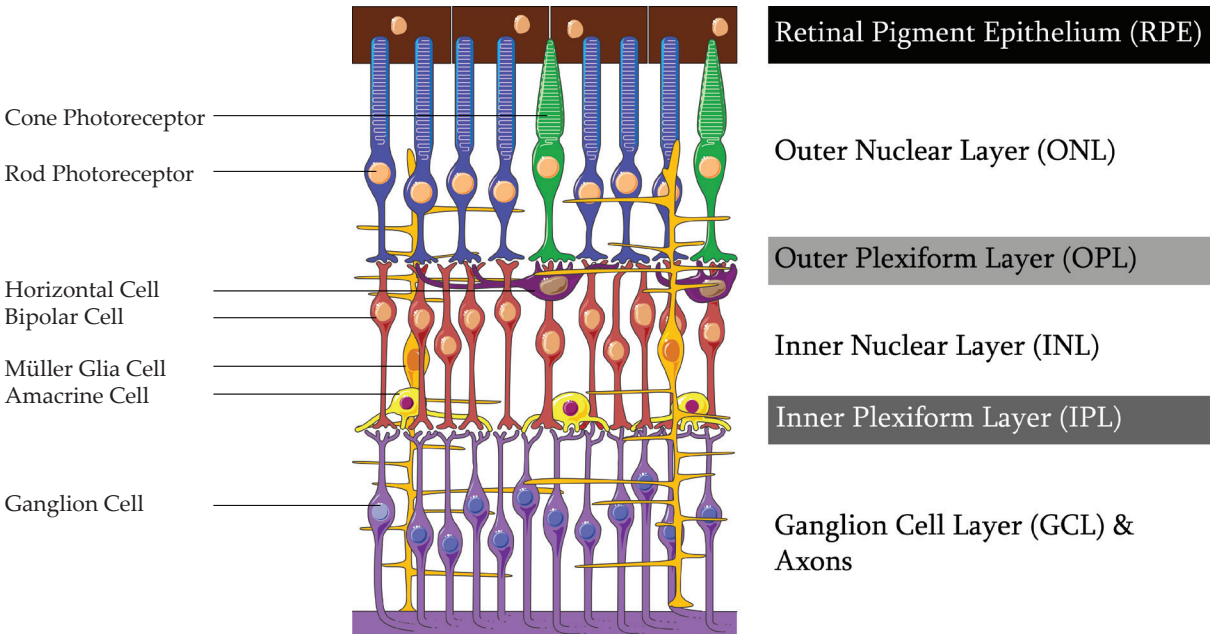

Figure 2: Schematic representation of a vertebrate retina.
Light passes through three nuclear layers before it hits the visual pigments located at the very back of the photoreceptors in the so-called outer segments. Vertebrate retinae are duplex retinae, meaning they harbor rod (blue) and cone (green) photoreceptors that work best either at scotopic or at bright light conditions. Photoreceptors depolarize in darkness and release glutamate into the synaptic cleft between photoreceptors, horizontal cells (purple) and bipolar cells (red). Horizontal cells are modulatory interneurons that enhance contrast vision and are involved in color oponency. Bipolar cells form synapses in the IPL with amacrine cells (yellow) and ganglion cells (violet). Amacrine cells are modulatory interneurons fulfilling several roles such as direction selectivity. Ganglion cells project to targets in the rest of the brain. Müller glia cells (orange) are responsible for the uptake of neurotransmitters from the synapse in order to prevent cells from excitotoxicity and to remove debris. They span across the whole retina.

cortex, to the superior colliculus, the mammalian homolog of the optic tectum, and to the suprachiasmatic nucleus among other brain areas (Leventhal et al. 1985).

1.2.2. Origins of retinal anatomy

To understand the evolutionary origin of the vertebrate retina, we have to go back to the last common ancestor of all Chordata, consisting of Vertebrata, Tunicata and Cephalochordata (Figure 2). Already Tunicata and Cephalochordata possess the ability to sense light at least at certain developmental stages and react accordingly. Recent studies date back the split of chordates from the ancestral deuterostome about 700 million years ago (mya) (Erwin et al. 2011). About 550 to 500 mya two rounds of whole genome duplications took place at the base of the vertebrate lineage, providing the genetic basis of greater organismal complexity that is also represented in the visual system (Crow, Wagner 2006; Lamb et al. 2007; Lamb 2013). In this section, ancestral and intermediate forms of light sensing organs will be discussed.

1.2.2.1. Cephalochordata

In the cephalochordate amphioxus four light sensing region were described (Lacalli 2004). The frontal eye has been proposed to be a homolog to the vertebrate eye and will be discussed here in more detail. Ciliary photoreceptors (named row 1 cell (Lacalli 2004)) are surrounded by pigmented cells and express typical photoreceptor markers like retinal homeobox (rx), Pax4/6, Otx, c-opsin1 and c-opsin3 (Vopalensky et al. 2012; Figure 3).

The origin of the amphioxus genome predates the time where the vertebrate-specific two rounds of whole genome duplications occurred, which are thought to lead to new innovations in the light perception and processing machinery (Lamb 2013). For example, the amphioxus genome does not harbor a transducin gene, which plays a crucial role in the phototransduction cascade, but another inhibitory Gi-alpha subunit with similar properties of the

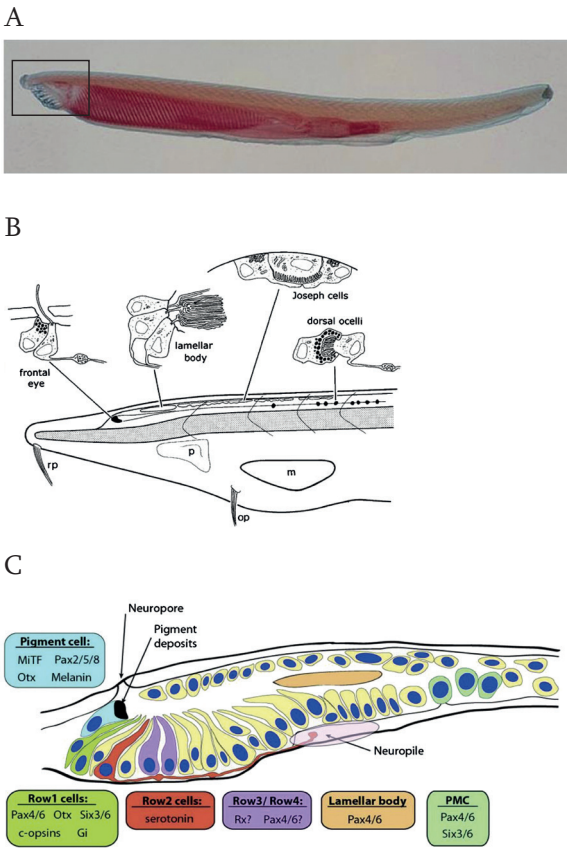

Figure 3: Anatomy and genomic finger print of the amphioxus frontal eye.
A: Photograph of an adult amphioxus. Box indicates magnified region in schematic representations in B and C.
B: Schematic representation of the head region of amphioxus depicting all light sensing organs and photoreceptor types. Frontal eye and lamellar body both contain ciliary photoreceptors whereas Joseph cells and dorsal ocelli contain rhabdomeric photoreceptors.
C: Schematic representation and fingerprint of the frontal eye. Row 1 cells are light sensing cells expressing typical vertebrate photoreceptor markers such as c-opsin or Pax4/6.
Picture adapted from (Lamb 2013).

vertebrate transducin was found to be expressed in row 1 cells, supporting the hypothesis that those cells are the precursors of vertebrate retinal photoreceptors (Yau, Hardie 2009; Vopalensky et al. 2012; Lamb 2013). Row 1 cells are directly adjacent to row 2 cells that in turn project to the neuropile. The amphioxus neuropile serves as a control region for locomotor behavior and is comparable to the vertebrate diencephalic locomotor region of the hypothalamus, similar to where melanopsin containing bipolar cells project and entrain the circadian rhythm (Lacalli, Kelly 2000; Hattar et al. 2006). Row 2 cells are homologous to retinal ganglion cells. Retinal ganglion cells are sister cells to amacrine and horizontal cells since they share specification and effector genes. Together this indicates that these cells share a common ancestry and row 2 cells seem to be the ancestral state of ganglion, horizontal and amacrine cells (Arendt 2003; Vopalensky et al. 2012).

1.2.2.2. Tunicata

Tunicata were longly classified as the lowest chordate group based on morphological data. Sequencing of tunicate and cephalochordate genomes however revealed that phylogenetically cephalochordates are more basal and tunicates represent the true sister group of vertebrates (Delsuc et al. 2006; Putnam et al. 2008). It is now assumed that simpler tunicate morphology and lifestyle is an adaptation to their ecological niche. This simplification is also reflected in the light sensing compartment of Tunicata (Delsuc et al. 2006).

Adult sea squirts (*Ciona intestinalis*) are sessile and show some light-evoked behaviors such as siphon contraction or gamete release but lack a defined light sensing organ. Two opsin genes that are orthologs of vertebrate ciliary opsins have been found to be expressed in adult sea

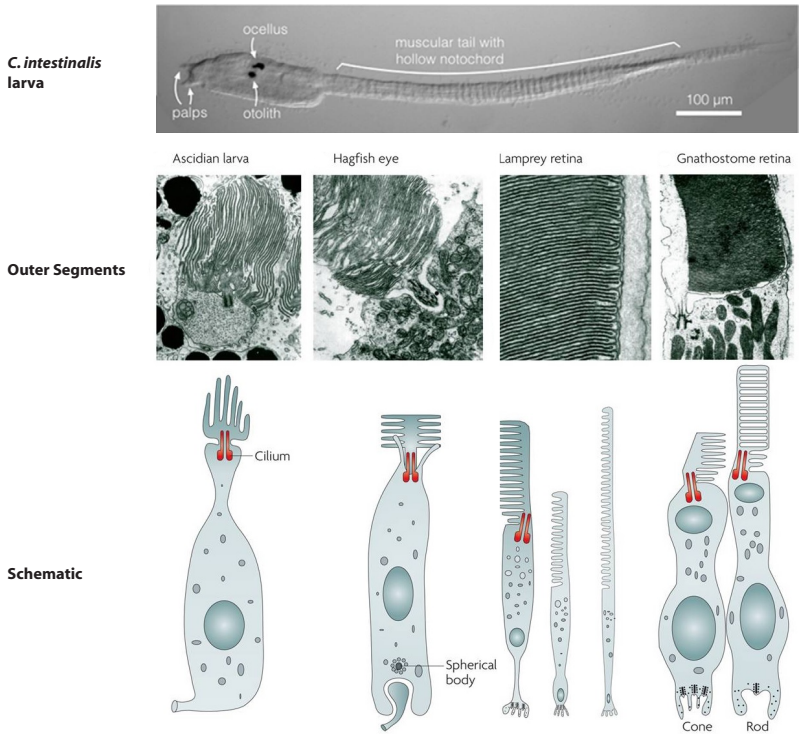

Figure 4: Ciona intestinalis larva and different types of photoreceptors found in chordates.
Photograph of a *C.intestinalis* larva at the hatching stage. The ocellus is the light sensing organ in Ciona embryos.
Lower part shows schematic representation of different ciliated chordate photoreceptors and electron microscopic pictures of the outer segments. In ascidian larvae and in hagfish the outer segment is rather unorganized. In lampreys five distinct types of photoreceptors are present, each expressing a different opsin gene (Lamb 2013). The outer segments of lamprey photoreceptors are continuous and morphologically resemble cones of higher vertebrates. The photoreceptors of Gnathostomata can morphologically and functionally be separated into rods and cones. Picture modified from (Kourakis, Smith 2015; Lamb 2013).

squirts in several tissues (Kusakabe, Tsuda 2007). In its larval stages, Ciona exhibit a light sensing spot called ocellus with photoreceptor cells expressing ci-opsin1 that are surrounded by one pigmented cell (Kusakabe et al. 2001)(Figure 4). Recent studies showed that the ci-opsin1 gene depicts an intermediate form between vertebrate and invertebrate visual opsins (Kojima et al. 2017).

1.2.2.3. Agnatha

The jawless vertebrate class, the Agnatha, consists of two extant groups, hagfishes and lampreys. The phylogenetic classification of hagfishes has been extensively debated as they were thought to be a sister group to lampreys. Studies using molecular data showed that the extant Agnatha form a monophyletic group (Figure 1) (Delarbre et al. 2002; Heimberg et al. 2010; Oisi et al. 2013). As mentioned before, after the split of chordates and vertebrates, two rounds of whole genome duplications took place in the vertebrate lineage. Duplication of genes are thought to be the molecular basis for innovation, thus the two round of whole genome duplication at the base of the vertebrate lineage migth have been necessary to develop more complex light-sensing organs and more specialized phototransduction cascades (Lamb et al. 2007; Vopalensky et al. 2012).

The assumption that hagfishes represent an ancient vertebrate species, fits very well with the retinal morphology. Hagfish eyes are located under a patch of translucent skin and possess only a bilayer neuronal retina with photoreceptors directly contacting projection neurons. No evidence for bipolar, amacrine or horizontal cells have been found (Kobayashi 1964; Holmberg 1970; Holmberg 1971). The lacks of a lens, ocular muscles or a cornea were seen as further evidence of an ancestral retinal state of hagfishes (Fernholm, Holmberg 1975; Locket, Jørgensen 1998). Hagfishes appear to be almost blind with extremely delayed reaction to light. Removal of the eyes prolonged the response even further but did not abolish it completely. Due to the lack of a pineal organ in hagfish it is assumed that the retina mainly serves as a pace-control for circadian rhythm rather than image-forming vision (Kobayashi 1964; Lamb 2013). Direct projections of retinal ganglion cells to the hypothalamus rather than an optic tectum is in line with this assumption (Kusunoki, Amemiya 1983).

The second class of Cyclostomata consists of lampreys. Lampreys have camera-type eye with extraocular muscles, a lens and an iris. All major cell types, photoreceptors, bipolar, ganglion, amacrine, horizontal and Müller glia cells, are present in the retina (Lamb 2013). Larval stages of lampreys are blind and the retina is buried under a translucent skin patch, similar to the hagfish retina. In larval stages the retina is undifferentiated and during a five year long metamorphosis the retina differentiates similarly to the differentiation of the retina of higher vertebrates, generating ganglion cells, amacrine cells, horizontal cells, photoreceptors and in the end bipolar cells (Rubinson, Cain 1989; Lamb 2013). Interestingly, layering seems slightly more rudimentary with most ganglion cells located in the innermost part of the INL followed by the IPL (Fritzsch, Collin 1990).

Two classes of photoreceptors can be found in the lamprey retina, termed long and short photoreceptors. Both morphologically resemble cone photoreceptors by having a continuous cell membrane forming the outer segments (Dickson, Graves 1979) (Figure 4). Interestingly, it has now been shown that despite their morphological similarities, short lamprey photoreceptors exhibit rod-like photosensitivity by expressing a lamprey rhodopsin homolog, whereas long photoreceptors show cone-like properties (Ishikawa et al. 1987; Bowmaker 2008; Morshedian, Fain 2015).

Lampreys and higher vertebrates use bipolar cells to increase the processing power in the retina. Interestingly, bipolar cells share a number of physiological and morphological features with photoreceptors. For example, photoreceptors and bipolar cells have quite similar axonal terminals using a specialized synaptic structure called ribbon synapse, enabling simultaneous release of a high number of synaptic vesicles. Moreover, ON-bipolar cells use metabotropic signaling via G-protein signaling, while photoreceptors use G-protein signalling to process light stimuli. Therefore it is assumed that either bipolar cells evolved from photoreceptors or that they share a common ancestral cell type (Lamb et al. 2007; Lamb et al. 2008).

Although there is now good evidence that lampreys and hagfish are a monophyletic group, the evolutionary status of the hagfish retina is still highly debated. Many authors claim that the retina of the common ancestor of cyclostomes must have been a lamprey-style retina and consequently the hagfish retina underwent extensive degeneration in the course of evolution as a result of adaptation to their burrowing life style and evolutionary niche (Holmberg 1977; Stock, Whitt 1992; Locket, Jørgensen 1998). On the other hand it is argued that the eyes of larval lamprey and hagfish share strong morphological similarities and therefore the hagfish eye could resemble an arrested stage of development (Lamb et al. 2007; Lamb 2013). Further it is argued that degeneration of different cell types and additionally rewiring ganglion cells to project to hypothalamic regions instead of the optic tectum seems rather unlikely and too complex (Lamb et al. 2008). Nevertheless, retinae of the two extant cyclostome groups depict at least partially intermediate stages between chordate light sensing organs and higher vertebrate's eyes.

1.2.2.4. Gnathostomata

The eyes and the retina of all jawed vertebrates (Gnathostomata) share remarkable similarities in morphology and function. Photoreceptors can be morphologically divided into rod and cone type photoreceptors. Lamprey photoreceptors are morphologically identical to Gnathostomata cones where the cell membrane in the outer segments is rather continuous, but lamprey short photoreceptors exhibit rod-like features suggesting that the duplex retina was invented before the split of Agnatha and Gnathostomata (Morshedian, Fain 2015, 2017).

The invention of the duplex retina allowed further adaptations at the level of the photoreceptors. Several groups of fishes, Amphibia, Reptilia, birds, Monotremata and Marsupilalia possess oil droplets in cones. In some species they are pigmented and it is thought that they act as spectral filters and guide the light to the outer segments. Since such droplets are present in lungfish but absent in Agnatha, they must have appeared after the split of Agnatha and Gnathostomata. The absence of oil droplets in cones of placental mammals is thought to be a consequence of the nocturnal phase of the common ancestor of placental mammals. Nevertheless, species without oil droplets in cones have been described in all major vertebrate classes indicating that these droplets were lost independently several times during vertebrate evolution (Bowmaker 2008; Lamb 2013).

Most vertebrate species have a cone-dominated retina. However, mammals represent an exception in having a rod-dominated retina. This is thought to be a consequence of the nocturnal bottleneck the mammal ancestor underwent (Heesy, Hall 2010). Under scotopic conditions, not enough photons hit the retina to activate cones. Consequently, mammals adapted their visual system to rod-dominated retinae (Bowmaker 2008; Lamb 2013). Recently the molecular basis of this adaption was resolved. In mammals the differentiation into rods and cones is controlled by the two transcription factors Maf-family neural retina leucine zipper protein

(NRL) and thyroid hormone receptor β2 (TRβ2) (Ng et al. 2011). Short-wavelength-sensitive cone-fate resembles the default state in mammalian retina (Hunt, Peichl 2014). NRL knockout mice resulted in a retina with predominant s-cones while mice lacking TRβ2 have s-cones instead of medium wavelength sensitive cones (m-cones) (Ng et al. 2011). A subset of s-cone precursors in mice differentiates into rods by ectopic expression of NRL and therefore rodents and likely other mammals have a bigger proportion of rods than cones (Kim et al. 2016). How rod differentiate in lower vertebrate is not entirely clear. In zebrafish NRL is expressed in all photoreceptor cells and can therefore not be the sole rod-determining factor (Stenkamp 2011).

Other cell types also show adaptations to the nocturnal bottleneck in the mammalian lineage, mainly in the count of cell type subtypes. This topic is further covered in Chapters 1.2.3 and 1.2.4.

1.2.3. Signaling in the vertebrate retina

In vertebrates, light has to pass through the entire retina and hits the visual pigment in the photoreceptor outer segment at the very back of the retina. Photoreceptors are depolarized in darkness and tonically release glutamate. When light hits the retina, photoreceptors hyperpolarize gradually with light intensity and subsequently the glutamate release is gradually diminished. Glutamate released by photoreceptors reaches the dendrites of bipolar cells that in turn use glutamate to signal to ganglion cells. This section focuses on the different cell types and the synaptic signaling in the retina.

The visual pigment is located in the photoreceptor outer segments and comprises an opsin protein and a 11-cis retinal, a vitamin A derivate. When light hits 11-cis retinal it undergoes a conformational change into all-trans retinal that cannot bind to opsin anymore. Free opsin in turn activates the G-protein transducin where the guanosine diphosphate (GDP) of the α subunit is exchanged by guanosine triphosphate (GTP) and the α subunit dissociates from transducin. Subsequently, the α subunit activates cyclic guanosine monophosphate (cGMP) phosphodiesterase (PDE) which in turn breaks down cGMP to GMP. cGMP acts as a second messenger in photoreceptors, opening cGMP gated cation channels. Lower levels of local intracellular cGMP lead to the closure of these cation channels and subsequent hyperpolarization of the cell. Therefore photoreceptor cells are depolarized in darkness. Their resting membrane potentials range between -35 and -45mV and hyperpolarize up to -75mV upon a light stimulus (Thoreson 2007). Hence, photoreceptors release glutamate tonically in darkness and this release is gradually diminished with the intensity of a light stimulus (Baylor, Hodgkin 1973; Thoreson 2007).

The depolarization of a photoreceptor leads to the opening of voltage-gated calcium channels in the synaptic terminal and subsequent calcium-influx leads to the exocytosis of synaptic vesicles and subsequent release of glutamate into the synaptic cleft. Tonic release of glutamate is enabled by a highly specialized ribbon synapse at the photoreceptor terminal. While 10-100 vesicles cluster at the release site of a conventional synapse, up to 170’000 release-ready glutamate-filled vesicles have been found in the ribbon-synapse of a single lizard cone (Choi et al. 2005).

Photoreceptors form synapses with bipolar and horizontal cells in the OPL. Horizontal cells are modulatory interneurons as they are depolarized by glutamate released from photoreceptors and in turn release γ-Aminobutyric acid (GABA). Cones express $GABA_A$-receptors (GABA-gated chloride channel) and thus hyperpolarize upon GABA signaling from horizontal cells. Horizontal cells contact multiple cones and play crucial roles in contrast vision and col-

or opponency (for reviews see (Kamermans, Spekreijse 1999; Thoreson, Mangel 2012)). Horizontal cells further contact ON- and OFF-bipolar cells. Interestingly, all bipolar cells express $GABA_A$-receptors on their dendritic tip. Nevertheless it was shown that application of GABA depolarizes ON-bipolar cells but hyperpolarizes OFF-bipolar cells. This differences might be explained by different chloride equilibrium potentials of ON- and OFF-bipolar cells (Thoreson, Mangel 2012). Horizontal cells can be morphologically and molecularly divided into four different subgroups. H1 or B-type horizontal cells are axon-bearing horizontal cells, contacting exclusively rod photoreceptors. H2 or A-type and H3 and H4 (C-type) horizontal cells are axon-less and cover smaller regions in the retina, only contacting cone synapses. Most mammalian species have A- and B-type horizontal cells, but some rodents and marsupials only use the H1 subtype which is thought to be an adaptation to an extremely rod-dominated retina. Some bird, reptile and fish species use the full spectrum of four horizontal cell subtypes (Thoreson, Mangel 2012). Taken together, horizontal cells are important for contrast vision and color opponency by a negative feedback-loop with photoreceptors and a feedforward-loop to bipolar cells.

Bipolar cells receive their main input from glutamate released by photoreceptor cells. In the mammalian retina ten different subtypes of bipolar cells have been described, while in lower vertebrates such as teleost fishes up to 22 subtypes exist (Connaughton et al. 2004; Euler et al. 2014). Rods only contact one specific subtype of bipolar cells called rod bipolar cells. At least nine different bipolar subtypes have been described to form synapses with cones and exhibit distinct function in processing different aspects visual stimuli (for review see (Masland 2012a)). Bipolar cells fall into two major categories, namely ON- and OFF-bipolar cells. OFF-bipolar cells express ionotropic glutamate receptors such as AMPA and kainate receptors on their dendritic tips and thus depolarize when light is off and glutamate is released by photoreceptors. ON-bipolar cells in turn express metabotropic glutamate receptor 6 (mGluR6) on their dendritic tips. Upon glutamate binding, mGluR6 mediates via G-protein signalling closure of cation-selective TRPM1 channels which in turn leads to hyperpolarization of ON-bipolar cells. Therefore ON-bipolar cells are sign-inverting and OFF-bipolar cells are sign-conserving compared to the photoreceptor membrane potential. Rod bipolar cells exhibit properties similar to ON-bipolar cells (for review see (Euler et al. 2014)).

ON- and OFF-bipolar cells form synapses with ganglion cells and amacrine cells in the IPL. Like photoreceptors, bipolar cells use ribbon synapses at their axonal terminal and release of glutamate is tuned by the depolarization-state of the cell. Amacrine cells can be grouped according to the spread of their dendrites into wide field, medium field and narrow field. Morphologically and molecularly they can be further classified into at least 29 different subtypes in mammals and 28 in zebrafish (Bloomfield 2009; Jusuf, Harris 2009; Masland 2012b). Surprisingly little is known about specific function of different amacrine subtypes. Besides integrating and modulating signals from bipolar cells to ganglion cells, two further roles have been described in more detail. Direction-selective ganglion cells have been described to fire action potentials whenever the stimulus moves into the preferred direction of the ganglion cells. This selectivity has been shown to be acetylcholine- and GABA- dependent. Starburst amacrine cells release both, acetylcholine and GABA. Electrophysiological measurements have proved involvement of starburst amacrine cells in direction-selectivity (Bloomfield 2009; Masland 2012b). A second very important role fulfill AII amacrine cells. Rod bipolar cells do not form synapses with ganglion cells directly but with AII and A17 amacrine cells. Whereas A17 amacrine cells signal back to the rod bipolar cells via GABAergic synapse, AII amacrine cells are depolarized upon glutamate signaling of rod bipolar cells. AII amacrine cells form gap junctions with other AII amacrine cells as well as cone ON-bipolar cells and thus piggy-

back the rod signal to the cone signaling pathway (Demb, Singer 2012).

The last cell type that gets light-evoked signals are retinal ganglion cells. Retinal ganglion cells express AMPA and kainate receptors at their dendritic tips thus depolarize upon glutamate signaling of bipolar cells. As described above, they get modulatory input from amacrine cells. Morphologically between 11 and 15 different subtypes of ganglion cells have been described for fishes and mammals but recent studies suggest up to 40 different subtypes based on functional and molecular implications (Mangrum et al. 2002; Baden et al. 2016). They can roughly be classified as ON- and OFF-center ganglion cells and ON/OFF-center ganglion cells.

Retinal ganglion subtypes need to process and deliver all aspects of vision, such as contrast, color and luminance to their distinct target sites. Furthermore, all classes have direction selective subtypes. A specific subset of ganglion cells was described to be light-sensing itself by expressing melanopsin. These cells project to the suprachiasmatic nucleus of the thalamus, where they entrain the circadian clock besides other important roles such as the pupillary reflex (Hattar et al. 2002; Hattar et al. 2006).

Taken together, vertebrates use glutamatergic signaling in the retina for processing visual information and delivery to the corresponding target site. Regulation of synaptic glutamate-concentration is therefore crucial for proper signal transmission and termination. This topic will be further covered in a following section.

1.2.4. Evolution of vertebrate color vision – the opsin gene family

Gene families are a group of genes that share similar properties and descend from a common ancestor. Genome-shaping events lead to the adaptation of single family members to specific tasks and eventually to higher organismal complexity. Thus, we can study gene families and tracing their evolution by comparing expression and properties of gene family homologs from different vertebrate groups.

One such gene family is the opsin gene family. Color vision in vertebrates is dependent on visual opsins, as discussed above. Among others, the G-protein-coupled receptor (GPCR) family-A comprises the opsin gene family. Opsin genes can be further divided according to their G-protein subtypes into ciliary-opsins, rhabdomeric-opsins and photo-isomerases. C-opsins and r-opsins are used by most animals as visual opsins (Bowmaker 2008; Shichida, Matsuyama 2009). Arthropods use r-opsins in their rhabdomeric photoreceptors. In this case, light hitting the photoreceptors leads, via G-protein signaling, to the opening of transient receptor potential channels (TRPC) and subsequently to the depolarization of the cell, which is in contrast to the light-evoked hyperpolarization in vertebrate photoreceptors (Shichida, Matsuyama 2009).

Visual opsins used by chordates are c-opsins (Vopalensky et al. 2012; Lamb 2013). In higher vertebrates, opsins are named according to their absorption spectra. Long-wavelength-sensitive opsins (LWS) have absorption maxima between 495-570 nm in the green/red range, short-wavelength-sensitive opsin 1 and 2 (SWS1 and SWS2) in the UV-blue (355-450 nm) and blue (415-480 nm), rhodopsin-like 2 (RH2) in the green range (470-530 nm) and rhodopsins (RH1), that is expressed in rods, show absorption maxima between 460-530 nm depending on the species (Bowmaker 2008). Opsins consist of seven transmembrane domains that form a binding site for the chromophore 11-cis retinal (Figure 5).

Thus, by simply taking the visual opsin gene number and their absorption maxima into account, we can follow the evolution of the opsin gene family and draw conclusions about the

complexity of color vision in the corresponding species.

Already basal vertebrates such as lampreys harbor five visual opsin genes in their genome. While they possess an ortholog for SWS1, SWS2 and LWS, somewhat surprisingly they possess two rhodopsin-like genes that cluster together between RH1 and RH2 with approximately the same evolutionary distance to both (Collin et al. 2003) (Figure 5). This suggests that the common ancestor of all vertebrates must have had two visual opsin genes that gave rise to eight opsin genes after the two rounds of whole genome duplications at the base of the vertebrate lineage. The subsequent loss of three genes led to a final number of five opsin genes at the base of the vertebrate clade. After these duplication events, opsin genes adjusted the absorption maxima accordingly. Changes of only a single amino acid in an opsin gene can result in a shift of absorption maxima of up to 30 nm (for reviews see (Lamb et al. 2007; Bowmaker 2008; Lamb 2013)). Phylogenetic analysis and characterization of numerous opsin genes led to the assumption that the common ancestor of vertebrates was able to process four different wave-lengths of light, indicating similar complexity of color vision as several extant vertebrate groups show (Lamb 2013).

After the additional round of whole genome duplication, zebrafish have retained nine visual opsin genes. Nevertheless, functionally zebrafish are tetrachromates, expressing similar opsin genes in the same cone subtypes (Cameron 2002; Endeman et al. 2013). Interestingly, the higher number of genes did not lead to increased complexity of the system in this case and it remains unclear why so many opsin genes have been retained in zebrafish. While zebrafish seem to have duplicated the RH2 gene twice and retained all copies, the very same gene is lost in the amphibian lineage, indicating a loss shortly after the split of the Amphibia from other vertebrates (Bowmaker 2008). Although exceptions exist, the majority of reptiles and birds species retained all five visual opsins. Several gene loss events occurred in the mammalian lineage. These events are associated with the nocturnal-bottleneck of a common ancestor of all mammals as mentioned before (Jacobs 2013; Lamb 2013). The common ancestor of all mammals lost RH2 before the split of Monotremata from Eutheria and Marsupilalia. While Monotremata further lost SWS1, some marsupial species have retained the three remaining cone opsins but all eutherian species have lost SWS2. In the eutherian lineage further gene loss seems to have occurred. For example, marine mammals are monochromates. Humans and other primates in contrast have duplicated the LWS gene and shifted the absorption maxima of the two copies to distinct green and red (for review see (Bowmaker 2008; Jacobs 2013)) (Figure 5).

While cones mediate color vision in bright light conditions at high speed, high sensitivity and high contrast, rods are even more sensitive to light and can respond to a single photon. Because RH1 evolved from an ancestral cone-type opsin, cones are evolutionary older than rods (Okano et al. 1992; Lamb 2013). Interestingly, the higher sensitivity to light of rods is not due to the adaptation of rhodopsin but rather due to a change in the amplification of the light stimuli. For example, rhodopsin is activated for longer than other opsins by slowing down the shut-off reactions subsequently leading to the activation of more transducin G-protein (Shichida, Matsuyama 2009; Lamb 2013).

To sum up, the opsin gene family depicts an example of a dynamic gene family where two rounds of whole genome duplication at the base of the vertebrate clade led to an increased complexity of the visual system. Countless adaptations in absorption maxima as well as in gene number took place which can be nicely correlated to species specific demands for the perception of different colors of light. The loss of several opsin genes and thus perception of several different colors in mammals is most likely followed by simplification in the processing machinery.

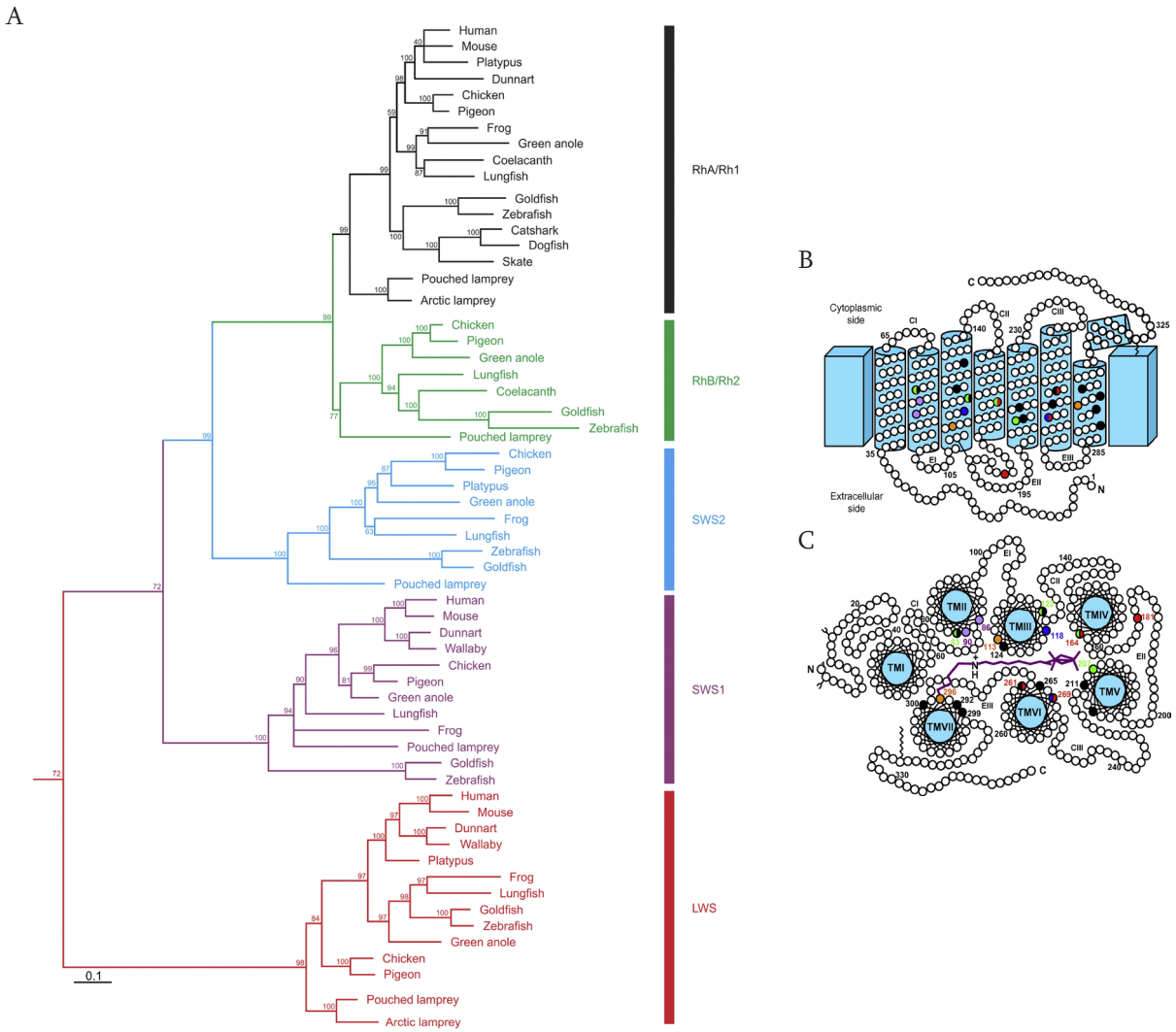

Figure 5: Phylogeny and membrane topology of vertebrate visual opsins.
A: Phylogenetic tree of the vertebrate visual opsins shows grouping into RH1/RHA, RH2/RHB, SWS1, SWS2 and LWS according to different absorption maxima. Numbers indicate branch support values and the scale bar represents required amino acids substitutions to generate the corresponding tree. Modified from (Collin et al. 2009). Side (B) and top (C) view of the membrane topology of visual opsins. Opsins contain seven transmembrane α-helices. Numbering is referred to bovine rhodopsin. Lysine 296 (orange) covalently binds the chromophore retinal (violet). Sites that are primarily involved in spectral tuning of opsins are depicted with different colors; LWS red, RH2 green, SWS1 violet, SWS2 blue and RH1 black. Adapted from (Bowmaker, Hunt 2006).

1.3. The Solute Carrier Family 1 gene family

One group of genes that is involved in processing visual information in the retina is the gene family of the EAATs that belong to the SLC1 gene family. In this thesis we investigate whether adaptations in the complexity of the visual system are reflected by the EAATs.

Glutamate is the main excitatory amino acid in the retina and the remaining central nervous system. Proper signal propagation and termination relies on fast removal of glutamate from the synaptic cleft. EAATs are responsible for the reuptakte of glutamate from the synaptic cleft. They are so-called secondary active transporter that transport glutamate against its concentration gradient together with three sodium ions and one proton into the cell while one potassium ion is counter-transported (Figure 6). Besides the important role in glutamate transport, a thermodynamically uncoupled anion conductance has been described for EAATs (for review see (Fahlke et al. 2016)). In mammals five EAATs (EAAT1-5) and two neutral amino acid transporter comprise the SLC1 gene family (Kanai, Hediger 2004).

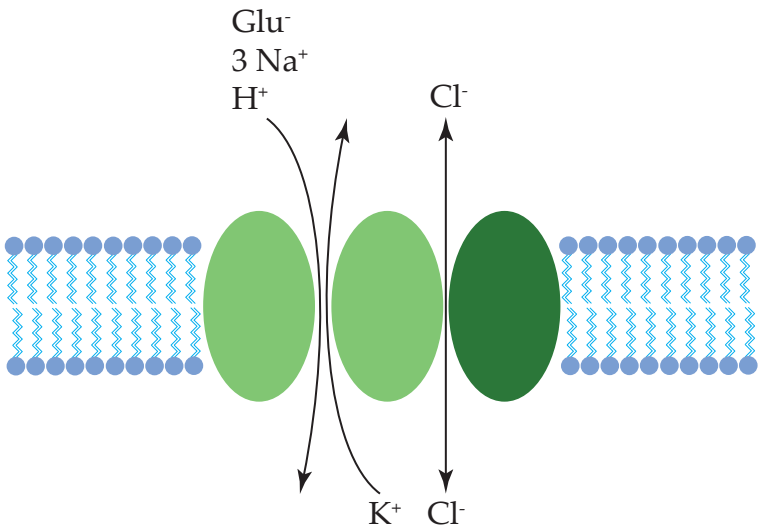

Figure 6: EAAT mediated secondary active glutamate transport.
Schematic representation of an EAAT located in the cellular membrane. The transport domain is depicted in light green, dark green represents the trimerization domain. Glutamate is transported together with three sodium ions and one proton while one potassium ion is counter-transported, resulting in a net flux of two positive charges into the cell. Movement of the transpoport domain upon glutamate transport opens an anion pore and anions can pass in either direction. This anion conductance is therefore thermodynamically uncoupled form the glutamate transport (Machtens et al. 2015; Fahlke et al. 2016).

1.3.1. Membrane topology of Excitatory Amino Acid Transporters

EAATs are evolutionary old and homologs of the glutamate transporter have been found in the archae *Pyrococcus horikoshii* (Glt_{Ph}). Much of what is known about the protein structure and membrane topology of EAATs has been studied in Glt_{Ph}. Conservation between Glt_{Ph} and EAATs is highest in the structural domain (Slotboom et al. 1996; Grunewald, Kanner 2000; Yernool et al. 2004). Eight transmembrane domains (TM) and two re-entrant hairpin loops (HP) form an EAAT protomer that in turn forms homotrimers (Yernool et al. 2004) (Figure 7). Each protomer works independently from the other protomers in the trimer and can be in different transport states (Akyuz et al. 2013; Erkens et al. 2013). In heterologous expression systems it was shown that EAAT3 and EAAT4 can form heterotrimers but such hetrerotrimerizations were never shown *in vivo* (Nothmann et al. 2011). TM1, TM2, TM4 and TM5 build the trimerization domain that is essential for anchoring the protein in the cell membrane. The transport domain is formed by TM3, TM6, TM7, TM8 as well as HP1 and HP2 (Reyes et al. 2009; Vandenberg, Ryan 2013) (Figure 7). In its outward facing state, Glt_{Ph} forms a bowl-shaped basin that faces the extracellular space and is half of the depth of the cellular membrane. This configuration allows HP2 to act as an extracellular gate whereas HP1 acts as the intracellular counterpart (Yernool et al. 2004).

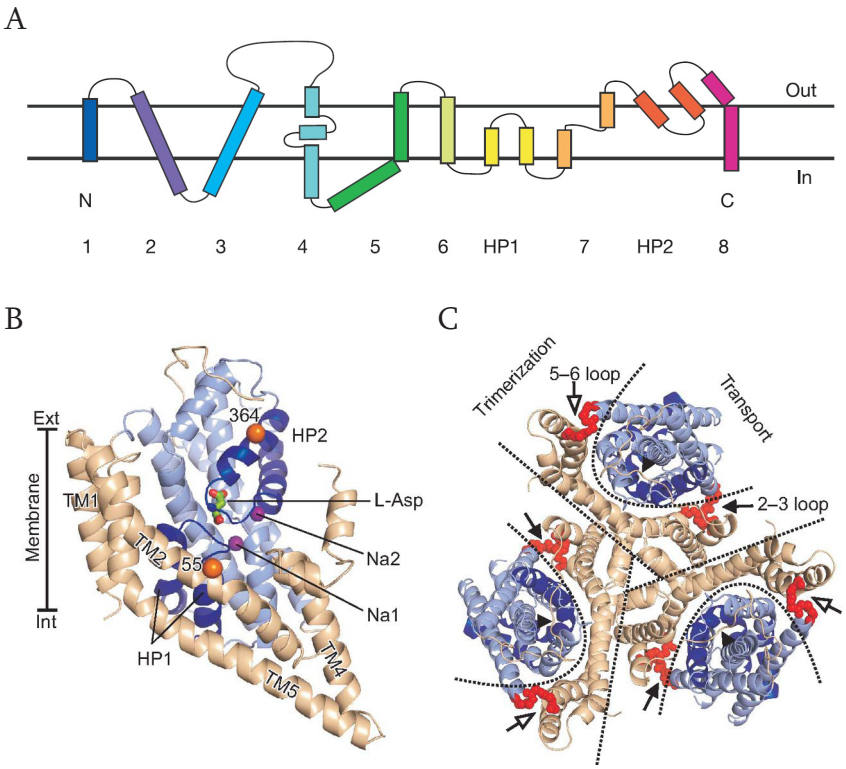

Figure 7: Membrane topology and crystal structure of Glt_{Ph}.
EAAT and Glt_{Ph} are transmembrane domain proteins consisting of eight TMs and two HPs (A). Side view of a schematic representation of Glt_{Ph} (B) and view from extracellular side onto a Glt_{Ph} trimer (C). Brown helices indicate the trimerization domains whereas blue helices show the transport domains. Straight dashed lines in C show protomer assembly in trimer-state (Vandenberg, Ryan 2013).
Modified from (Yernool et al. 2004) (A) and (Reyes et al. 2009; Vandenberg, Ryan 2013) (B, C).

1.3.2. Biophysical properties of EAATs

1.3.2.1. Glutamate transport of EAATs

As for the crystal structure of EAATs, much about molecular transport mechanisms of the EAATs was studied using the archeal EAAT homolog Glt_{Ph} as a model. Unlike EAAT, Glt_{Ph} is favoring aspartate over glutamate. It as well co-transports three sodium ions but no counter-transport was observed (Yernool et al. 2004; Akyuz et al. 2013; Erkens et al. 2013).

The binding site for the first Na^+ is located below the aspartate/glutamate binding site and is formed by amino acid residues from TM7 and TM8. The second binding site for Na^+ is located below HP2 where the binding site is formed by parts of TM7 and HP2 (Boudker et al. 2007). Binding of the first Na^+ moves HP2 in a way to free the binding site for the substrate and the second Na^+ binding site (Verdon et al. 2014; Ji et al. 2016). The location of the third Na^+ was more difficult to elaborate since binding of the third Na^+ would lead to closure of HP2 and subsequent transport of the substrate and co-transported ions. Nevertheless, Bastug and co-workers found the third Na^+ binding site to be associated with side chains of amino acids from TM3 and TM7. They further propose the binding sequence Na3 – Na1 – Asp – Na2 to be the favored order in which Na^+ and the substrate bind to the transporter due to allosteric reasons (Bastug et al. 2012).

Following substrate and ion binding and closure of HP2, the transporter undergoes large, elevator-like, conformational changes that involve movements of the transport domain relatively to the trimerization domain (Reyes et al. 2009; Ji et al. 2016). Opening of the intracellular gate HP1 leads then to the release of substrate and co-transported ions. This transporter-state is called inward-facing.

1.3.2.2. Anion conductance of EAATs

Besides transporting glutamate against its concentration gradient, EAATs fulfill a role as glutamate-gated anion channel (Fairman et al. 1995; Ryan, Vandenberg 2005). While it was shown that the anion (in physiological conditions mostly Cl^-) permeates in a from the glutamate transport uncoupled manner, the mechanisms of anion permeation were only recently resolved (Machtens et al. 2015). Based on electrophysiological recordings, it was assumed for a long time that the translocation between outward- and inward facing transporter state could lead to an opening of a chloride pore but it became already evident that anion permeation and glutamate transport are structurally divided (Seal et al. 2001; Ryan, Vandenberg 2002).

Machtens and colleagues showed that anions are transported during extremely short intermediate transporter states that involve lateral movement of the transport domain by combining molecular dynamics simulations with fluorescence spectroscopy and subsequent electrophysiological recordings (Machtens et al. 2015). These lateral movements of the transport domain lead to the formation of an aqueous pore between the trimerization and the transport domain. They further showed that this pore is perfectly anion selective and unselective for transporter substrates (Machtens et al. 2015; Fahlke et al. 2016). Most side chains that reach the anion pore are hydrophobic, with the exception of positively charged arginine 276 that localized at the tip of HP1. Mutagenesis of R276 leads to the loss of anion-selectivity and results in an unselective ion pore (Borre, Kanner 2004; Machtens et al. 2015).

1.3.2.3. Properties of different SLC1 family members

Traditionally EAATs have been roughly divided into mainly glial-expressed (EAAT1 and EAAT2) and mainly neuronal-expressed EAATs. This further indicates functional diversity and it was shown that EAAT1 and EAAT2 are high capacity transporters with the main purpose of transporting glutamate from the synaptic cleft into the cell and by that they are tightly controlling the extracellular glutamate concentration. Knockout of EAAT1 leads to amygdala-kindling and subsequent epileptic seizures in mice and similar, EAAT2 knockout mice develop epilepsy and neurodegeneration (Rothstein et al. 1996; Tanaka 1997; Watanabe et al. 2000). Furthermore, EAAT1 and EAAT2 show comparatively low conductance for anions, suggesting they are not involved in altering membrane potentials of glia cells (Wadiche et al. 1995; Wadiche, Kavanaugh 1998).

Mammalian EAAT3, EAAT4 and EAAT5 are predominantly expressed in neurons and show lower affinity to glutamate but higher anion conductance compared to EAAT1 and EAAT2 (Wadiche et al. 1995; Fairman et al. 1995; Arriza et al. 1997; Kanai et al. 2013). Although EAAT3 is expressed in neurons all over the brain, EAAT3 knockout mice do not show any neurological phenotype. Since EAAT3 is also expressed in the proximal tubules of the kidney, glutamate and aspartate reuptake from the urine is decreased (Rothstein et al. 1994; Peghini et al. 1997). Because EAAT3 shows high affinity to L-cysteine it might play a role in cell metabolism rather than in synaptic transmission (Zerangue, Kavanaugh 1996b). EAAT4 was shown to be expressed mainly in cerebellar Purkinje cells and knockout of EAAT4 leads to typical cerebellar dysfunction phenotypes such as motor deficits and subsequent neurodegeneration (Nagao et al. 1997; Perkins et al. 2016). EAAT5 is expressed in retinal bipolar cells and photoreceptors (Eliasof et al. 1998; Pow, Barnett 2000). For rod bipolar and ON-bipolar cells it was shown that EAAT5 acts on the resting membrane potential by shoveling chloride into the cell when glutamate is present and thus keeping the cell hyperpolarized in this way (Wersinger et al. 2006; Tse et al. 2014).

The two neutral amino acid transporters ASCT1 and ASCT2 show some similarity to glutamate transporters. ASCTs transport substrate amino acids together with three sodium ions but no counter-transport of potassium has been found for ASCTs (Zerangue, Kavanaugh 1996a; Kanai et al. 2013). As for EAATs, ASCT exhibit thermodynamically uncoupled anion conductance. Due to the lack of potassium counter-transport it is assumed that ASCTs work as homo- or heteroexchanger of neutral amino acids (Zerangue, Kavanaugh 1996a; Kanai et al. 2013). Expression of ASCT is not limited to neuronal tissues thus they are involved in amino acid homeostasis in neurons as well as in other parts of the body (for review see (Kanai et al. 2013)).

1.3.2.4. Phylogeny of vertebrate SLC1 gene family

The SLC1 gene family is a rather old gene family. Already archaeal prokaryotes used a SLC1 ortholog to sense food in their environment. In human and other mammals, the SLC1 gene family consists of five EAAT and two ASCT genes. Gesemann and coworkers found, by extensive phylogenetic analysis of the vertebrate lineage, two additional members of the SLC1 gene family, EAAT6 and EAAT7, which are present in lower vertebrates such as Reptilia and Amphibia (Gesemann et al. 2010). In the teleost zebrafish, a total of eleven EAAT and two ASCT genes have been found. They have retained two paralogs for EAAT1, EAAT2, EAAT5 and EAAT6 after the teleost-specific whole genome duplication. The common ancestor of birds and reptiles still possessed seven EAAT genes, but while EAAT7 and SLC1A5 have been lost in the bird lineage, the situation in the Reptilia clade is more complex. Gesemann and co-work-

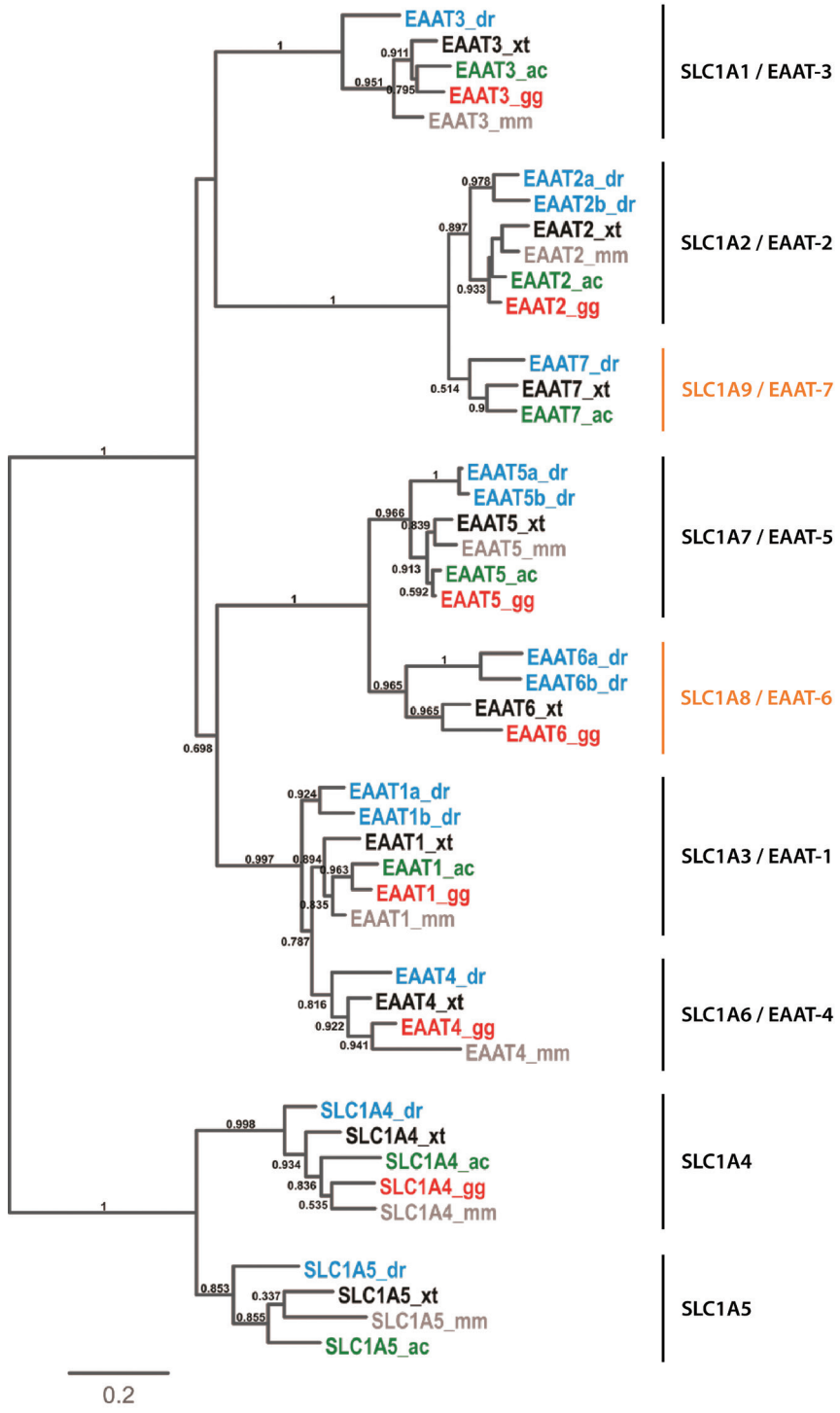

Figure 8: Phylogeny of the vertebrate SLC1 gene family.
Maximum likelihood phylogeny of the vertebrate SLC1 gene family (A). Two additional subgroups (EAAT6 and EAAT7) are present partially in non-mammalian vertebrates (indicated in orange). Numbers indicate branch support values and the scalebar shows amino acid substitutions necessary to build the corresponding tree. For clarity, only one representative species of the majoir vertebrate clades were included into the tree (dr: *Danio rerio*, zebrafish, teleost fishes; xt: *Xenopus tropicalis*, western clawed frog, Amphibia; ac: *Anolis carolinensis*, green anole lizard, Reptilia; gg: *Gallus gallus*, chicken, Aves; mm: *Mus musculus*, house mouse, Mammalia).

ers reported the loss of EAAT4 and EAAT6 in anole lizards. Nevertheless, database search revealed that still seven EAAT genes are present in the genome of *Gekko japonicus*, while Burmese python and chinese soft shell turtle have lost EAAT7 (Gesemann et al. 2010; our own unpublished data).

Further gene loss occurred before the split of Monotremata and Theria, where EAAT7 was lost. All Theria have additionally lost EAAT6. Taken together, EAAT6 and EAAT7 have been non-functionalized several times independently in the course of vertebrate evolution.

SLC1 nomenclature	EAAT nomenclature	Other names
SLC1A1	EAAT3	EAAC1
SLC1A2	EAAT2	GLT-1
SLC1A3	EAAT1	GLAST, GLAST-1
SLC1A4		ASCT1
SLC1A5		ASCT2
SLC1A6	EAAT4	
SLC1A7	EAAT5	
SLC1A8	EAAT6	
SLC1A9	EAAT7	

Table 1: Nomenclature of the SLC1 gene family and corresponding EAAT nomenclature and other commonly used names.

1.4. Objectives of the thesis

This thesis aims to shed light on the evolutionary history of the SLC1 gene family using different experimental approaches.

After a duplication event, one of the two copies of the ancestral gene is released from selective pressure and subsequently accumulates mutations. Such mutations can affect regulatory or coding sequences and the two copies can split ancestral functions of the gene between the two copies what is called sub-functionalization. In less frequent cases, one copy can as well gain a new function and thus serve a new task, what is called neo-functionalization. In a majority of cases accumulated mutations in one copy will lead to non-functionalization and the copy is lost in the genome (Glasauer, Neuhauss 2014).

Chapter 1 of this thesis focuses mainly on glial expressed EAAT1 and EAAT2. Zebrafish retained two paralogs for each of the two genes, which led to sub-functionalization on the expression level in both cases. Interestingly we found a switch of expression patterns between EAAT1 and EAAT2 in mice by comparative expression analysis in the retina of selected vertebrate species of the major clades. Analysis of the biophysical properties of EAAT1 and EAAT2 orthologs was performed in order to find hints why such a switch could happen.

In Chapter 2 we show an example of sub-functionalization using the zebrafish EAAT2 paralogs as a model. Taking advantage of morpholino-mediated gene knockdown it was shown that EAAT2a and EAAT2b play distinct roles in retinal signal transmission.

Chapter 3 deals with retinal EAAT5, EAAT6 and EAAT7. EAAT6 and EAAT7 were lost during

the course of mammalian evolution. Expression analysis shows almost restricted expression in the retina for both EAAT orthologs. Elucidating the biophysical properties of EAAT7 reveals clear glutamate-gated anion channel properties, similar to EAAT5. We speculate that along with the loss of several opsin genes the whole processing machinery in the retina was simplified, ultimately leading to the loss of EAAT6 and EAAT7 in mammals.

Chapter 4 is unrelated to the evolutionary history of the SLC1 gene family. It contains a published study about the role of MAM domain containing glycosylphosphatidylinositol anchor 2 (MDGA2) and its role in axon outgrowth and migration of zebrafish cranial motoneurons.

1.5. References

Akyuz, Nurunisa; Altman, Roger B.; Blanchard, Scott C.; Boudker, Olga (2013): Transport dynamics in a glutamate transporter homolog. In *Nature* 502 (7469), pp. 114–118. DOI: 10.1038/nature12265.

Arendt, Detlev (2003): Evolution of eyes and photoreceptor cell types. In *The International journal of developmental biology* 47 (7-8), pp. 563–571.

Arriza, J. L.; Eliasof, S.; Kavanaugh, M. P.; Amara, S. G. (1997): Excitatory amino acid transporter 5, a retinal glutamate transporter coupled to a chloride conductance. In *Proceedings of the National Academy of Sciences of the United States of America* 94 (8), pp. 4155–4160.

Baden, Tom; Berens, Philipp; Franke, Katrin; Román Rosón, Miroslav; Bethge, Matthias; Euler, Thomas (2016): The functional diversity of retinal ganglion cells in the mouse. In *Nature* 529 (7586), pp. 345–350. DOI: 10.1038/nature16468.

Bastug, Turgut; Heinzelmann, Germano; Kuyucak, Serdar; Salim, Marietta; Vandenberg, Robert J.; Ryan, Renae M. (2012): Position of the third Na+ site in the aspartate transporter GltPh and the human glutamate transporter, EAAT1. In *PloS one* 7 (3), e33058. DOI: 10.1371/journal.pone.0033058.

Baylor, D. A.; Hodgkin, A. L. (1973): Detection and resolution of visual stimuli by turtle photoreceptors. In *The Journal of physiology* 234 (1), pp. 163–198.

Bloomfield, S. A. (2009): Retinal Amacrine Cells. In Larry R. Squire (Ed.): Encyclopedia of neuroscience. [Amsterdam]: Elsevier, pp. 171–179.

Borre, Lars; Kanner, Baruch I. (2004): Arginine 445 controls the coupling between glutamate and cations in the neuronal transporter EAAC-1. In *The Journal of biological chemistry* 279 (4), pp. 2513–2519. DOI: 10.1074/jbc.M311446200.

Boudker, Olga; Ryan, Renae M.; Yernool, Dinesh; Shimamoto, Keiko; Gouaux, Eric (2007): Coupling substrate and ion binding to extracellular gate of a sodium-dependent aspartate transporter. In *Nature* 445 (7126), pp. 387–393. DOI: 10.1038/nature05455.

Bowmaker, James K. (2008): Evolution of vertebrate visual pigments. In *Vision Research* 48 (20), pp. 2022–2041. DOI: 10.1016/j.visres.2008.03.025.

Bowmaker, James K.; Hunt, David M. (2006): Evolution of vertebrate visual pigments. In *Current biology : CB* 16 (13), R484-9. DOI: 10.1016/j.cub.2006.06.016.

Cameron, David A. (2002): Mapping absorbance spectra, cone fractions, and neuronal mechanisms to photopic spectral sensitivity in the zebrafish. In *Vis. Neurosci.* 19 (03), pp. 365–372. DOI: 10.1017/S0952523802192121.

Campbell, Neil A.; Reece, Jane B. (2015): Biology. A global approach. 10th edition, global edition. Boston: Pearson.

Choi, Sue-Yeon; Borghuis, Bart G.; Borghuis, Bart; Rea, Ruth; Levitan, Edwin S.; Sterling, Peter; Kramer, Richard H. (2005): Encoding light intensity by the cone photoreceptor synapse. In *Neuron* 48 (4), pp. 555–562. DOI: 10.1016/j.neuron.2005.09.011.

Collin, Shaun P.; Davies, Wayne L.; Hart, Nathan S.; Hunt, David M. (2009): The evolution of

early vertebrate photoreceptors. In *Philosophical transactions of the Royal Society of London. Series B, Biological sciences* 364 (1531), pp. 2925–2940. DOI: 10.1098/rstb.2009.0099.

Collin, Shaun P.; Knight, Maree A.; Davies, Wayne L.; Potter, Ian C.; Hunt, David M.; Trezise, Ann E.O. (2003): Ancient colour vision. Multiple opsin genes in the ancestral vertebrates. In *Current Biology* 13 (22), R864-R865. DOI: 10.1016/j.cub.2003.10.044.

Connaughton, V. P.; Graham, D.; Nelson, R. (2004): Identification and morphological classification of horizontal, bipolar, and amacrine cells within the zebrafish retina. In *The Journal of comparative neurology* 477 (4), pp. 371–385. DOI: 10.1002/cne.20261.

Crow, Karen D.; Wagner, Günter P. (2006): Proceedings of the SMBE Tri-National Young Investigators' Workshop 2005. What is the role of genome duplication in the evolution of complexity and diversity? In *Molecular biology and evolution* 23 (5), pp. 887–892. DOI: 10.1093/molbev/msj083.

Delarbre, Christiane; Gallut, Cyril; Barriel, Veronique; Janvier, Philippe; Gachelin, Gabriel (2002): Complete mitochondrial DNA of the hagfish, Eptatretus burgeri: the comparative analysis of mitochondrial DNA sequences strongly supports the cyclostome monophyly. In *Molecular phylogenetics and evolution* 22 (2), pp. 184–192. DOI: 10.1006/mpev.2001.1045.

Delsuc, Frédéric; Brinkmann, Henner; Chourrout, Daniel; Philippe, Hervé (2006): Tunicates and not cephalochordates are the closest living relatives of vertebrates. In *Nature* 439 (7079), pp. 965–968. DOI: 10.1038/nature04336.

Demb, Jonathan B.; Singer, Joshua H. (2012): Intrinsic properties and functional circuitry of the AII amacrine cell. In *Visual neuroscience* 29 (1), pp. 51–60. DOI: 10.1017/S0952523811000368.

Dickson, D.Howard; Graves, Debra A. (1979): Fine structure of the lamprey photoreceptors and retinal pigment epithelium (Petromyzon marinus L.). In *Experimental Eye Research* 29 (1), pp. 45–60. DOI: 10.1016/0014-4835(79)90165-9.

Eliasof, S.; Arriza, J. L.; Leighton, B. H.; Kavanaugh, M. P.; Amara, S. G. (1998): Excitatory amino acid transporters of the salamander retina. Identification, localization, and function. In *The Journal of neuroscience* 18 (2), pp. 698–712.

Endeman, Duco; Klaassen, Lauw J.; Kamermans, Maarten (2013): Action spectra of zebrafish cone photoreceptors. In *PloS one* 8 (7), e68540. DOI: 10.1371/journal.pone.0068540.

Erkens, Guus B.; Hänelt, Inga; Goudsmits, Joris M. H.; Slotboom, Dirk Jan; van Oijen, Antoine M. (2013): Unsynchronised subunit motion in single trimeric sodium-coupled aspartate transporters. In *Nature* 502 (7469), pp. 119–123. DOI: 10.1038/nature12538.

Erwin, Douglas H.; Laflamme, Marc; Tweedt, Sarah M.; Sperling, Erik A.; Pisani, Davide; Peterson, Kevin J. (2011): The Cambrian conundrum: early divergence and later ecological success in the early history of animals. In *Science (New York, N.Y.)* 334 (6059), pp. 1091–1097. DOI: 10.1126/science.1206375.

Euler, Thomas; Haverkamp, Silke; Schubert, Timm; Baden, Tom (2014): Retinal bipolar cells. Elementary building blocks of vision. In *Nat Rev Neurosci* 15 (8), pp. 507–519. DOI: 10.1038/nrn3783.

Fahlke, Christoph; Kortzak, Daniel; Machtens, Jan-Philipp (2016): Molecular physiology of

EAAT anion channels. In *Pflugers Archiv : European journal of physiology* 468 (3), pp. 491–502. DOI: 10.1007/s00424-015-1768-3.

Fairman, W. A.; Vandenberg, R. J.; Arriza, J. L.; Kavanaugh, M. P.; Amara, S. G. (1995): An excitatory amino-acid transporter with properties of a ligand-gated chloride channel. In *Nature* 375 (6532), pp. 599–603. DOI: 10.1038/375599a0.

Fernholm, Bo; Holmberg, Kaj (1975): The eyes in three genera of hagfish (Eptatretus, paramyxine andMyxine)—A case of degenerative evolution. In *Vision Research* 15 (2), 253-IN4. DOI: 10.1016/0042-6989(75)90215-1.

Fritzsch, Bernd; Collin, Shaun P. (1990): Dendritic distribution of two populations of ganglion cells and the retinopetal fibers in the retina of the silver lamprey (Ichthyomyzon unicuspis). In *Vis Neurosci* 4 (06), pp. 533–545. DOI: 10.1017/S0952523800005745.

Gesemann, Matthias; Lesslauer, Annegret; Maurer, Colette M.; Schönthaler, Helia B.; Neuhauss, Stephan C. F. (2010): Phylogenetic analysis of the vertebrate excitatory/neutral amino acid transporter (SLC1/EAAT) family reveals lineage specific subfamilies. In *BMC evolutionary biology* 10, p. 117. DOI: 10.1186/1471-2148-10-117.

Glasauer, Stella M. K.; Neuhauss, Stephan C. F. (2014): Whole-genome duplication in teleost fishes and its evolutionary consequences. In *Molecular genetics and genomics : MGG* 289 (6), pp. 1045–1060. DOI: 10.1007/s00438-014-0889-2.

Grunewald, M.; Kanner, B. I. (2000): The accessibility of a novel reentrant loop of the glutamate transporter GLT-1 is restricted by its substrate. In *The Journal of biological chemistry* 275 (13), pp. 9684–9689.

Hattar, S.; Liao, H. W.; Takao, M.; Berson, D. M.; Yau, K. W. (2002): Melanopsin-containing retinal ganglion cells: architecture, projections, and intrinsic photosensitivity. In *Science (New York, N.Y.)* 295 (5557), pp. 1065–1070. DOI: 10.1126/science.1069609.

Hattar, Samer; Kumar, Monica; Park, Alexander; Tong, Patrick; Tung, Jonathan; Yau, King-Wai; Berson, David M. (2006): Central projections of melanopsin-expressing retinal ganglion cells in the mouse. In *The Journal of comparative neurology* 497 (3), pp. 326–349. DOI: 10.1002/cne.20970.

Heesy, Christopher P.; Hall, Margaret I. (2010): The nocturnal bottleneck and the evolution of mammalian vision. In *Brain, behavior and evolution* 75 (3), pp. 195–203. DOI: 10.1159/000314278.

Heimberg, Alysha M.; Cowper-Sal-lari, Richard; Sémon, Marie; Donoghue, Philip C. J.; Peterson, Kevin J. (2010): microRNAs reveal the interrelationships of hagfish, lampreys, and gnathostomes and the nature of the ancestral vertebrate. In *Proceedings of the National Academy of Sciences of the United States of America* 107 (45), pp. 19379–19383. DOI: 10.1073/pnas.1010350107.

Holmberg, K. (1970): The hagfish retina. Fine structure of retinal cells in Myxine glutinosa, L., with special reference to receptor and epithelial cells. In *Zeitschrift fur Zellforschung und mikroskopische Anatomie (Vienna, Austria : 1948)* 111 (4), pp. 519–538.

Holmberg, Kaj (1971): The hagfish retina. Electron microscopic study comparing receptor and epithelial cells in the pacific hagfish, Polistotrema stouti, with those in the atlantic hagfish, Myxine glutinosa. In *Z. Zellforsch.* 121 (2), pp. 249–269. DOI: 10.1007/BF00340676.

Holmberg, Kaj (1977): The cyclostome retina. In : The visual system in vertebrates: Springer, pp. 47–66.

Hunt, David M.; Peichl, Leo (2014): S cones: Evolution, retinal distribution, development, and spectral sensitivity. In *Visual neuroscience* 31 (2), pp. 115–138. DOI: 10.1017/S0952523813000242.

Ishikawa, Makoto; Takao, Masashi; Washioka, Hiroshi; Tokunaga, Fumio; Watanabe, Hiroshi; Tonosaki, Akira (1987): Demonstration of rod and cone photoreceptors in the lamprey retina by freeze-replication and immunofluorescence. In *Z. Zellforsch.* 249 (2). DOI: 10.1007/BF00215506.

Jacobs, Gerald H. (2013): Losses of functional opsin genes, short-wavelength cone photopigments, and color vision--a significant trend in the evolution of mammalian vision. In *Visual neuroscience* 30 (1-2), pp. 39–53. DOI: 10.1017/S0952523812000429.

Ji, Yurui; Postis, Vincent L. G.; Wang, Yingying; Bartlam, Mark; Goldman, Adrian (2016): Transport mechanism of a glutamate transporter homolog GltPh. In *Biochemical Society transactions* 44 (3), pp. 898–904. DOI: 10.1042/BST20160055.

Jusuf, Patricia R.; Harris, William A. (2009): Ptf1a is expressed transiently in all types of amacrine cells in the embryonic zebrafish retina. In *Neural development* 4, p. 34. DOI: 10.1186/1749-8104-4-34.

Kamermans, M.; Spekreijse, H. (1999): The feedback pathway from horizontal cells to cones. In *Vision Research* 39 (15), pp. 2449–2468. DOI: 10.1016/S0042-6989(99)00043-7.

Kanai, Yoshikatsu; Clémençon, Benjamin; Simonin, Alexandre; Leuenberger, Michele; Lochner, Martin; Weisstanner, Martin; Hediger, Matthias A. (2013): The SLC1 high-affinity glutamate and neutral amino acid transporter family. In *Molecular aspects of medicine* 34 (2-3), pp. 108–120. DOI: 10.1016/j.mam.2013.01.001.

Kanai, Yoshikatsu; Hediger, Matthias A. (2004): The glutamate/neutral amino acid transporter family SLC1: molecular, physiological and pharmacological aspects. In *Pflugers Archiv : European journal of physiology* 447 (5), pp. 469–479. DOI: 10.1007/s00424-003-1146-4.

Kim, Jung-Woong; Yang, Hyun-Jin; Oel, Adam Phillip; Brooks, Matthew John; Jia, Li; Plachetzki, David Charles et al. (2016): Recruitment of Rod Photoreceptors from Short-Wavelength-Sensitive Cones during the Evolution of Nocturnal Vision in Mammals. In *Developmental cell* 37 (6), pp. 520–532. DOI: 10.1016/j.devcel.2016.05.023.

Kobayashi, Hiroshi (1964): On the photo-perceptive function in the eye of the hagfish, Myxine garmani Jordan et Snyder. In *J Natl Fish Univ* 13, pp. 67–83.

Kojima, Keiichi; Yamashita, Takahiro; Imamoto, Yasushi; Kusakabe, Takehiro G.; Tsuda, Motoyuki; Shichida, Yoshinori (2017): Evolutionary steps involving counterion displacement in a tunicate opsin. In *Proceedings of the National Academy of Sciences of the United States of America* 114 (23), pp. 6028–6033. DOI: 10.1073/pnas.1701088114.

Kourakis, Matthew J.; Smith, William C. (2015): An organismal perspective on C. intestinalis development, origins and diversification. In *eLife* 4. DOI: 10.7554/eLife.06024.

Kusakabe, T.; Kusakabe, R.; Kawakami, I.; Satou, Y.; Satoh, N.; Tsuda, M. (2001): Ci-opsin1, a vertebrate-type opsin gene, expressed in the larval ocellus of the ascidian Ciona intestinalis. In

FEBS letters 506 (1), pp. 69–72.

Kusakabe, Takehiro; Tsuda, Motoyuki (2007): Photoreceptive systems in ascidians. In *Photochemistry and photobiology* 83 (2), pp. 248–252. DOI: 10.1562/2006-07-11-IR-965.

Kusunoki, Toyokazu; Amemiya, Fumiaki (1983): Retinal projections in the hagfish, Eptatretus burgeri. In *Brain Research* 262 (2), pp. 295–298. DOI: 10.1016/0006-8993(83)91021-1.

Lacalli, Thurston C. (2004): Sensory systems in amphioxus: a window on the ancestral chordate condition. In *Brain, behavior and evolution* 64 (3), pp. 148–162. DOI: 10.1159/000079744.

Lacalli, Thurston C.; Kelly, Samantha J. (2000): The infundibular balance organ in amphioxus larvae and related aspects of cerebral vesicle organization. In *Acta Zoologica* 81 (1), pp. 37–47. DOI: 10.1046/j.1463-6395.2000.00036.x.

Lamb, Trevor D. (2013): Evolution of phototransduction, vertebrate photoreceptors and retina. In *Progress in retinal and eye research* 36, pp. 52–119. DOI: 10.1016/j.preteyeres.2013.06.001.

Lamb, Trevor D.; Collin, Shaun P.; Pugh, Edward N. (2007): Evolution of the vertebrate eye: opsins, photoreceptors, retina and eye cup. In *Nature reviews. Neuroscience* 8 (12), pp. 960–976. DOI: 10.1038/nrn2283.

Lamb, Trevor D.; Pugh, Edward N.; Collin, Shaun P. (2008): The Origin of the Vertebrate Eye. In *Evo Edu Outreach* 1 (4), pp. 415–426. DOI: 10.1007/s12052-008-0091-2.

Leventhal, A. G.; Rodieck, R. W.; Dreher, B. (1985): Central projections of cat retinal ganglion cells. In *The Journal of comparative neurology* 237 (2), pp. 216–226. DOI: 10.1002/cne.902370206.

Locket, N. Adam; Jørgensen, Jørgen Mørup (1998): The eyes of hagfishes. In : The biology of hagfishes: Springer, pp. 541–556.

Machtens, Jan-Philipp; Kortzak, Daniel; Lansche, Christine; Leinenweber, Ariane; Kilian, Petra; Begemann, Birgit et al. (2015): Mechanisms of anion conduction by coupled glutamate transporters. In *Cell* 160 (3), pp. 542–553. DOI: 10.1016/j.cell.2014.12.035.

Mangrum, Wells I.; Dowling, John E.; Cohen, Ethan D. (2002): A morphological classification of ganglion cells in the zebrafish retina. In *Vis Neurosci* 19 (06), pp. 767–779. DOI: 10.1017/S0952523802196076.

Masland, Richard H. (2012a): The neuronal organization of the retina. In *Neuron* 76 (2), pp. 266–280. DOI: 10.1016/j.neuron.2012.10.002.

Masland, Richard H. (2012b): The tasks of amacrine cells. In *Vis Neurosci* 29 (01), pp. 3–9. DOI: 10.1017/S0952523811000344.

Morshedian, Ala; Fain, Gordon L. (2015): Single-photon sensitivity of lamprey rods with cone-like outer segments. In *Current biology : CB* 25 (4), pp. 484–487. DOI: 10.1016/j.cub.2014.12.031.

Morshedian, Ala; Fain, Gordon L. (2017): The evolution of rod photoreceptors. In *Philosophical transactions of the Royal Society of London. Series B, Biological sciences* 372 (1717). DOI: 10.1098/rstb.2016.0074.

Nagao, S.; Kwak, S.; Kanazawa, I. (1997): EAAT4, a glutamate transporter with properties of a chloride channel, is predominantly localized in Purkinje cell dendrites, and forms parasagittal

compartments in rat cerebellum. In *Neuroscience* 78 (4), pp. 929–933.

Ng, Lily; Lu, Ailing; Swaroop, Alok; Sharlin, David S.; Swaroop, Anand; Forrest, Douglas (2011): Two transcription factors can direct three photoreceptor outcomes from rod precursor cells in mouse retinal development. In *The Journal of neuroscience* 31 (31), pp. 11118–11125. DOI: 10.1523/JNEUROSCI.1709-11.2011.

Nothmann, Doreen; Leinenweber, Ariane; Torres-Salazar, Delany; Kovermann, Peter; Hotzy, Jasmin; Gameiro, Armanda et al. (2011): Hetero-oligomerization of neuronal glutamate transporters. In *The Journal of biological chemistry* 286 (5), pp. 3935–3943. DOI: 10.1074/jbc.M110.187492.

Oisi, Yasuhiro; Ota, Kinya G.; Kuraku, Shigehiro; Fujimoto, Satoko; Kuratani, Shigeru (2013): Craniofacial development of hagfishes and the evolution of vertebrates. In *Nature* 493 (7431), pp. 175–180. DOI: 10.1038/nature11794.

Okano, T.; Kojima, D.; Fukada, Y.; Shichida, Y.; Yoshizawa, T. (1992): Primary structures of chicken cone visual pigments: vertebrate rhodopsins have evolved out of cone visual pigments. In *Proceedings of the National Academy of Sciences of the United States of America* 89 (13), pp. 5932–5936.

Peghini, P.; Janzen, J.; Stoffel, W. (1997): Glutamate transporter EAAC-1-deficient mice develop dicarboxylic aminoaciduria and behavioral abnormalities but no neurodegeneration. In *The EMBO journal* 16 (13), pp. 3822–3832. DOI: 10.1093/emboj/16.13.3822.

Perkins, Emma; Suminaite, Daumante; Jackson, Mandy (2016): Cerebellar ataxias: β-III spectrin's interactions suggest common pathogenic pathways. In *The Journal of physiology* 594 (16), pp. 4661–4676. DOI: 10.1113/JP271195.

Pow, D. V.; Barnett, N. L. (2000): Developmental expression of excitatory amino acid transporter 5. A photoreceptor and bipolar cell glutamate transporter in rat retina. In *Neuroscience letters* 280 (1), pp. 21–24.

Putnam, Nicholas H.; Butts, Thomas; Ferrier, David E. K.; Furlong, Rebecca F.; Hellsten, Uffe; Kawashima, Takeshi et al. (2008): The amphioxus genome and the evolution of the chordate karyotype. In *Nature* 453 (7198), pp. 1064–1071. DOI: 10.1038/nature06967.

Reyes, Nicolas; Ginter, Christopher; Boudker, Olga (2009): Transport mechanism of a bacterial homolog of glutamate transporters. In *Nature* 462 (7275), pp. 880–885. DOI: 10.1038/nature08616.

Robles, Estuardo; Laurell, Eva; Baier, Herwig (2014): The retinal projectome reveals brain-area-specific visual representations generated by ganglion cell diversity. In *Current biology : CB* 24 (18), pp. 2085–2096. DOI: 10.1016/j.cub.2014.07.080.

Rothstein, Jeffrey D.; Dykes-Hoberg, Margaret; Pardo, Carlos A.; Bristol, Lynn A.; Jin, Lin; Kuncl, Ralph W. et al. (1996): Knockout of Glutamate Transporters Reveals a Major Role for Astroglial Transport in Excitotoxicity and Clearance of Glutamate. In *Neuron* 16 (3), pp. 675–686. DOI: 10.1016/S0896-6273(00)80086-0.

Rothstein, Jeffrey D.; Martin, Lee; Levey, Allan I.; Dykes-Hoberg, Margaret; Jin, Lin; Wu, David et al. (1994): Localization of neuronal and glial glutamate transporters. In *Neuron* 13 (3), pp. 713–725. DOI: 10.1016/0896-6273(94)90038-8.

Rubinson, Kalman; Cain, Hilary (1989): Neural differentiation in the retina of the larval sea lamprey (Petromyzon marinus). In *Vis Neurosci* 3 (03), pp. 241–248. DOI: 10.1017/S0952523800009998.

Ryan, Renae M.; Vandenberg, Robert J. (2002): Distinct conformational states mediate the transport and anion channel properties of the glutamate transporter EAAT-1. In *The Journal of biological chemistry* 277 (16), pp. 13494–13500. DOI: 10.1074/jbc.M109970200.

Ryan, Renae M.; Vandenberg, Robert J. (2005): A channel in a transporter. In *Clinical and experimental pharmacology & physiology* 32 (1-2), pp. 1–6. DOI: 10.1111/j.1440-1681.2005.04164.x.

Seal, R. P.; Shigeri, Y.; Eliasof, S.; Leighton, B. H.; Amara, S. G. (2001): Sulfhydryl modification of V449C in the glutamate transporter EAAT1 abolishes substrate transport but not the substrate-gated anion conductance. In *Proceedings of the National Academy of Sciences of the United States of America* 98 (26), pp. 15324–15329. DOI: 10.1073/pnas.011400198.

Shichida, Yoshinori; Matsuyama, Take (2009): Evolution of opsins and phototransduction. In *Philosophical transactions of the Royal Society of London. Series B, Biological sciences* 364 (1531), pp. 2881–2895. DOI: 10.1098/rstb.2009.0051.

Slotboom, D. J.; Lolkema, J. S.; Konings, W. N. (1996): Membrane topology of the C-terminal half of the neuronal, glial, and bacterial glutamate transporter family. In *The Journal of biological chemistry* 271 (49), pp. 31317–31321.

Stellwag, Edmund J. (2004): Are genome evolution, organism complexity and species diversity linked? In *Integrative and comparative biology* 44 (5), pp. 358–365. DOI: 10.1093/icb/44.5.358.

Stenkamp, Deborah L. (2011): The rod photoreceptor lineage of teleost fish. In *Progress in retinal and eye research* 30 (6), pp. 395–404. DOI: 10.1016/j.preteyeres.2011.06.004.

Stock, D.; Whitt, G. (1992): Evidence from 18S ribosomal RNA sequences that lampreys and hagfishes form a natural group. In *Science* 257 (5071), pp. 787–789. DOI: 10.1126/science.1496398.

Tanaka, K. (1997): Epilepsy and Exacerbation of Brain Injury in Mice Lacking the Glutamate Transporter GLT-1. In *Science* 276 (5319), pp. 1699–1702. DOI: 10.1126/science.276.5319.1699.

Thoreson, Wallace B. (2007): Kinetics of synaptic transmission at ribbon synapses of rods and cones. In *Molecular neurobiology* 36 (3), pp. 205–223. DOI: 10.1007/s12035-007-0019-9.

Thoreson, Wallace B.; Mangel, Stuart C. (2012): Lateral interactions in the outer retina. In *Progress in retinal and eye research* 31 (5), pp. 407–441. DOI: 10.1016/j.preteyeres.2012.04.003.

Tse, Dennis Y.; Chung, Inyoung; Wu, Samuel M. (2014): Possible roles of glutamate transporter EAAT5 in mouse cone depolarizing bipolar cell light responses. In *Vision Research* 103, pp. 63–74. DOI: 10.1016/j.visres.2014.06.005.

Vandenberg, Robert J.; Ryan, Renae M. (2013): Mechanisms of glutamate transport. In *Physiological reviews* 93 (4), pp. 1621–1657. DOI: 10.1152/physrev.00007.2013.

Verdon, Grégory; Oh, SeCheol; Serio, Ryan N.; Boudker, Olga (2014): Coupled ion binding and structural transitions along the transport cycle of glutamate transporters. In *eLife* 3, e02283. DOI: 10.7554/eLife.02283.

Vopalensky, Pavel; Pergner, Jiri; Liegertova, Michaela; Benito-Gutierrez, Elia; Arendt, Detlev;

Kozmik, Zbynek (2012): Molecular analysis of the amphioxus frontal eye unravels the evolutionary origin of the retina and pigment cells of the vertebrate eye. In *Proceedings of the National Academy of Sciences of the United States of America* 109 (38), pp. 15383–15388. DOI: 10.1073/pnas.1207580109.

Wadiche, J. I.; Kavanaugh, M. P. (1998): Macroscopic and microscopic properties of a cloned glutamate transporter/chloride channel. In *The Journal of neuroscience* 18 (19), pp. 7650–7661.

Wadiche, Jacques I.; Amara, Susan G.; Kavanaugh, Michael P. (1995): Ion fluxes associated with excitatory amino acid transport. In *Neuron* 15 (3), pp. 721–728. DOI: 10.1016/0896-6273(95)90159-0.

Watanabe, Takemi; Morimoto, Kiyoshi; Hirao, Toru; Suwaki, Hiroshi; Watase, Kei; Tanaka, Kohi chi (2000): Amygdala-Kindling and Pentylenetetrazole-Induced Seizures in Glutamate Transporter GLAST-Deficient Mice. In *Epilepsia* 41 (s9), pp. 49–50. DOI: 10.1111/j.1528-1157.2000.tb02222.x.

Wersinger, Eric; Schwab, Yannick; Sahel, José-Alain; Rendon, Alvaro; Pow, David V.; Picaud, Serge; Roux, Michel J. (2006): The glutamate transporter EAAT5 works as a presynaptic receptor in mouse rod bipolar cells. In *The Journal of physiology* 577 (Pt 1), pp. 221–234. DOI: 10.1113/jphysiol.2006.118281.

Yau, King-Wai; Hardie, Roger C. (2009): Phototransduction motifs and variations. In *Cell* 139 (2), pp. 246–264. DOI: 10.1016/j.cell.2009.09.029.

Yernool, Dinesh; Boudker, Olga; Jin, Yan; Gouaux, Eric (2004): Structure of a glutamate transporter homolog from Pyrococcus horikoshii. In *Nature* 431 (7010), pp. 811–818. DOI: 10.1038/nature03018.

Zerangue, N.; Kavanaugh, M. P. (1996a): ASCT-1 is a neutral amino acid exchanger with chloride channel activity. In *The Journal of biological chemistry* 271 (45), pp. 27991–27994.

Zerangue, N.; Kavanaugh, M. P. (1996b): Interaction of L-cysteine with a human excitatory amino acid transporter. In *The Journal of physiology* 493 (Pt 2), pp. 419–423.

Chapter 2

Evolutionary Adaptations of EAAT1 and EAAT2 in the Course of Higher Vertebrate Evolution

André Lehnherr[1,2], Peter Kovermann[3], Matthias Gesemann[1], Christoph Fahlke[3], Stephan C.F. Neuhauss[1]

[1] Institute of Molecular Life Sciences, University of Zurich, Winterthurerstrasse 190, 8057 Zürich, Switzerland
[2] Life Science Zürich Graduate Program – Neuroscience, 8057 Zürich, Switzerland
[3] Institute of Complex Systems, Zelluläre Biophysik (ICS-4), Forschungszentrum Jülich, Leo-Brandt-Strasse, 52425 Jülich, Germany

Report on a research project

Personal contribution:
Planning and performing of experiments, preparation of all figures and manuscript

2.1. Abstract

Excitatory amino acid transporters (EAATs) are crucial for terminating excitatory glutamatergic synaptic signals by removing glutamate out of the synapse against its electrochemical gradient. Besides glutamate transport, an anion conductance that can regulate neuronal excitability has been described for EAAT proteins. While EAATs expressed in glia cells are thought to mainly take up glutamate, neuronal expressed EAATs are expected to exhibit larger anion conductance. In this study, we focus on EAAT1 (GLAST) and EAAT2 (GLT-1) that are mainly expressed in glial cells. Due to an additional teleost-specific whole genome duplication, two paralogs for EAAT1 and EAAT2 are found in zebrafish. Using expression analysis, electrophysiological recordings and ancestral reconstruction of EAAT sequences, we show that duplicated genes adapted their expression and biophysical properties accordingly and define potential amino acid substitutions necessary for such changes. Further we show that EAAT1 and EAAT2 functions seem to be interchangeable in mice and therefore expression patterns could switch without any evolutionary necessity.

2.2. Introduction

Glutamate is the main excitatory neurotransmitter in the central nervous system. Proper clearance of glutamate from the synaptic cleft is therefore essential to shape and terminate excitatory signaling as well as to prevent excitotoxicity. EAATs are responsible for glutamate clearance from synapses. Several diseases, such as schizophrenia, amyloid lateral sclerosis or epilepsy have been associated with EAAT malfunctioning (Amara, Fontana 2002; Medrano et al. 2013; Ohnuma et al. 1998; Tanaka 1997; Yi, Hazell 2006). EAAT genes belong together with neutral amino acid transporters to the Solute Carrier Family 1 (SLC1) gene family (Gesemann et al. 2010; Kanai, Hediger 2004).

EAATs transport glutamate against its electrochemical gradient. This is achieved by the co-transport of three sodium ions and one proton and the simultaneous counter-transport of one potassium ion. Besides glutamate transport, a thermodynamically uncoupled chloride conductance was reported for EAATs (Wadiche et al. 1995; Wadiche, Kavanaugh 1998; Zerangue, Kavanaugh 1996). The opening probability of the chloride pore is increased during glutamate transport cycles due to associated movements of the transport domain (Boudker et al. 2007; Reyes et al. 2009; Machtens et al. 2015). Glutamate affinities, as well as anion conductance vary remarkably between different EAATs (Wadiche et al. 1995; Arriza et al. 1997). While EAAT1 and EAAT2 are mainly expressed in glia cells in the brain and exhibit low anion conductance, EAAT3, EAAT4 and EAAT5 are mainly expressed in neuronal cells, exhibiting larger anion conductance (reviewd by Rose et al. 2016).

EAAT genes form homotrimers where each subunit is built by seven transmembrane domains (TM) and two re-entering hairpin loops (HP). Since the first description of the protein structure of the archaeal glutamate transporter homologue Glt_{Ph}, transport mechanisms and associated protein structures have as well been intensively studied for EAATs. Glutamate and coupled ion transport involve binding to HP1 and translocation of HP1 and HP2 allows glutamate transport against its electrochemical gradient. However, it was found that none of these conformational changes would allow the opening of an anion-selective pore of the transporter. Only recently, molecular dynamics simulations revealed that in presence of membrane voltage a movement of the transport domain happens that allows the anion-pore to open for short periods (Rose et al. 2016; Machtens et al. 2015).

The phylogeny of vertebrate EAAT genes has been thoroughly studied (Gesemann et al. 2010). While amphibians harbor nine SLC1 genes, mammals only contain seven SLC1 genes, namely five EAAT and two neutral amino acid transporter genes. Due to an additional round of whole genome duplication in the teleost lineage, additional paralogs yield 13 SLC1 genes in zebrafish, 11 of them coding for EAATs. The most common fate of paralogous genes after whole genome duplications (also referred to as ohnologs) is functional inactivation (non-functionalization) due to the release of selective pressure (reviewed by Glasauer, Neuhauss 2014). In the case of the SLC1 gene family, ohnologs have been overproportionally retained arguing for them being under positive selective pressure. Therefore, an evolutionary advantage, resulting from either sub-functionalization or neo-functionalization events, must result in keeping those duplicates.

In this study, we take advantage of different approaches to study the fate of duplicated genes and trace their evolutionary history. We performed expression analyses of EAAT1 and EAAT2 genes in different vertebrate species and compare their expression patterns in the conserved anatomical structure of the retina. Subsequent description of biophysical properties of the transporters by electrophysiological recordings give insights into evolutionary adaptations of duplicated genes as well as into possible discovery of new sites with important roles in anion conductance and glutamate affinity. We find higher proportion of anion conductance in the zebrafish EAAT1b and EAAT2b proteins compared to their respective paralogs. While in both cases none of the known amino acid residues that are important for higher anion conductance are altered, we describe several candidate amino acid residues that could lead to these differences. To our surprise we found that expression of EAAT1 and EAAT2 in mice retina is not consistent with other investigated vertebrate species. Furthermore, biophysical properties of the two EAAT homologues indicate functional redundancy.

2.3. Methods

2.3.1. Zebrafish husbandry

Zebrafish were kept at 26°C under a 14h/10h dark/light cycle. Breeding and raising was done as previously described (Mullins et al. 1994).

2.3.2. Reconstruction of ancestral EAATs, estimation of evolutionary rates and alignment

cDNA sequences for *eaat* genes were published before (Gesemann et al. 2010). For reconstruction of the ancestral sequences of the ancestor of the zebrafish or the common ancestor of mice, chicken, anole lizard and *Xenopus tropicalis eaat1* or *eaat2* genes MEGA7 software package (Kumar et al. 2016) was used. Sequences were aligned using MUSCLE (Edgar 2004) and ancestral sequences were calculated via a maximum likelihood phylogeny using the Jones-Taylor-Thornton substitution model (Jones et al. 1992) and assuming eight discrete gamma categories. More species sequences were included for calculation of the relative evolutionary rate. The relative evolutionary rate was calculated using MEGA7 software package (Kumar et al. 2016).

CLC Main Work Bench (Qiagen) software was used for the graphical alignment and representations were arranged in Corel Draw.

2.3.3. Cloning of EAAT-1 and EAAT-2 and heterologous expression in tsA201 cells

Total RNA was isolated from brains and eyes of zebrafish, *Xenopus tropicalis*, anole lizard,

chicken and mice using Reliaprep RNA tissue miniprep kit (Promega) and cDNA was transcribed with SuperScript III First-Strand Synthesis kit (Invitrogen).

Full length expression constructs were PCR amplified using gene specific primer pairs (Table 2) with Phusion High-Fidelity DNA Polymerase (ThermoFisher Scientific) introducing restriction sites for cloning into pRcCMV vector with an N-terminal YFP tag.

tsA201 cells (Sigma Aldrich) were cultured in DMEM medium containing 10% FCS (Gibco) at 37°C and 10% CO_2. Transient transfection of tsA201 cells was performed using $Ca_3(PO_4)_2$ transfection method as previously described elsewhere (Leinenweber et al. 2011). Two days after transfection, cells showing fluorescence in the membrane, were used for electrophysiological experiments.

For In situ hybridization, fragments of around 900bp were PCR amplified using gene specific primer and Qiagen Fast Cycling PCR kit (Qiagen) (Table 3). PCR products were subsequently ligated into TOPO PCRII vector (Invitrogen).

2.3.4. *In situ* hybridization

Digoxigenin-labelled (DIG) RNA *in situ* hybridization probes were synthesized as described before (Niklaus et al. 2017). In brief, plasmids containing fragments of the *eaat* genes were linearized for SP6 or T7 *in vitro* transcription of RNA probes. DIG-RNA probes were transcribed using DIG-RNA-labelling kit (Roche Diagnostics).

Whole-mount in situ hybridization of 3 days post fertilization (dpf) zebrafish larvae or Nieuwkoop and Faber stage (NF; Nieuwkoop, Faber 1994) 40 *Xenopus tropicalis* tadpoles and in situ hybridization on retinal transverse cross-sections were performed as previously described (Huang et al. 2012). Briefly, tissues were fixed in 4% paraformaldehyde (PFA) over night (ON) at 4°C. Before hybridization, the tissue was treated with proteinase K and postfixed in 4%PFA. Hybridization with RNA probes was performed at 65°C ON followed by several stringency washes. The tissue was then blocked in 1x Blocking Solution (Roche Diagnostics) in TNT (100 mM Tris HCl pH 7.5, 150 mM NaCl, 0.5% Tween 20) and anti-DIG conjugated to alkaline phosphatase was diluted 1:5000 in 1x blocking solution in TNT and incubated ON at 4°C. After several washes in TNT, the tissue was stained in staining buffer containing NBT and BCIP (Roche Diagnostics) and staining was stopped in PBT. The stained tissue was then postfixed in 4% PFA before mounting for microscopy. Zebrafish larvae were mounted in Glycerol while *Xenopus* tadpoles were cleared and mounted in BABB. Retinal sections were mounted with Kaiser's Gelatine. No further adaptations were needed for in situ hybridizations of different specie's tissues. Imaging was performed with an Olympus BX61 microscope and Adobe Photoshop and Illustrator were used to process and assemble figures.

2.3.5. Electrophysiology

Standard whole cell patch clamp recordings were performed using a Multiclamp 700b (Molecular Devices) amplifier. Borosilicate glass electrodes were pulled and used with resistances between 2.5 and 7 MΩ. Voltage-errors were reduced by compensation of more than 80% of the series resistance. Recorded currents were filtered at 10 kHz and digitized by a Digidata 1440A (Molecular Devices) digitizer with a sampling rate of 5 kHz. In order to distinguish between glutamate transport currents and anion currents, currents were measured in absence and presence of extracellular anions. Standard external solution contained 140mM $NaNO_3$, 4mM KCl, 2mM $CaCl_2$, 1mM $MgCl_2$, 1mM Glutamate and 5mM HEPES and pH was set to 7.4.

In anion-free solutions, all anions were equimolar replaced by the corresponding gluconate salt and for determining glutamate induced currents, baseline values were measured in the absence of glutamate. In order to avoid an outflux of anions, the intracellular solution contained 110mM KGluconate, 5mM EGTA, 2mM MgGluconate and 10mM HEPES and pH was adjusted to 7.4 with KOH. All experiments were carried out using agar bridges with 3M KCl in 1% Agarose to connect the Ag/AgCl electrode. Liquid junction potential differences were calculated in pClamp 10.3 Molecular Devices) and protocols adjusted accordingly.

Amplitudes of glutamate associated currents were measured at physiological -75mV and anion current amplitudes were measured at +75mV. The ratio between glutamate transport currents and anion currents is used as a measure for the anion permeability of different *eaat* genes.

Currents were analyzed using pClamp 10.3 (Molecular Devices) software and for plots and statistical analysis Prism 7 (GraphPad) was used. Reversal potentials were interpolated by calculating a four-parameter logistic regression.

2.3.6. Pharmacological measurements

To test effects of known EAAT1 and EAAT2 antagonists on the zebrafish orthologs, TFB-TBOA (1μM), UCPH101 (10μM) or WAY21363 (10μM) were applied in bath solutions mentioned before. Effect sizes were calculated from Cohen's coefficients (d_{Co}) and assessed as $d_{Co} < 0.2$ (*no*), $0.2 \leq d_{Co} < 0.5$ (*weak*), $0.5 \leq d_{Co} < 0.8$ (*medial*) and $0.8 \leq d_{Co} < 1.3$ (*large*).

2.4. Results

2.4.1. Expression patterns of EAAT1 and EAAT2

To differentiate between neuronal and glial expression patterns of *eaat1* and *eaat2*, RNA *in situ* hybridization was performed. Retinal sections provide a valid model for comparative expression analysis since its structure as well as its cell types are conserved across all vertebrate species (reviewed by Lamb et al. 2007).

Figure 1: Expression patterns of eaat1 and eaat2 in adult retinal sections (A) of zebrafish, *Xenopus*, anole lizard, chicken and mouse and larval zebrafish and *Xenopus tropicalis* tadpoles (B).
A: In adult retinal sections of *Xenopus*, anole lizards and chicken, *eaat1* shows expression in bipolar cells and photoreceptors. In mouse *eaat1* is expressed in Müller glia cells while no expression of either *eaat1* paralog was found in zebrafish retina.
eaat2a and *eaat2b* show expression in photoreceptors and Müller glia cells in zebrafish. *eaat2a* is stronger expressed in Müller glia cells while *eaat2b* expression is higher in photoreceptors. In *Xenopus*, anole lizards and chicken, *eaat2* is expressed in Müller glia cells and in photoreceptors. The mouse *eaat2* orthologue shows expression on photoreceptors, bipolar and ganglion cells.
Schematic representation of the retina: Dark brown cells: retinal pigment epithelium (RPE), blue and green: rod and cone photoreceptor cells, violet: horizontal cells, red: bipolar cells, orange: Müller glia cells, yellow: amacrine cells, violet: ganglion cells. Scale bar represents 50μm
B: Expression of *eaat1a* in 3dpf zebrafish larvae was observed in neuromast cells of the lateral line organ and in the inner ear while *eaat1b* is expressed in glia cells of the brain. Those expression patterns are consitent with the expression of *eaat1* in *Xenopus* tadpoles.
Both *eaat2* paralogs are expressed in glia cells of the zebrafish brain while in *Xenopus eaat2* is expressed in neuronal cells. Scale bar represents 100 μm.

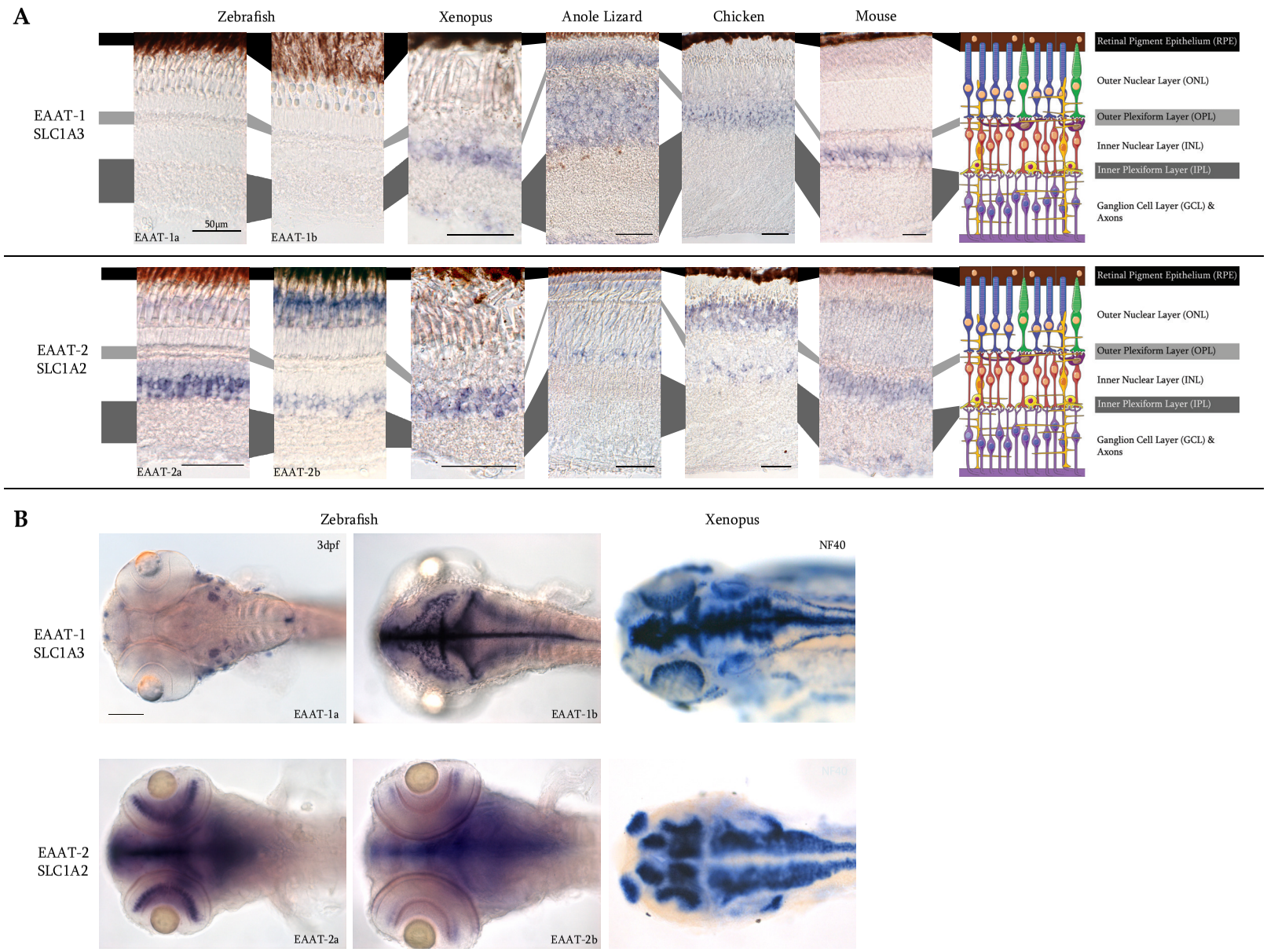
A
Zebrafish
Xenopus
Anole Lizard
Chicken
Mouse
EAAT-1
SLC1A3
50µm
EAAT-1a
EAAT-1b
Retinal Pigment Epithelium (RPE)
Outer Nuclear Layer (ONL)
Outer Plexiform Layer (OPL)
Inner Nuclear Layer (INL)
Inner Plexiform Layer (IPL)
Ganglion Cell Layer (GCL) & Axons
EAAT-2
SLC1A2
EAAT-2a
EAAT-2b
B
Zebrafish
Xenopus
3dpf
NF40
EAAT-1
SLC1A3
EAAT-1a
EAAT-1b
EAAT-2
SLC1A2
EAAT-2a
EAAT-2b

None of the two zebrafish *eaat1* paralogs show expression in the retina, while the *Xenopus*, anole lizard and chicken orthologs are expressed in bipolar cells and photoreceptors in the retina. In contrast, mice *eaat1* is expressed in Müller glia cells (Figure 1A).

Since no expression for *eaat1* was found in zebrafish retina, we further investigated the expression patterns in larval zebrafish and *Xenopus* tadpoles outside of the retina. Here we found *eaat1a* to be expressed in neuromast cells of the lateral line organ and in the inner ear while *eaat1b* shows expression in glia cells of the zebrafish brain. In *Xenopus*, *eaat1* is expressed as well in neuromast cells, the inner ear and in glia cells (Figure 1B).

In line with previous findings, *eaat2a* shows strong expression in Müller glia cells and weaker expression in photoreceptors, while *eaat2b* in turn shows strong expression in photoreceptors and weaker expression in Müller glia cells (Figure 1A, Niklaus et al. 2017). In *Xenopus*, lizards and chicken expression of *eaat2* orthologs was found in Müller glia cells and photoreceptors, but in mice *eaat2* is expressed in photoreceptors, bipolar and ganglion cells. In larval zebrafish, we found both *eaat2* paralogs to be expressed in glia cells of the brain while *Xenopus* tadpoles seem to express *eaat2* only in neuronal tissues (Figure 1B).

Taken together, we found consistent expression of *eaat2* in photoreceptors and Müller glia cells while *eaat1* is expressed in bipolar cells. However, in mice those expression patterns are switched, begging the question if this exchange is also reflected in biophysical properties of these transporters.

2.4.2. Biophysical properties of EAAT1 and EAAT2

After determining the expression patterns of EAAT1 and EAAT2 in retinal sections and embryonic zebrafish and *Xenopus*, we can address possible roles in glutamate clearance and signal transmission. Given the dual functionality of EAAT, we hypothesize that glial transporters are mainly involved in clearance of glutamate, hence sporting large glutamate transport currents while only weakly affecting the membrane potential. Conversely, neuronal EAATs would be expected to influence the membrane potential by a large anion conductance and a smaller glutamate transport capability.

In order to measure the biophysical properties of the various EAATs, we transfected tsA201 cells with YFP-tagged EAAT-constructs. The different constructs varied in their fluorescence intensity as well as subcellular distribution of the fluorescence. While some constructs almost exclusively exhibit fluorescence in the cell membrane, EAAT2 of anole lizards is not at all transported to the cell membrane and accumulates intracellularly (data not shown). Therefore, we cannot directly compare elicited currents of different constructs, but we can calculate the ratio of glutamate transport associated currents and anion currents. Those ratios are by their nature not depending on expression levels allowing comparisons between different constructs.

Figure 2: Current-Voltage relationship plots of EAAT1 and EAAT2 transfected tsA201 cells.
All measured constructs exhibit distinct glutamate transport currents at negative membrane potentials and anion currents at positive membrane potentials. Displayed currents are not corrected for differences in expression of the corresponding EAAT gene and can therefore not be compared directly with each other. EAAT2 of anole lizard could not be measured because the protein aggregated intracellularly.
Blue lines indicate baseline values of transfected cells in the absence of glutamate or anions other than gluconate. Orange lines show glutamate transport induced currents in absence of anions other than gluconate. Gray lines show currents of glutamate transport and NO_3-flux into the cell.
Error bars represent standard error means. Note different scales for current axes.

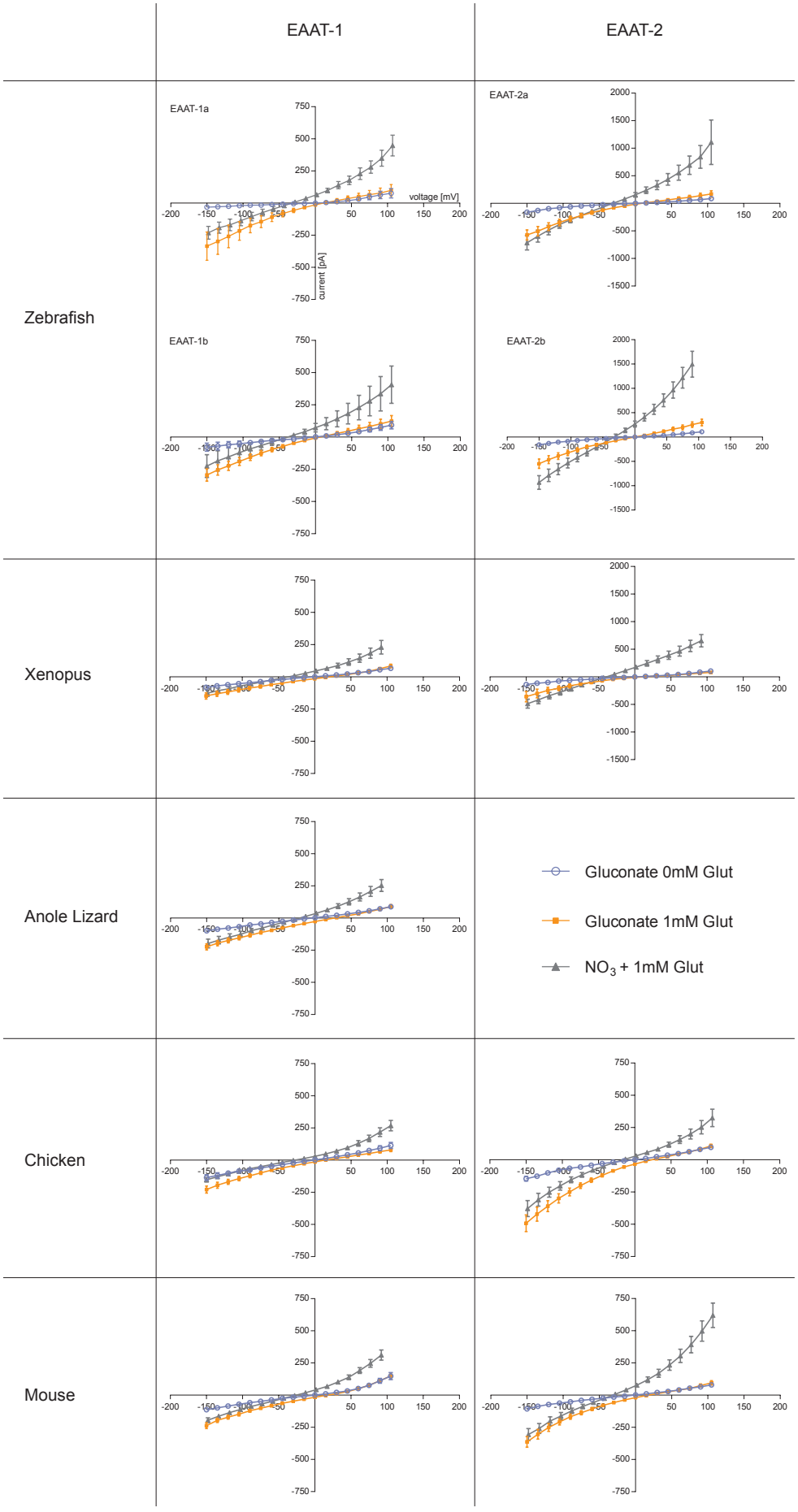
EAAT-1
EAAT-2
Zebrafish
Xenopus
Anole Lizard
Chicken
Mouse
EAAT-1a
EAAT-2a
EAAT-1b
EAAT-2b
voltage [mV]
current [pA]
Gluconate 0mM Glut
Gluconate 1mM Glut
NO3 + 1mM Glut

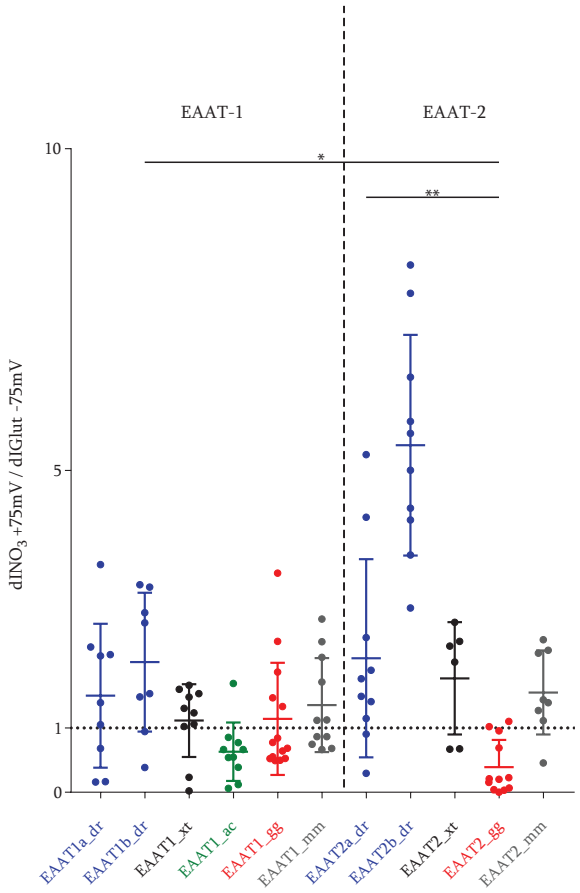

Figure 3: Ratio between anion currents measured at 75mV and glutamate transport currents measured at -75mV.
Amplitudes of glutamate induced currents were measured at a membrane potential of -75mV while NO_3-current amplitudes were measured at +75mV.
All investigated EAAT1 orthologs exhibit statistically indifferent ratios although EAAT1b show a slight increased ratio.
EAAT2 show larger ratios between anion and glutamate transport currents. The chicken EAAT2 orthologue shows significantly less anion currents than EAAT1b and EAAT2a of zebrafish (ANOVA, $p \leq 0.05$ and $p \leq 0.01$ respectively). Note that EAAT2b displays highly significant different transport ratio compared to all other constructs (not shown in figure for clarity, $p \leq 0.0001$). Bars represent the mean and the 95% confidence interval.
dr: *Danio rerio*, zebrafish,; xt: *Xenopus tropicalis*, western clawed frog; ac: *Anolis carolinensis*, american green anole lizard; gg: *Gallus gallus*, Chicken; mm: *Mus musculus*, house mouse.

Glutamate transport associated currents were measured under anion-free conditions where we replaced intra- and extracellular anions by equimolar amounts of gluconate. The anion gluconate is too big to permeate the EAAT anion pore. Under these conditions, application of glutamate solely induces currents elicited by glutamate transport (Figure 2, orange curves). Application of extracellular NO_3^- together with glutamate in turn allowed us to measure anion influx at positive membrane potentials (Figure 2, grey curves). Since we expect the anion permeability to be similar in all EAAT isoforms, we plotted the reversal potential of all measured constructs allowing us to exclude unhealthy or leaky cells from analysis (Figure S1).

Figure 2 shows current-voltage relationship curves for all measured EAAT1 and EAAT2 orthologs. Clearly, all constructs exhibit distinct glutamate transport associated currents as well as anion currents to a variable extent. Although differences in expression levels cannot be taken into account, EAAT2 show in general higher currents compared to EAAT1 and the b-paralogs of zebrafish EAAT1 and EAAT2 exhibit larger anion currents than their corresponding a-paralog. When comparing the ratios between glutamate transport currents and anion currents it becomes obvious that zebrafish EAAT1 and EAAT2 paralogs show adaptations in their biophysical properties according to their expression. While EAAT1a, that is expressed in neuromast cells of the lateral line organ and in the inner ear (Figure 1), show a mean ratio of 1.5 ± 0.37 (n=9), the mean ratio of EAAT1b, that is mainly expressed by glia cells in the brain, is higher (2.02 ± 0.38, n=8). In line with our hypothesis, EAAT2b, that shows higher expression in photoreceptors, shows a significant higher proportion of anion current (5.39 ± 0.54, n=10, $p < 0.0001$) compared to all other investigated constructs and therefore is even highly significantly different from glial-expressed EAAT2a (2.08 ±0.49, n=10, $p < 0.0001$)

(Figure 3). Two transporters, namely the lizard EAAT1 (0.63 ± 0.14, n=10) and chicken EAAT2 (0.39 ± 0.12, n=12) show an average transport ration below 1, meaning that more current is elicited by the glutamate transport than by anion permeation (Figure 3).

2.4.3. Action of EAAT1- and EAAT2-specific blockers on zebrafish orthologs

Several antagonists for specific blocking of different EAAT isoforms have been described. Here we test whether known antagonists for EAAT1 and EAAT2 act similarly on the corresponding zebrafish ortholog.

TFB-TBOA has been described to be a an antagonist for both, EAAT1 and EAAT2 (Shimamoto et al. 2004). UCPH-101 was found to inhibit EAAT1 more than 400 times stronger than other EAAT isoforms and binding sites for the antagonist have been identified (Jensen et al. 2009; Abrahamsen et al. 2013). The most potent specific blocker for EAAT2 known is WAY-213613 (Dunlop et al. 2005).

Figure 4A-D show the effect on current-voltage relationship plots of the tested EAAT1 and EAAT2 antagonists on tsA201 cells that transiently express zebrafish EAAT1 and EAAT2 isoforms. Due to the replacement of intracellular anions with gluconate, only glutamate transport currents are measured at negative membrane potentials and in this way we can distinguish the effects of those antagonists on glutamate transport and anion permeability. In Figure 4D current amplitudes at -150mV are plotted. None of the blockers can reduce the current amplitude significantly. Interestingly WAY213613, an EAAT2 specific antagonist, blocks as well both EAAT1 paralogs while UCPH101 selectively blocks currents only in the zebrafish EAAT1 paralogs. We calculated the ratio of glutamate transport current amplitude or the anion current amplitude respectively before and after application of the blockers and found that WAY-213613 blocks glutamate transport more efficiently than anion conductance for EAAT1a and EAAT1b (Figure S2). Further investigations are needed to proof this since we could only measure from limited number of cells so far. In order to gain more insight into the blocking efficiency, effect size was calculated (Table 1). EAAT1a gets blocked by all investigated antagonists effectively and the effect size is very large for UCPH101 and at positive membrane potentials as well for TFB-TBOA and WAY213613. EAAT1b on the other hand gets blocked by TFB-TBOA and UCPH101 but WAY213613 only shows a medial effect size at negative membrane potentials and no effect at positive membrane potentials. TFB-TBOA and WAY213613 have a medial effect size for both EAAT2a and EAAT2b at positive as well as at negative membrane potentials (Table 1).

	TFB-TBOA				UCPH101				WAY21636			
	-150mV		+105mV		-150mV		+105mV		-150mV		+105mV	
	d	Effect size	*d*	Effect size	*d*	Effect size	*d*	Effect size	*d*	Effect size	*d*	Effect size
EAAT1a	0.726	0.635	**1.164**	**0.503**	**2.124**	**0.728**	**1.508**	**0.602**	0.786	0.366	**1.328**	**0.553**
EAAT1b	0.424	0.207	0.465	0.227	**0.870**	**0.399**	0.257	0.127	*0.161*	*0.080*	*-0.270*	*-0.134*
EAAT2a	0.637	0.304	0.670	0.318	*0.001*	*0.001*	*-0.391*	*-0.192*	0.517	0.250	0.600	0.287
EAAT2b	**0.924**	**0.419**	0.626	0.296	*-1.031*	*-0.458*	*-0.777*	*-0.362*	0.604	0.289	0.305	0.151

Table 1: Effect size and Cohen's d for application of TFB-TBOA, UCPH101 and WAY213613 at negative and positive membrane potential. Bold: dco >0.8 for large effect size, italic: dco <0.2 for no effect.

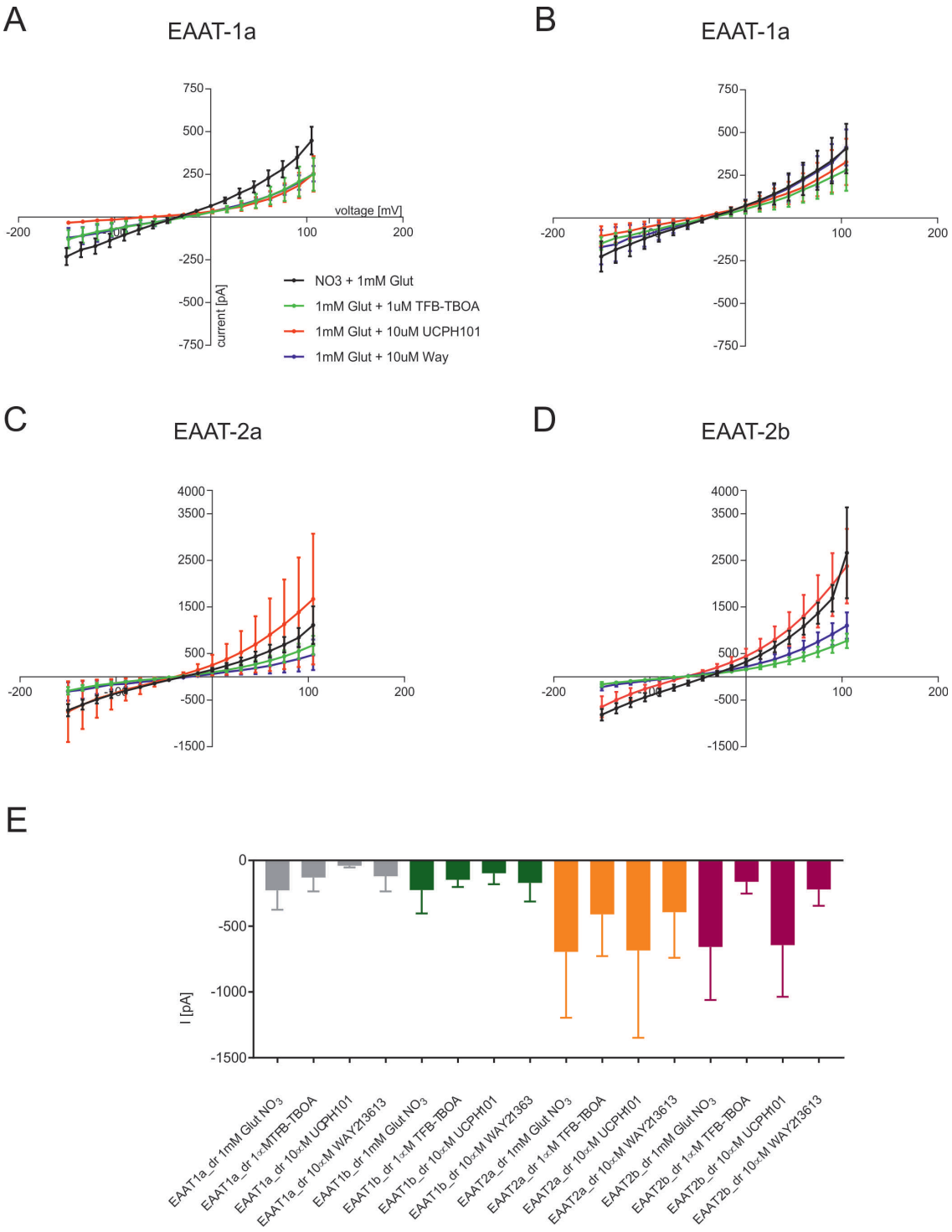

Figure 4: Effects of specific blockers on the zebraish EAAT1 and EAAT2 orthologs.
Current-voltage relationship plots for EAAT1a (A), EAAT1b (B), EAAT2a (C) and EAAT2b (D) from zebrafish. Black lines indicate transport currents induced by application of 1mM glutamate and with extracellular NO_3. Green lines show currents elicited by application of 1µM TFB-TBOA to the solution, red lines represent application of 10µM UCPH101 and blue lines show currents after application of 10µM WAY21313. Dots represent mean of several measures and error bars represent standard error of the mean.
E: Current amplitudes measured at -150mV. No significant differences were found for none of the measured EAATs, but all tested constructs clearly reduce current amplitude of EAAT1a and EAAT1b. No such effect was observed after application of UCPH101 to EAAT2a or EAAT2b. TFB-TBOA and WAY213613 clearly reduce current amplitudes of EAAT2a and EAAT2b. Error bars represent standard deviations.

2.4.4. Specific amino acid changes in duplicated zebrafish genes

The observed differences in expression patterns as well as in biophysical properties between the retained EAAT1 and EAAT2 paralogs in zebrafish raised the interest in potential amino acid changes that could lead to such differences. Reconstructing the common ancestor of the zebrafish genes and the common ancestor of all other investigated vertebrate species might give insight into changes that led to differences between the zebrafish EAAT1 and EAAT2 paralogs (phylogenetic tree used for ancestral reconstruction Figure S3).

Recent studies resolved the protein structure and anion pore-forming residues of EAATs and possible interaction sites for UCPH101 (Abrahamsen et al. 2013; Machtens et al. 2015). Such amino acids are of high interest because changes in those residues may be the basis of different biophysical properties between the zebrafish EAAT1 and EAAT2 paralogs. To our surprise, when we aligned the two zebrafish EAAT1 paralogs with their common ancestor and the ancestor of higher vertebrates, there were neither changes in the known anion pore-forming residues nor in the UCPH101 interaction site (Figure 5). Subsequent calculation of the evolutionary rate revealed several amino acid substitutions of EAAT1b with a low evolutionary rate and are therefore considered as either conserved structural or functional domains (Figure 5, Table S1). Of those, EAAT1b Ile55 and Val59 in the first and Ile284, Ile300 and Ile301 in the fifth transmembrane domain and in the vicinity of known anion pore-forming residues are of special interest. Furthermore, five EAAT1b specific amino acid substitutions with low evolutionary rate were found in TM6 (Met319, Gly322, Tyr328, Val332, Ile333). TM6 is part of the transport domain but facing the cell membrane (Reyes et al. 2009).

Ile53 and Tyr57 in TM1 are valid candidates for substitution of EAAT2b that could possibly lead to a higher anion conductance (Figure 6). Further EAAT2b-specific changes are found in TM4c (Ile225, Val230), in TM5 (Arg259, Ile270, Asn284), and in HP1a (Lys326, Leu330, Val336) (Figure 6). While changes in TM4c as well as in HP1a are more likely to be associated with substrate transport, changes in TM5 could be located in the anion-pore region and therefore modulate anion conductance (Ji et al. 2016; Reyes et al. 2009).

To sum up, several possible candidate substitutions for EAAT1 and EAAT2 that lead to altered anion conductance have been identified. Of special interest are EAAT1b Ile284 and its corresponding position in EAAT2b, Ile270, because it is surrounded by known pore-forming residues. Since both, EAAT1b and EAAT2b show higher proportions of anion conductance compared to glutamate transport currents, this change could play a crucial role in adaptation of anion conductance.

2.5. Discussion

Since the first description of the X-ray crystal structure of the archeal glutamate transporter homologue Glt_{Ph} (Yernool et al. 2004), subsequent reports of amino acid residues important for trimerization and transport have been made for either EAATs or Glt_{Ph} (Reyes et al. 2009; Machtens et al. 2015; Kovermann et al. 2010; Boudker et al. 2007). We combine expression analysis, electrophysiology and evolutionary analysis for the first time to find evolutionary adaptations necessary for keeping duplicated genes in the genome and amino acids associated with such adaptations.

To know whether expression patterns are conserved between different vertebrate species, we performed *in situ* hybridization on retinal sections. To our surprise, we found that lower vertebrate species show expression of EAAT1 in bipolar cells but zebrafish do not express either of

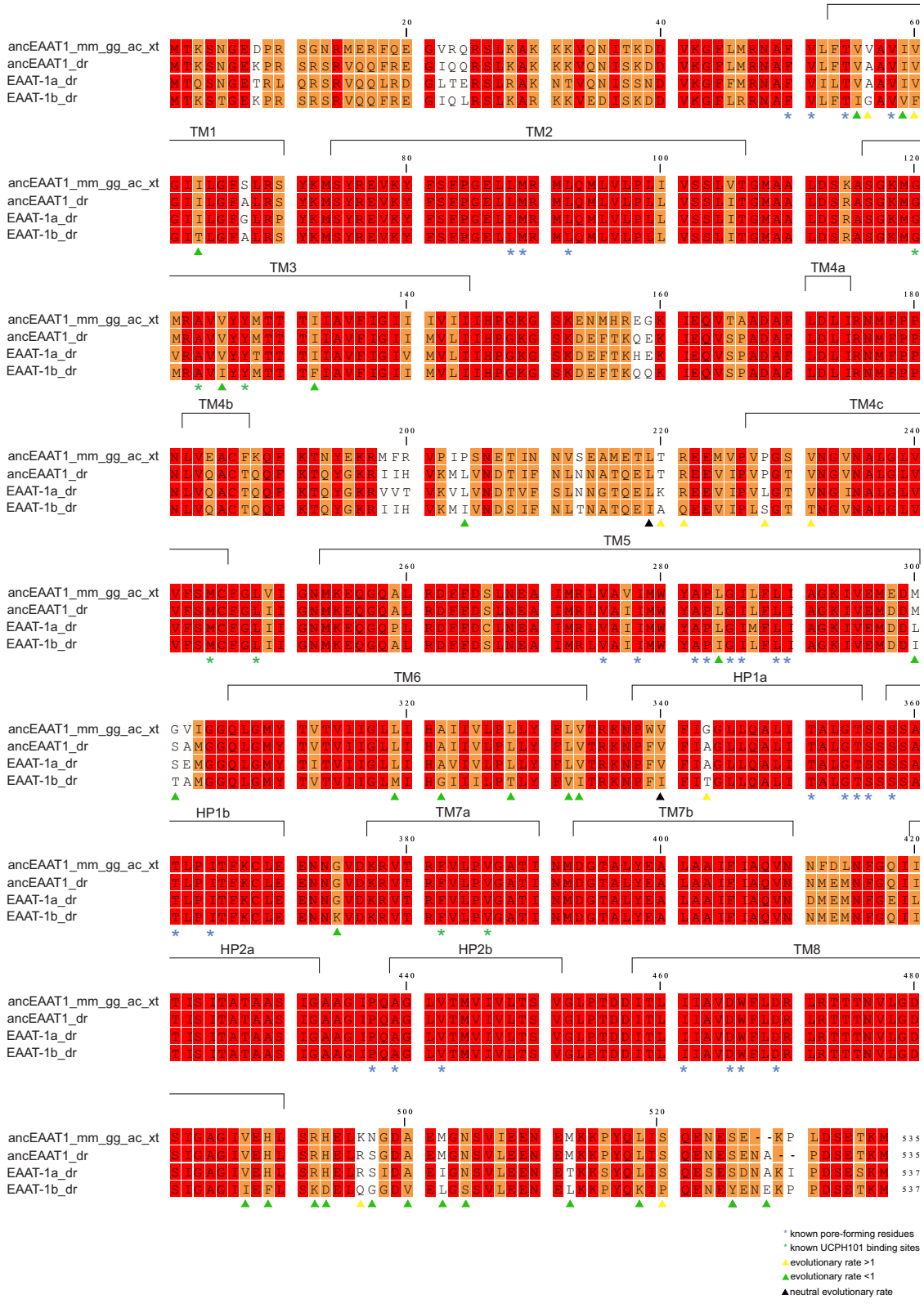

Figure 5: Alignment of Reconstructed Ancestral Sequences and Zebrafish EAAT1 paralogs.
For clarity, conserved amino acids are with red background, orange background represents changes in one of the sequences, and white background indicates two different substitutions at the given position. Known pore-forming residues are marked with blue asterisks and UCPH101 binding sites with green asterisks. Evolutionary rate of EAAT1b specific amino acid substitutions are marked with differently colored triangles.

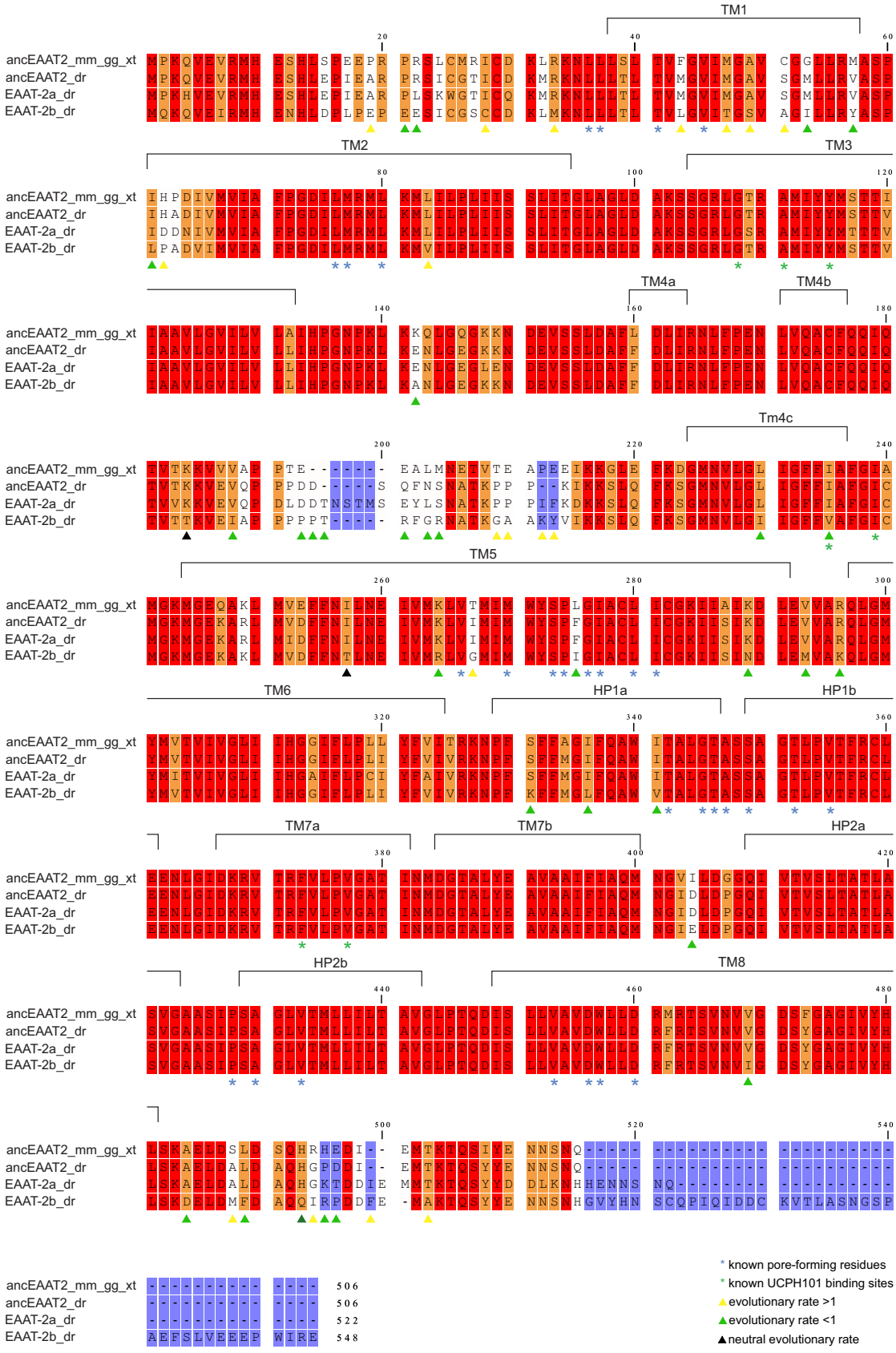
TM1
TM2
TM3
TM4a
TM4b
Tm4c
TM5
TM6
HP1a
HP1b
TM7a
TM7b
HP2a
HP2b
TM8
ancEAAT2_mm_gg_xt
ancEAAT2_dr
EAAT-2a_dr
EAAT-2b_dr
506
506
522
548
* known pore-forming residues
* known UCPH101 binding sites
evolutionary rate >1
evolutionary rate <1
neutral evolutionary rate

Figure 6: Alignment of Reconstructed Ancestral Sequences and Zebrafish EAAT2 paralogs.
For clarity, conserved amino acids are with red background, orange background represents changes in one of the sequences, and white background indicates two different substitutions and blue background shows amino acid positions where all amino acids differ in the alignment. Known pore-forming residues are marked with blue asterisks and UCPH101 binding sites with green asterisks. Evolutionary rate of EAAT1b specific amino acid substitutions are marked with differently colored triangles.

their two paralogs in the retina (Figure 1A). Expression analysis in larvae revealed expression of EAAT1 paralogs in glia cells, neuromast cells of the lateral line organ and in the inner ear. In mice in turn we found expression in Müller glia cells as previously described (Figure 1A; Derouiche, Rauen 1995). Expression of EAAT1 in the inner ear and in glia cells in the brain was reported for mice and is in line with our findings in zebrafish and *Xenopus* tadpoles (Figure 1B; Jin et al. 2003; Shibata et al. 1997). Hence EAAT1 expression is conserved in the inner ear and the lateral line organ in aquatic vertebrates and in glia cells in the brain. In the retina EAAT1 is expressed in photoreceptors and bipolar cells of amphibians, reptiles and birds, whereas mammals express EAAT1 in Müller glia cells and teleosts do not express neither of the EAAT1 paralogs in the retina.

Like the differences of expression patterns between lower vertebrates and mice of EAAT1 we found expression patterns of EAAT2 to be different in the mice retina. In all examined species, EAAT2 is expressed in photoreceptors and in bipolar cells but in mice it is exclusively expressed in Müller glia cells as previously reported (Figure 1A; Reye et al. 2002).

Such changes in expression patterns are caused by sequence changes in *cis*-regulatory elements. It is likely that changes in expression patterns are followed by biophysical adaptations to match changed expression sites. While we expect a high ratio of anion currents compared to glutamate transport currents for neuronal expressed EAATs, a low ratio is expected for EAATs mainly expressed in glia cells. To test this hypothesis, we recorded glutamate transport currents and anion currents separately and calculated the transport ratio (dI_{NO3}/dI_{Glut}). While the mice EAAT1 ortholog exhibits a transport ratio of 1.355 ± 0.730, the EAAT2 ortholog transport ratio is 1.551 ± 0.653 and therefore not statistically significantly different from each other (Figure 3). Michaelis-Menten constants, describing the substrate dose necessary for half-maximal activation of the transporter, were reported to be almost identical for the human EAAT1 and EAAT2 orthologs (EAAT1 Km = 22 ± 3μM; EAAT2 Km = 25 ± 3μM; (Jensen, Bräuner-Osborne 2004)). Since differences in expression levels between different EAAT orthologs were not taken into account, we cannot directly compare measured values in the current-voltage relationship plot and therefore we don't know whether the higher currents measured for EAAT2 are due to more efficient transport or just an artefact of differences in expression.

Those unexpected findings raise the question why the expression patterns of EAAT1 and EAAT2 have changed in mice, since both show virtually indistinguishable biophysical properties. If two genes are so similar in function, one would expect that one becomes redundant and relieved of selective pressure, thereby purged from the genome (non-functionalization). The presence of two different EAATs with similar properties may be explained by a chance distribution of one of the two proteins that are functionally required. If the distribution of expression patterns for EAAT1 and EAAT2 is random, one would expect it to be more diverse. However, we only found differences in mice. Another explanation could be the dosage of the two transporters. It might be that the two EAATs proteins are expressed at different concentrations. Co-expressing them in several tissues, different specific functional concentrations can be achieved.

While we did not find major differences between mice EAAT1 and EAAT2 genes, zebrafish EAAT1 as well as EAAT2 duplicated paralogs show distinct sub-functionalization in expression and transport properties. Aligning EAAT1a and EAAT1b with their theoretical common ancestor (ancEAAT1_dr) as well as the common ancestor of mice, chicken, lizard and *Xenopus* (ancEAAT1_mm_gg_ac_xt) shows several distinct amino acid changes in the sequence of EAAT1b. Several of these amino acid changes show a low evolutionary rate, meaning that those sites are conserved and therefore pointing towards a key role in protein function or structure. In TM1, Ile55 and Val59 are in close vicinity to known anion pore-forming amino acids and may therefore be crucial for either anion-selectivity or pore formation (Machtens et al. 2015). Further positions of interest near pore-forming amino acids are Ile300 and Thr301 and especially Ile284 in TM5. Notably, several changes occurred as well in TM6 which belongs to the transport domain. The transport of glutamate together with sodium and protons and the counter-transport of potassium involve movements of parts of the transporter through the lipid bilayer of the cell membrane (Reyes et al. 2009). TM6 and the structurally symmetrical TM3 move in the lipid bilayer and therefore enable HP1 and HP2 to move into the transport pore and out of it again (Reyes et al. 2009). So far, no mutations in this region have been described and therefore we can only speculate about effects of these substitutions. Gly322 of EAAT1b derived from an Ala at the corresponding site of EAAT1a and the ancestral sequences. EAAT2b and the ancestral forms of EAAT2 show a Gly at the same site (Gly309) but in turn EAAT2a substituted Gly309 to Ala309. Although EAAT1b and EAAT2a show very similar ratios between glutamate-transport associated currents and anion currents, a direct effect of this substitution is rather unlikely since this region was not reported to be important for pore-formation or anion selectivity (Machtens et al. 2015). Since TM6 interacts with the lipid bilayer of the cell membrane, such substitutions could cause altered translocation of the transporter and therefore change the velocity of the transport cycle.

Like EAAT1b, distinct amino acid substitutions potentially causing differences in biophysical properties can be found for EAAT2b. Ile53 and Tyr57 in TM1 are, due to their vicinity to known pore-forming residues, valid candidates causing such changes. Further Arg259 and Asn284 in TM5 could be causing described differences between EAAT2a and EAAT2b. Probably the most promising candidate is Ile270 which corresponds to Ile284 in EAAT1b as described before, since both, EAAT1b and EAAT2b, show higher ratio of anion conductance compared to glutamate transport currents.

Further substitutions in EAAT2b in TM4c, HP1a and TM8 can't be associated with anion selectivity or known anion pore-forming residues. While HP1a is facing intracellular space and its translocation is required for glutamate to enter the cell, TM4c and TM8 harbor glutamate interaction sites (Reyes et al. 2009). Those substitutions could potentially account for previously reported differences in glutamate sensitivity between EAAT2a and EAAT2b (Niklaus et al. 2017).

For several species, effects of blocking or knockdown of either EAAT1 or EAAT2 on retinal function have been described. For instance, loss of mice EAAT1 results in reduced b-wave amplitude in electroretinography (ERG) (Harada et al. 1998). The same effect was observed after application of UCPH101 to the retina before ERG measurement (Tse et al. 2014). The authors assigned the reduction of the b-wave to excess glutamate in the synapse between photoreceptors and bipolar cells, due to the lack of EAAT1 on Müller glia cells. Similar to these findings, knockdown of EAAT2a in zebrafish, which is mainly expressed in Müller glia cells in the retina, leads to a reduction of the b-wave amplitude (Niklaus et al. 2017). Interestingly, knockdown of EAAT2b, which is mainly expressed in photoreceptors, didn't result in a strong phenotype. In line with these findings, knockout or pharmacological knockdown of

EAAT2 in mice did not provoke a clear retinal phenotype (Harada et al. 1998; Tse et al. 2014; Niklaus et al. 2017). With the exception of EAAT1 in zebrafish, we found EAAT1 and EAAT2 to be expressed in retinae of all other investigated species. Here we propose that duplication and subsequent sub-functionalization of the two EAAT2 paralogs made expression of EAAT1 in zebrafish redundant. Phenotypic similarities between knockdown of EAAT1 in mice and EAAT2a in zebrafish as well as knockdown of EAAT2 in mice and knockdown of EAAT2b in zebrafish support this hypothesis (Harada et al. 1998; Tse et al. 2014; Niklaus et al. 2017).

Duplication of EAAT1 and EAAT2 in zebrafish allowed adaptations in protein function as well as in expression patterns. All other investigated constructs show similar expression patterns and biophysical properties. Therefore we think that EAAT2 of *Xenopus* and chicken fulfill similar physiological tasks as EAAT2a in zebrafish, while EAAT1 of *Xenopus*, anole lizards and chickens share similar function in retinae with mice EAAT2.

Here we hypothesize that EAATs with similar ratios of glutamate transport currents and anion currents and possibly similar glutamate affinity would be interchangeable and would therefore be as well redundant. To test this hypothesis, mice EAAT1 or EAAT2 will be expressed in EAAT2a deficient zebrafish. Homozygous EAAT2a deficient zebrafish are not viable and therefore expression of a substitute EAAT should lead to a rescue of the lethal phenotype (A. Hotz, unpublished data).

Further, to test effects of amino acid substitutions with low evolutionary rates between zebrafish EAAT1a and EAAT1b or EAAT2a and EAAT2b respectively, site directed mutagenesis will be performed to unravel possible involvement of those amino acids in anion selectivity and conductance.

Taken together we could show that despite their very similar biophysical properties, EAAT1 and EAAT2 changed their expression pattern in mice compared to other vertebrate species. Furthermore, we identified several possible candidate amino acid substitutions in the zebrafish EAAT1 and EAAT2 paralogs that potentially led to distinct differences in transport and anion conductance properties of the different paralogs.

2.6. Acknowledgement

We thank the Loffing Lab (Institute of Anatomy, UZH) for mice, Stemple Lab (Sanger Institute, London) for *Xenopus tropicalis*, Janine Daum (FMI, Basel) for anole lizard and Bell Schweiz AG for chicken tissue donations. Furthermore, we thank Colette Steinegger for her help with cloning and Kara Kristiansen and Marin Walther for excellent technical and animal support.

2.7. Appendix

2.7.1. Supplementary Figures

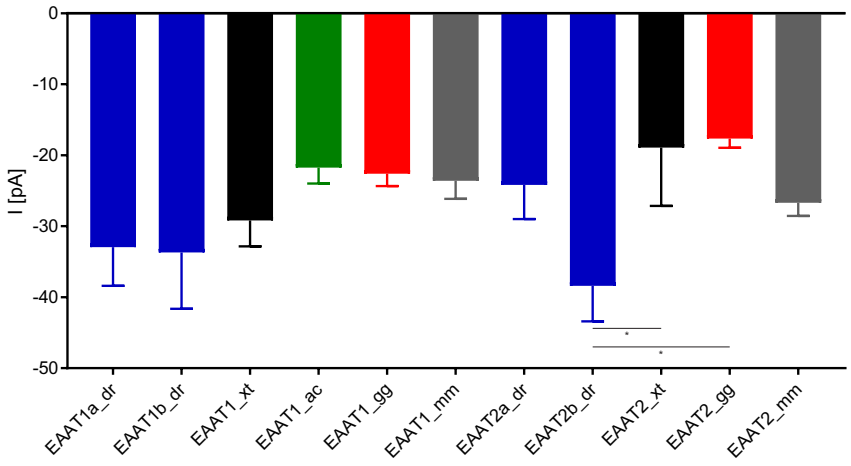

Figure S1 Reversal potential of investigated EAAT1 and EAAT2 orthologs.
Reversal potentials were interpolated via a four-parameter logistic regression. Bars show the mean of reversal potential and error bars represent standard deviation. All constructs show similar reversal potentials. Since anion conductivity is thought to be similar for all genes, inclusion of unhealthy or leaky cells into the statistical analysis can be excluded. Error bars represent standard error mean.

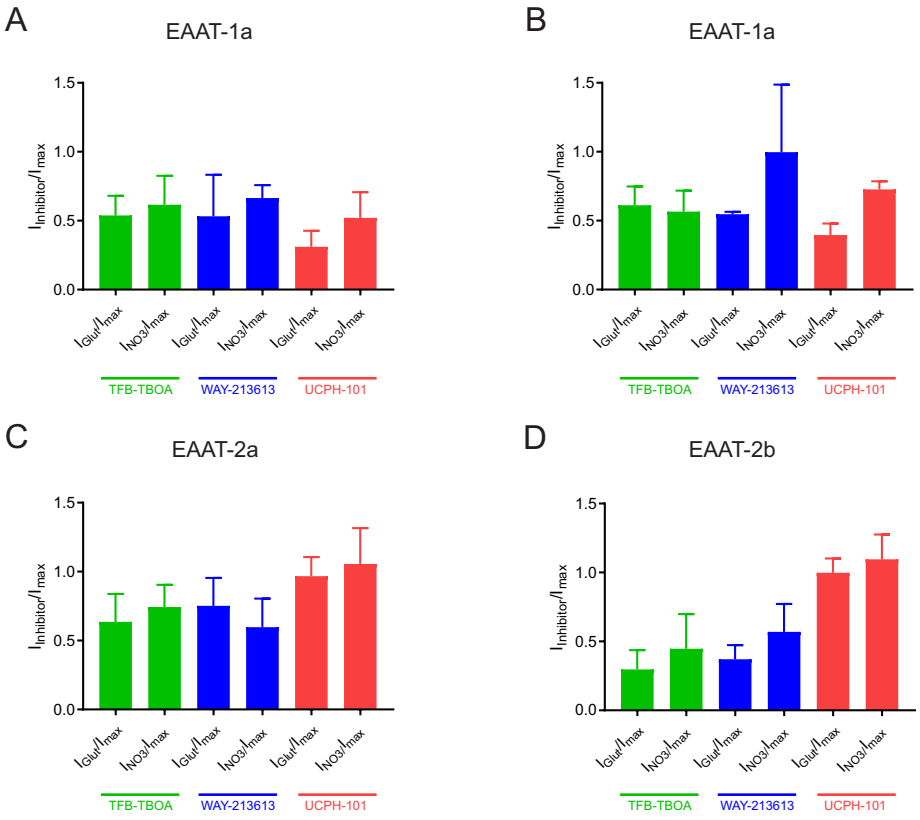

Figure S2: Blocking effect on glutamate transport currents and anion currents.
Green bars represent ratios between maximal measured current amplitudes at -150mV for glutamate transport currents and at +105mV for NO3-currents after application of 1µm TFB-TBOA, blue bars after 10µm WAY213613 and red bars after 10µm UCPH101 application. Interestingly, application of UCPH101 on EAAT1a and EAAT1b seems to reduce glutamate transport currents more than anion currents. All differences between glutamate transport currents and anion currents are statistically not significant (student's t-test, $p > 0.05$). Error bars represent the standard deviation from the mean.

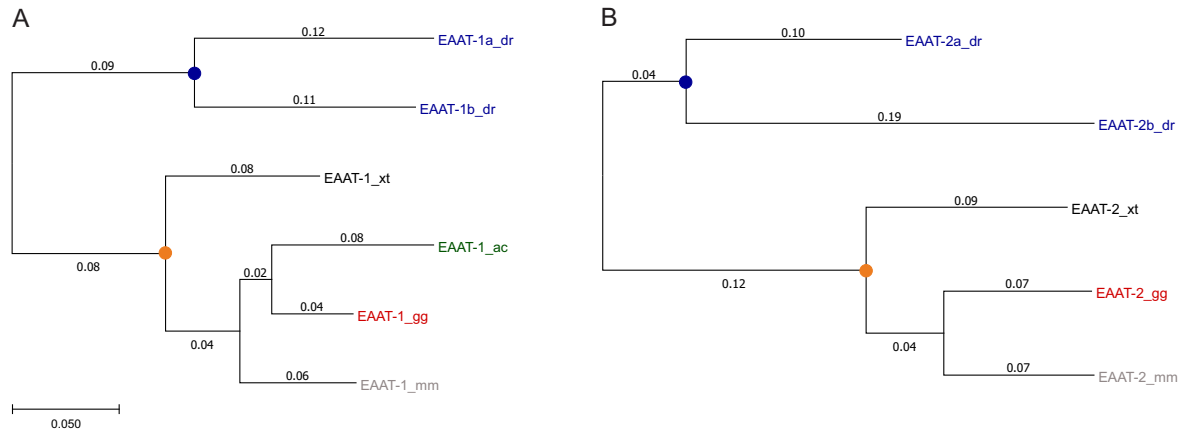

Figure S3: Phylogenetic Trees for EAAT1 (A) and EAAT2 (B).
Positions of reconstructed ancestral sequences are marked with circles. Blue corresponds to ancEAAT1_dr (A) and ancEAAT2_dr respectively. Orange circles correspond to ancEAAT1_mm_gg_ac_xt (A) or ancEAAT2_mm_gg_xt.

EAAT1b	I55	G56	V59	F60	T63	I125	F132	I204	S208	I219
evolutionary rate	0.156	2.207	0.133	1.262	0.564	0.218	0.116	0.156	0.206	0.998
EAAT1b	A220	Q221	S228	T231	I284	I300	T301	M319	G322	T328
evolutionary rate	4.688	4.435	4.156	4.084	0.635	0.218	0.131	0.785	0.126	0.230
EAAT1b	V332	I333	I340	T343	K374	I487	F489	K492	D493	Q496
evolutionary rate	G497	V500	L502	S504	K518	P520	Y525	E528		
EAAT1b	0.230	0.131	0.166	0.218	0.479	1.605	0.175	0.230		
evolutionary rate	0.144	0.972	0.893	4.429	0.206	0.126	0.126	0.218	0.230	1.129
EAAT2b	E19	E21	E22	C28	M33	L43	T47	S49	A51	I53
evolutionary rate	1.495	0.666	0.116	1.889	3.103	6.766	4.467	1.439	2.709	0.192
EAAT2b	Y57	L61	P62	V83	A142	T184	I188	P193	P194	T195
evolutionary rate	0.604	0.617	5.363	1.539	0.106	0.986	0.133	0.143	0.108	0.192
EAAT2b	R196	G198	R199	G204	A205	K207	Y208	V209	I225	V230
evolutionary rate	0.116	0.113	0.224	1.619	6.770	6.773	3.469	2.930	0.111	0.113
EAAT2b	T252	R259	G262	I270	N284	M288	K291	K326	L331	V336
evolutionary rate	1.064	0.192	1.171	0.204	0.130	0.116	0.131	0.200	0.200	0.106
EAAT2b	E399	I464	D479	M483	F484	Q488	I489	R490	P491	F494
evolutionary rate	0.192	0.204	0.143	1.889	0.130	0.722	1.549	0.719	0.638	1.117
EAAT2b	A497									
evolutionary rate	1.086									

Table S1: Specific amino acid changes of EAAT1b and EAAT2b compared to ancestors and a-paralog and calculated evolutionary rate for the corresponding site.

2.7.2. Primers used in this study

Gene	Primer	Sequence 5′ to 3′
eaat1a_dr	EAAT1a_dr_1s_BsiWI	GTTGTTCGTACGAGATGACTCAGAGTAACGGGG
	EAAT1a_dr_1s_BsiWI	GTTGTTGCGGCCGCTTACATTTTGCTCTCGCT
eaat1b_dr	EAAT1b_dr_1s_BsiWI	GTTGTTCGTACGAGATGACCAAAAGCACAGGG
	EAAT1b_dr_1614as_NotI	GTTGTTGCGGCCGCCTACATCTTGGTCTCGCTG
eaat1_xt	EAAT1_xt_1s_BsiWI	GTTGTTCGTACGAGATGACTAAAAGCAACGGG
	EAAT1_xt_1629as_NotI	GTTGTTGCGGCCGCTTACATTTTTGTTTCACTGTCT
eaat1_gg	EAAT1_gg_1s_BsiWI	GTTGTTCGTACGAGATGACTAAAGGTAACGGAGA
	EAAT1_gg_1632as_NotI	GTTGTTGCGGCCGCTACATCTTGGTTTCACTGTC
eaat1_ac	EAAT1_ac_1s_BsiWI	GTTGTTCGTACGAGATGACTAAAAGTAACGGAGAA
	EAAT1_gg_1632as_NotI	GTTGTTGCGGCCGCTTACATCTTGGTTTCACTGTC
eaat1_mm	EAAT1_mm_1s_BsiWI	GTTGTTCGTACGAGATGACCAAAAGCAACGG
	EAAT1_mm_1632as_NotI	GTTGTTGCGGCCGCTACATCTTGGTTTCGCTG
eaat2a_dr	EAAT2a_dr_1s_Acc65I	GTTGTTGGTACCAGATGCCGAAGCACGTGG
	EAAT2a_dr_1569as_NotI	GTTGTTGCGGCCGCTTACTGGTTGGAGTTGTTTTC
eaat2b_dr	EAAT2b_dr_1s_Acc65I	GTTGTTGGTACCAGATGCAGAAGCAAGTGGAG
	EAAT2b_dr_1647as_NotI	GTTGTTGCGGCCGCTTACTCGCGAATCCATG
eaat2_xt	EAAT2_xt_1s_BsiWI	GTTGTTCGTACGAGATGGCATCGACAGAAGG
	EAAT2_xt_1707as_NotI	GTTGTTGCGGCCGCTCACCCTTCCAGTGGCT
eaat2_gg	EAAT2_gg_1s_Acc65I	GTTGTTGGTACCAGATGCCGAAGCAAGTAGAA
	EAAT2_gg_1701as_NotI	GTTGTTGCGGCCGCTTAGTTTTCACGTTTCCAA
eaat2_ac	EAAT2_ac_1s_Acc65I	GTTGTTGGTACCAGATGGCATCGACCGACG
	EAAT2_ac_1722as_NotI	GTTGTTGCGGCCGCTTATTTCTCCTGTTTCCAAG
eaat2_mm	EAAT2_mm_1s_BsiWI	GTTGTTCGTACGAGATGGCATCAACAGAGGGT
	EAAT2_mm_1719as_EcoRI	GTTGTTGAATTCTTATTTTTCACGTTTCCAA

Table S2: Primers used for cloning of expression constructs.

Gene	Primer	Sequence 5′ to 3′
eaat1a_dr	EAAT1a_dr_-0009s	CCTCCAGACATGACTCAGAG
	EAAT1a_dr_0644s	GCACGCAGGAGCTCAAAC
	EAAT1a_dr_0957as	CAGCAGGCCAATGATGAC
	EAAT1a_dr_1651as	AAACCTCCAGGAAATGAAAC
eaat1b_dr	EAAT1b_dr_-0005s	ACAGCATGACCAAAAGCAC
	EAAT1b_dr_0640s	AACGCTACGCAGGAGATC
	EAAT1b_dr_0951as	GCCGATGATCACCGTAAC
	EAAT1b_dr_1625as	AACATCAGCCTCTACATCTTG
eaat1_xt	EAAT1_xt_-0033s	CCCAACAAGAGGCATTTG
	EAAT1_xt_0760s	GGGTTGGTCATTGGAAAC
	EAAT1_xt_0976as	GCAGTCCTACAATAACCGTG
	EAAT1_xt_1636as	GGATCTTTTACATTTTTGTTTC
eaat1_gg	EAAT1_gg_-0013s	TTCTGCAAGATAAATGACTAAG
	EAAT1_gg_0737s	TGGTGGTTTTTTCAATAAGC
	EAAT1_gg_0914as	TCCATCTCAACAATTTTTCC
	EAAT1_gg_1649as	AGACTCATGCCTTCTTTACC

Gene	Primer	Sequence 5′ to 3′
eaat1_ac	EAAT1_ac_0001s	ATGACTAAAAGTAACGGAGAAG
	EAAT1_ac_0841s	CGGCTGGTTGCACTAATC
	EAAT1_ac_0985as	GGATGAGCAAGCCAATG
	EAAT1_ac_1637as	CTGCCTTACATCTTGGTTTC
eaat1_mm	EAAT1_mm-0034s	GCAAGGACGTGATAAATTC
	EAAT1_mm0748s	TCCATGTGCTTCGGTTTC
	EAAT1_mm0923as	CCCATGTCTTCCATCTCAAC
	EAAT1_mm1691as	GGATACATTGTAGAACAGTTTCC
eaat2a_dr	EAAT-2a_dr_-0009s	TTGTGGATGATGCCGAAG
	EAAT-2a_dr_0664s	AAGAGCGGCATGAATGTG
	EAAT-2a_dr_0970as	TGGCGAAGTAGATGCAGG
	EAAT-2a_dr_1686as	TTAATCGTTTTTCCAGGGTTC
eaat2b_dr	EAAT-2b_dr_-0003s	AAGATGCAGAAGCAAGTGG
	EAAT-2b_dr_0649s	AAGAGCGGCATGAATGTG
	EAAT-2b_dr_0932as	AATATGCCTCCATGAATAATG
	EAAT-2b_dr_1653as	GCTGTGTTACTCGCGAATC
eaat2_xt	EAAT2_xt_-0002s	CCATGGCATCGACAGAAG
	EAAT2_xt_0780s	GCTGATGGTCGAGTTTTTC
	EAAT2_xt_0991as	GCAGCGGCAGGAATATG
	EAAT2_xt_1749as	GCAAAGGGTCTTCGTGAAG
eaat2_gg	EAAT2_gg_-0009s	GCCAACAATATGCCGAAG
	EAAT2_gg_0753s	AGACCAAGCCAAGATGATG
	EAAT2_gg_0943as	GGCCCACAATCACAGTTAC
	EAAT2_gg_1727as	AAAGATGGAGCTGGGAATC
eaat2_ac	EAAT2_ac_0001s	ATGGCATCGACCGACG
	EAAT2_ac_0865s	GGTATTGCCTGTCTCATTTG
	EAAT2_ac_1003as	AGTACAACGAAGGCAAGAAG
	EAAT2_ac_1744as	ACAGAGCTGTATTGTTCTTCC
eaat2_mm	EAAT2_mm-0003s	GCCATGGCATCAACAGAG
	EAAT2_mm0735s	CGGATTCTTTATTGCTTTC
	EAAT2_mm0897as	GATCTTCCCACAAATCAAGC
	EAAT2_mm1728as	ATCGGGTCATTATTTTTCAC

Table S3: Primes used for In situ probes.

2.8. References

Abrahamsen, Bjarke; Schneider, Nicole; Erichsen, Mette N.; Huynh, Tri H. V.; Fahlke, Christoph; Bunch, Lennart; Jensen, Anders A. (2013): Allosteric modulation of an excitatory amino acid transporter: the subtype-selective inhibitor UCPH-101 exerts sustained inhibition of EAAT1 through an intramonomeric site in the trimerization domain. In *The Journal of neuroscience* 33 (3), pp. 1068–1087. DOI: 10.1523/JNEUROSCI.3396-12.2013.

Amara, Susan G.; Fontana, Andreia C.K (2002): Excitatory amino acid transporters. Keeping up with glutamate. In *Neurochemistry international* 41 (5), pp. 313–318. DOI: 10.1016/S0197-0186(02)00018-9.

Arriza, J. L.; Eliasof, S.; Kavanaugh, M. P.; Amara, S. G. (1997): Excitatory amino acid transporter 5, a retinal glutamate transporter coupled to a chloride conductance. In *Proceedings of the National Academy of Sciences of the United States of America* 94 (8), pp. 4155–4160.

Boudker, Olga; Ryan, Renae M.; Yernool, Dinesh; Shimamoto, Keiko; Gouaux, Eric (2007): Coupling substrate and ion binding to extracellular gate of a sodium-dependent aspartate transporter. In *Nature* 445 (7126), pp. 387–393. DOI: 10.1038/nature05455.

Derouiche, A.; Rauen, T. (1995): Coincidence of L-glutamate/L-aspartate transporter (GLAST) and glutamine synthetase (GS) immunoreactions in retinal glia: evidence for coupling of GLAST and GS in transmitter clearance. In *Journal of neuroscience research* 42 (1), pp. 131–143. DOI: 10.1002/jnr.490420115.

Dunlop, John; McIlvain, H. Beal; Carrick, Tikva A.; Jow, Brian; Lu, Qiang; Kowal, Dianne et al. (2005): Characterization of novel aryl-ether, biaryl, and fluorene aspartic acid and diaminopropionic acid analogs as potent inhibitors of the high-affinity glutamate transporter EAAT2. In *Molecular pharmacology* 68 (4), pp. 974–982. DOI: 10.1124/mol.105.012005.

Edgar, Robert C. (2004): MUSCLE: multiple sequence alignment with high accuracy and high throughput. In *Nucleic acids research* 32 (5), pp. 1792–1797. DOI: 10.1093/nar/gkh340.

Gesemann, Matthias; Lesslauer, Annegret; Maurer, Colette M.; Schönthaler, Helia B.; Neuhauss, Stephan C. F. (2010): Phylogenetic analysis of the vertebrate excitatory/neutral amino acid transporter (SLC1/EAAT) family reveals lineage specific subfamilies. In *BMC evolutionary biology* 10, p. 117. DOI: 10.1186/1471-2148-10-117.

Glasauer, Stella M. K.; Neuhauss, Stephan C. F. (2014): Whole-genome duplication in teleost fishes and its evolutionary consequences. In *Molecular genetics and genomics : MGG* 289 (6), pp. 1045–1060. DOI: 10.1007/s00438-014-0889-2.

Harada, T.; Harada, C.; Watanabe, M.; Inoue, Y.; Sakagawa, T.; Nakayama, N. et al. (1998): Functions of the two glutamate transporters GLAST and GLT-1 in the retina. In *Proceedings of the National Academy of Sciences of the United States of America* 95 (8), pp. 4663–4666.

Huang, Ying-Yu; Haug, Marion F.; Gesemann, Matthias; Neuhauss, Stephan C. F. (2012): Novel expression patterns of metabotropic glutamate receptor 6 in the zebrafish nervous system. In *PloS one* 7 (4), e35256. DOI: 10.1371/journal.pone.0035256.

Jensen, Anders A.; Bräuner-Osborne, Hans (2004): Pharmacological characterization of human excitatory amino acid transporters EAAT1, EAAT2 and EAAT3 in a fluorescence-based membrane potential assay. In *Biochemical pharmacology* 67 (11), pp. 2115–2127. DOI: 10.1016/j.bcp.2004.02.013.

Jensen, Anders A.; Erichsen, Mette N.; Nielsen, Christina W.; Stensbøl, Tine B.; Kehler, Jan; Bunch, Lennart (2009): Discovery of the first selective inhibitor of excitatory amino acid transporter subtype 1. In *Journal of medicinal chemistry* 52 (4), pp. 912–915. DOI: 10.1021/jm8013458.

Ji, Yurui; Postis, Vincent L. G.; Wang, Yingying; Bartlam, Mark; Goldman, Adrian (2016): Transport mechanism of a glutamate transporter homologue GltPh. In *Biochemical Society transactions* 44 (3), pp. 898–904. DOI: 10.1042/BST20160055.

Jin, Zhen-Hua; Kikuchi, Toshihiko; Tanaka, Kohichi; Kobayashi, Toshimitsu (2003): Expression of glutamate transporter GLAST in the developing mice cochlea. In *The Tohoku journal of*

experimental medicine 200 (3), pp. 137–144.

Jones, David T.; Taylor, William R.; Thornton, Janet M. (1992): The rapid generation of mutation data matrices from protein sequences. In *Bioinformatics* 8 (3), pp. 275–282. DOI: 10.1093/bioinformatics/8.3.275.

Kanai, Yoshikatsu; Hediger, Matthias A. (2004): The glutamate/neutral amino acid transporter family SLC1: molecular, physiological and pharmacological aspects. In *Pflugers Archiv : European journal of physiology* 447 (5), pp. 469–479. DOI: 10.1007/s00424-003-1146-4.

Kovermann, Peter; Machtens, Jan-Philipp; Ewers, David; Fahlke, Christoph (2010): A conserved aspartate determines pore properties of anion channels associated with excitatory amino acid transporter 4 (EAAT4). In *The Journal of biological chemistry* 285 (31), pp. 23676–23686. DOI: 10.1074/jbc.M110.126557.

Kumar, Sudhir; Stecher, Glen; Tamura, Koichiro (2016): MEGA7: Molecular Evolutionary Genetics Analysis Version 7.0 for Bigger Datasets. In *Molecular biology and evolution* 33 (7), pp. 1870–1874. DOI: 10.1093/molbev/msw054.

Lamb, Trevor D.; Collin, Shaun P.; Pugh, Edward N. (2007): Evolution of the vertebrate eye: opsins, photoreceptors, retina and eye cup. In *Nature reviews. Neuroscience* 8 (12), pp. 960–976. DOI: 10.1038/nrn2283.

Leinenweber, Ariane; Machtens, Jan-Philipp; Begemann, Birgit; Fahlke, Christoph (2011): Regulation of glial glutamate transporters by C-terminal domains. In *The Journal of biological chemistry* 286 (3), pp. 1927–1937. DOI: 10.1074/jbc.M110.153486.

Machtens, Jan-Philipp; Kortzak, Daniel; Lansche, Christine; Leinenweber, Ariane; Kilian, Petra; Begemann, Birgit et al. (2015): Mechanisms of anion conduction by coupled glutamate transporters. In *Cell* 160 (3), pp. 542–553. DOI: 10.1016/j.cell.2014.12.035.

Medrano, M. C.; Gerrikagoitia, I.; Martínez-Millán, L.; Mendiguren, A.; Pineda, J. (2013): Functional and morphological characterization of glutamate transporters in the rat locus coeruleus. In *Br. J. Pharmacol.* 169 (8), pp. 1781–1794. DOI: 10.1111/bph.12235.

Mullins, M. C.; Hammerschmidt, M.; Haffter, P.; Nüsslein-Volhard, C. (1994): Large-scale mutagenesis in the zebrafish: in search of genes controlling development in a vertebrate. In *Current biology : CB* 4 (3), pp. 189–202.

Nieuwkoop, P. D.; Faber, Jacob (1994): Normal table of Xenopus laevis (Daudin). A systematical and chronological survey of the development from the fertilized egg till the end of metamorphosis. New York: Garland Publishing.

Niklaus, Stephanie; Cadetti, Lucia; Vom Berg-Maurer, Colette M.; Lehnherr, André; Hotz, Adriana L.; Forster, Ian C. et al. (2017): Shaping of Signal Transmission at the Photoreceptor Synapse by EAAT2 Glutamate Transporters. In *eNeuro* 4 (3). DOI: 10.1523/ENEURO.0339-16.2017.

Ohnuma, T.; Augood, S. J.; Arai, H.; McKenna, P. J.; Emson, P. C. (1998): Expression of the human excitatory amino acid transporter 2 and metabotropic glutamate receptors 3 and 5 in the prefrontal cortex from normal individuals and patients with schizophrenia. In *Brain research. Molecular brain research* 56 (1-2), pp. 207–217.

Reye, Peter; Sullivan, Robert; Fletcher, Erica L.; Pow, David V. (2002): Distribution of two splice

variants of the glutamate transporter GLT1 in the retinas of humans, monkeys, rabbits, rats, cats, and chickens. In *The Journal of comparative neurology* 445 (1), pp. 1–12.

Reyes, Nicolas; Ginter, Christopher; Boudker, Olga (2009): Transport mechanism of a bacterial homologue of glutamate transporters. In *Nature* 462 (7275), pp. 880–885. DOI: 10.1038/nature08616.

Rose, Christine R.; Ziemens, Daniel; Untiet, Verena; Fahlke, Christoph (2016): Molecular and cellular physiology of sodium-dependent glutamate transporters. In *Brain research bulletin. DOI:* 10.1016/j.brainresbull.2016.12.013.

Shibata, T.; Yamada, K.; Watanabe, M.; Ikenaka, K.; Wada, K.; Tanaka, K.; Inoue, Y. (1997): Glutamate transporter GLAST is expressed in the radial glia-astrocyte lineage of developing mice spinal cord. In *The Journal of neuroscience* 17 (23), pp. 9212–9219.

Shimamoto, Keiko; Sakai, Ryuichi; Takaoka, Kiyo; Yumoto, Noboru; Nakajima, Terumi; Amara, Susan G.; Shigeri, Yasushi (2004): Characterization of novel L-threo-beta-benzyloxyaspartate derivatives, potent blockers of the glutamate transporters. In *Molecular pharmacology* 65 (4), pp. 1008–1015. DOI: 10.1124/mol.65.4.1008.

Tanaka, K. (1997): Epilepsy and Exacerbation of Brain Injury in Mice Lacking the Glutamate Transporter GLT-1. In *Science* 276 (5319), pp. 1699–1702. DOI: 10.1126/science.276.5319.1699.

Tse, Dennis Y.; Chung, Inyoung; Wu, Samuel M. (2014): Pharmacological inhibitions of glutamate transporters EAAT1 and EAAT2 compromise glutamate transport in photoreceptor to ON-bipolar cell synapses. In *Vision research* 103, pp. 49–62. DOI: 10.1016/j.visres.2014.07.020.

Wadiche, J. I.; Kavanaugh, M. P. (1998): Macroscopic and microscopic properties of a cloned glutamate transporter/chloride channel. In *The Journal of neuroscience* 18 (19), pp. 7650–7661.

Wadiche, Jacques I.; Amara, Susan G.; Kavanaugh, Michael P. (1995): Ion fluxes associated with excitatory amino acid transport. In *Neuron* 15 (3), pp. 721–728. DOI: 10.1016/0896-6273(95)90159-0.

Yernool, Dinesh; Boudker, Olga; Jin, Yan; Gouaux, Eric (2004): Structure of a glutamate transporter homologue from Pyrococcus horikoshii. In *Nature* 431 (7010), pp. 811–818. DOI: 10.1038/nature03018.

Yi, Jae-Hyuk; Hazell, Alan S. (2006): Excitotoxic mechanisms and the role of astrocytic glutamate transporters in traumatic brain injury. In *Neurochemistry international* 48 (5), pp. 394–403. DOI: 10.1016/j.neuint.2005.12.001.

Zerangue, N.; Kavanaugh, M. P. (1996): Flux coupling in a neuronal glutamate transporter. In *Nature* 383 (6601), pp. 634–637. DOI: 10.1038/383634a0.

Chapter 3

Shaping of Signal Transmission at the Photoreceptor Synapse by EAAT2 Glutamate Transporters

Stephanie Niklaus[1,3,*], Lucia Cadetti[1,*], Colette M. vom Berg-Maurer[1,4,] André Lehnherr[1,3], Adriana Hotz[1], Ian C. Forster[2], Matthias Gesemann[1] & Stephan C.F. Neuhauss[1,§]

[*] equal contribution

University of Zurich
[1]Institute of Molecular Life Sciences,
[2]Institute of Physiology,
[3]Life Science Zürich Graduate Program – Neuroscience,
Winterthurerstrasse 190, CH-8057 Zurich, Switzerland

[4]Present address: Eawag, Swiss Federal Institute of Aquatic Science and Technology, CH-8600 Dübendorf, Switzerland

[§] Corresponding author:
Prof. Dr. Stephan C. F. Neuhauss
Institute of Molecular Life Sciences
University of Zurich
Winterthurerstrasse 190
CH-8057 Zurich, Switzerland
stephan.neuhauss@imls.uzh.ch

Abbreviated title: EAAT2 glutamate transporters function at photoreceptor synapse

Article published in eNeuro

Personal contribution:
In situ hybridization on adult retinal section, cloning of expression constructs

eNeuro

New Research

Neuronal Excitability

Shaping of Signal Transmission at the Photoreceptor Synapse by EAAT2 Glutamate Transporters

Stephanie Niklaus,[1,3,*] Lucia Cadetti,[1,*] Colette M. vom Berg-Maurer,[1] André Lehnherr,[1,3] Adriana L. Hotz,[1] Ian C. Forster,[2] Matthias Gesemann,[1] and Stephan C.F. Neuhauss[1]

DOI:http://dx.doi.org/10.1523/ENEURO.0339-16.2017

[1]Institute of Molecular Life Sciences, University of Zurich, Zurich, CH-8057, Switzerland, [2]Institute of Physiology, Zurich, CH-8057, Switzerland, and [3]Life Science Zürich Graduate Program – Neuroscience, Zurich, CH-8057, Switzerland

Visual Abstract

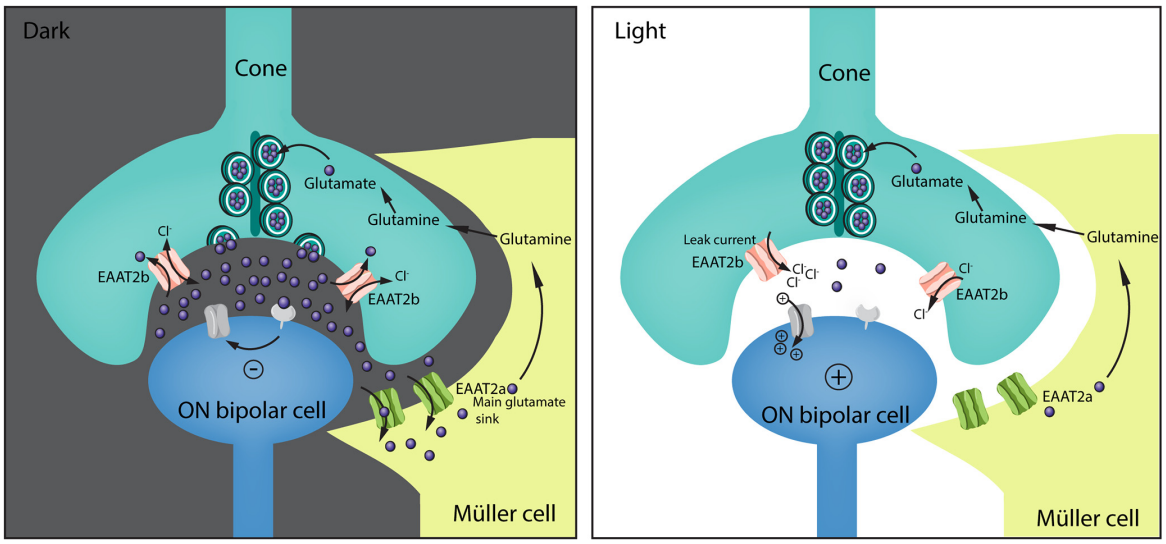

Photoreceptor ribbon synapses tonically release glutamate. To ensure efficient signal transmission and prevent glutamate toxicity, a highly efficient glutamate removal system provided by members of the SLC1 gene family is required. By using a combination of biophysical and *in vivo* studies, we elucidate the role of excitatory amino acid transporter 2 (EAAT2) proteins in synaptic glutamate homeostasis at the zebrafish photoreceptor synapse. The

Significance Statement

Glutamate transporters are key regulators of glutamate homeostasis. Here we analyze two players of glutamate homeostasis at the zebrafish photoreceptor synapse. This report demonstrates how paralogous glutamate transporters emerging from a whole-genome duplication event acquired a complementary expression pattern and adopted different biophysical characteristics that allow modulation of the synapse and signal transmission in a specialized manner.

main glutamate sink is provided by the glial EAAT2a, reflected by reduced electroretinographic responses in EAAT2a-depleted larvae. EAAT2b is located on the tips of cone pedicles and contributes little to glutamate reuptake. However, this transporter displays both a large chloride conductance and leak current, being important in stabilizing the cone resting potential. This work demonstrates not only how proteins originating from the same gene family can complement each other's expression profiles and biophysical properties, but also how presynaptic and glial transporters are coordinated to ensure efficient synaptic transmission at glutamatergic synapses of the central nervous system.

Key words: Excitatory amino acid transporter; glutamate; retina; zebrafish

Introduction

Excitatory amino acid transporters (EAATs) are high-affinity glutamate transporters that regulate the extracellular concentration of glutamate in the vertebrate brain and retina. The transport of glutamate is an electrogenic process driven by the cotransport of three sodium and one hydrogen and the countertransport of one potassium ion (Zerangue and Kavanaugh, 1996). In addition, a thermodynamically uncoupled chloride conductance, whose magnitude differs between EAATs, is associated with the glutamate transport. This chloride conductance can modulate the cell's membrane potential (Picaud et al., 1995; Palmer et al., 2003; Veruki et al., 2006; Wersinger et al., 2006). Photoreceptors possess highly specialized ribbon synapses, where vesicles are tethered to provide tonic release of glutamate (Morgans, 2000; Schmitz, 2009). In contrast to nonribbon synapses, where the depolarization of the presynaptic terminal induces the release of a few vesicles of neurotransmitter, cone ribbon synapses allow the simultaneous release of hundreds of vesicles. This can result in exceptionally high glutamate concentrations within the synapse, making efficient glutamate uptake capacities essential to ensure an optimal signal-to-noise ratio, precisely terminate a signal, and prevent neurotoxic glutamate concentrations (Morgans, 2000). As a consequence, EAATs are highly expressed in the retina. In mammals, the main retinal glutamate uptake is conducted by Müller glia cells through EAAT1 (GLAST; White and Neal, 1976; Harada et al., 1998; Rauen et al., 1998; Barnett and Pow, 2000; Rauen, 2000; Levinger et al., 2012; Tse et al., 2014). However, in most other vertebrates including zebrafish (*Danio rerio*), the glutamate transporter expressed on Müller glia cells is EAAT2 (GLT-1; Eliasof et al., 1998a, b). Interestingly, EAATs are also present at photoreceptor terminals, where glutamate uptake is accompanied by a subtle regulation of the presynaptic potential (Eliasof and Werblin, 1993; Vandenbranden et al., 1996; Gaal et al., 1998; Roska et al., 1998; Hasegawa et al., 2006; Rowan et al., 2010; Szmajda and Devries, 2011).

In the present study, we focus on the role of EAAT2 at the photoreceptor synapse of the cone-dominant zebrafish retina. The zebrafish genome harbors two *eaat2* genes that originated from a whole-genome duplication event ~350 million years ago (Gesemann et al., 2010b). For EAAT2, we found an unusual case of both spatial and functional subfunctionalization (division of the ancestral gene function among the two paralogs, as reviewed by Glasauer and Neuhauss [2014]). Biophysical properties of the transporters differ in dependence of their biological requirements. EAAT2a is expressed in Müller glia cells, and knockdown of this glial transporter significantly reduces the electroretinogram (ERG) b-wave amplitude, indicating that EAAT2a removes the main load of synaptic glutamate. EAAT2b is located presynaptically in cone pedicles. Loss of EAAT2b does not significantly reduce the ERG b-wave, suggesting that it interferes only slightly with the removal of cleft glutamate: its action could be limited to the cone presynaptic terminal in agreement with its proposed function of accelerating the transient cone response (Rowan et al., 2010). Furthermore, with its high chloride conductance and the presence of a significant leak current, EAAT2b may stabilize the dark resting potential of cones. This presents an intriguing case of divergent evolution of an ancestral protein leading to subfunctionalized proteins at the photoreceptor synapse, supporting vision through different mechanisms.

Methods

Fish maintenance

Zebrafish *(Danio rerio)* of the Tübingen and Wik strain were kept in a 14-h/10-h light/dark cycle under standard conditions as previously described (Mullins et al., 1994). Larval stages were raised in E3 embryo medium (5 mM NaCl, 0.17 mM KCl, 0.33 mM $CaCl_2$, 0.33 mM $MgSO_4$, 10^{-5}% methylene blue) at 28°C. All experiments were performed in accordance with the ARVO Statement for

Received November 10, 2016; accepted May 25, 2017; First published June 5, 2017.

Authors report no conflict of interest.

Authors' Contributions: SN performed histology and electroretinography, prepared Figs. 1–4, and wrote the manuscript; LC made oocyte recordings, prepared Fig. 5, and contributed to manuscript writing; CMvBM cloned the genes, did initial physiological and histological analyses, and wrote an earlier version of the manuscript; AL and ALH contributed to expression analyses; ICF contributed to oocyte recordings; MG contributed to cloning and phylogenetic analyses; SCFN conceived and coordinated the study and contributed to manuscript writing; and all authors edited and approved the manuscript.

Funding: This work was supported by the Swiss National Science Foundation (31003A_153289/1).

*S.N. and L.C. contributed equally to this work.

Colette M. vom Berg-Maurer's present address: Eawag, Swiss Federal Institute of Aquatic Science and Technology, 8600, Dübendorf, Switzerland.

Acknowledgments: We thank Kara Dannenhauer for excellent technical and animal support and Dr. Shoji Kawamura Kennedy for transgenic lines.

Correspondence should be addressed to Stephan C.F. Neuhauss, Institute of Molecular Life Sciences, University of Zurich, Winterthurerstrasse 190, CH-8057 Zurich, Switzerland. E-mail: stephan.neuhauss@imls.uzh.ch.

DOI:http://dx.doi.org/10.1523/ENEURO.0339-16.2017

the Use of Animals in Ophthalmic and Vision Research and were approved by the local authorities (Veterinäramt Zürich TV4206).

In situ hybridization

Cloning of the *eaat2* genes into the TOPO pCRII vector (TA Cloning Kit Dual Promoter, Invitrogen) is described elsewhere (Gesemann et al., 2010a). Plasmids containing the genes were linearized for SP6 and T7 *in vitro* transcription and purified with phenol-chloroform. Digoxigenin (DIG)-labeled antisense RNA probes were generated using DIG-RNA-labeling kit (Roche Diagnostics). Larval whole-mount and adult retina *in situ* hybridization was done on 5-d postfertilization (5-dpf) larvae and adult retinal cross sections. Detailed protocol of *in situ* hybridization is described by Huang et al. (2012). Briefly, the tissue was treated with proteinase K and postfixed with 4% paraformaldehyde (PFA) before prehybridization at 64°C. Hybridization of RNA probes was done at 64°C overnight. On day 2, after several stringency washes at 64°C, probes were blocked in 1× Roche blocking solution in Tris/NaCl/Tween. Anti-DIG AP antibody was applied overnight at 4°C. On day 3, after several washing steps, signal was detected by incubation in staining buffer. Stained embryos/retinal sections were fixed with PFA and imaged in glycerol (whole-mount) with an Olympus BX61 light microscope. Images were processed and assembled using Adobe Photoshop and Adobe Illustrator CS5.

Generation of antibodies

Chickens were immunized using the peptide H_2N-CKL KEN LGE GLE NDE V-$CONH_2$ to raise chicken anti-EAAT2a antibodies. Antibodies against EAAT2b were raised in guinea pigs using the peptides H_2N-CKL KAN LGE GKK NDE V-$CONH_2$ and H_2N-CKG AAK YVI KKS LQF KS-$CONH_2$. Antibodies were raised in a 87-d classic program and affinity-purified against the corresponding peptides by Eurogentec (Seraing, Belgium).

Immunohistochemistry

Larvae (5 dpf) or adult eyes were fixed in 4% PFA in PBS, pH 7.4, or 2% trichloroacetic acid for 30 min at room temperature. Samples were cryoprotected in 30% sucrose in PBS overnight at 4°C and embedded in cryomatrix (Tissue Tek OCT Compound, Sakura Finetek) using liquid N_2 to immediately freeze the samples. Sections of 16–18 μm were mounted onto Superfrost slides (Thermo Fisher Scientific). Slides were air-dried at room temperature and stored at –20°C. Before use, slides were thawed at 37°C for 30 min and washed in PBS, pH 7.4, for 10 min. Blocking solution (10% normal goat serum, 1% bovine serum albumin, 0.3% Tween 20 in PBS, pH 7.4) was applied for at least 45 min at room temperature, and primary antibodies diluted in blocking solution were incubated overnight at 4°C. The following antibodies were used: mouse anti–glutamine synthetase (EMD Millipore, MAB302) 1:700, mouse anti–Zpr-1 (Fret43, a commonly used marker labeling red-green double cones; Larison and Bremiller, 1990; Zebrafish International Resource Center) 1:400, chicken anti-EAAT2a 1:100, and guinea pig anti-EAAT2b 1:100. The immunoreaction was then detected using fluorescently labeled secondary antibodies (goat anti-mouse Alexa Fluor 488 or 568, goat anti–guinea pig Alexa Fluor 488 or 568, all from Invitrogen, and rabbit anti-chicken IgY Cy5 from Jackson ImmunoResearch or rabbit anti-chicken Alexa Fluor 488 from Invitrogen) diluted 1:1000 in PBS. Bodipy TR Methyl Ester (Invitrogen) was used to counterstain green fluorescence. It was applied 1:300 in PDT (PBS with 1% DMSO and 0.1% Triton) for 20 min after washing the secondary antibodies.

Slides were coverslipped and imaged with a SP5 and a TCS LSI confocal microscope (both Leica Microsystems). Images were then processed with Imaris (Bitplane) and postprocessed using Gimp imaging processing software, Adobe Photoshop, and Adobe Illustrator CS5.

Histology

Whole larvae were fixed in 4% PFA overnight at 4°C. Larvae were dehydrated in series of increasing ethanol concentrations in PBS (50%, 70%, 80%, 90%, 95%, and 100% ethanol). After dehydration, larvae were incubated in a 1:1 ethanol Technovit 7100 (Heraeus Kulzer) solution (1% Hardener 1 in Technovit 7100 basic solution) for 1 h followed by incubation in 100% Technovit solution overnight at room temperature. Larvae were then embedded in plastic molds in Technovit 7100 polymerization medium and dried at 37°C for 1 h. 3-μm-thick sections were prepared with a microtome, mounted onto slides, and dried at 60°C. Sections were stained with Richardson–Romeis (0.5% borax, 0.5% Azur II, 0.5% methylene blue), and slides were mounted with Entellan (Merck). Images were taken in the bright-field mode of a BX61 microscope (Olympus).

Gene knockdown

Two different EAAT2a translation-blocking morpholinos were used for injections into the one-cell stage of the zebrafish embryo. Titration injections were performed to find the optimal dose with highest knockdown efficiency but no toxic side effects. For EAAT2a morpholino 1, CATCATCCACAACTGTCAGGCTGGC (position –22 to –03), the injected amount was 1.3 ng. For EAAT2a morpholino 2, CGTGCTTCGGCATCATCCACAACTG (position –12 to –13), two different amounts were injected, 1.8 and 3.6 ng (referred to as low and high dose, respectively). EAAT2b morpholino 1, GATCTCCACTTGCTTCTGCATCTTC (position –04 to –21), was injected at a dose of 1.8 ng, and morpholino 2, GAGTTTCACAACAGTTTGCTAGACA (position –65 to –41), was injected at a dose of 9 ng.

Before dilution, stock morpholinos were heated to 65°C for 5 min and subsequently diluted with nuclease free H_2O to the desired concentration (injection mix contained 0.04% phenol red for color indication). The injection amount was 1 nl. The standard control morpholino was injected into sibling embryos. Injected embryos were raised in E3 containing methylene blue at 28°C until 5 dpf.

Efficiency of knockdown was quantified by measuring the fluorescence of antibody staining on wild-type (WT) and morphant retinal sections (imaged with the same confocal microscope settings). For EAAT2a, a region of interest (ROI) reaching from photoreceptors to basal processes of Müller cells was selected to measure the fluorescence. For EAAT2b, the ROI was placed over an area

of the outer plexiform layer (OPL). Because EAAT2b staining is present only in OPL, background fluorescence [ROI set on inner nuclear layer (INL)] was subtracted from fluorescence in OPL. Two ROIs were set per animal. One-way ANOVA with Tukey *post hoc* test was performed to statistically analyze the difference in fluorescence.

Assessment of retinal morphology in WT and EAAT2 knockdown animals

Retinal morphology of EAAT2a and EAAT2b morphant and WT animals was analyzed on cryosections, and several parameters were statistically compared. 5-dpf WT ($n = 13$) and larvae injected with EAAT2a MO 1 (1.3 ng; $n = 13$), EAAT2a MO 2 ($n = 12$), EAAT2b MO 1 (1.8 ng; $n = 13$), and EAAT2b MO 2 (9 ng; $n = 13$) were fixed, embedded in cryomatrix, and sectioned at 16 μm before immunofluorescent staining with Zpr-1 (EAAT2b morphants) and glutamine synthetase (EAAT2a morphants; see Materials and Methods, "Immunohistochemistry"). The retinal thickness was measured on confocal images using Fiji software. Retinal thickness was assessed on three different locations per larva. The average of the three measurements was used for statistical analysis. The length of Müller cells (in EAAT2a morphants) as well as the overall cone length (EAAT2b morphants) was assessed the same way. In total, three cones and three Müller cells per larvae were analyzed (same sample sizes as for retinal thickness analysis), and the average of the three measurements was used for statistical analysis. One-way ANOVA followed by Tukey *post hoc* test was performed using SPSS.

Electroretinography

ERG recordings were performed on 5-d-old morphant larvae of either sex and their control injected siblings as previously described by Makhankov et al. (2004) with some minor adaptations. Larvae were dark-adapted for at least 30 min, and all preparations before the actual recording were done under a red light, preventing bleaching of photoreceptors. The larval eye was removed from the eyecup and placed onto filter paper on top of a 1.5% agarose gel in E3, in which the reference electrode was inserted. The recording electrode (micropipette filled with E3) was placed onto the center of the cornea. 100-ms light stimuli of five different intensities (log-4 to log0) were given with an interstimulus interval of 7 s. The light intensity of log0 corresponds to 6800 lux or 75 W/m^2.

b-wave amplitudes and the time from light onset to the b-wave peak were compared using mixed repeated-measures ANOVA followed by Tukey and Games–Howell *post hoc* test. Results are shown in a box-and-whisker plot (b-wave amplitudes and time from light onset to peak), where the bottom and top of the box represent the first and third quartile, respectively, with the median represented as a line within the box and whiskers reaching to minimum and maximum values obtained.

Oocyte experiments

Xenopus oocytes were purchased from Ecocyte Bioscience or were obtained from the Institute of Physiology, University of Zurich. The oocytes were kept at 16°C for 2–5 d. Capped cRNA was microinjected into *Xenopus* oocytes (40–80 ng per oocyte), and membrane currents were recorded 2–4 d later.

With the exception of the chloride-free solution, the extracellular recording solution comprised (in mM) 96 NaCl, 2 KCl, 1.8 $CaCl_2$, 1 $MgCl_2$, and 5 HEPES, pH 7.5. L-Glutamate was obtained from Sigma; DL-TBOA (DL-threo-β-benzyloxyaspartic acid) was obtained from Tocris. For chloride-free solutions, all chloride salts were replaced with gluconate salts. To increase the uncoupled current, the oocytes were dialyzed in chloride-free solution for 24 h, and the recordings were then performed in a solution in which chloride was substituted with the more permeant ion SCN^-. The approximated chloride equilibrium potential, E_{Cl^-}, for the injected oocytes was estimated by calculating the reversal potential of $I_{Cl(Ca)}$ induced by 4-Br A23187 (Sigma), a calcium ionophore, as described by Wadiche et al. (1995).

Radiolabeled glutamate uptake was performed under voltage clamp at −60 mV (or −15 mV when uptake at the chloride equilibrium potential was investigated). Currents were recorded during application of 100 μM [^{3}H]L-glutamate for 100 s. The specific activity of the [^{3}H]L-Glutamate in this solution was 20 Ci/mol. For control, we used the same protocol on uninjected oocytes. After application of [^{3}H]L-glutamate, oocytes were first washed in Ringer solution and then lysed in a scintillation vial containing 2% SDS. Radioactivity was later measured. Two-electrode voltage-clamp recordings were performed using a Turbo Tex-03x amplifier (NPI), and signals were acquired with a Digidata 1440A (Molecular Devices). Recording electrodes with resistance <1 MΩ contained 3 M KCl. Currents were acquired at 10 kHz and low-pass filtered at 20 or 500 Hz in dependence of the recording protocol.

Data analysis was performed using Axon pClamp10 and GraphPad Prism software. To determine K_m, dose–response curves were fitted with the Michaelis–Menten relationship included with the GraphPad Prism software, $Y = I_{max} \times X/(K_m + X)$, where I_{max} is the maximum current in the same units as Y and K_m is the Michaelis–Menten constant, in the same unit as X.

Results

EAAT2 paralogs are complementarily expressed in the retina

A phylogenetic analysis of excitatory amino acid transporter genes revealed that the zebrafish genome harbors two *eaat2* (also called *glt-1* or *slc1a2*) genes (Gesemann et al., 2010a). Analyzing the transcript expression of the two transporters in the zebrafish retina, we found strong *eaat2a* expression in the INL in close proximity to the inner plexiform layer (IPL) and additionally very weak expression in photoreceptors (Fig. 1*A*, *B*). In contrast, *eaat2b* mRNA was present in the photoreceptor cell layer and in low concentration in the INL (Fig. 1*C*, *D*). Staining in the photoreceptor layer was present throughout all cone photoreceptors; however, the layer containing nuclei of rods was unstained, suggesting *eaat2b* to be cone specific.

To confirm cellular identity and obtain information about subcellular distribution of the protein, we generated paralog-

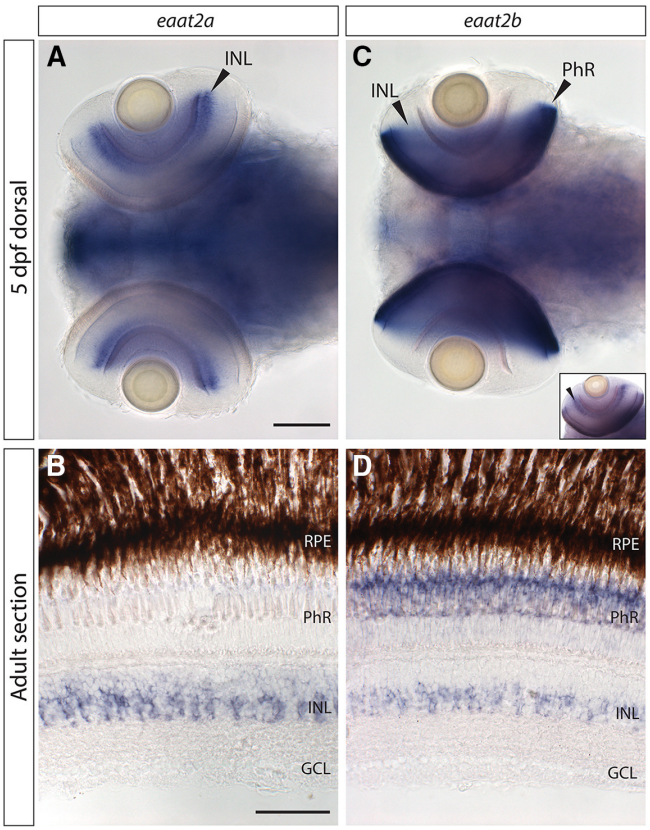

Figure 1. Transcript expression of excitatory amino acid transporter 2 (*eaat2*) paralogs. ***A***, ***B***, *eaat2a* mRNA is strongly expressed in the inner nuclear layer (INL) in the retina, in both 5-d postfertilization (5-dpf) larvae (***A***) and adult retina (***B***). Additionally, extremely low transcript levels can be found in photoreceptors (***B***). ***C***, ***D***, mRNA of *eaat2b* is expressed in photoreceptors and weakly in the INL throughout different developmental stages (***C***, in 5-dpf larvae; ***D***, in adult retinal sections). Small inset in ***C*** shows *eaat2b in situ* staining in an eye of a whole-mount larva that has been only shortly stained, to better visualize expression in the INL. Scale bar in ***A*** is 100 μm; also applies to ***C***. Scale bar in ***B*** corresponds to 50 μm; also applies to ***D***.

specific peptide antibodies. Consistent with the *in situ* hybridization data, immunostainings against EAAT2a on larval and adult retinal sections revealed expression of EAAT2a in Müller glia cell membranes (Fig. 2*A–F*). EAAT2a seems to be specific to Müller cells, as no immunofluorescent signal could be detected in photoreceptors. The staining intensity within Müller glia cells appeared increased in the OPL and IPL, where glutamatergic synapses are tightly ensheathed by Müller glia cells. The nature of the labeled cells was confirmed by double-labeling with the glial marker glutamine synthetase, which colocalizes with EAAT2a (Fig. 2*A*, *D*). Consistent with the mRNA distribution, we found dotted antibody staining against EAAT2b protein in the OPL (Fig. 2*G–N*). The appearance of the staining indicated localization of EAAT2b in cone pedicles, whereas rod spherules were devoid of EAAT2b protein. To further characterize the photoreceptor subtype-specific expression, we used transgenic fish lines expressing GFP in different photoreceptor cell types [Tg(zfSWS1–5.5A:EGFP), Tg(zfSWS2–3.5A:EGFP), Tg(zfRh1-3:EGFP); Hamaoka et al., 2002; Takechi et al., 2003, 2008]. EAAT2b is expressed in the presynaptic terminal of all cone subtypes (UV-, blue-, red-, and green-sensitive cones; Fig. 2*G–I*, *K–M*); however, consistent with the *in situ* hybridization results, rod terminals do not express this transporter (Fig. 2*J*). Remarkably, no EAAT2b immunofluorescence could be observed in cells of the INL, suggesting that local protein concentrations in the membranes of these cells are rather low, preventing immunostaining.

EAAT2 paralogs differentially shape signal transmission in the cone synapse

To characterize the function of EAAT2 transporters in zebrafish vision, we generated knockdown larvae using different morpholino antisense oligonucleotides. Quantification of fluorescence intensities in morphant and WT eyes demonstrated the efficiency of protein knockdown in 5-dpf larvae (Fig. 3).

Both EAAT2a- and EAAT2b-deficient animals showed no apparent overall morphologic abnormalities (Fig. 4*A–C*, *G–I*) or abnormalities in the cell shape of Müller glia cells (Fig. 4*D–F*) or red and green cones (Fig. 4*J–L*). Statistical analysis confirmed this assessment, as no sig-

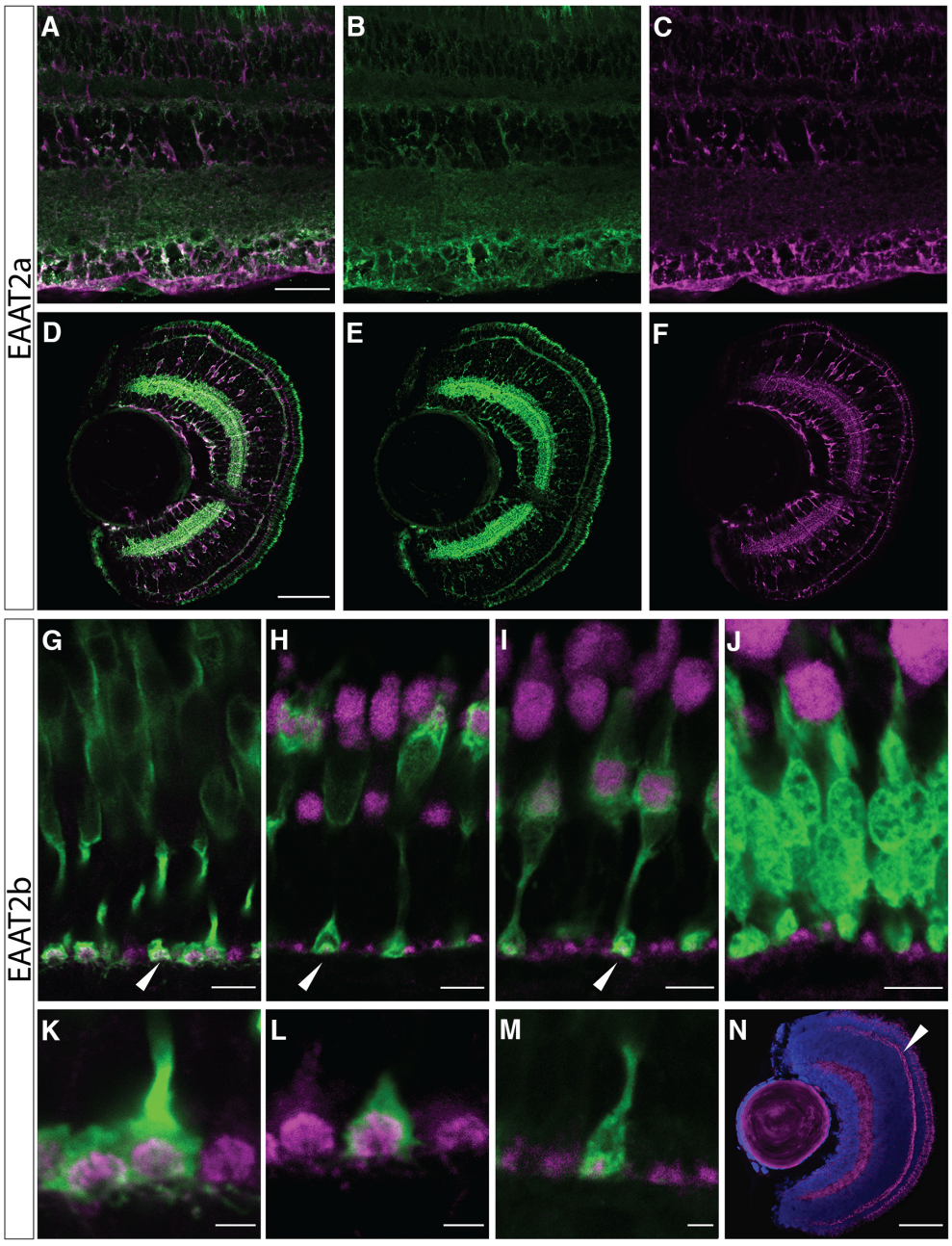

Figure 2. Protein expression of EAAT2 paralogs. ***A–F***, Double immunostaining of EAAT2a (green) and glutamine synthetase (magenta) in adult (***A***) and larval (5 dpf; ***D***) retinal sections confirm expression of EAAT2a in Müller glia cells. Separated channels are shown in ***B*** (adult), ***E*** (5 dpf; EAAT2a, green channel only), ***C*** (adult), and ***F*** (5 dpf; glutamine synthetase, magenta channel only). Scale bar in ***A*** is 30 μm; also applies to ***B*** and ***C***. Scale bar in ***D*** is 50 μm; also applies to ***E*** and ***F***. ***G–N***, EAAT2b protein is expressed in a dotted manner in the outer plexiform layer (OPL) in all cone pedicles, but it is not expressed in rods. EAAT2b antibody staining (magenta) on adult retinal sections stained with Zpr-1 (red-green double cones, ***G***) and on retinal sections of zebrafish expressing GFP in blue cones (***H***), UV cones (***I***), and rods (***J***) confirms that EAAT2b is cone specific and is spared from rod spherules. ***K–M*** show zoom-ins of the cone pedicles expressing EAAT2b (magenta) in red-green double cones (***K***), blue cones (***L***), and UV cones (***M***). ***N*** shows larval (5 dpf) expression of EAAT2b in magenta together with a nuclear counterstain (DAPI, blue). Scale bars in ***G–J*** are 7 μm. Scale bars in ***K–M*** are 2 μm. Scale bar in ***N*** is 30 μm.

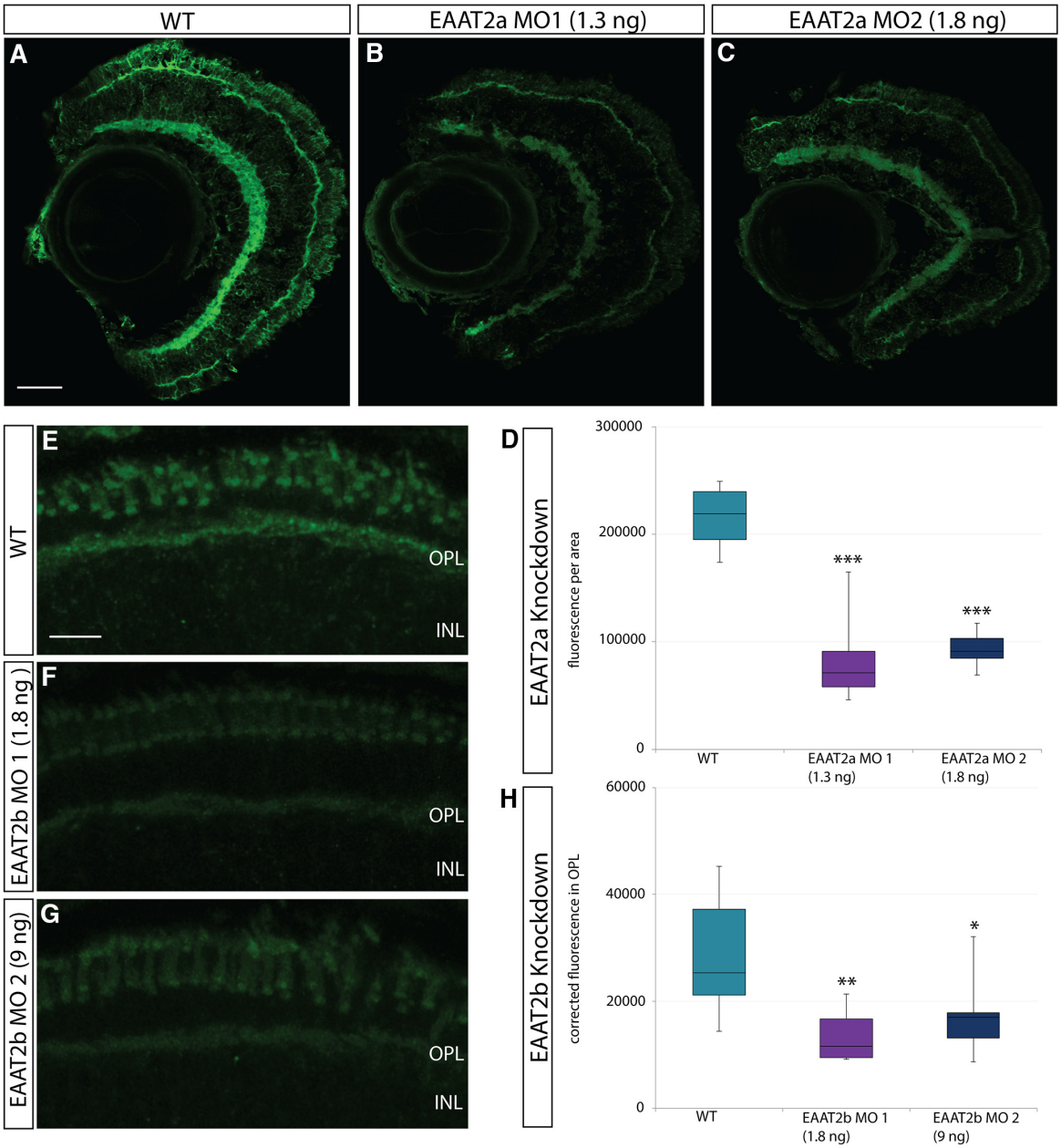

Figure 3. Confirmation of knockdown. ***A–C***, Immunostaining of EAAT2a on WT (***A***) and EAAT2a morphant [***B***, 1.3 ng EAAT2a morpholino (MO) 1; ***C***, 1.8 ng EAAT2a MO 2] retinal sections (5 dpf). ***D***, Box-and-whisker plot of analysis of fluorescence of WT, EAAT2a MO 1, and EAAT2a MO 2 injected animals stained with anti-EAAT2a antibody. Statistical analysis reveals a highly significant ($p < 0.001$) reduction of fluorescence for both MOs. ***E–G***, Retinal sections of WT (***E***) and EAAT2b morphant (***F***, 1.8 ng EAAT2b MO 1; ***G***, 9 ng EAAT2b MO 2) larvae stained with anti-EAAT2b antibody. ***H***, Fluorescence was measured in the OPL, and background fluorescence (taken from area in INL) was subtracted. Fluorescence of WT and morphant immunostaining is plotted in a box-and-whisker plot and shows a significant ($p < 0.01$) and slightly significant ($p < 0.05$) decrease in fluorescence in animals injected with 1.8 ng EAAT2b MO 1 and 9 ng EAAT2b MO 2, respectively. EAAT2a WT, $n = 6$; EAAT2a MO 1, $n = 8$; EAAT2a MO 2, $n = 8$; EAAT2b WT, $n = 10$; EAAT2b MO 1, $n = 10$; EAAT2b MO 2, $n = 10$. Scale bar in ***A*** is 30 μm; also applies to ***B*** and ***C***. Scale bar in ***E*** is 10 μm; also applies to ***F*** and ***G***.

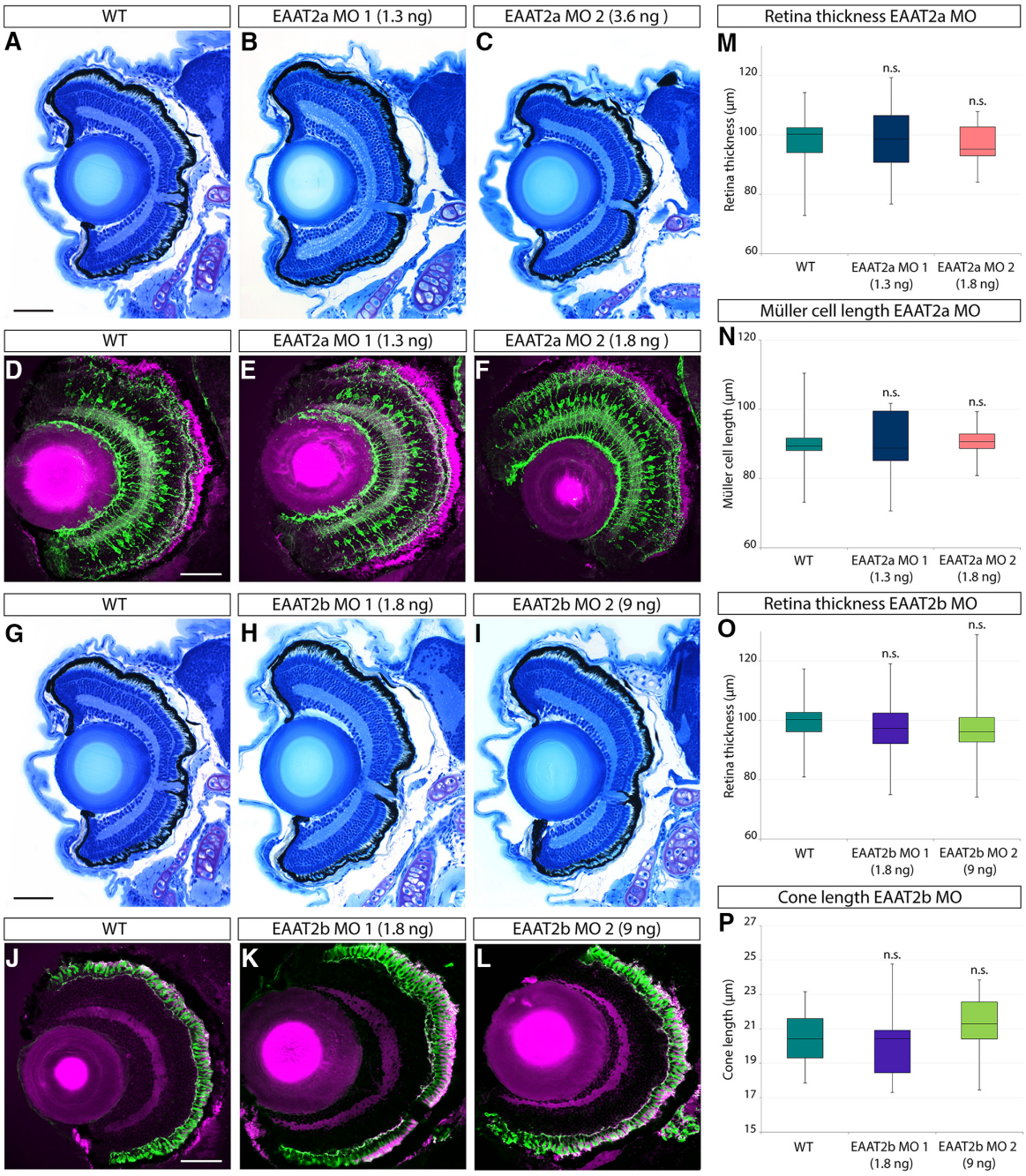

Figure 4. Retinal histology of EAAT2 morphant zebrafish larvae. Histologic analysis of retinal sections of WT, EAAT2a, and EAAT2b morphant zebrafish larvae (5 dpf) stained with Richardson–Romeis (***A–C*** and ***G–I***). Immunostaining of glutamine synthetase (green) labeling Müller glia cells counterstained with Bodipy (magenta; ***D–F***) of WT and EAAT2a morphant (***E***, EAAT2a MO 1; ***F***, EAAT2a MO 2) 5-dpf retinal sections. Anti–Zpr-1 immunostaining (labeling red and green cones, shown in green) on WT (***J***) and EAAT2b morphant (***K***, EAAT2b MO 1; ***L***, EAAT2b MO 2) retinal sections counterstained with Bodipy (magenta). Knockdown of neither EAAT2a (***B***, EAAT2a MO 1; ***C***, EAAT2a MO 2) nor EAAT2b (***H***, EAAT2b MO 1; ***I***, EAAT2b MO 2) causes any defect in retinal lamination. Thickness of the retina was assessed on WT and morphant larvae and did not reveal any significant difference in the thickness of the retina in either EAAT2a or EAAT2b morphants (***M***, ***O***), yielding *p* values of 0.997 and 0.935 for EAAT2a MO 1 and EAAT2a MO 2, respectively, and 0.658 and 0.922 for EAAT2b MO 1 and EAAT2b MO 2 (all in comparison to WT). Moreover, knockdown of EAAT2a does not significantly influence Müller glia cell length

continued
(***N***), nor does the loss of EAAT2b result in cone length alteration (***P***). Statistical analysis of the cell length yielded *p* values of 0.969 and 0.989 for EAAT2a MO 1 and EAAT2a MO 2, respectively, and 0.911 and 0.631 for EAAT2b MO 1 and EAAT2b MO 2 (in comparison to WT). All scale bars are 50 μm. Scale bar in ***A*** also applies to ***B*** and ***C***; scale bar in ***D*** also applies to ***E*** and ***F***; scale bar in ***G*** also applies to ***H*** and ***I***; and scale bar in ***J*** also applies to ***K*** and ***L***.

nificant difference in retinal thickness between WT and EAAT2a (Fig. 4*M*) or EAAT2b morphant larvae (Fig. 4*O*) could be detected. Furthermore, neither the length of Müller cells (Fig. 4*N*) nor that of cones (Fig. 4*P*) was influenced by knockdown of EAAT2a and EAAT2b, respectively, indicating that the knockdown does not impair retinal development. However, EAAT2a morphant larvae displayed behavioral changes (no quantifications done) and abnormal body bends, similar to the ones described in *tnt* mutants that carry a point mutation in *eaat2a* (McKeown et al., 2012).

To analyze the functional role of EAAT2 in the zebrafish retina, we performed ERG on 5-d-old morphant larvae. The ERG measures the sum field potential generated by retinal cells on light exposure. We used the amplitude of the b-wave at varying light intensities as a functional readout of outer retinal function. The b-wave reflects the activation of ON bipolar cells after photoreceptor hyperpolarization after a light stimulus. In a typical WT ERG, the large b-wave masks the a-wave, resulting in no or only a tiny a-wave visible. At 5 d, rods are not yet functionally integrated into the larval retina; therefore, the measured light responses are exclusively cone driven (Branchek, 1984; Branchek and Bremiller, 1984). To analyze the ERG kinetics, the time from light stimulus onset to the peak of the b-wave was compared between control and morphant animals.

Loss of EAAT2a leads to a reduction of the ON response. EAAT2a-deficient larvae showed a highly significant reduction in b-wave amplitude throughout all different light intensities tested, indicating that this glial transporter is fundamental for uptake of the synaptic glutamate (Fig. 5*A*). b-wave amplitudes of larvae injected with 1.3 ng morpholino 1 or low-dose morpholino 2 were diminished by >40% throughout all different light intensity flashes. b-wave amplitudes of larvae injected with high-dose morpholino 2 showed a reduction of 75% or more in comparison to WT and control injected larvae. Furthermore, we show a clear dose dependence of morpholino 2, leading to significant differences in the b-wave amplitude between low- and high-dose EAAT2a morphants. This was observed for all light intensities except the lowest intensity stimulus (log-4). However, even at high doses of injected EAAT2a morpholino, we could still observe a small ERG b-wave, indicating that there is either no complete protein knockdown or that different glutamate transporters present at the first visual synapse take over a comparable function.

In contrast to EAAT2a, knockdown of EAAT2b resulted in only a mild ERG phenotype. The medians of ERG b-wave amplitudes of EAAT2b morphant larvae were slightly reduced compared with WT and control morphant ERG, but were statistically significant only for some light intensities (see legend, Fig. 5*B*).

To artificially augment glutamate concentrations in the cleft and disrupt the glutamate–glutamine cycle between photoreceptors and Müller glia cells, double injections of 1.3 ng EAAT2a and 9 ng EAAT2b morpholino were performed. Interestingly, except for dim light conditions, b-wave amplitudes of double-knockdown larvae were significantly lower than those of EAAT2a morphants (Fig. 5*C*). This nicely demonstrates the function of EAAT2b by illustrating that glutamate clearing capacity has further been neutralized in the EAAT2 double morphants.

Knockdown of EAAT2a affected not only the b-wave amplitude, but also its kinetics. In general, the ERG response in EAAT2a-depleted animals was slower (representative ERG traces shown in Fig. 5*D*) than in WT or control animals (Fig. 5*E*). The time to peak at low light intensity stimuli (log-4) was significantly increased in EAAT2a-depleted larvae. Also at bright light (log0), the ERG response was still decelerated, resulting in a significant increase in the time to peak in EAAT2a-depleted animals (Fig. 6*A*, *B*). Because ON bipolar cell activity is decreased and delayed in EAAT2a morphants, the b-wave no longer dominates the a-wave. Therefore, the a-wave (electronegative wave preceding the positive b-wave) becomes apparent in an EAAT2a morphant ERG (Fig. 5*E*). ERG kinetics in EAAT2b-depleted larvae is unaffected (Fig. 6*C*, *D*; representative ERG traces are shown in Fig. 5*F*).

Biophysical properties of EAAT2 paralogs

Glutamate uptake by EAAT proteins is electrogenic, being associated with the movement of charges through the cell membrane: three Na^+ ions and one proton enter the cell for each transport cycle, and one K^+ ion moves out (Zerangue and Kavanaugh, 1996; Levy et al., 1998; Owe et al., 2006). In addition, on binding of glutamate and sodium, a thermodynamically uncoupled chloride current is associated with these transporters (Fairman et al., 1995; Wadiche and Kavanaugh, 1998). These intrinsic electrogenic properties of glutamate transporters allow evaluation of their electrical properties by expressing them in *Xenopus* oocytes.

Approximately 48 h after microinjection of *eaat2a* or *eaat2b* mRNA, *Xenopus* oocytes displayed glutamate-evoked currents (I_{Glu}) that were absent in uninjected oocytes. In oocytes voltage-clamped to negative potentials, increasing doses of glutamate evoked an increasing inward current (Fig. 7*A*, *B*, insets). The normalized amplitude of I_{Glu} for different glutamate concentrations was fitted with the Michaelis–Menten equation (Fig. 7*A*, *B*) to yield a K_m of 19.6 $\pm$ 2.7 μM (n = 6) for EAAT2a and 3.1 $\pm$ 0.6 μM (n = 8) for EAAT2b (see Materials and Methods). When voltage-clamping the oocytes to different potentials and measuring I_{Glu} in the steady state, we found that at sufficiently positive potentials, I_{Glu} reversed for both

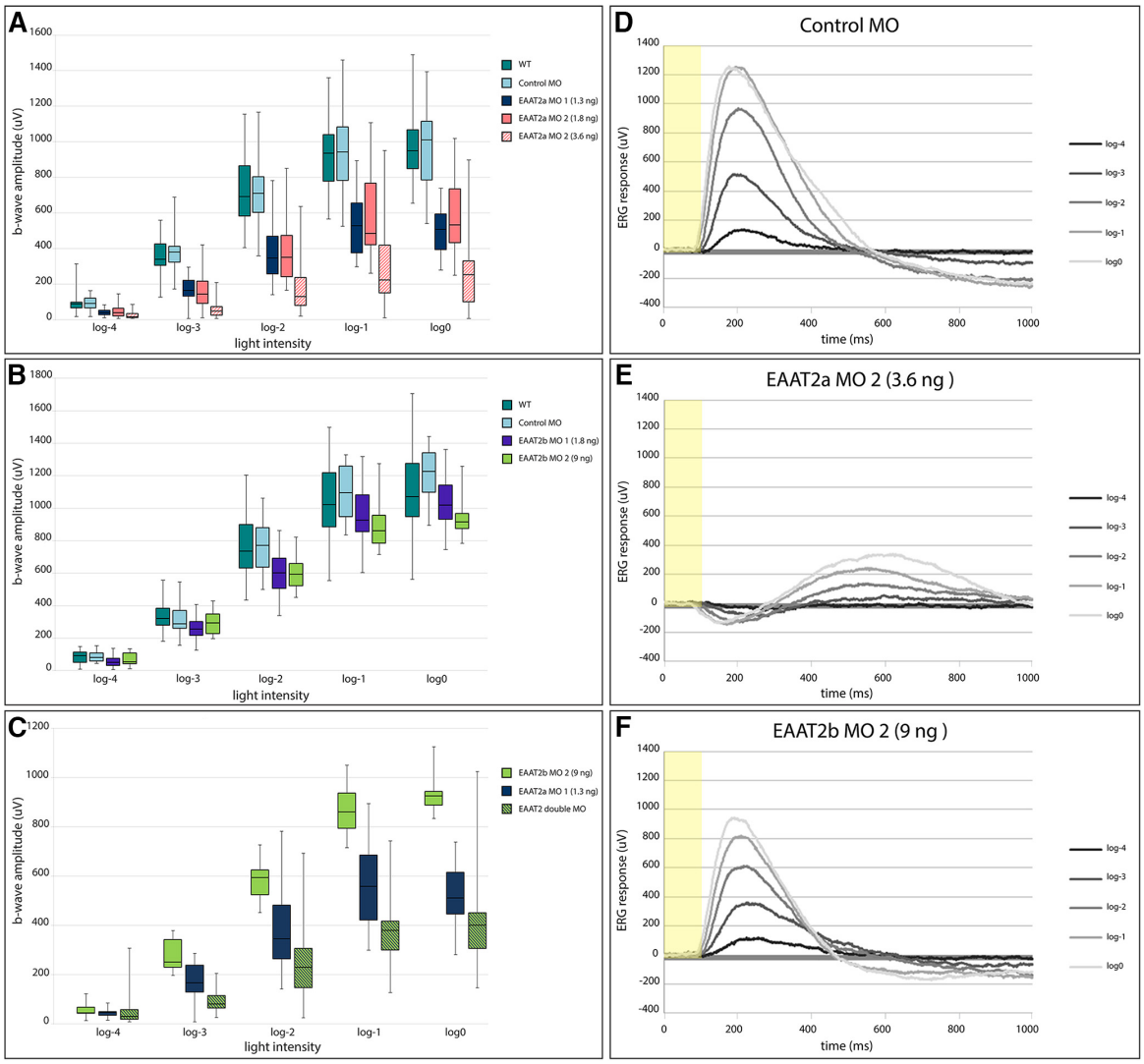

Figure 5. Box-and-whisker plots of ERG b-wave amplitudes of EAAT2a and EAAT2b morphant zebrafish larvae and representative ERG traces. ***A***, Knockdown of EAAT2a results in a highly significant ($p < 0.001$) reduction of the ERG b-wave amplitude in comparison to both WT and control injected animals throughout all light intensities (log-4 to log0). For EAAT2a MO 2, we could demonstrate a dose dependence, resulting in a highly significant difference ($p < 0.001$) between the low dose (1.8 ng) and the high dose (3.6 ng) for the bright light intensities (log-1 and log0) and a significant difference ($p < 0.01$) for the medium light intensities (log-3 and log-2). WT, $n = 33$; control MO, $n = 25$; EAAT2a MO 1, $n = 23$; 1.8 ng EAAT2a MO 2, $n = 27$; 3.6 ng EAAT2a MO 2, $n = 24$. ***B***, Knockdown of EAAT2b only mildly interferes with the ERG b-wave. There is an overall tendency in EAAT2b-depleted animals to have a slightly reduced ERG b-wave amplitude. This results in a slight statistical significance ($p < 0.05$) between WT and EAAT2b morphant (MO 1) at log-4 and a highly significant ($p < 0.001$) reduction at log-3 and log-2. Further, there is a slightly significant ($p < 0.05$) reduction between EAAT2b morphants (MO 1) and control morphants for log-2. When using EAAT2b MO 2, we obtained a significant ($p < 0.01$) reduction of the ERG b-wave amplitude in comparison to control morphants at log0 and in comparison to WT at log-2. WT, $n = 39$; control MO, $n = 11$; EAAT2b MO 1, $n = 39$; EAAT2b MO 2, $n = 16$. ***C***, The function of EAAT2b could be demonstrated by double knockdown of both EAAT2 paralogs. Under such conditions, when glutamate uptake by Müller glia cells was impaired, we could show an even further reduction of the ERG b-wave amplitude in the double morphants in comparison to EAAT2a morphant larvae [slightly significant ($p < 0.05$) at log0, significant ($p < 0.01$) at log-1, and highly significant ($p < 0.001$) at log-3 and log-2]. EAAT2a MO 1, $n = 23$; EAAT2b MO 2, $n = 16$; double MO, $n = 32$. ***D–F***, Representative ERG traces of control MO injected larvae (***D***), EAAT2a morphant (***E***, high dose of MO 2), and EAAT2b morphant (MO 2) larvae (***F***). Yellow bar represents light stimulus (starting at time 0, ending at 100 ms).

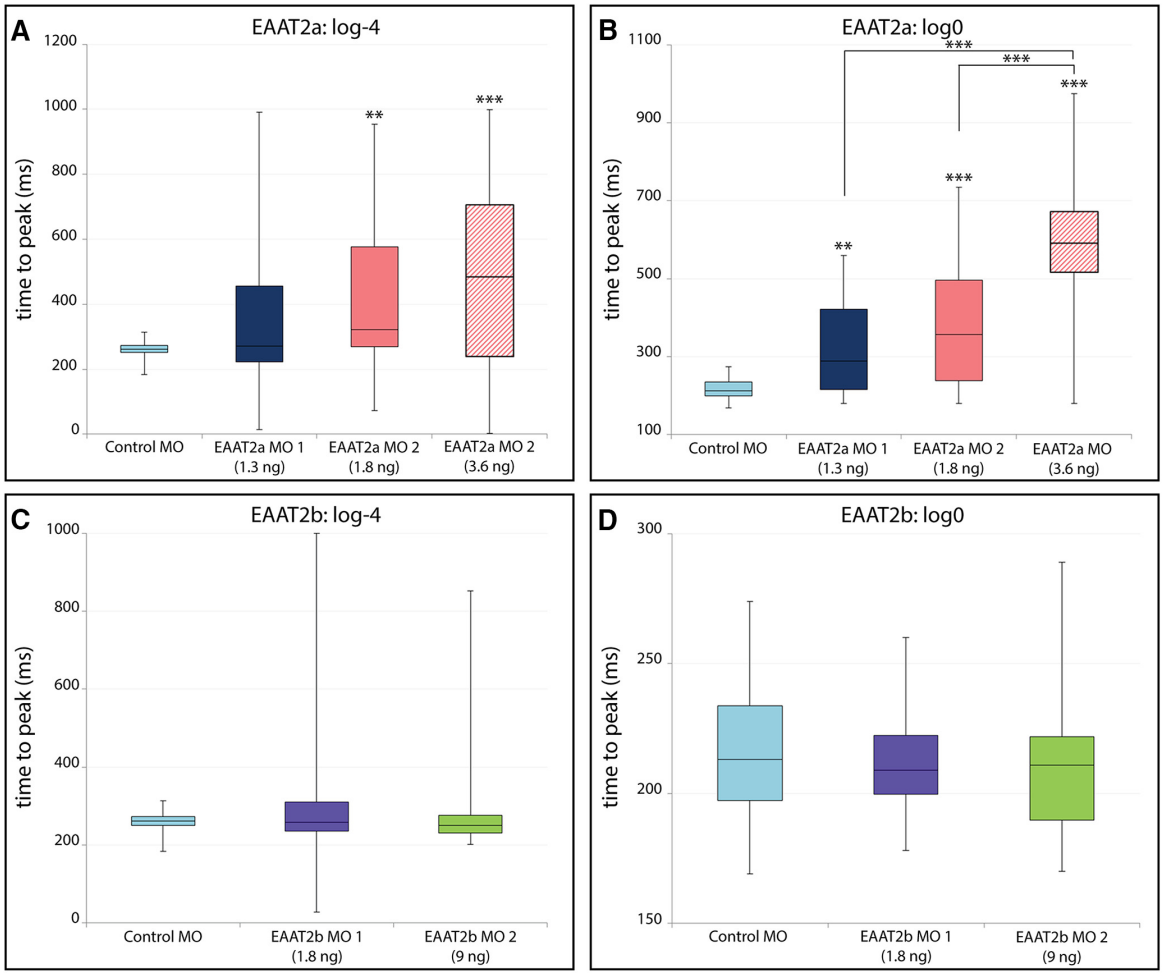

Figure 6. Time-to-peak analysis of ERG recordings. Box-and-whisker plots of time (ms) from onset of light stimulus (0 ms) to the peak of the b-wave. EAAT2a morphant larvae display changed ERG kinetics. At low light levels (***A***), low and high doses of EAAT2a MO 2 result in significant ($p < 0.01$) and highly significant ($p < 0.001$) increases in the time to peak, respectively. At bright light levels (***B***), EAAT2a morphant (MO 1) larvae show a significant ($p < 0.01$) increase in the time to peak, whereas both levels of MO 2 result in a highly significant ($p < 0.001$) increase in the time to peak. ERG response of EAAT2b morphant fish was not decelerated in dim light conditions (***C***) or in bright light (***D***).

EAAT2a- and EAAT2b-injected oocytes (Fig. 7*C*, *D*, black). This outward current was more prominent for EAAT2b-expressing oocytes. Such an outward current has been described for human EAAT1 and EAAT3 and salamander sEAAT1, sEAAT2, and sEAAT5 (Eliasof and Werblin, 1993; Wadiche et al., 1995; Eliasof et al., 1998a, b) and shown to be due to the uncoupled chloride conductance that is associated with the transporter itself.

The more prominent outward current in EAAT2b-injected oocytes suggested that a larger chloride conductance was associated with this paralog. To verify this hypothesis, we recorded I_{Glu} in a bath solution in which chloride was substituted with gluconate. Gluconate cannot permeate the chloride channel; therefore, for potentials that are positive to the chloride equilibrium potential, no current carried by an inward chloride flux should be recorded. For EAAT2a-injected oocytes, there was no difference between the glutamate current recorded in control solution and that recorded in chloride-free solution (Fig. 7*C*). Conversely, for EAAT2b-injected oocytes, the glutamate-induced outward current was abolished at positive potentials when recorded in a gluconate-based solution, whereas the inward current was only minimally affected (Fig. 7*D*). The chloride current is therefore a significant component of the total glutamate-induced current.

To estimate how much of the total I_{Glu} was due to the uncoupled chloride component, we calculated the charge-to-flux ratio (the charge transferred per molecule of glutamate taken up), using bath-applied tritiated gluta-

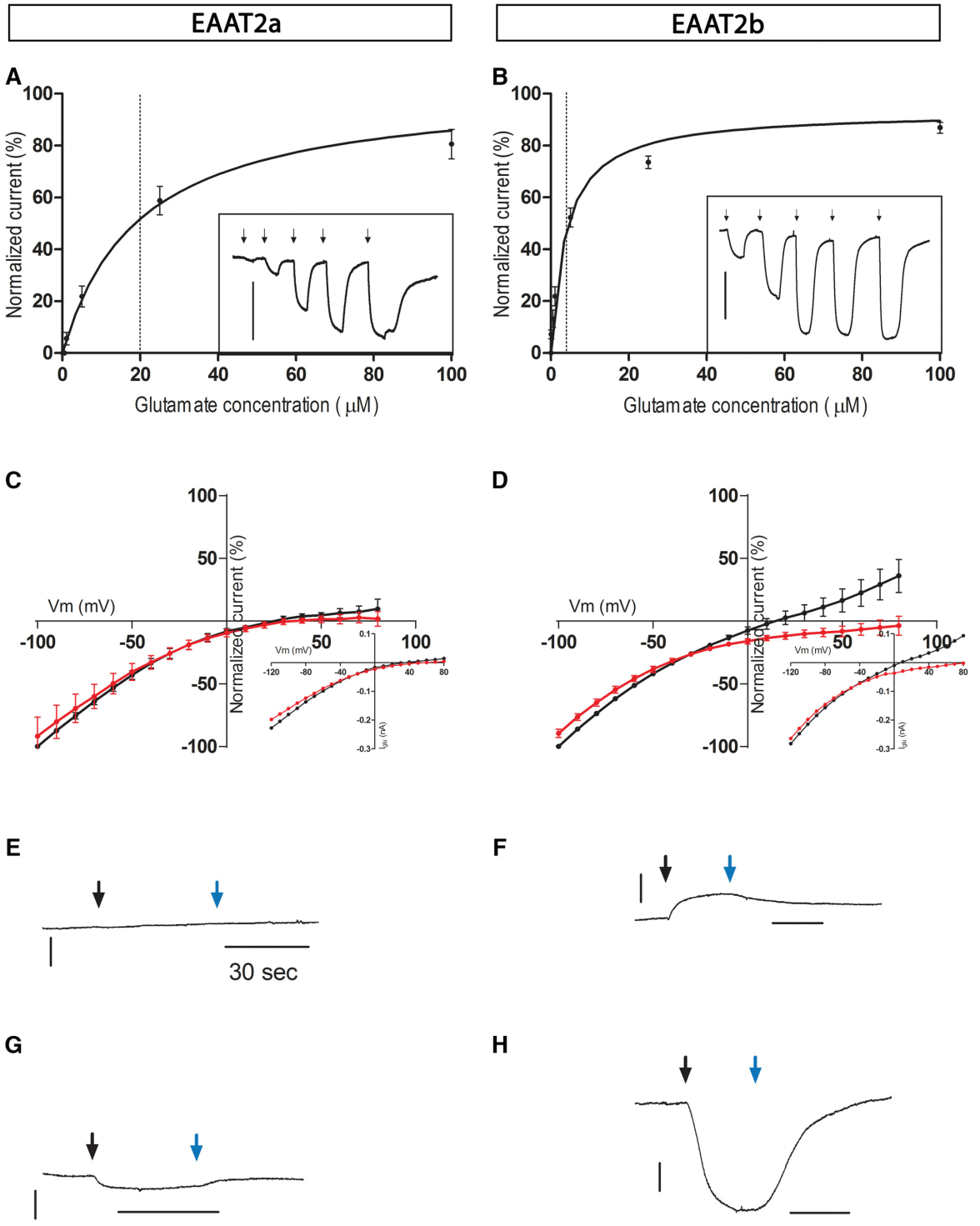

Figure 7. Two-electrode voltage clamp recordings from EAAT2a- and EAAT2b-expressing oocytes. ***A***, ***B***, Glutamate-evoked currents normalized to the saturating current induced by 500 μM glutamate in EAAT2a-expressing (***A***) and EAAT2b-expressing (***B***) oocytes (n = 8) and fitted with the Michaelis–Menten equation. The oocytes were voltage clamped at –50 mV. For clarity, fitted curves were

continued
plotted only up to 100 μM. In the insets, inward currents were induced by increasing concentrations of L-glutamate (1, 5, 25, 100, and 500 μM) in representative oocytes. The arrows indicate when glutamate was applied. Scale bar is 20 nA. ***C***, ***D***, Voltage dependence of EAAT2a-mediated (C) and EAAT2b-mediated (D) currents ($n = 5$) induced by 100 μM L-glutamate in control solution (black) and a chloride-free solution (red). The data from each cell were normalized to the response elicited by 100 μM L-glutamate in control solution at −100 mV. Insets show I-V recordings from representative oocytes in normal buffer. Data under both conditions are recorded from the same cells; oocytes are from three different batches. ***E–H***, TBOA reveals a leak current. TBOA (100 mM) was applied alone (black arrow) in control medium to EAAT2a (***E***) and EAAT2b (***F***) injected oocytes. In EAAT2b injected oocytes, it evoked an outward current. When oocytes were dialyzed with a chloride-free solution for 24 h and the control perfusing medium was exchanged with a solution containing SCN^- as the main negative ion, TBOA induced an inward current in EAAT2a and EAAT2b injected oocytes (***G***, ***H***). Blue arrows indicate wash from TBOA. Scale bar is 10 nA.

mate. This ratio is independent of functional expression-level efficiency and provides a reliable measure of the current elicited by each molecule of glutamate. At a holding potential of −60 mV, the calculated charge-to-flux ratios were significantly different ($p < 0.0008$, two-tailed *t* test) for EAAT2a (1.7 ± 0.4, $n = 8$) and EAAT2b (4.5 ± 1.7, $n = 8$) injected oocytes.

However, at this potential, the recorded current is due to both the chloride conductance and the stoichiometrically transported ions (Na^+, K^+, and H^+). To confirm that the difference between the two ratios was indeed due to chloride flux, we repeated the uptake experiment at −15 mV, the calculated chloride equilibrium potential (see Materials and Methods). The charge-to-flux ratio did not differ for the two transporters (1.2 ± 0.2 for EAAT2a and 1.3 ± 0.3 for EAAT2b) at this potential. Therefore, we concluded that the observed difference in charge-to-flux ratio at −60 mV was indeed due to differences in chloride conductance. Moreover, the charge-to-flux ratio at −60 mV for EAAT2a was not significantly different from the uptake at −15 mV (ANOVA plus Tukey *post hoc* test), which indicated that the larger charge-to-flux ratio measured at −60 mV with EAAT2b-injected oocytes was mostly due to uncoupled chloride current.

EAAT2a and EAAT2b differ in their leak currents

To determine whether currents were induced only by the ligand glutamate, we checked whether DL-TBOA, a nontransportable antagonist, could block I_{Glu} in EAAT2a- and EAAT2b-injected oocytes. DL-TBOA blocked the glutamate-induced current as expected, but also revealed a current in EAAT2b (not in EAAT2a) injected oocytes in the absence of glutamate (Fig. 7*E*, *F*). Indeed, the antagonist blocks the channel, preventing the ions from flowing through it, and unmasks ion slippage through the transporter in the absence of substrate (glutamate in this case; Shimamoto et al., 2004).

The leak current (determined by subtracting the current in DL-TBOA from the current recorded in absence of antagonist) was inward at negative potentials and outward for potentials more positive than −16 mV (not shown). Leak currents have been described for most electrogenic carriers (Sonders and Amara, 1996; Ryan et al., 2004; Vandenberg et al., 2008; Andrini et al., 2008), but their function is often not clear. For some transporters, the ions contributing to the leak current can be the same ones that are translocated, whereas for others they are different. The calculated oocyte chloride equilibrium potential is close to the reversal potential of the EAAT2b leak current, suggesting that chloride flows through EAAT2b in the absence of glutamate. In contrast to EAAT2b, we never observed an outward current at negative potentials in the presence of DL-TBOA in EAAT2a-injected oocytes ($n = 6$).

To test whether the absence of a leak current in EAAT2a could be due to the absence of such ion slippage or to a negligible chloride conductance associated with the transporter, we recorded the DL-TBOA–induced currents in a solution in which chloride was substituted with SCN^-. When DL-TBOA alone was applied to the SCN^- bathing solution, an inward current was observed in all EAAT2b-injected oocytes at negative potentials (Fig. 7*H*): in these experimental conditions, SCN^- was indeed flowing into the oocyte through the EAAT2b before DL-TBOA closed the leak. Under these same conditions, even EAAT2a oocytes displayed an inward current, although small compared with the one elicited in EAAT2b-injected oocytes (Fig. 7*G*). This current was too small to be measured in EAAT2a-expressing oocytes bathed in standard Ringer solution, suggesting that only EAAT2b has a leak current that could exert an important physiologic role.

Discussion

The synaptic clearance of glutamate by EAATs is essential to maintain synaptic function in the CNS (Zhou and Danbolt, 2013). In this study, we focused on zebrafish EAAT2 proteins that are expressed at the photoreceptor synapse. This paralogous gene pair originated from a genome-duplication event ~350 million years ago. Intriguingly, we found the two paralogous genes and their proteins to be complementarily expressed in two distinct retinal cell types: cone photoreceptors and Müller glia cells. Although high mRNA expression levels of *eaat2a* are observed in the INL, only low transcript levels can be seen in photoreceptors. On the other hand, mRNA expression levels of *eaat2b* are high in photoreceptors and low in the INL. This weak INL expression of *eaat2b* and even lower transcript levels of *eaat2a* in photoreceptors might be a remnant of the ancestral *eaat2* gene expression, which was, before the whole-genome duplication, likely expressed in both Müller glia cells and photoreceptors. Interestingly, protein expression of the corresponding *eaats* in these cells could not be detected using our immunofluorescence protocol. Whether this is due to the generally low protein concentration in the membrane of these cells or degradation of EAAT2b in Müller cells and

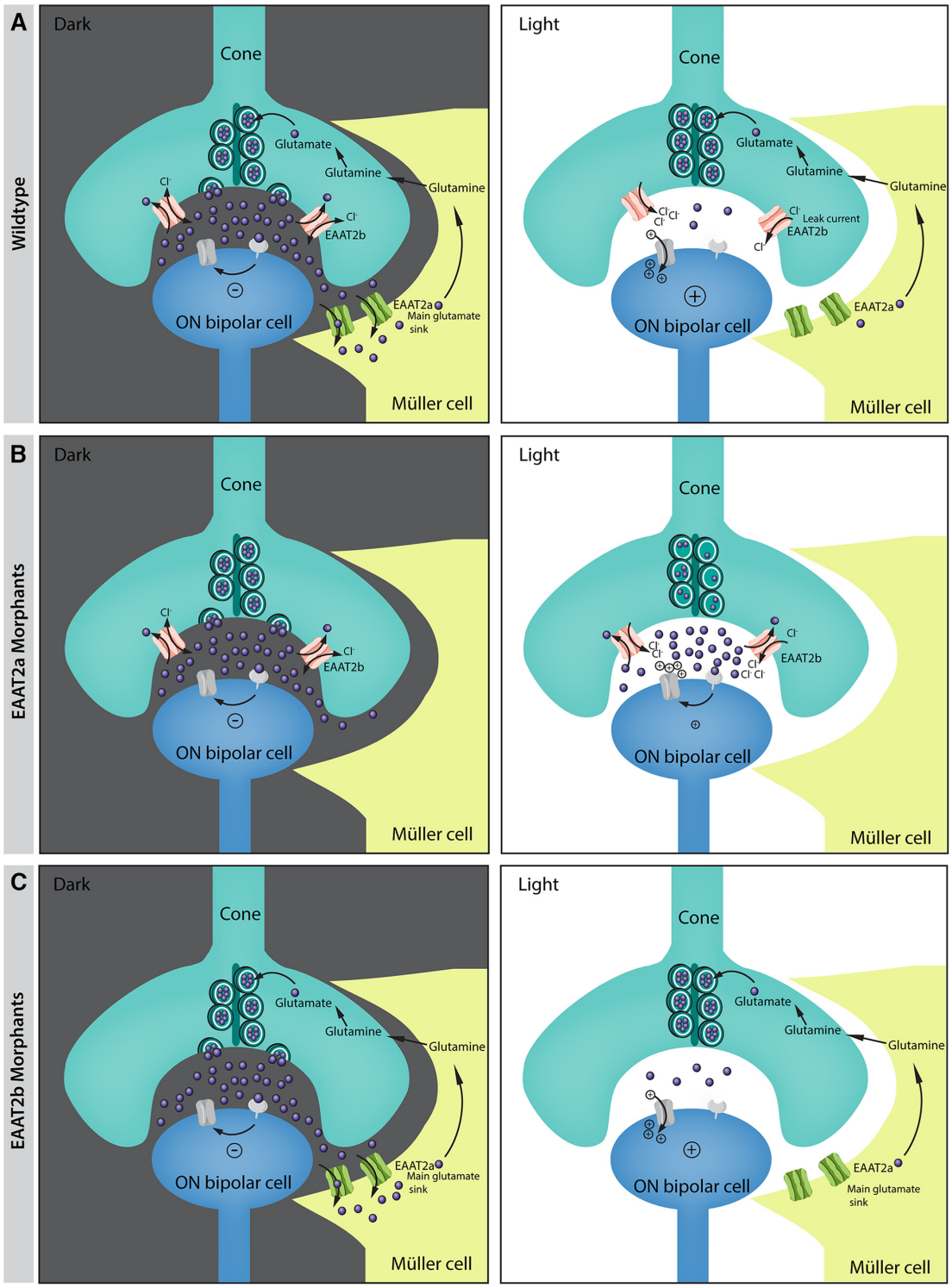

Figure 8. Schematics of photoreceptor synapse in light and dark. Illustration of changes in the photoreceptor synapse between light and dark in WT (***A***) and EAAT2a (***B***) and EAAT2b (***C***) morphants. EAAT2a on Müller glia cells is responsible for the uptake of the main

continued
load of glutamate. The uptaken glutamate in Müller cells is recycled via the glutamate–glutamine cycle. In EAAT2a morphants (***B***), the main load of glutamate is not being taken up and the cleft glutamate concentrations remain high, even during bright light stimuli. This may lead to binding of glutamate to postsynaptic receptors and therefore to a decreased ON-response in comparison to WT animals. The presynaptic transporter EAAT2b has a large Cl^- conductance with a large leak current in absence of glutamate. During a light stimulus, when photoreceptors hyperpolarize and very few glutamate remains in the synaptic cleft, Cl^- leaves the photoreceptor (leak current) and brings back the membrane potential closer to the dark resting potential. Because of the lack of such a leak current in EAAT2b morphants, cones remain in a slightly more hyperpolarized state.

EAAT2a in cones remains to be analyzed. The case of EAAT2 represents a rare case in which the subfunctionalization event led to a change not only in expression pattern but also in biophysical properties that can be directly linked to the biological function.

Unfortunately, morpholino antisense nucleotides are effective in knocking down protein only until ~5 dpf. At this stage, the small size of the larval retina prevents patch-clamp recordings of outer and inner retinal neurons. Furthermore, no paralog-specific pharmacologic inhibitors are available that would allow examination of the transporters in the adult retina by single-cell recordings. Therefore, functional analysis was conducted by ERG recordings. The ERG measures sum field potential changes of the retina evoked by changes in illumination. It has proven to be a robust measure of photoreceptor responses and subsequent bipolar cell activation. The ERG is a standard approach to measure outer retina function not only in model organisms, but also in the clinic (Perlman, 1995).

Knockdown of the glial transporter EAAT2a shows a highly significant reduction in the ERG b-wave, implying that glutamate levels in the synaptic cleft remain elevated even during a light stimulus, saturating postsynaptic glutamatergic receptors (Fig. 8*B*). This is consistent with the increased time to peak recorded for the b-wave in these animals. This delay is likely due to elevated glutamate levels in the cleft, even after light stimulation. In darkness, photoreceptors tonically release glutamate, which binds to the postsynaptic metabotropic glutamate receptor 6b (Nomura et al., 1994; Huang et al., 2012). This leads, via a signaling cascade, to the closure of the cation-conducting ion channel TRPM1 (Morgans et al., 2009). During a light stimulus, photoreceptors become more hyperpolarized, which results in a decreased number of vesicles fusing at the presynapse. This, together with glutamate transporters clearing the synaptic glutamate, results in reduced concentrations of glutamate in the synaptic cleft, to an extent depending on the light stimulus intensity (Fig. 8*A*). In EAAT2a-depleted animals, glutamate levels do not decrease during a light stimulus to the same extent as in WT animals, implying reduced and delayed ON bipolar cell depolarization (Fig. 8*B*). Müller glia cell processes wrap around and coat photoreceptor synapses but do not invaginate the synapse (Burris et al., 2002). Thus released glutamate needs to diffuse from the presynaptic release site to the glial glutamate transporter EAAT2a on Müller cell processes, where it is being taken up. Such a system, with the main transporter being outside the synaptic cleft, prevents direct competition of transporter with the postsynaptic receptors and therefore keeps interference of the glutamate uptake with signal propagation to a minimum (Gaal et al., 1998; Roska et al., 1998). In accordance with being expressed on glia cells rather than neurons, we could not associate EAAT2a with high chloride conductance or with a high leak current, which implies that its primary function is high-capacity glutamate transport and not modulation of membrane potentials.

Loss of the presynaptic glutamate transporter EAAT2b only slightly modulates the ERG b-wave, indicating that synaptic glutamate levels in knockdown animals must still be comparable to the ones in WT (Fig. 8*C*). The fact that the kinetics of the EAAT2b morphant ERG does not significantly differ from that in control animals further reveals that EAAT2b does not have a high glutamate turnover rate. However, EAAT2b shows a high affinity to glutamate; hence, it must either be significantly outnumbered by EAAT2a or have a lower cycling rate or capture efficiency (likelihood of glutamate being transported versus released again) than EAAT2a. Glutamate transporters have been shown to buffer glutamate and thereby shape signal transmission after a quantal event in a fast time frame, despite having slow turnover rates (Wadiche et al., 1995; Diamond and Jahr, 1997; Wadiche and Kavanaugh, 1998). Furthermore, EAAT1–3 are thought to have a capture efficiency of 0.5, indicating that the likelihood of being released again equals the likelihood of being transported (Cavelier and Attwell, 2005; Beart and O'Shea, 2007; Tilleux and Hermans, 2007). Therefore, we assume that glutamate released by photoreceptors can bind and unbind several transporters within the cleft, before being taken up by glial transporters that surround the synapse in high numbers (Diamond and Jahr, 1997; Wadiche and Jahr, 2001; Bergles et al., 2002).

In addition, our ERG results suggest that the main vesicular glutamate pool of cones is not being replenished by presynaptic glutamate uptake via EAAT2b; otherwise EAAT2b knockdown would result in a depletion of the presynaptic vesicles, which would give us a more drastic phenotype. Glutamate vesicles of cones therefore seem to be mainly filled by glutamate recycled via the glutamate–glutamine cycle between Müller cells and photoreceptors (Fig. 8*A*), revealing another difference between cones and rods, which are thought to possess an almost self-sustaining glutamate uptake system (Hasegawa et al., 2006).

ERG recordings on double morphant zebrafish indicate that upon loss of both EAAT2 paralogs, glutamate uptake is further neutralized. The resulting difference in the b-wave amplitude between EAAT2a single loss and EAAT2 double knockdown is (1) the result of photoreceptors possessing a limited pool of glutamate-filled vesicles (as both the glutamate–glutamine cycle via Müller glia

cells and the presynaptic uptake of glutamate are inhibited); (2) the result of an increased glutamate level in the synaptic cleft, even during light stimuli; or (3) both.

Binding of glutamate by EAAT2b is accompanied by the opening of chloride conductance that generates a large component of the total current. The chloride driving force and ionic flux direction depend on the chloride equilibrium potential that we suppose for zebrafish cones is between −40 and −50 mV. These estimates stem from data obtain in goldfish (–50 mV; Vroman et al., 2014), salamanders (–46 mV; Thoreson and Bryson, 2004), and turtle (–47 mV; Kaneko and Tachibana, 1986) cones. As the cone dark resting potential of zebrafish is around −40 mV (Endeman et al., 2013), very close to the chloride equilibrium potential (E_{Cl-}), the flux of chloride that accompanies glutamate transport of EAAT2b will force the cone to return to potentials close to the dark resting potential, giving rise to previously described positive feedback (Szmajda and Devries, 2011). The presence of the large leak current that we have described for EAAT2b in the absence of glutamate will push the cone toward the resting potential, even when glutamate in the cleft is extremely low. Accordingly, a prolonged and strong light stimulus will speed up the repolarization at light off (Rowan et al., 2010), stabilizing the resting potential at depolarized potentials (Fig. 8*C*). The lack of such a chloride leak in EAAT2b knockdown larvae would maintain the cones in a slightly hyperpolarized status in darkness and therefore contribute to the observed slight b-wave reduction. This effect would become more evident in the double knockdown larvae. Indeed, in this case, the postsynaptic glutamatergic receptors would be partially saturated owing to the increased glutamate concentration in the cleft, and the hyperpolarization of the cones in darkness (and their possible loss of readily available vesicles) would further reduce the difference in cleft glutamate between dark and light conditions.

It is intriguing that the zebrafish retina acquired a system with subfunctionalized EAAT2 proteins that is comparable to the one present in the mouse retina with different EAATs. In contrast to zebrafish, mice use EAAT2 as the presynaptic transporter, whereas EAAT1 (GLAST) on Müller cells constitutes the main glutamate sink of the photoreceptor synapse (Tse et al., 2014).

References

Andrini O, Ghezzi C, Murer H, Forster IC (2008) The leak mode of type II Na(+)-P(i) cotransporters. Channels (Austin, Tex.) 2:346–357. Medline

Barnett NL, Pow DV (2000) Antisense knockdown of GLAST, a glial glutamate transporter, compromises retinal function. Invest Ophthalmol Vis Sci 41:585–591. Medline

Beart PM, O'Shea RD (2007) Transporters for L-glutamate: an update on their molecular pharmacology and pathological involvement. Br J Pharmacol 150:5–17. CrossRef Medline

Bergles DE, Tzingounis AV, Jahr CE (2002) Comparison of coupled and uncoupled currents during glutamate uptake by GLT-1 transporters. J Neurosci 22:10153–10162.

Branchek T (1984) The development of photoreceptors in the zebrafish, brachydanio rerio. II. Function. J Comp Neur 224:116–122. CrossRef Medline

Branchek T, Bremiller R (1984) The development of photoreceptors in the zebrafish, Brachydanio rerio. I. Structure. J Comp Neur 224:107–115. CrossRef Medline

Burris C, Klug K, Ngo IT, Sterling P, Schein S (2002) How Müller glial cells in macaque fovea coat and isolate the synaptic terminals of cone photoreceptors. J Comp Neur 453:100–111. CrossRef Medline

Cavelier P, Attwell D (2005) Tonic release of glutamate by a DIDS-sensitive mechanism in rat hippocampal slices. J Physiol 564:397–410. CrossRef Medline

Diamond JS, Jahr CE (1997) Transporters buffer synaptically released glutamate on a submillisecond time scale. J Neurosci 17:4672–4687. Medline

Eliasof S, Arriza JL, Leighton BH, Amara SG, Kavanaugh MP (1998a) Localization and function of five glutamate transporters cloned from the salamander retina. Vis Res 38:1443–1454.

Eliasof S, Arriza JL, Leighton BH, Kavanaugh MP, Amara SG (1998b) Excitatory amino acid transporters of the salamander retina: identification, localization, and function. J Neurosci 18:698–712.

Eliasof S, Werblin F (1993) Characterization of the glutamate transporter in retinal cones of the tiger salamander. J Neurosci 13:402–411. Medline

Endeman D, Klaassen LJ, Kamermans M (2013) Action spectra of zebrafish cone photoreceptors. PloS One 8:e68540. CrossRef Medline

Fairman WA, Vandenberg RJ, Arriza JL, Kavanaugh MP, Amara SG (1995) An excitatory amino-acid transporter with properties of a ligand-gated chloride channel. Nature 375:599–603. CrossRef Medline

Gaal L, Roska B, Picaud SA, Wu SM, Marc R, Werblin FS (1998) Postsynaptic response kinetics are controlled by a glutamate transporter at cone photoreceptors. J Neurophysiol 79:190–196. Medline

Gesemann M, Lesslauer A, Maurer CM, Schönthaler HB, Neuhauss SC (2010a) Phylogenetic analysis of the vertebrate excitatory/neutral amino acid transporter (SLC1/EAAT) family reveals lineage specific subfamilies. BMC Evol Biol 10:117.

Gesemann M, Maurer CM, Neuhauss SC, Stephan CF (2010b) Excitatory amino acid transporters in the zebrafish: Letter to "Expression and functional analysis of Na(+)-dependent glutamate transporters from zebrafish brain" from Rico et al., Brain Res Bull 83:202–206.

Glasauer SS, Neuhauss SC (2014) Whole-genome duplication in teleost fishes and its evolutionary consequences. Mol Genet Genom 289:1045–1060. CrossRef Medline

Hamaoka T, Takechi M, Chinen A, Nishiwaki Y, Kawamura S (2002) Visualization of rod photoreceptor development using GFP-transgenic zebrafish. Genesis (New York) 34:215–220.

Harada T, Harada C, Watanabe M, Inoue Y, Sakagawa T, Nakayama N, Sasaki S, Okuyama S, Watase K, Wada K, Tanaka K (1998) Functions of the two glutamate transporters GLAST and GLT-1 in the retina. Proc Natl Acad Sci U S A 95:4663–4666. Medline

Hasegawa J, Obara T, Tanaka K, Tachibana M (2006) High-density presynaptic transporters are required for glutamate removal from the first visual synapse. Neuron 50:63–74. CrossRef Medline

Huang Y-Y, Haug MF, Gesemann M, Neuhauss SC (2012) Novel expression patterns of metabotropic glutamate receptor 6 in the zebrafish nervous system. PloS One 7:e35256. CrossRef Medline

Kaneko A, Tachibana M (1986) Effects of gamma-aminobutyric acid on isolated cone photoreceptors of the turtle retina. J Physiol 373:443–461. Medline

Larison KD, Bremiller R (1990) Early onset of phenotype and cell patterning in the embryonic zebrafish retina. Development (Cambridge, England) 109:567–576.

Levinger E, Zemel E, Perlman I (2012) The effects of excitatory amino acids and their transporters on function and structure of the distal retina in albino rabbits. Doc Ophthalmol 125:249–265. CrossRef Medline

Levy LM, Warr O, Attwell D (1998) Stoichiometry of the glial glutamate transporter GLT-1 expressed inducibly in a Chinese hamster

ovary cell line selected for low endogenous Na+-dependent glutamate uptake. J Neurosci 18:9620–9628.
Makhankov YV, Rinner O, Neuhauss SC (2004) An inexpensive device for non-invasive electroretinography in small aquatic vertebrates. J Neurosci Methods 135:205–210. CrossRef Medline
McKeown KA, Moreno R, Hall VL, Ribera AB, Downes GB (2012) Disruption of Eaat2b, a glutamate transporter, results in abnormal motor behaviors in developing zebrafish. Dev Biol 362:162–171. CrossRef Medline
Morgans CW (2000) Neurotransmitter release at ribbon synapses in the retina. Immunol Cell Biol 78:442–446. CrossRef Medline
Morgans CW, Zhang J, Jeffrey BG, Nelson SM, Burke NS, Duvoisin RM, Brown RL (2009) TRPM1 is required for the depolarizing light response in retinal ON-bipolar cells. Proc Natl Acad Sci U S A 106:19174–19178. CrossRef Medline
Mullins MC, Hammerschmidt M, Haffter P, Nüsslein-Volhard C (1994) Large-scale mutagenesis in the zebrafish: in search of genes controlling development in a vertebrate. Curr Biol 4:189–202. CrossRef
Nomura A, Shigemoto R, Nakamura Y, Okamoto N, Mizuno N, Nakanishi S (1994) Developmentally regulated postsynaptic localization of a metabotropic glutamate receptor in rat rod bipolar cells. Cell 77:361–369. Medline
Owe SG, Marcaggi P, Attwell D (2006) The ionic stoichiometry of the GLAST glutamate transporter in salamander retinal glia. J Physiol 577:591–599. CrossRef Medline
Palmer MJ, Taschenberger H, Hull C, Tremere L, von Gersdorff H (2003) Synaptic activation of presynaptic glutamate transporter currents in nerve terminals. J Neurosci 23:4831–4841.
Perlman I (1995) The Electroretinogram: ERG. In: Webvision: The Organization of the Retina and Visual System (Kolb H, Fernandez E, Nelson R, eds). University of Utah, Salt Lake City, UT.
Picaud SA, Larsson HP, Grant GB, Lecar H, Werblin FS (1995) Glutamate-gated chloride channel with glutamate-transporter-like properties in cone photoreceptors of the tiger salamander. J Neurophysiol 74:1760–1771. Medline
Rauen T (2000) Diversity of glutamate transporter expression and function in the mammalian retina. Amino Acids 19:53–62. Medline
Rauen T, Taylor WR, Kuhlbrodt K, Wiessner M (1998) High-affinity glutamate transporters in the rat retina: a major role of the glial glutamate transporter GLAST-1 in transmitter clearance. Cell Tissue Res 291:19–31. CrossRef
Roska B, Gaal L, Werblin FS (1998) Voltage-dependent uptake is a major determinant of glutamate concentration at the cone synapse: an analytical study. J Neurophysiol 80:1951–1960. Medline
Rowan MJ, Ripps H, Shen W (2010) Fast glutamate uptake via EAAT2 shapes the cone-mediated light offset response in bipolar cells. J Physiol 588:3943–3956. CrossRef Medline
Ryan RM, Mitrovic AD, Vandenberg RJ (2004) The chloride permeation pathway of a glutamate transporter and its proximity to the glutamate translocation pathway. J Biol Chem 279:20742–20751. CrossRef Medline
Schmitz F (2009) The making of synaptic ribbons: how they are built and what they do. Neurosci 15:611–624. CrossRef
Shimamoto K, Sakai R, Takaoka K, Yumoto N, Nakajima T, Amara SG, Shigeri Y (2004) Characterization of novel L-threo-beta-benzyloxyaspartate derivatives, potent blockers of the glutamate transporters. Mol Pharmacol 65:1008–1015. CrossRef Medline
Sonders MS, Amara SG (1996) Channels in transporters. Curr Opin Neurobiol 6:294–302. Medline
Szmajda BA, Devries SH (2011) Glutamate spillover between mammalian cone photoreceptors. J Neurosci 31:13431–13441. CrossRef
Takechi M, Hamaoka T, Kawamura S (2003) Fluorescence visualization of ultraviolet-sensitive cone photoreceptor development in living zebrafish. FEBS Lett 553:90–94. Medline
Takechi M, Seno S, Kawamura S (2008) Identification of cis-acting elements repressing blue opsin expression in zebrafish UV cones and pineal cells. J Biol Chem 283:31625–31632. CrossRef Medline
Thoreson WB, Bryson EJ (2004) Chloride equilibrium potential in salamander cones. BMC Neurosci 5:53. CrossRef Medline
Tilleux S, Hermans E (2007) Neuroinflammation and regulation of glial glutamate uptake in neurological disorders. J Neurosci Res 85:2059–2070. CrossRef Medline
Tse DY, Chung I, Wu SM (2014) Pharmacological inhibitions of glutamate transporters EAAT1 and EAAT2 compromise glutamate transport in photoreceptor to ON-bipolar cell synapses. Vis Res 103:49–62. CrossRef Medline
Vandenberg RJ, Huang S, Ryan RM (2008) Slips, leaks and channels in glutamate transporters. Channels (Austin) 2:51–58. CrossRef
Vandenbranden CA, Verweij J, Kamermans M, Müller LJ, Ruijter JM, Vrensen GF, Spekreijse H (1996) Clearance of neurotransmitter from the cone synaptic cleft in goldfish retina. Vis Res 36:3859–3874. Medline
Veruki ML, Mørkve SH, Hartveit E (2006) Activation of a presynaptic glutamate transporter regulates synaptic transmission through electrical signaling. Nat Neurosci 9:1388–1396. CrossRef Medline
Vroman R, Klaassen LJ, Howlett MHC, Cenedese V, Klooster J, Sjoerdsma T, Kamermans M (2014) Extracellular ATP hydrolysis inhibits synaptic transmission by increasing pH buffering in the synaptic cleft. PLoS Biol 12:e1001864. CrossRef
Wadiche JI, Amara SG, Kavanaugh MP (1995) Ion fluxes associated with excitatory amino acid transport. Neuron 15:721–728. Medline
Wadiche JI, Jahr CE (2001) Multivesicular release at climbing fiber-Purkinje cell synapses. Neuron 32:301–313. Medline
Wadiche JI, Kavanaugh MP (1998) Macroscopic and microscopic properties of a cloned glutamate transporter/chloride channel. J Neurosci 18:7650–7661. Medline
Wersinger E, Schwab Y, Sahel J-A, Rendon A, Pow DV, Picaud S, Roux MJ (2006) The glutamate transporter EAAT5 works as a presynaptic receptor in mouse rod bipolar cells. J Physiol 577:221–234. CrossRef Medline
White RD, Neal MJ (1976) The uptake of L-glutamate by the retina. Brain Res 111:79–93. Medline
Zerangue N, Kavanaugh MP (1996) Flux coupling in a neuronal glutamate transporter. Nature 383:634–637. CrossRef Medline
Zhou Y, Danbolt NC (2013) GABA and glutamate transporters in brain. Front Endocrinol 4:165. CrossRef Medline

Chapter 4

Life History of the EAAT Protein Family in the Vertebrate Retina

André Lehnherr[1,2], Peter Kovermann[3], Matthias Gesemann[1], Christoph Fahlke[3], Stephan C.F. Neuhauss[1]

[1] Institute of Molecular Life Sciences, University of Zurich, Winterthurerstrasse 190, 8057 Zürich, Switzerland
[2] Life Science Zürich Graduate Program – Neuroscience, 8057 Zürich, Switzerland
[3] Institute of Complex Systems, Zelluläre Biophysik (ICS-4), Forschungszentrum Jülich, Leo-Brandt-Strasse, 52425 Jülich, Germany

Report on a research project

Personal contribution:

Performing all experiments except for cloning of in situ hybridization probes for zebrafish EAAT5, EAAT6 and EAAT7 orthologs, preparation of all figures, writing the manuscript

4.1. Abstract

Processing of visual information in the retina is dependent on glutamatergic signaling. Synaptic glutamate-concentrations are tightly controlled by Excitatory Amino Acid Transporters (EAATs). Moreover, EAATs exhibit thermodynamically uncoupled anion conductance and are able to alter cellular membrane potentials. Seven EAAT subgroups have been described in vertebrates of which five (EAAT1-5) are present in the mammalian lineage.

In zebrafish, two EAAT6 paralogs, and one EAAT7 ortholog were described and all of them are expressed in neuronal cells in the retina. While both EAAT6 paralogs are expressed in photoreceptors, EAAT7 is expressed by retinal bipolar cells and co-localizes with EAAT5b expression. Knockdown of EAAT5b as well as EAAT7 led to smaller ERG b-wave only in red-light measurements, indicating an important role of EAAT7 in processing of red-light stimuli. In this study we examine the expression patterns and biophysical properties of EAAT5, EAAT6 and EAAT7 in the retinae of representative species of the major clades of higher vertebrates. We found EAAT5 to be expressed in photoreceptors and bipolar cells in all investigated species. EAAT6 is expressed in photoreceptors of zebrafish and *Xenopus*. While in chicken bipolar cells express EAAT6, anole lizards as well as mammals have lost EAAT6. EAAT7 in turn is expressed in bipolar cells of zebrafish, *Xenopus* and anole lizards while birds and mammals have lost EAAT7.

We show that EAAT7 of all investigated species exhibits high anion conductance allowing the transporter to alter cellular membrane potentials. Moreover, the zebrafish EAAT5b paralog exhibits similar biophysical properties. These findings are in line with the proposed roles of these transporters in processing visual information. For EAAT6 on the other hand we were not able to measure any glutamate-induced currents. We speculate that EAAT6 plays a role in transporting metabolites into photoreceptors rather than in processing of stimuli.

During the nocturnal phase of the common ancestor of mammals, the mammalian retina adapted to scotopic vision and most mammals can process two different wave-lengths of light instead of four. We show that this simplification in retinal complexity is mirrored as well in the EAAT gene family by the loss of EAAT6 and EAAT7 in the mammalian lineage.

4.2. Introduction

Humans as well as many other vertebrate species are highly dependent on their visual sense. The retina at the back of the eye is the light sensing organ in vertebrate species. The anatomical structure and cell types are conserved in all major vertebrate classes although Agnatha show less complexity in the structure of their retinae (for review see (Lamb et al. 2007)).

Photoreceptors in the retina tonically release glutamate in darkness that is sensed by two different types of bipolar cells; sign-conserving OFF-bipolar cells and sign-inversing ON-bipolar cells. OFF-bipolar cells express ionotropic glutamate receptors on their dendritic tips and depolarize when glutamate is present in the synaptic cleft between photoreceptors and OFF-bipolar cells. ON-bipolar cells in turn express metabotropic glutamate receptors 6 (mGluR6) that close unspecific cation channels via intracellular G-protein signaling. Further currents induced by chloride flux through the cell membrane upon glutamate application were described and later excitatory amino acid transporter 5 (EAAT5) was identified to elicit these currents in different model organisms. It was further shown that chloride conductance elicited by EAAT5 keeps the cell hyperpolarized at bipolar cell resting potential by allowing chloride to enter the

cell against its concentration gradient by passive flux (Grant, Dowling 1995; Arriza et al. 1997; Eliasof et al. 1998; Billups, Attwell 2002; Wong et al. 2005).

Excitatory amino acid transporters (EAATs) play a crucial role in clearing glutamate from the synaptic cleft and prevent cells from excitotoxicity. EAATs are secondary active glutamate transporters and accumulate glutamate in the cell by using the electrochemical gradients of sodium and potassium. Glutamate transport is driven by the co-transport of three sodium ions and one proton, while one potassium ion is counter-transported per cycle (Wadiche et al. 1995; Zerangue, Kavanaugh 1996a). EAATs are not only transporters. Besides the transport function, EAATs exhibit an intrinsic chloride conductance (Wadiche, Kavanaugh 1998; Eliasof et al. 1998).

EAATs and neutral amino acid transporters are members of the solute carrier family 1 (SLC1) gene family. Originally five EAATs and two neutral amino acid transporters were described and studied intensively (for review see (Kanai, Hediger 2004; Fahlke et al. 2016)). Gesemann and coworkers showed that during vertebrate evolution in total seven subclasses of EAATs (EAAT1-7) existed but in human and other placental mammals only five EAAT genes were retained (for phylogeny see Figure S4) (Gesemann et al. 2010). Eleven EAAT genes are present in the genome of zebrafish in total, while *Xenopus* retained seven, Sauropsida retained six EAAT genes but from different subgroups. Apparently, two EAAT genes became redundant and subsequently disappeared in the course of vertebrate evolution.

In order to elaborate the evolutionary history of the SLC1 gene family and to understand how EAAT6 and EAAT7 became redundant, we need to identify expression patterns of those genes in different vertebrate classes and characterize the corresponding biophysical properties. In this study we compare expression patterns of EAAT5, EAAT6 and EAAT7 orthologs of selected vertebrate groups. Moreover, we electrophysiologically characterize the glutamate transporters by analyzing glutamate transport and anion channel currents with whole cell patch clamp recordings.

4.3. Methods

4.3.1. Zebrafish husbandry

Adult zebrafish of WIK and Tübingen (Tü) wildtype strains were kept under a 14h/10h light/dark-cycle. Breeding and raising of larval fish was performed as previously described elsewhere (Mullins et al. 1994).

4.3.2. Cloning of EAAT-5, EAAT-6 and EAAT-7 genes and heterologous expression in tsA201 cells and *Xenopus* oocytes

Reliaprep RNA tissue miniprep kit (Promega) was used to isolate total RNA from brains and eyes of zebrafish, *Xenopus tropicalis*, anole lizard, chicken and mice. cDNA was transcribed with SuperScript III First-Strand Synthesis kit (Invitrogen).

Overlapping fragments of around 900bp were PCR amplified using gene specific primers (Table S1) and Qiagen Fast Cycling PCR kit (Qiagen) for generation of in situ hybridization probes. PCR products were subsequently ligated into TOPO PCRII vectors (Invitrogen).

For expression constructs, coding regions were PCR amplified using gene specific primers

(Table S2) and Phusion High-Fidelity DNA Polymerase (ThermoFisher Scientific). Restriction sites were introduced to generate N-terminal YFP-fusion proteins and to clone into pRcCMV vector.

tsA201 cells (Sigma Aldrich) were cultured at 37°C and 10% CO_2 in DMEM medium containing 10% FCS (Gibco). $Ca_3(PO_4)_2$ transfection method was used to transiently express EAAT genes in tsA201 as described before (Machtens et al. 2015). Typically, two days after transfection, single cells exhibiting fluorescence in the membrane were used for electrophysiological recordings.

cRNA for injection into *Xenopus* oocytes were synthesized from NotI linearized plasmids using mMESSAGE mMACHINE T7 Transcription Kit and Poly(A) Tailing Kit (Ambion). 25ng cRNA were injected into *Xenopus* oocytes (Ecocyte) and fluorescence checked 1-5 days after injections. For recordings, oocytes were selected for YFP fluorescence under an Olympus MVX10 binocular.

4.3.3. *In situ* hybridization

Digoxigenin-labelled (DIG) RNA in situ probes for the different EAAT genes were synthesized as described before (Huang et al. 2012). Briefly, linearized plasmids were SP6 or T7 *in vitro* transcribed to RNA probes using DIG-RNA-labelling kit (Roche Diagnostics).

In situ hybridization on retinal cross-sections was performed as previously described (Huang et al. 2012). Tissues were fixed overnight (ON) at 4°C in 4% paraformaldehyde (PFA), subsequently dehydrated in 30% sucrose in PBS and frozen in OCT medium. Cryo-sections of 14µm thickness were cut. Before hybridization, retinal sections treated with proteinase K and postfixed in 4%PFA. RNA probes were applied ON at hybridization temperature of 65°C. Subsequent blocking was performed in 1x Blocking Solution (Roche Diagnostics) in TNT (100 mM Tris HCl pH 7.5, 150 mM NaCl, 0.5% Tween 20). Anti-DIG conjugated to alkaline phosphatase was diluted 1:5000 in 1x Blocking Solution in TNT and incubated ON at 4°C. Unbound antibodies were washed out by several washes in TNT and staining was performed with staining buffer containing NBT and BCIP (Roche Diagnostics). Staining reactions were stopped and tissue postfixed in 4% PFA. For imaging, retinal sections were mounted in Kaiser's Gelatine. Imaging was performed with an Olympus BX61 microscope and Adobe Photoshop and Illustrator were used to process and assemble figures.

4.3.4. Electrophysiology

Standard whole cell patch clamp recordings were performed using a Multiclamp 700b (Molecular Devices) amplifier. Borosilicate glass electrodes were pulled and used with resistances between 2.5 and 7 MΩ. Compensation of 80% of the series resistance reduced voltage-errors. Recorded currents were filtered at 10 kHz and digitized by a Digidata 1440A (Molecular Devices) digitizer at a sampling rate of 5 kHz. To record anion currents, currents were measured using standard external solution containing 140mM $NaNO_3$, 4mM KCl, 2mM $CaCl_2$, 1mM $MgCl_2$, 1mM Glutamate and 5mM HEPES and pH was set to 7.4. For recordings of glutamate transport induced currents, all anions were equimolar replaced by the corresponding gluconate salt. Intracellular solutions contained 110mM KGluconate, 5mM EGTA, 2mM MgGluconate and 10mM HEPES and pH was adjusted to 7.4 with KOH. Using this intracellular solution allows recording of glutamate transport currents isolated since gluconate cannot pass through EAAT anion pores. All experiments were carried out using agar bridges with 3M KCl in 1%

Agarose to connect the Ag/AgCl electrode. Liquid junction potential differences were calculated in pClamp 10.3 Molecular Devices) and protocols adjusted accordingly.

Amplitudes of glutamate associated currents were measured at physiological -75mV and anion current amplitudes were measured at +75mV. The ratio between anion currents and glutamate transport associated currents is used as a measure for anion flux for different EAAT genes.

Recordings from RNA injected *Xenopus* oocytes were performed as described before (Niklaus et al. 2017). Two-electrode voltage-clamp (TEVC) recordings were performed using a Turbo Tex-03x amplifier (NPI). Signals were recorded by a Digidata 1440A (Molecular Devices). Recording electrodes were pulled and used with resistances below 1 MΩ. Electrodes were filled with 3M KCl. Currents were recorded at 10kHz and lowpass filtered at 20Hz. To enhance anion currents, the extracellular solution contained 96mM $NaNO_3$, 2mM KCl, 1.8mM $CaCl_2$, 1mM $MgCl_2$ and 5mM HEPES, the pH was set to 7.4. For anion-free recording, nitrate and chloride were equimolar replaced by gluconate salts.

Currents were analyzed using pClamp 10.3 (Molecular Devices) software and for plots and statistical analysis Prism 7 (GraphPad) was used. Reversal potentials were interpolated by calculating a four-parameter logistic regression.

4.4. Results

4.4.1. *eaat5*, *eaat6* and *eaat7* show neuronal expression patterns in adult retinal sections.

In zebrafish, the mRNA of both *eaat5* paralogs are expressed in photoreceptors and bipolar cells. *eaat5a* is stronger expressed in photoreceptors whereas *eaat5b* expression is higher in bipolar cells. In general, expression of *eaat5* mRNA in photoreceptors, bipolar cells and ganglion cells was shown in retinae of all examined vertebrate species (*Xenopus*, anole lizards, chicken and mice) (Figure 1).

No *eaat6* orthologs were found in reptilian or mammalian genomes (Gesemann et al. 2010). *Xenopus eaat6* as well as zebrafish *eaat6a* and *eaat6b* are all expressed in photoreceptor cells, while the chicken *eaat6* ortholog shows expression in bipolar cells (Figure 1).

Genomes of teleost fish, *Xenopus* and anole lizards harbor *eaat7* genes, which are consistently expressed in retinal bipolar cells of all investigated species (Gesemann et al., 2010) (Figure 1).

Figure 1: Retinal expression patterns of *eaat5*, *eaat6* and *eaat7* mRNA in vertebrates.
mRNA of *eaat5* show expression in photoreceptors and bipolar cells of mouse, chicken, anole lizard, *Xenopus* and zebrafish retina. In zebrafish, *eaat5a* shows stronger expression in photoreceptors whereas *eaat5b* seems to be stronger expressed in bipolar cells.
Both zebrafish *eaat6* paralogs and *Xenopus eaat6* are expressed in photoreceptors. In chicken retina, *eaat6* shows expression in bipolar cells.
All cloned and examined *eaat7* orthologs show expression in bipolar cells.
Schematic representation of the retina: Dark brown cells: retinal pigment epithelium (RPE), orange and green: rod and cone photoreceptor cells, violet: horizontal cells, red: bipolar cells, light green: Müller glia cells, yellow: amacrine cells, blue: ganglion cells. Scale bar represents 50μm.

Zebrafish
Xenopus
Anole Lizard
Chicken
Mouse
EAAT-5
SLC1A7
EAAT-6
SLC1A8
EAAT-7
SLC1A9
EAAT-5a
EAAT-5b
EAAT-6a
EAAT-6b
Retinal Pigment Epithelium (RPE)
Outer Nuclear Layer (ONL)
Outer Plexiform Layer (OPL)
Inner Nuclear Layer (INL)
Inner Plexiform Layer (IPL)
Ganglion Cell Layer (GCL) & Axons

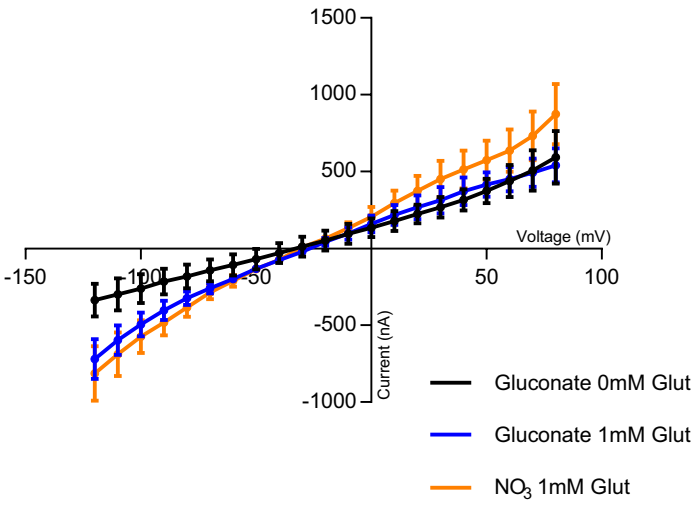

Figure 2: Current-voltage relationship plot for EAAT5b of zebrafish.
Traces represent different extracellular solutions. Black: all anions replaced by impermeable gluconate, no glutamate; blue: all anions replaced by impermeable gluconate, 1mM glutamate; orange: standard recording solution containing nitrate and chloride as well as 1mM glutamate. At negative membrane potentials, application of glutamate induces an inward current (orange and blue line) consisting of glutamate transport currents and anion currents. An outward current is observed at positive membrane potentials, indicating an anion conductance for EAAT5b.

4.4.2. Expression of EAAT5 and EAAT6 orthologs in tsA201 cells and *Xenopus* oocytes

Expression of EAAT5 and EAAT6 paralogs in tsA201 cells resulted in intracellular accumulation of the protein and little or no protein localizing in the cell membrane (data not shown). As a consequence, we tried to express zebrafish EAAT5b, EAAT6a and EAAT6b, together with EAAT2a as control, in *Xenopus laevis* oocytes. Surprisingly, we see expression of these constructs in oocytes but to different extents (Figure S1). While EAAT2a, like in tsA201 cells, shows high expression levels, EAAT5b, EAAT6a and EAAT6b show clearly lower expression.

4.4.3. Biophysical properties of EAAT5b and EAAT6b from zebrafish

To characterize the biophysical properties for those transporters, we performed TEVC recordings on oocytes injected with cRNA from zebrafish EAAT5b and EAAT6b. We found that EAAT5b exhibits a robust outward current at positive membrane potentials with anions in the perfusion solution, which disappeares upon anion depletion. This suggests that the zebrafish EAAT5b isoform is permeable for anions (Figure 2).

Recorded inward currents of EAAT5b at negative potentials are the sum of glutamate transport-associated currents and currents brought by anion conductance through EAAT5b. Unlike in tsA201 cells, it is problematic to control intracellular ion concentrations, and therefore we didn't separate glutamate transport and anion currents. However, the IV curves show a major increase in transport current under anion-free conditions, which is not observed at positive voltages (Figure 2).

Application of glutamate to EAAT6b injected *Xenopus* oocytes did not provoke any measurable currents neither with anion-free recording solution nor with recording solution containing nitrate (data not shown).

4.4.4. Biophysical properties of EAAT7

Here we describe for the first time biophysical properties of EAAT7. Clearly, all examined EAAT7 orthologs exhibit glutamate transport currents and anion currents (Figure 3; Figure 4). Because we don't have a measure for expression levels, we can't directly compare elicited currents of EAAT7 from different species.

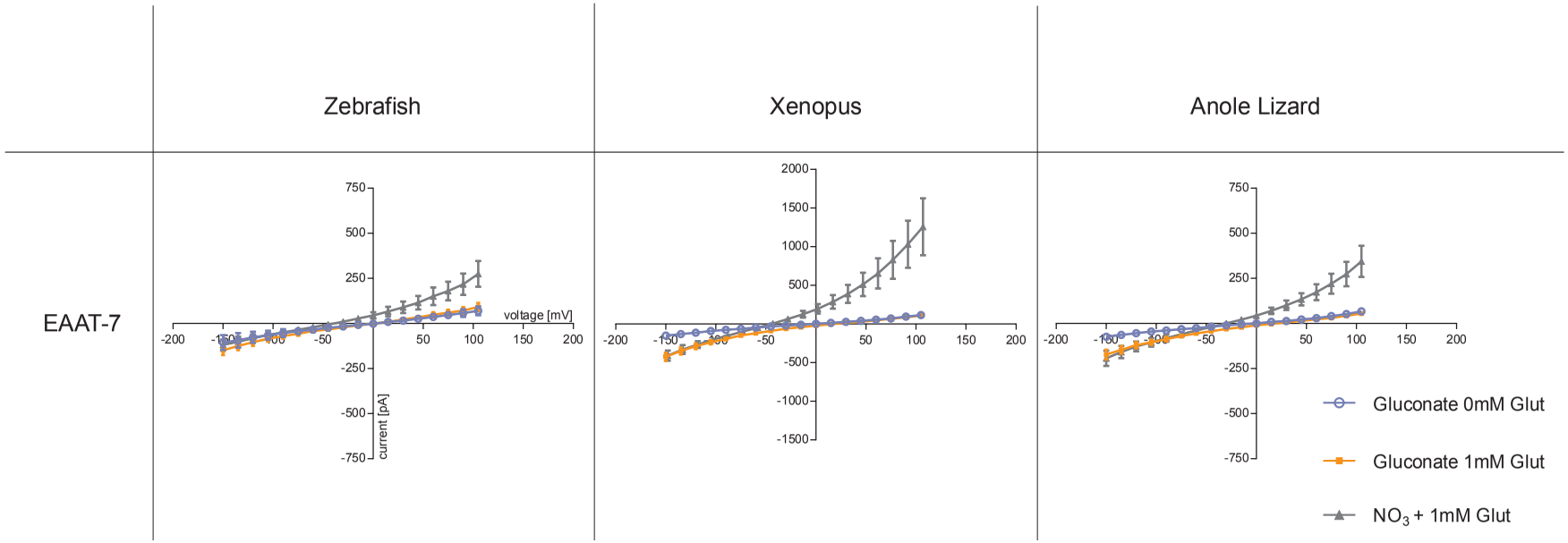

Figure 3: Current-voltage relationship plot of EAAT7 orthologs of zebrafish, *Xenopus* and anole lizard.
Examined EAAT7 orthologs all show enhanced inward currents at negative membrane potentials after application of glutamate (orange). Applying extracellular NO3 leads to outward currents at positive membrane potentials (black), indicating anion conductance for zebrafish (n=10), *Xenopus* (n=6) and anole lizard (n=11) EAAT7 orthologs. *Xenopus* EAAT7 shows bigger currents than corresponding zebrafish and anole lizard orthologs. This may be partially explained by different expression levels.

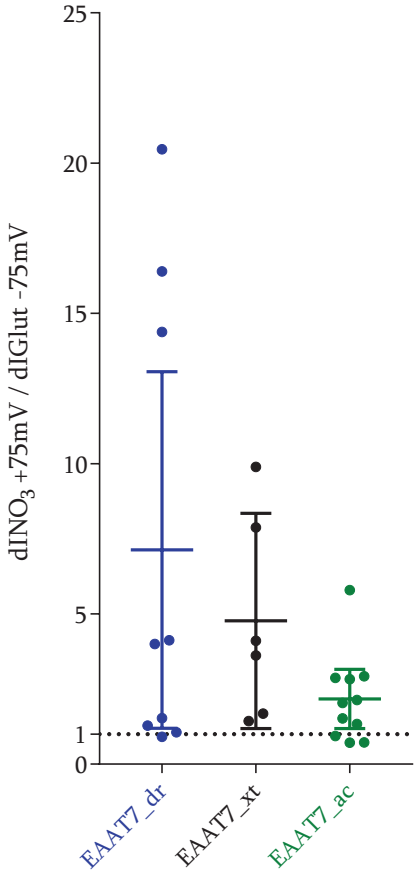

Figure 4: Ratio between anion currents and glutamate transport currents of zebafish, *Xenopus* and anole lizard EAAT7 orthologs.
Amplitudes of glutamate induced current amplitudes were measured at a membrane potential of -75mV while NO3-current amplitudes were measured at +75mV.
Although it seems like the zebrafish (7.13 ± 2.52, n=9) and *Xenopus* (4.77 ± 1.39, n=6) EAAT7 orthologs show higher ratios than the lizard EAAT7 (2.17 ± 0.44, n=11), all examined EAAT7 orthologs show statistically indifferent ratios between anion currents and glutamate transport currents (ANOVA, $p > 0.05$). Since all ratios are clearly higher than one, we conclude that EAAT7 acts as a glutamate-gated anion channel.
Bars showing mean ratio and 95% confidence interval.
Abbreviations: dr: *Danio rerio* – zebrafish; xt: *Xenopus tropicalis* – Western clawed frog; ac: *Anolis carolinensis* – American green anole lizard.

To be able to make a comparison between EAAT7 orthologs from different species, we calculated the ratio between anion currents elicited at a membrane potential of +75mV and glutamate transport-associated currents at -75mV (dI_{NO3}/dI_{Glu}, Figure 4). The zebrafish EAAT7 orhtolog shows the biggest ratio (7.13 ± 2.52, n=9), while the *Xenopus* ortholog (4.77 ± 1.39, n=6) and especially the ortholog of anole lizards (2.17 ± 0.44, n=11) show lower ratios. Statistical testing revealed no significant differences between these ratios.

Clearly, all examined EAAT7 show a high ratio between anion currents and glutamate transport currents indicating that EAAT7 act as glutamate-gated anion channels but still showing a remarkable glutamate transport current. For all cells included into analysis, the reversal potential was calculated. No significant differences between different EAAT7 orthologs have been found. Since similar anion permeability is expected for different EAAT isoforms, this indicates that no leaky or unhealthy cells were taken into analysis (Figure S2).

4.5. Discussion

In mammals, five EAAT subtypes named EAAT1-5 have been described (for review (Kanai et al. 2013; Jensen et al. 2015). Later it was shown that inconsistent numbers of EAAT genes in different vertebrate classes occur, due to several gene duplication and gene loss events during vertebrate evolution. In lower vertebrate classes such as teleost fishes or Amphibia, two additional subtypes named EAAT6 and EAAT7 have been described (Gesemann et al. 2010). Here we describe expression patterns of EAAT5, EAAT6 and EAAT7 in retinal sections from representative species of the different vertebrate classes for the first time. Furthermore, we could show that EAAT7 clearly can act as a glutamate-gated anion channel by electrophysiological

recordings.

EAAT5 has been reported to be expressed almost exclusively in retinae of mammals, Amphibia and fishes (Arriza et al. 1997; Eliasof et al. 1998; Palmer et al. 2003). Consistent with these findings, we found EAAT5 to be expressed in photoreceptors and bipolar cells in all examined vertebrate species but we found that the two EAAT5 paralogs of zebrafish show a sub-functionalization in expression patterns. While *eaat5a* mRNA seems to be stronger expressed in photoreceptors, *eaat5b* mRNA in turn shows stronger expression in bipolar cells. Immunohistochemical staining revealed that the EAAT5a protein localizes most likely on bipolar cells whereas EAAT5b clearly localizes in dendritic tips of ON-bipolar cells (Niklaus 2017). Both EAAT6 paralogs from zebrafish as well as EAAT6 from *Xenopus* show exclusive expression in photoreceptors. While anole lizards did not retain an EAAT6 ortholog, chicken express EAAT6 in bipolar cells. Nevertheless, the EAAT6a protein has been reported to localize on horizontal cells processes while EAAT6b localizes at the base of cone photoreceptor inner segments (Niklaus 2017). Reptiles, Amphibia and teleosts have retained EAAT7 and in the investigated species we found *eaat7* mRNA to localize in bipolar cells. This staining is in line with the reported localization of EAAT7 protein in ON-bipolar cells and a subset of rod photoreceptors (Niklaus 2017). The change in expression patterns of EAAT6 in birds from photoreceptors to bipolar cells led us to the assumption that the loss of EAAT7 in birds led to adaptation of EAAT6 expression patterns. Whether this adaptation is reflected by the biophysical properties of the chicken EAAT6 homolog requires further investigations.

In order to elaborate possible roles of EAAT5, EAAT6 and EAAT7 in synaptic transmission in the retina,we expressed EAAT5, EAAT6 and EAAT7 orthologs in tsA201 cells for subsequent electrophysiological recordings of biophysical properties. While all investigated EAAT7 homologs localize to the cell surface membrane, EAAT5 and EAAT6 orthologs accumulate intracellularly and do not show expression at the cell membrane (data not shown). Expression of cRNA in *Xenopus* oocytes and subsequent TEVC recordings provide an established alternative to standard whole cell patch clamp on transfected tsA201 cells (i.e. Arriza et al. 1997). Therefore, we expressed zebrafish EAAT5b, EAAT6a and EAAT6b genes as well as EAAT2a as a control in *Xenopus laevis* oocytes and could confirm expression of these constructs in oocytes (Figure S1). We could record glutamate induced currents from EAAT5b injected oocytes (Figure 2). EAAT5b shows clear inward currents after glutamate application at negative membrane potentials. Application of glutamate together with nitrate as a permeable anion revealed an outward current at positive membrane potentials. Like other EAAT5 homologs, EAAT5b can act as a glutamate-gated anion channel (Arriza et al. 1997; Schneider et al. 2014). Knockdown of EAAT5b in zebrafish leads to a reduced ERG b-wave after red-light stimuli (Niklaus 2017). The b-wave describes the field potential of depolarizing ON-bipolar cells. EAAT5b protein was shown to localize at the dendritic tips of ON-bipolar cells that are in contact with all cone-subtypes and as well with a minority of rods (Niklaus 2017). The pronounced anion current of EAAT5b will therefore push the ON-bipolar cells towards their resting potential whenever glutamate is present in the synaptic cleft. Consequently, these ON-bipolar cells are pushed towards hyperpolarized states by the glutamate that is released by photoreceptors in darkness. In EAAT5b knockout zebrafish, ON-bipolar cells which express EAAT5b are not hyperpolarized by glutamate and thus the diminished glutamate release upon a red-light stimulus is not reducing the ERG b-wave to the same extent as in the wildtype situation.

For EAAT6b we could so far not record any current elicited by the application of glutamate (data not shown). Although we cannot exclude that low expression levels could mask such currents, other possible roles of EAAT6b have to be considered. Previous studies in our lab

showed that the EAAT6b protein localizes at the level of the outer limiting membrane, where Müller glia cells end-feets form adherence junctions between each other and cone photoreceptors inner segments (Bunt-Milam et al. 1985; Niklaus 2017). Clearly, the hypothesis that EAAT6b associated glutamate uptake is involved in redox homeostasis, similar to what was shown for EAAT3, is challenged by the fact that we could not record glutamate transport currents so far (Rothstein et al. 1994; Shashidharan et al. 1997; Niklaus 2017). In line with our findings, Eliasof and co-workers reported no measurable glutamate transport currents for the EAAT6 ortholog of tiger salamanders (Eliasof et al. 1998). EAAT3 has been shown to serve another important role by not only transporting glutamate but as well L-cysteine (Zerangue, Kavanaugh 1996b). L-cysteine is the limiting factor of the glutathione synthesis pathway and glutathione in turn is important in maintaining intracellular redox potential and is therefore protecting cells from oxidative stress. Similar, EAAT6b was proposed to act as a L-cysteine transporter (Niklaus 2017). Besides this potential role of EAAT6b, other possible duties have to be considered. Marcaggi et al. showed that isolated Müller cells can release glutamate and aspartate by reversed transport cycle of EAAT1 (Marcaggi et al. 2005). Glutamate and aspartate could be taken up by photoreceptors which in turn could process these amino acids into oxaloacetate. Oxaloacetate is used as a substrate in the citric acid cycle, the most important aerobic metabolic pathway. Photoreceptors are known to be highly energy demanding cells and such mechanisms could provide alternative energy sources.

We characterized biophysical properties of EAAT7 orthologs in tsA201 cells. In anion-free measurements, application of glutamate leads to a pronounced inward current at negative membrane potentials (Figure 3). When extracellular nitrate is applied, all investigated EAAT7 show clear outward current at positive membrane potentials, suggesting selective inward flux of the anion. By comparing anion current amplitudes and glutamate transport current amplitudes, we showed that investigated EAAT7 show high proportions of anion currents and are therefore classified as glutamate-gated anion channels. Interestingly, the anion to transport current ratios vary remarkably between different EAAT7 orthologs. While zebrafish and *Xenopus* EAAT7 homologs display a relatively high ratio, the ratio for lizard EAAT7 is smaller (statistically insignificant; Figure 4).

Eliasof and colleagues investigated four EAAT genes that are expressed in the tiger salamander retina (Eliasof et al. 1998). Due to their similarity with known EAAT2 and EAAT5 proteins, they were named EAAT2a, EAAT2b, EAAT5a and EAAT5b. Phylogenetic analysis allowed us to allocate those genes to different EAAT subgroups. Consequently, EAAT2a belongs to the EAAT2 subgroup whereas EAAT2b is an EAAT7 paralog. EAAT5a groups clearly with other EAAT5 while EAAT5b groups with EAAT6 (Figure S4). For EAAT5 they showed that almost all of the glutamate elicited currents were brought out by anion flux while EAAT7 in salamander did not show conclusive channel properties in their case but they report clear chloride conductivity.

Depolarization of ON-bipolar cells relies on two different types of postsynaptic glutamate receptors. Binding of glutamate to mGluR6 mediates closure of unselective cation channels thus hyperpolarizing the cells (Nakajima et al. 1993). The second glutamate receptor involved in hyperpolarization of ON-bipolar cells is EAAT5 (Grant, Dowling 1995; Wong et al. 2005; Tse et al. 2014). Blocking of EAAT5 leads to a reduction of the ERG b-wave due to the lack of hyperpolarizing chloride influx through the transporter (Tse et al. 2014). Studies in our lab showed that EAAT5b and EAAT7 are expressed in close proximity in ON-bipolar dendrites. Knockout of EAAT7 showed a significant reduction of the b-wave under red light in spectral ERG measurements. Double knockout of EAAT5b and EAAT7 leads to a further decrease of

the b-wave in red-light measurements (Niklaus 2017). Although the majority of vertebrate species are having the predisposition for trichromatic vision, several exceptions have been reported. The common ancestor of all mammals was nocturnal and as a consequence of the lack of light, UV-violet and red light perception degenerated during the course of placental mammal evolution. Only humans together with old world and some new world monkeys regained red light perception (for reviews (Surridge et al. 2003; Lamb et al. 2007)). Consequently, it seems likely that together with the loss of perception of red light, the machinery for red light processing in the retina became redundant. Opsins are the light sensing proteins in photoreceptor cells. Different subclasses of opsins show distinct absorption maxima (λ_{max}). Rhodopsin (Rh1) is expressed in rod photoreceptors and important for dim-light vision and shows λ_{max} of roughly 500nm. Opsins expressed in cones are classified into long- to middle-wave class (LWS, red to green sensitive), middle-wave class (RH2, green sensitive), short-wave class 1 (SWS1, violet-ultraviolet sensitive) and a second short wave class 2 (SWS2, sensitive to blue-violet light) (Lamb et al. 2007; Bowmaker 2008). Intuitively one would think that the nocturnal ancestor of all mammals has lost UV-violet and red sensitive opsins. But studies have shown that the distribution of visual pigments is more complex than thought. The zebrafish genome harbors eight cone-specific opsin genes: one SWS1, one SWS2, four RH2 and two LWS homologs (Chinen et al. 2003). Although all of these opsin genes have been shown to have a distinct absorption maxima, *in vivo* studies showed that zebrafish are in fact tetrachromats using UV-, S-, M- and L-type cones (Cameron 2002; Endeman et al. 2013). *Xenopus* in turn have lost a RH2 gene but express all other opsins. Interestingly, a small subpopulation of rods expresses as well SWS2 which are therefore sensitive to blue light (Witkovsky et al. 1981). All four cone opsins are present in anole lizards thus they are potentially tetrachromats. The retina of anole lizards is lacking rod photoreceptors but a functional rhodopsin gene is present in the genome (Kawamura, Yokoyama 1998). Diurnal birds have similar visual systems to the one of anole lizards but rods are found in avian retinae (for review (Hart, Hunt 2007)). Nocturnal animals perceive less light and as a consequence retinae of nocturnal vertebrates contain mainly rods and have less opsins compared to diurnal animals. Since all mammals share a common nocturnal ancestor, they possess rod-dominated retinae with fewer visual pigments. In monotremes, two orthologs to LWS and SWS2 have been found and marsupials have been shown to be trichromats, although so far only two cone opsins, a SWS1 and a LWS ortholog, have been found (for review (Bowmaker 2008)). Placental mammals, except primates, are dichromats using a LWS and a SWS1 gene for color perception. In most cases the LWS is altered and the absorption maximum is shifted to green ranges. In old world monkeys, some new world monkeys and humans, the LWS gene was duplicated and one copy shifted the absorption maximum again to the red range, thus making these species trichromats (see overview Figure S3; for reviews see (Yokoyama 2000; Bowmaker 2008). It is true, that the loss of green-sensitive RH2 and UV-sensitive SWS1 corresponds with the loss of EAAT7 and EAAT6 in the vertebrate lineage (Bowmaker 2008; Gesemann et al. 2010). We showed that EAAT7 is expressed exclusively in bipolar cells and while EAAT7 is missing in birds, expression of EAAT6 changed from photoreceptors to bipolar receptors. Monotremes diverged from other mammals around 200 million years ago (mya) during the nocturnal phase of ancestral mammals. This could explain why monotremes have retained a different subset of visual pigments and additionally EAAT6 compared to other mammals. Here we can only speculate that the loss of several visual pigments during vertebrate evolution has led to subsequent loss of genes that are involved in the processing machinery of the visual stimuli, in this case EAAT6 and EAAT7.

Lepidosauromorpha, in our study represented by green anole lizards, lost EAAT6 but retained EAAT7 while birds retained EAAT6 but lost EAAT7 (Gesemann et al. 2010). This leads to the

assumption that EAAT6 and EAAT7 still were present in the genome of the common ancestor of the Sauropsida (Gesemann et al. 2010). Since an all-cone retina is specific for anole lizards but not for other Lepidosauromorpha species, loss of EAAT6 cannot be associated with the loss of rods. In addition, both Sauropsida subgroups are potentially tetrachromats and use four different cone opsin genes for color perception and loss of either EAAT6 or EAAT7 can therefore not be a secondary loss in the processing machinery. Most likely, redundancy of these genes led to the non-functionalization of one of the two genes and by chance the two Sauropsida subgroups lost different EAAT homologs.

4.6. Outlook

Elaboration of biophysical properties of zebrafish EAAT6a and EAAT6b and other EAAT6 orthologs will help us to understand possible roles of EAAT6 in signal transmission or involvement in transport or substrates for metabolic processes. Two-electrode voltage clamp recordings from oocytes injected with different EAAT6 orthologs will be carried out in order to shine light on transport and possible channel properties. Of special interest is the chicken EAAT6 homolog. Expression patterns changed in birds from photoreceptors to bipolar cells and adaptations to new expression patterns are likely.

From an evolutionary point of view, it will be interesting to investigate the biophysical properties further. Not only for the two zebrafish paralogs but as well for the representative species from Amphibia, reptiles and birds.

4.7. Appendix

4.7.1. Supplementary figures

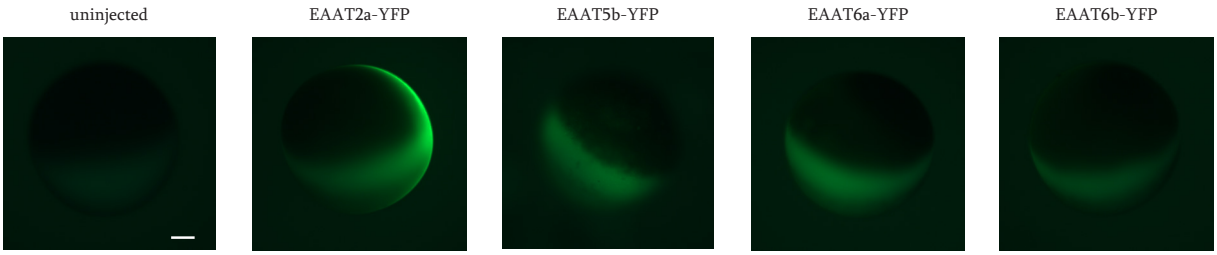

Figure S1: *Xenopus laevis* oocytes expressing EAAT-YFP fusion proteins.
Uninjected control oocytes do not exhibit fluorescence. EAAT2a-YFP construct as a positive control show high fluorescence intensities while expression levels of EAAT5b, EAAT6a and EAAT6b are lower. Scale bar represents 200µm.

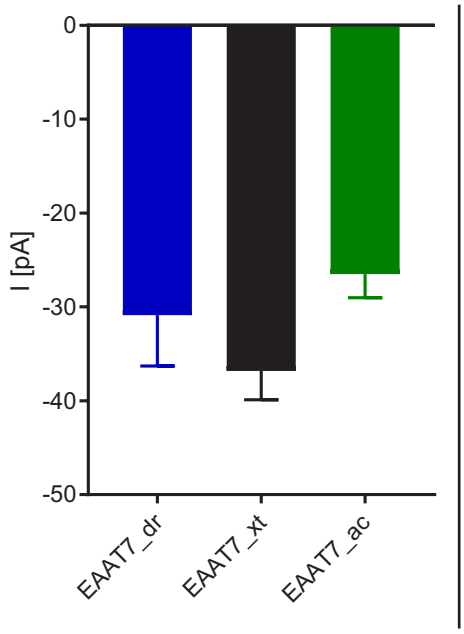

Figure S2: Reversal potential of investigated EAAT7 constructs expressed in tsA201 cells.
Reversal potentials of tsA201 cells transfected with different EAAT7 orthologs are statistically insignificant (ordinary one-way ANOVA, $p > 0.24$). This suggests that no leaky or unhealthy cells are included into analysis.

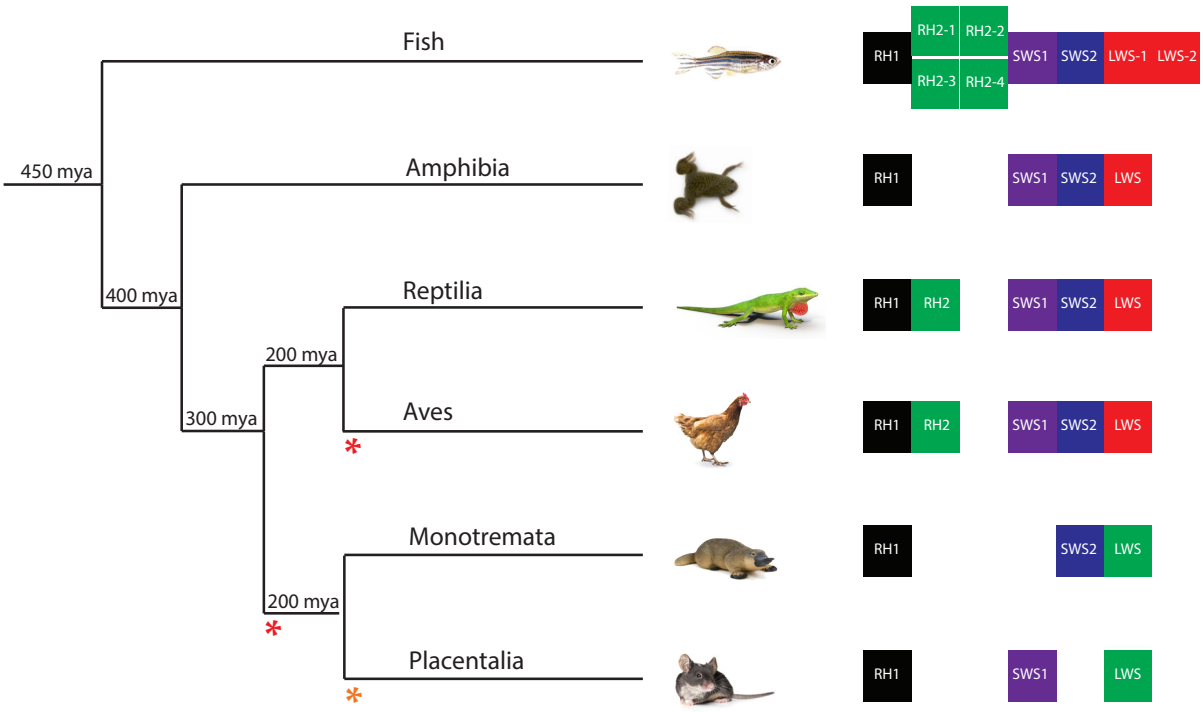

Figure S3: Schematic representation of a vertebrate phylogeny and opsin genes in different vertebrate classes.
Teleost fish harbor eight opsin and one rhodopsin genes in the genome. Functionally they are tetrachromates, expressing duplicated genes in the same cone types. Amphibian species lost middle-wavelength sensitive RH2 while birds and reptiles possess all four opsins and are tetrachromates. The nocturnal phase of the common ancestor of all mammals led to the loss of several opsin genes. Surprisingly, monotremes lost RH2 and UV-violet sensitive SWS1 but retained blue-sensitive SWS2, while placental mammals lost RH2 and SWS2. Most mammals adapted their LWS to absorptions maxima in the green light range. Humans together with primates duplicated LWS, leading to the adaptation of one copy to red light absorption maxima.
Nummers indicate approximate time of the last common ancestor in million years (mya). Red asterisks indicate the loss of EAAT7 in the aviana and mammalian lineage. Orange asterisk indicate the loss of EAAT6 in the clade of the Placentalia.

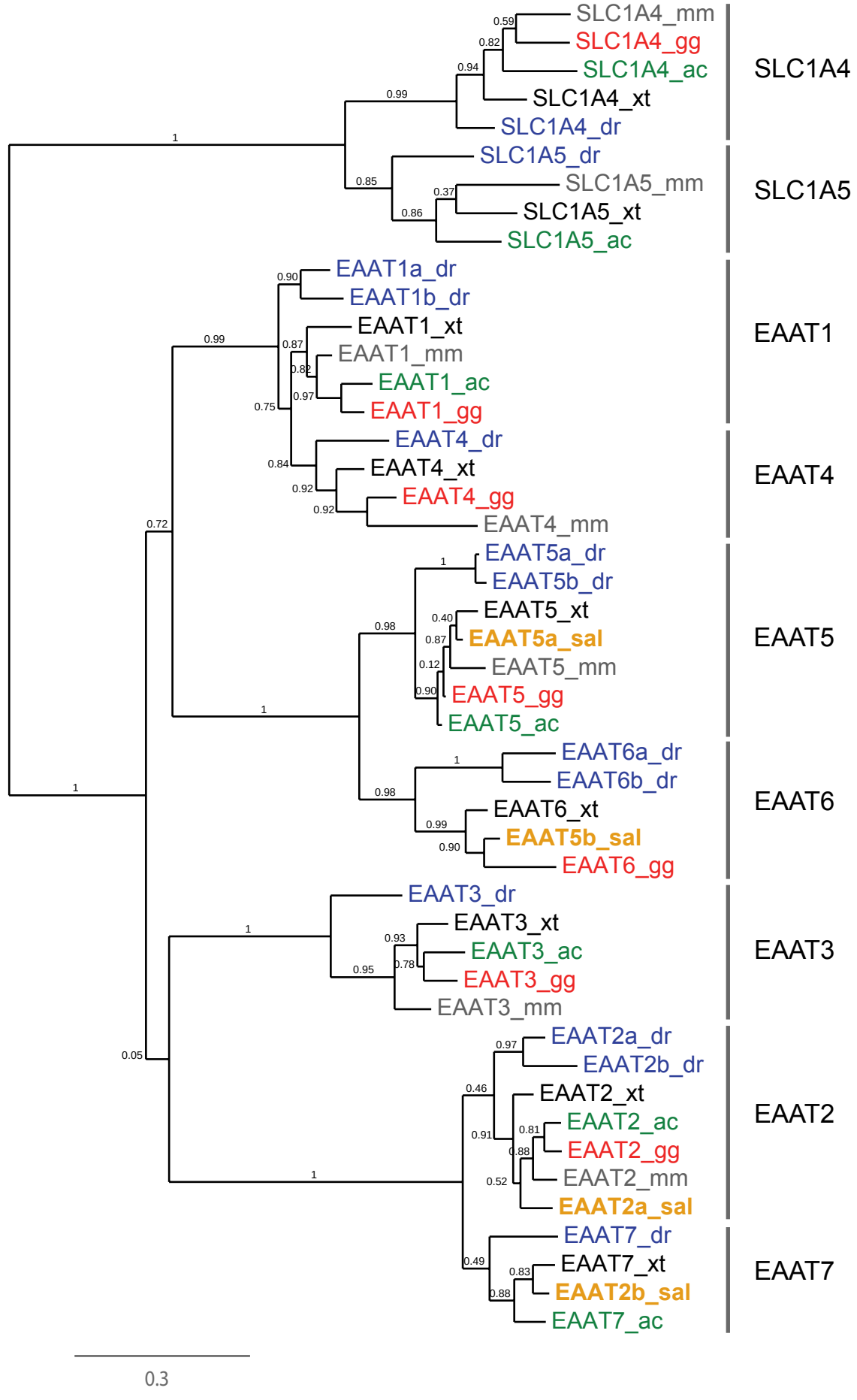
SLC1A4_mm
SLC1A4_gg
SLC1A4_ac
SLC1A4_xt
SLC1A4_dr
SLC1A5_dr
SLC1A5_mm
SLC1A5_xt
SLC1A5_ac
EAAT1a_dr
EAAT1b_dr
EAAT1_xt
EAAT1_mm
EAAT1_ac
EAAT1_gg
EAAT4_dr
EAAT4_xt
EAAT4_gg
EAAT4_mm
EAAT5a_dr
EAAT5b_dr
EAAT5_xt
EAAT5a_sal
EAAT5_mm
EAAT5_gg
EAAT5_ac
EAAT6a_dr
EAAT6b_dr
EAAT6_xt
EAAT5b_sal
EAAT6_gg
EAAT3_dr
EAAT3_xt
EAAT3_ac
EAAT3_gg
EAAT3_mm
EAAT2a_dr
EAAT2b_dr
EAAT2_xt
EAAT2_ac
EAAT2_gg
EAAT2_mm
EAAT2a_sal
EAAT7_dr
EAAT7_xt
EAAT2b_sal
EAAT7_ac
SLC1A4
SLC1A5
EAAT1
EAAT4
EAAT5
EAAT6
EAAT3
EAAT2
EAAT7
0.3

Figure S4: Phylogenetic tree of the SLC1 gene family including tiger salamander EAAT2a, EAAT2b, EAAT5a and EAAT5b orthologs.
Maximum likelihood phylogeny of the SLC1 gene family of investigated vertebrate species together with published EAAT2 and EAAT5 orthologs from tiger salamander (Eliasof et al. 1998; Gesemann et al. 2010). While the salamander EAAT2a groups with other EAAT2 orthologs, EAAT2b falls into the EAAT7 group, suggesting that the salamander EAAT2b is actually an EAAT7 ortholog.
Similarly, the salamander EAAT5a gene clearly groups together with other EAAT5 homologues while EAAT5b groups into the EAAT6 class.
The scale bar shows percentage of amino acid substitutions that are required to generate the corresponding tree (0.3 equals 30%). The numbers indicate branch support values.

4.7.2. Primers used in this study

1. Gene	Primer	Sequence 5′ to 3′
eaat5a_dr	EAAT5a_dr_0016_s	GTGTGGAGCCGTGTTAAA
	EAAT5a_dr_0525_as	GGGTTCCAGGGTTCAATG
eaat5b_dr	EAAT5b_dr_0135_s	GGAGCAGGAAGTCAAGTA
	EAAT5b_dr_0600_as	GTCCGTCCCATTATCGTC
eaat5_xt	EAAT5_xt_-0003s	ACAATGGCAGGGTCTTGTG
	EAAT5_xt_0750s	CTTCTGCCAGTGCTTAAATG
	EAAT5_xt_0951as	CATGAGAGGAAGAATGAAAG
	EAAT5_xt_1703as	GCCTGCAGTTAGACATTAGTC
eaat5_ac	EAAT5_ac_-0001s	CATGGCAGTGGGCTTTG
	EAAT5_ac_0866S	CTATTGGGAAGAAGCTTGG
	EAAT5_ac_0987as	GATGAAGACAATGGGGTC
	EAAT5_ac_1709as	AGAAGTAACAGCTACACATTGG
eaat5_gg	EAAT5_gg_-0001s	CATGGCGGTGGCTCTG
	EAAT5_gg_0728s	GTGGTGTTCCTTTGGTCAG
	EAAT5_gg_0861as	AGGGTCGTCCATTTCTAAG
	EAAT5_gg_1704as	CGGTTACACGTTCGTTTC
eaat5_mm	EAAT5_mm_-0040s	CTGACAGTGCATGGAATGG
	EAAT5_mm_0740s	GCTTCTGTCAGTGCCTTAATG
	EAAT5_mm_0915as	GACCACCAGCCCACAAAC
	EAAT5_mm_1688as	CTGCAGGTTCACACGTTG
eaat6a_dr	EAAT6a_dr_0017_s	CTATAAGTGTCCGGGAGT
	EAAT6a_dr_0535_as	GGGTTCCAGGGTTCAATG
eaat6b_dr	EAAT6b_dr_-0012_s	CCCTGGAGAAACATGGTG
	EAAT6b_1687_as	GTGCCCATTGGTAGTGTAAC
eaat6_xt	EAAT6_xt_-0002s	GGATGTCCACGTGTGACC
	EAAT6_xt_0768s	TGAAGCAGTGATGAAATTG
	EAAT6_xt_0956as	AGGAACAAGAGTGGCAATAG
	EAAT6_xt_1611as	AATCACCATTTAGACCAAGC
eaat6_gg	EAAT6_gg_-0008s	CACTGTCCATGGGCTCTG
	EAAT6_gg_0763s	GCCGTGATGAAATCGTC
	EAAT6_gg_0904as	CCGACACCACAGTGATTG
	EAAT6_gg_1607as	AGTGCTGCGACCTACACC
eaat7_dr	EAAT7_dr_142_s	GTAATAGCAGGCACAGTGATG
	EAAT7_dr_1001_as	CCCAGAGCAGTGATCCAAG
eaat7_xt	EAAT7_xt_-0002s	GGATGACCAATCACATTGAG
	EAAT7_xt_0769s	GAGCAGGCCAAATTAATG
	EAAT7_xt_0895as	TTCCTGCAATTTTTCCAC
	EAAT7_xt_1632as	ACTAGGCAGGGAGGTGTAG
eaat7_ac	EAAT7_ac_0001s	ATGACTAACCATGTGGAGGTG
	EAAT7_ac_0775s	CCCATGGCTGATTTCTTC
	EAAT7_ac_0895as	CTTTGATAGCTGCAATCTTG
	EAAT7_ac_1725as	GGATCTAGTCGCCTTCTTTC

Table S1: Primers used for cloning of in situ probes.

Gene	Primer	Sequence 5′ to 3′
eaat5b_dr	EAAT5b_dr_-6s_BsrGI	GTTGTTTGTACAAGCTCACGATGGCCGTGG
	EAAT5b_dr_1743as_NotI	GTTGTTGCGGCCGCCTATACATTAGTCTCAAGACCG
eaat6a_dr	EAAT6a_dr_1s_BsrGI	GTTGTTTGTACAAGATGGCACCTACATTCTCTATA
	EAAT6a_dr_1617as_NotI	GTTGTTGCGGCCGCTCAGACTTGACATATATTGTAGTA
eaat6b_dr	EAAT6b_dr_1s_BsiWI	GTTGTTCGTACGAGATGGTGGAATATTTTAAGAATA
	EAAT6b_dr_1653as_NotI	GTTGTTGCGGCCGCTTAGACTTGGCAAAGGTTG
eaat7_dr	EAAT7_dr_1s_Acc65I	GTTGTTGGTACCAGATGACGAATAAACATTTGGG
	EAAT7_dr_2016as_NotI	GTTGTTGCGGCCGCTTAGGGCAGATCACATGG
eaat7_xt	EAAT7_xt_1s_BsiWI	GTTGTTCGTACGAGATGACCAATCACATTGAGG
	EAAT7_xt_1674as_NotI	GTTGTAGCGGCCGCTTCTAAAGACGCATTGCTTG
eaat7_ac	EAAT7_ac_1s_BsrGI	GTTGTTTGTACAAGATGACTAACCATGTGGAGGT
	EAAT7_ac_1722as_NotI	GTTGTTGCGGCCGCCTAGTCGCCTTCTTTCTTCT

Table S2: Primers used for cloning of expression constructs.

4.8. References

Arriza, J. L.; Eliasof, S.; Kavanaugh, M. P.; Amara, S. G. (1997): Excitatory amino acid transporter 5, a retinal glutamate transporter coupled to a chloride conductance. In *Proceedings of the National Academy of Sciences of the United States of America* 94 (8), pp. 4155–4160.

Billups, Daniela; Attwell, David (2002): Control of intracellular chloride concentration and GABA response polarity in rat retinal ON bipolar cells. In *The Journal of physiology* 545 (1), pp. 183–198. DOI: 10.1113/jphysiol.2002.024877.

Bowmaker, James K. (2008): Evolution of vertebrate visual pigments. In *Vision research* 48 (20), pp. 2022–2041. DOI: 10.1016/j.visres.2008.03.025.

Bunt-Milam, A. H.; Saari, J. C.; Klock, I. B.; Garwin, G. G. (1985): Zonulae adherentes pore size in the external limiting membrane of the rabbit retina. In *Investigative ophthalmology & visual science* 26 (10), pp. 1377–1380.

Cameron, David A. (2002): Mapping absorbance spectra, cone fractions, and neuronal mechanisms to photopic spectral sensitivity in the zebrafish. In *Vis. Neurosci.* 19 (03), pp. 365–372. DOI: 10.1017/S0952523802192121.

Chinen, Akito; Hamaoka, Takanori; Yamada, Yukihiro; Kawamura, Shoji (2003): Gene duplication and spectral diversification of cone visual pigments of zebrafish. In *Genetics* 163 (2), pp. 663–675.

Eliasof, S.; Arriza, J. L.; Leighton, B. H.; Amara, S. G.; Kavanaugh, M. P. (1998): Localization and function of five glutamate transporters cloned from the salamander retina. In *Vision research* 38 (10), pp. 1443–1454.

Endeman, Duco; Klaassen, Lauw J.; Kamermans, Maarten (2013): Action spectra of zebrafish cone photoreceptors. In *PloS one* 8 (7), e68540. DOI: 10.1371/journal.pone.0068540.

Fahlke, Christoph; Kortzak, Daniel; Machtens, Jan-Philipp (2016): Molecular physiology of EAAT anion channels. In *Pflugers Archiv : European journal of physiology* 468 (3), pp. 491–502. DOI: 10.1007/s00424-015-1768-3.

Gesemann, Matthias; Lesslauer, Annegret; Maurer, Colette M.; Schönthaler, Helia B.; Neuhauss, Stephan C. F. (2010): Phylogenetic analysis of the vertebrate excitatory/neutral amino acid transporter (SLC1/EAAT) family reveals lineage specific subfamilies. In *BMC evolutionary biology* 10, p. 117. DOI: 10.1186/1471-2148-10-117.

Grant, G. B.; Dowling, J. E. (1995): A glutamate-activated chloride current in cone-driven ON bipolar cells of the white perch retina. In *The Journal of neuroscience* 15 (5 Pt 2), pp. 3852–3862.

Hart, Nathan S.; Hunt, David M. (2007): Avian visual pigments: characteristics, spectral tuning, and evolution. In *The American naturalist* 169 Suppl 1, S7-26. DOI: 10.1086/510141.

Huang, Ying-Yu; Haug, Marion F.; Gesemann, Matthias; Neuhauss, Stephan C. F. (2012): Novel expression patterns of metabotropic glutamate receptor 6 in the zebrafish nervous system. In *PloS one* 7 (4), e35256. DOI: 10.1371/journal.pone.0035256.

Jensen, Anders A.; Fahlke, Christoph; Bjørn-Yoshimoto, Walden E.; Bunch, Lennart (2015): Ex-

citatory amino acid transporters: recent insights into molecular mechanisms, novel modes of modulation and new therapeutic possibilities. In *Current opinion in pharmacology* 20, pp. 116–123. DOI: 10.1016/j.coph.2014.10.008.

Kanai, Yoshikatsu; Clémençon, Benjamin; Simonin, Alexandre; Leuenberger, Michele; Lochner, Martin; Weisstanner, Martin; Hediger, Matthias A. (2013): The SLC1 high-affinity glutamate and neutral amino acid transporter family. In *Molecular aspects of medicine* 34 (2-3), pp. 108–120. DOI: 10.1016/j.mam.2013.01.001.

Kanai, Yoshikatsu; Hediger, Matthias A. (2004): The glutamate/neutral amino acid transporter family SLC1: molecular, physiological and pharmacological aspects. In *Pflugers Archiv : European journal of physiology* 447 (5), pp. 469–479. DOI: 10.1007/s00424-003-1146-4.

Kawamura, Shoji; Yokoyama, Shozo (1998): Functional characterization of visual and nonvisual pigments of American chameleon (Anolis carolinensis). In *Vision research* 38 (1), pp. 37–44. DOI: 10.1016/S0042-6989(97)00160-0.

Lamb, Trevor D.; Collin, Shaun P.; Pugh, Edward N. (2007): Evolution of the vertebrate eye: opsins, photoreceptors, retina and eye cup. In *Nature reviews. Neuroscience* 8 (12), pp. 960–976. DOI: 10.1038/nrn2283.

Machtens, Jan-Philipp; Kortzak, Daniel; Lansche, Christine; Leinenweber, Ariane; Kilian, Petra; Begemann, Birgit et al. (2015): Mechanisms of anion conduction by coupled glutamate transporters. In *Cell* 160 (3), pp. 542–553. DOI: 10.1016/j.cell.2014.12.035.

Marcaggi, Païkan; Hirji, Nashila; Attwell, David (2005): Release of L-aspartate by reversal of glutamate transporters. In *Neuropharmacology* 49 (6), pp. 843–849. DOI: 10.1016/j.neuropharm.2005.07.011.

Mullins, M. C.; Hammerschmidt, M.; Haffter, P.; Nüsslein-Volhard, C. (1994): Large-scale mutagenesis in the zebrafish: in search of genes controlling development in a vertebrate. In *Current biology : CB* 4 (3), pp. 189–202.

Nakajima, Y.; Iwakabe, H.; Akazawa, C.; Nawa, H.; Shigemoto, R.; Mizuno, N.; Nakanishi, S. (1993): Molecular characterization of a novel retinal metabotropic glutamate receptor mGluR6 with a high agonist selectivity for L-2-amino-4-phosphonobutyrate. In *The Journal of biological chemistry* 268 (16), pp. 11868–11873.

Niklaus, Stephanie (2017): Glutamate Homeostasis in the Zebrafish outer Retina. Diss. Univ. Zürich. - Ref.: Stephan C.F. Neuhauss; Korref.: Christian Grimm, Martin Müller. Zürich.

Niklaus, Stephanie; Cadetti, Lucia; Vom Berg-Maurer, Colette M.; Lehnherr, André; Hotz, Adriana L.; Forster, Ian C. et al. (2017): Shaping of Signal Transmission at the Photoreceptor Synapse by EAAT2 Glutamate Transporters. In *eNeuro* 4 (3). DOI: 10.1523/ENEURO.0339-16.2017.

Palmer, Mary J.; Taschenberger, Holger; Hull, Court; Tremere, Liisa; Gersdorff, Henrique von (2003): Synaptic activation of presynaptic glutamate transporter currents in nerve terminals. In *The Journal of neuroscience* 23 (12), pp. 4831–4841.

Rothstein, Jeffrey D.; Martin, Lee; Levey, Allan I.; Dykes-Hoberg, Margaret; Jin, Lin; Wu, David et al. (1994): Localization of neuronal and glial glutamate transporters. In *Neuron* 13 (3), pp. 713–725. DOI: 10.1016/0896-6273(94)90038-8.

Schneider, Nicole; Cordeiro, Sönke; Machtens, Jan-Philipp; Braams, Simona; Rauen, Thomas; Fahlke, Christoph (2014): Functional properties of the retinal glutamate transporters GLT-1c and EAAT5. In *The Journal of biological chemistry* 289 (3), pp. 1815–1824. DOI: 10.1074/jbc.M113.517177.

Shashidharan, P.; Huntley, George W.; Murray, Jacinta M.; Buku, Angeliki; Moran, Thomas; Walsh, Michael J. et al. (1997): Immunohistochemical localization of the neuron-specific glutamate transporter EAAC1 (EAAT3) in rat brain and spinal cord revealed by a novel monoclonal antibody. In *Brain Research* 773 (1-2), pp. 139–148. DOI: 10.1016/S0006-8993(97)00921-9.

Surridge, Alison K.; Osorio, Daniel; Mundy, Nicholas I. (2003): Evolution and selection of trichromatic vision in primates. In *Trends in Ecology & Evolution* 18 (4), pp. 198–205. DOI: 10.1016/S0169-5347(03)00012-0.

Tse, Dennis Y.; Chung, Inyoung; Wu, Samuel M. (2014): Possible roles of glutamate transporter EAAT5 in mouse cone depolarizing bipolar cell light responses. In *Vision research* 103, pp. 63–74. DOI: 10.1016/j.visres.2014.06.005.

Wadiche, J. I.; Kavanaugh, M. P. (1998): Macroscopic and microscopic properties of a cloned glutamate transporter/chloride channel. In *The Journal of neuroscience* 18 (19), pp. 7650–7661.

Wadiche, Jacques I.; Amara, Susan G.; Kavanaugh, Michael P. (1995): Ion fluxes associated with excitatory amino acid transport. In *Neuron* 15 (3), pp. 721–728. DOI: 10.1016/0896-6273(95)90159-0.

Witkovsky, Paul; Levine, Joseph S.; Engbretson, Gustav A.; Hassin, Guido; MacNichol, Edward F. (1981): A microspectrophotometric study of normal and artificial visual pigments in the photoreceptors ofXenopus laevis. In *Vision research* 21 (6), pp. 867–873. DOI: 10.1016/0042-6989(81)90187-5.

Wong, Kwoon Y.; Adolph, Alan R.; Dowling, John E. (2005): Retinal bipolar cell input mechanisms in giant danio. I. Electroretinographic analysis. In *Journal of neurophysiology* 93 (1), pp. 84–93. DOI: 10.1152/jn.00259.2004.

Yokoyama, Shozo (2000): Molecular evolution of vertebrate visual pigments. In *Progress in Retinal and Eye Research* 19 (4), pp. 385–419. DOI: 10.1016/S1350-9462(00)00002-1.

Zerangue, N.; Kavanaugh, M. P. (1996a): Flux coupling in a neuronal glutamate transporter. In *Nature* 383 (6601), pp. 634–637. DOI: 10.1038/383634a0.

Zerangue, N.; Kavanaugh, M. P. (1996b): Interaction of L-cysteine with a human excitatory amino acid transporter. In *The Journal of physiology* 493 (Pt 2), pp. 419–423.

Chapter 5

Proper Migration and Axon Outgrowth of Zebrafish Cranial Motoneuron Subpopulations Require the Cell Adhesion Molecule MDGA2A

Esther Ingold[1*], Colette M. vom Berg Maurer[2*], Christoph J. Burckhardt[2*], André Lehnherr[2*], Philip Rieder[1], Philip J. Keller[3] , Ernst H. Stelzer[3], Urs F. Greber[2], Stephan F. Neuhauss[2], and Matthias Gesemann[1,2]

[*] equal contribution

[1]Brain Research Institute of the University Zurich and Swiss Federal Institute of Technology (ETH), Department of Biology, 8057 Zurich,
[2]Institute of Molecular Life Sciences, University of Zurich, 8057 Zurich, Switzerland
[3] EMBL Heidelberg, Meyerhofstraße 1, 69117 Heidelberg, Germany

Author for correspondence:
Dr. Matthias Gesemann, Institute of Molecular Life Sciences, University of Zurich, Winterthurerstrasse 190, CH-8057 Zurich, Switzerland.
E-mail: matthias.gesemann@imls.uzh.ch

Running title: Role of zebrafish MDGA2A in cranial motoneurons

Article published in Biology Open

Personal contribution:
In situ hybridization, conformation of MDGA2A morpholino knockdown phenotype with MO-A and MO-B, preparation of Figure S4 and associated experiments, all revisions, proofing and editing of the manuscript

The Company of Biologists

© 2015. Published by The Company of Biologists Ltd | Biology Open (2015) 4, 146–154 doi:10.1242/bio.20148482

RESEARCH ARTICLE

Proper migration and axon outgrowth of zebrafish cranial motoneuron subpopulations require the cell adhesion molecule MDGA2A

Esther Ingold[1,*], Colette M. vom Berg-Maurer[2,*], Christoph J. Burckhardt[2,*], André Lehnherr[2,*], Philip Rieder[1], Philip J. Keller[3], Ernst H. Stelzer[3], Urs F. Greber[2], Stephan C. F. Neuhauss[2] and Matthias Gesemann[1,2,‡]

ABSTRACT

The formation of functional neuronal circuits relies on accurate migration and proper axonal outgrowth of neuronal precursors. On the route to their targets migrating cells and growing axons depend on both, directional information from neurotropic cues and adhesive interactions mediated via extracellular matrix molecules or neighbouring cells. The inactivation of guidance cues or the interference with cell adhesion can cause severe defects in neuronal migration and axon guidance. In this study we have analyzed the function of the MAM domain containing glycosylphosphatidylinositol anchor 2A (MDGA2A) protein in zebrafish cranial motoneuron development. MDGA2A is prominently expressed in distinct clusters of cranial motoneurons, especially in the ones of the trigeminal and facial nerves. Analyses of MDGA2A knockdown embryos by light sheet and confocal microscopy revealed impaired migration and aberrant axonal outgrowth of these neurons; suggesting that adhesive interactions mediated by MDGA2A are required for the proper arrangement and outgrowth of cranial motoneuron subtypes.

KEY WORDS: Zebrafish, MDGA, Cranial motoneurons, Digital light sheet microscopy, Cell migration, Cell adhesion, Axon guidance

INTRODUCTION

During the formation of the nervous system subsets of postmitotic neuroblasts delaminate from primary neuroepithelia and migrate over considerable distances to settle in different regions of the growing organism. These migratory cells follow stereotypic pathways detecting even miniature concentration differences of attractive and repulsive neurotropic cues or changes in the adhesive properties of the surrounding tissue. Therefore miss-regulation of either neurotropic or adhesive molecules often leads to aberrant migration and ectopic clustering of neuronal populations.

[1]Brain Research Institute of the University Zurich and Swiss Federal Institute of Technology (ETH), Department of Biology, 8057 Zurich, Switzerland. [2]Institute of Molecular Life Sciences, University of Zurich, 8057 Zurich, Switzerland. [3]EMBL Heidelberg, Meyerhofstraße 1, 69117 Heidelberg, Germany.
*These authors contributed equally to this work

‡Author for correspondence (matthias.gesemann@imls.uzh.ch)

Received 12 April 2014; Accepted 10 November 2014

Following neuronal migration and terminal differentiation, neurons have to properly connect with corresponding targets in order to integrate the information flow throughout the nervous system. In analogy to neuronal migration, elongating neurites also grow along predetermined pathways relying on instructional information from attractive and repulsive cues and growth promoting adhesive environments. Cell-cell and cell-substrate interactions via adhesion molecules, especially by molecules belonging to the immunoglobulin superfamily, have been shown to be crucial for nervous system development (Maness and Schachner, 2007). This has been demonstrated by countless *in vitro* assays, antibody perturbation assays as well as loss and gain of function experiments (Bingham et al., 2002).

Due to its relatively simple segmental organization, the developing hindbrain has been the focus of many studies (Bingham et al., 2010). As hindbrain development is essentially conserved among vertebrates, knowledge derived from one species can potentially give insights into hindbrain development in other species (Gilland and Baker, 1993; Moens et al., 1998; Moens and Prince, 2002; Gilland and Baker, 2005). In our study we have focused on the development of the zebrafish hindbrain, especially studying migration and axonal outgrowth of branchiomotoneurons (Drapeau et al., 2002). The concise and segmental organization as well as the stereotype migration and axonal outgrowth pattern have made branchiomotoneurons an attractive model system. Branchio- as well as somato- and viscera-motoneurons represent subgroups of cranial motoneurons whose axons exit the CNS at predetermined exit points (for reviews, see Chandrasekhar, 2004; Song, 2007). Neurons from specific nuclei form different cranial nerve bundles innervating the muscle masses of the branchial (pharyngeal) arches. While somatomotoneurons, innervating extraocular muscles, cluster in the oculomotor (cranial nerve III), the trochlear (IV) and the abducens (VI) motor nuclei; branchiomotoneurons (BMN) build up the trigeminal (V), facial (VII) glossopharyngeal (IX) and vagal (X) nuclei. In zebrafish BMN migration and axon outgrowth is initiated within the first 24 h of development. BMN precursors are generated in specific rhombomeres, which subsequently migrate towards their final destination at characteristic dorsolateral and rostrocaudal positions within the developing hindbrain. For example motoneuron precursors of the facial nerve originating in rhombomere 4 migrate as far as rhombomeres 6 and 7 (Chandrasekhar, 2004; Song, 2007). These cells project axons via specific motor nerves into the periphery. The generation of transgenic zebrafish where GFP expression is driven by the islet1 promoter has proven valuable to study the generation, positioning and axon outgrowth of branchiomotoneurons (Higashijima et al., 2000).

RESEARCH ARTICLE Biology Open (2015) 4, 146–154 doi:10.1242/bio.20148482

Using this Isl1-GFP transgenic line the involvement of planar cell polarity (PCP) pathway genes such as Stbm/Vangl2/tri (Jessen et al., 2002; Sittaramane et al., 2009), prickle1a (Carreira-Barbosa et al., 2003), prickle1b (Rohrschneider et al., 2007), scribble1 (Wada et al., 2005), Celsr2 and Frizzled3a (Wada et al., 2006), col/hdac1 (Nambiar et al., 2007), as well as the PCP effector gene Nhsl1b (Walsh et al., 2011) in the migration of branchiomotoneurons has already been demonstrated. However, besides the genes from the planar cell polarity pathway, other factors must be involved in motoneuron migration in the hindbrain, as several aspects of the migration appear normal in vangl2 mutants (Bingham et al., 2010). Furthermore, a "collective mode" of migration that requires the interaction between migrating facial BMNs themselves and is independent of PCP proteins has been suggested to work together with PCP-dependent mechanisms to drive directed migration of facial BMNs *in vivo* (Walsh et al., 2011). Recent studies also suggest that fucosylated glycans, such as gmds/twd expressed by neuroepithelial cells (Ohata et al., 2009), may repulse migrating vagal motoneurons preventing radial/apical migration (Ohata et al., 2011). Moreover, TAG1, laminin and cadherin mediated signals have been shown to be involved in guiding branchiomotoneurons (Sittaramane et al., 2009; Grant and Moens, 2010; Stockinger et al., 2011). In addition, interaction between motor nerves and sensory nerves are required for the proper axonal growth of trigeminal but not facial nerves (Cox et al., 2011), but the molecules mediating this interaction remain unknown. Interestingly, recently it has been shown that facial branchiomotoneuron migration also depends on the interaction of migrating neurons with axons of the medial longitudinal fascicle (MLF), as preventing MLF axons from entering the hindbrain results in staling of FBMN migration (Wanner and Prince 2013).

We have recently identified a novel group of cell adhesion molecules, called MDGAs (for MAM domain containing glycosylphosphatidylinositol anchor proteins) (Gesemann et al., 2001; Litwack et al., 2004). MDGAs, which belong to the immunoglobulin superfamily of cell adhesion molecules (for review, see Maness and Schachner, 2007), have been shown to be expressed in the spinal cord of different species including rat (Litwack et al., 2004), chicken (Joset et al., 2011) and medaka (Sano et al., 2009). For chicken it has been demonstrated that inactivation of MDGA2 by RNA interference or function blocking antibodies leads to outgrowth defects of commissural interneurons (Joset et al., 2011). Subsequent experiments have demonstrated that MDGA2 interacts homophilically and that interactions between commissural interneurons and MDGA2 positive ipsilateral projecting neurons are important for proper rostral growth of commissural interneurons (Joset et al., 2011).

In order to explore additional roles of MDGA in nervous system development, we have now analyzed MDGAs in the zebrafish *Danio rerio*. In zebrafish three different MDGAs are present; MDGA1, MDGA2A and MDGA2B. Of these, MDGA2A is highly expressed in subsets of migrating cranial motoneurons. Using morpholino mediated knockdown experiments, we could demonstrate that the absence of MDGA2A leads to migration defects of trigeminal neurons as well as aberrant axonal growth and defasciculation of facial branchiomotor axons.

RESULTS

Through comparative database searches with rat, human and chicken MDGA sequences, we found and subsequently cloned three orthologous zebrafish MDGA genes, namely MDGA1, MDGA2A and MDGA2B (for a phylogenetic comparison, see supplementary material Fig. S1). The amino acid sequence of zebrafish MDGA1 shows 59% and the one of zebrafish MDGA2A and -2B 76% and 74% identity with the corresponding rat orthologs. As the homology between individual domains of MDGAs varies significantly, a detailed homology analysis is given in supplementary material Fig. S1. While some data about the RNA distribution and functional properties of rat (Litwack et al., 2004; Takeuchi and O'Leary, 2006; Takeuchi et al., 2007), mice (Ishikawa et al., 2011), chicken (Fujimura et al., 2006; Joset et al., 2011) and medaka (Sano et al., 2009) MDGAs is available, no such information exists for the zebrafish embryo. We therefore performed in situ hybridization assays in zebrafish embryos at different stages of development, to test whether MDGA gene expression correlates with specific aspects of nervous system development.

Zebrafish MDGAs are expressed in the spinal cord and in defined brain areas

Since rat and chicken MDGAs are highly expressed in the developing spinal cord (Litwack et al., 2004; Joset et al., 2011), we started our analysis in the corresponding region of the zebrafish embryo. As expected from rat and chicken studies, zebrafish MDGA transcripts are expressed in distinct interneuron subpopulations within the dorsal and mediolateral part of the embryonic spinal cord (Fig. 1A–C). MDGA1 and MDGA2B transcripts can be observed at regions where dorsal commissural interneurons are located. In addition, MDGA2A and MDGA2B messages are expressed in cell pools that coincide with the location of intermediate and ventral interneuron subpopulations. In the spinal cord MDGA1 positive cells can further be found in a narrow band of mediolateral located interneurons as well as within the dorsal ventricular zone (Fig. 1A), from where newborn cells spread laterally.

Interestingly, MDGA transcripts are also abundantly expressed in the zebrafish brain. At two days post fertilization, MDGA1 riboprobes label distinct clusters of neurons that stretch bilaterally alongside the medial border of the eyes (Fig. 1D,G). The anterior region encompasses the ventral thalamus (asterisks in Fig. 1D,G) and the hypothalamus (arrow in Fig. 1D,G), whereas the posterior cell clusters represent low level staining of branchiomotoneurons. MDGA1 transcripts are also highly expressed in cells of the peripheral nervous system. Three well discernible cell clusters, the anterior and posterior lateral line ganglia as well as cells associated with the otic placode such as cells of the statoacoustic ganglion (gVIII) prominently express MDGA1 (arrowheads in Fig. 1D,G).

MDGA2A transcripts are localized in distinct neuronal clusters corresponding to motoneurons of several cranial nerves (Fig. 1E,H). Among them are motoneurons of the oculomotor (nIII) and trochlear (nIV) nerve in the midbrain (asterisks in Fig. 1E,H), as well as BMNs of the trigeminal, facial and vagal nerve in the hindbrain (Fig. 1E,H, nV/nVII/nX). In addition, MDGA2A transcripts are also weakly expressed in muscle tissue, such as the sternohyoideus (sh) and in mandibular muscles (data not shown). Expression in head muscles can also be seen for MDGA2B transcript. In addition, MDGA2B is expressed in the telencephalon, the ventral thalamus, the tegmentum, the hypothalamus and at low levels also in subpopulation of cranial motoneurons (Fig. 1F,I).

RESEARCH ARTICLE Biology Open (2015) 4, 146–154 doi:10.1242/bio.20148482

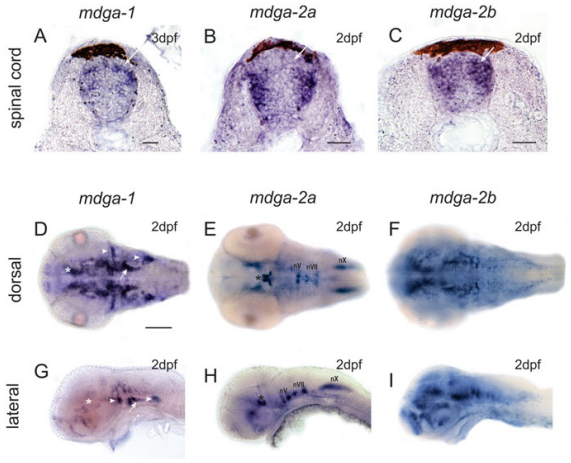

Fig. 1. MDGAs are expressed in the developing zebrafish spinal cord and brain. (A-C) Cross-section through larval zebrafish spinal cords. MDGA1 and MDGA2B staining can be observed at regions where dorsal commissural interneurons are located (white arrow). Additional staining for MDGA2A and MDGA2B can be observed in pools of intermediate and ventral interneuron. MDGA1 positive cells can be found in a narrow band of mediolateral located interneurons. Scale bars represent 25 µm. (D–F) Dorsal and (G–I) lateral view of MDGA whole mount in situ hybridizations of 2dpf larval zebrafish. MDGA1 riboprobes label the ventral thalamus (asterisks in D,G) and the hypothalamus (arrow in D,G). Three well discernible cell clusters in the peripheral nervous system, namely the anterior and posterior lateral line ganglia as well as cells associated with the otic placode such as cells of the statoacoustic ganglion (gVIII) also prominently express MDGA1 (arrowheads in D,G). MDGA2A transcripts can be found in the motoneurons of the oculomotor (nIII) and trochlear (nIV) nerve in the midbrain (asterisks in E,H), as well as branchiomotoneurons of the trigeminal, facial and vagal nerve in the hindbrain (E,H, nV/nVII/nX). MDGA2B is expressed in the telencephalon, the ventral thalamus, the tegmentum, the hypothalamus and at low levels also in subpopulation (nVII and nX) of cranial motoneurons (F,I). Scale bars in D equals 100 µm.

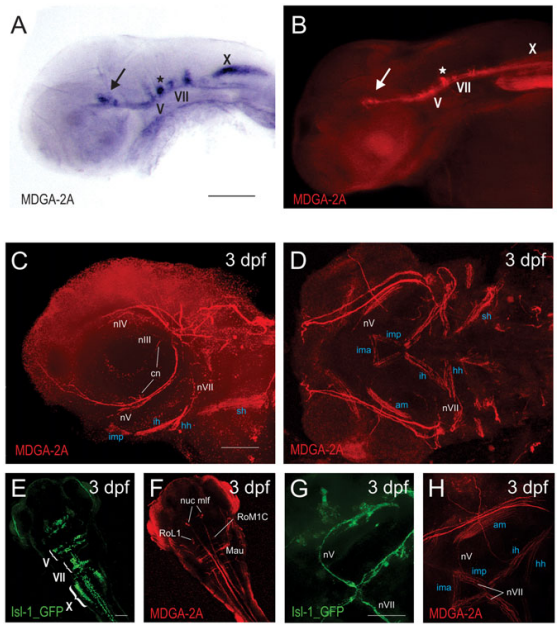

Fig. 2. Antibodies against MDGA2A label neurons and axons of branchiomotoneurons. (A,B) Comparison between MDGA2A RNA and protein distribution demonstrates that the MDGA2A antibody highlights identical structures as seen with MDGA2A riboprobes. Neurons and axons of the oculomotor (arrow), the trigeminal (V) and the facial (VII) nerve are clearly MDGA2A positive (A,B). (C,D,F,H) At 3dpf MDGA2A is located on specific nerves. MDGA2A antibodies highlight branches of the ciliary nerve (cn), the oculomotor nerve (nIII), the trochlear cranial nerve (nIV), several branches of the trigeminal nerve (nV) and the facial nerve (nVII) (C,D). MDGA2A positive nV axons run ventrally along the caudal edge of the eye. The distal nV innervates the imp and merges with both the contralateral nV and the distal tip of the seventh nerve (nVII) at the midline (H). Moreover neurons and axons of medial longitudinal fascicle (mlf), the Mauthner neurons (Mau) and neurons of the reticular formation (RoM1C, RoL1) express MDGA2A (F). (E,G) Isl-1 GFP staining in cranial motoneurons. As previously reported Isl-1 GFP transgenic zebrafish display intense cranial motoneurons V, VII and X staining (E). Moreover staining in the trigeminal as well as the facial nerve can easily be seen (G). Abbreviations: am, adductor hyomandibulae; cn, ciliary nerve; hh, hyohyal muscle; ih, interhyal muscle; ima, intermandibularis anterior; imp, intermandibularis posterior; Mau, mauthner neurons; nuc, mlf nucleus of the medial longitudinal fascicle; nV, trigeminal nerve (neurons); nVII, facial nerve (neurons); nX, vagal nerve (neurons); RoL1 and RoM1C, neurons of the reticular formation; sh, sternoid muscle. Scale bars equal 100 µm.

MDGA2A is expressed in axonal tracts of cranial motoneurons during development

The concise and segmentally arranged cell bodies and their stereotype axonal course have made BMNs an easily accessible system for studying different aspects of neuronal development, such as tangential migration and axon pathfinding (Bingham et al., 2002). Moreover, transgenic zebrafish lines with BMNs expressing GFP under the control of the Islet 1 promoter have substantially contributed to deciphering the molecular aspects of their development. In this transgenic zebrafish line, the Islet1 promoter/enhancer sequence drives GFP expression in cranial motoneurons, some of the cranial sensory neurons, and several other groups of cells (Fig. 2E,G; Higashijima et al., 2000). As MDGA2A is highly expressed in cranial motoneurons, we generated peptide antibodies against MDGA2A to analyze the distribution and potential role of MDGA2A in developing cranial neurons. In agreement with the RNA distribution pattern, MDGA2A antibodies stained neuronal cell bodies and axonal tracts and to a lesser extend head muscles. In the hindbrain, branchiomotoneurons are stained by MDGA2A antibodies (Fig. 2A,B). Among the MDGA2A positive cranial nerves are tracts of the oculomotor (nIII) and trochlear (nIV) nerves. The ciliary nerve (cn, part of nIII) innervating the lens muscle as well as a branch of nIV that innervates the superior oblique muscle are clearly MDGA2A positive (Fig. 2C). Additional axons expressing MDGA2A are the trigeminal (nV) and facial (nVII) motor nerves, innervating muscles in the jaw and jaw-support structures (Schilling and Kimmel, 1997; Chandrasekhar, 2004), as well as axons within the vagal motor nerve (nX) (Fig. 2C,D,H).

In addition to structures in the hindbrain, the MDGA2A antibody recognizes a number of neurons and axons in the central and peripheral nervous system (Fig. 2F; supplementary material Fig. S2). Among them are axons of the presumptive spino-occipital nerve (supplementary material Fig. S2), the bilaterally arranged nuclei of the medial longitudinal fascicle (nuc mlf; Fig. 2F) and its axonal tracts (mlf; supplementary material Fig. S2), reticulospinal neurons such as the assumed RoM1C and

RESEARCH ARTICLE Biology Open (2015) 4, 146–154 doi:10.1242/bio.20148482

RoL1 neurons as well as the large Mauthner neurons. Moreover, the lateral line system and components of the statoacoustic ganglion, both of which innervate hair cells of the head, trunk, tail and the inner ear are MDGA2A positive (for more information, see supplementary material Fig. S2).

In summary, MDGA2A protein is prominently expressed in several neuronal subpopulations and their axons during the period of neuronal migration and axon outgrowth, suggesting a potential role for this molecule in mediating adhesive interactions during these processes. To test such a hypothesis, we selectively downregulated MDGA2A protein synthesis using morpholino antisense oligonucleotides and analyzed occurring phenotypes.

MDGA2A deprivation leads to impaired migration and axonal growth of branchiomotoneurons

Since MDGA2A message is present in subgroups of branchiomotoneurons, namely the trigeminal, facial and vagal motoneurons, we further analyzed the effect of MDGA2A protein knockdown in Islet1-GFP transgenic zebrafish embryos. To analyze the efficiency of protein knockdown in MDGA2A morpholino treated zebrafish we compared antibody stainings in wildtype (wt) and MDGA2A knockdown animals. Neurons and axons that are clearly stained in wt fish, lack corresponding immunoreactivity in MDGA2A knockdown zebrafish (Fig. 3A–D; supplementary material Fig. S4C). Interestingly, several cranial motoneuron migration and axon outgrowth defects could be observed in Islet1-GFP MDGA2A knockdown animals. While in wt zebrafish migration of trigeminal BMNs occurs within the limits of their rhombomere (r) of origin resulting in the formation of an anterior and posterior trigeminal motor nucleus in r2 and r3, respectively; in MDGA2A morphants, trigeminal motoneurons (V) fail to undergo their proper migration pattern and settle at various ectopic positions (arrows in Fig. 3F). Also, neurons within clusters appear disorganized, accumulating in a pile, instead of settling in the characteristic lateral trigeminal clusters. Interestingly, motoneurons of the facial nerve (VII) have left their place of origin in r4 and undergone appropriate caudal migration. However, their number in the forming clusters seems to be reduced. Moreover, the bilateral branches of the vagal motor nucleus appear more prominent, as if containing more cells than normal.

Examination of the corresponding axon tracts in uninjected and morphant embryos suggest that fewer axons run in axonal tracts of MDGA2A deprived embryos (Fig. 3G,H). Interestingly, their course and innervation pattern is still maintained in MDGA2A knockdown animals, indicating that proper pathfinding of growing trigeminal and facial motoneurons can still occur. Nevertheless, many axons seem to stall along the axonal path, leaving a reduced number to reach their muscle targets. While the reduced number of axons running in these tracts may be caused by errors originating from the absence of MDGA2A, this phenotype may also be caused by migration defects of the mentioned branchiomotoneurons. In order to study these phenotypes in more detail *in vivo*, we performed time- lapse light sheet microscopy.

Live light sheet microscopy of zebrafish branchiomotoneuron development confirms MDGA2A knockdown phenotypes

To observe branchiomotoneuron migration and axon outgrowth in real time, Isl-l:GFP fish were imaged by digital scanned light sheet microscopy (DSLM) between 24–36 hpf. Image stacks

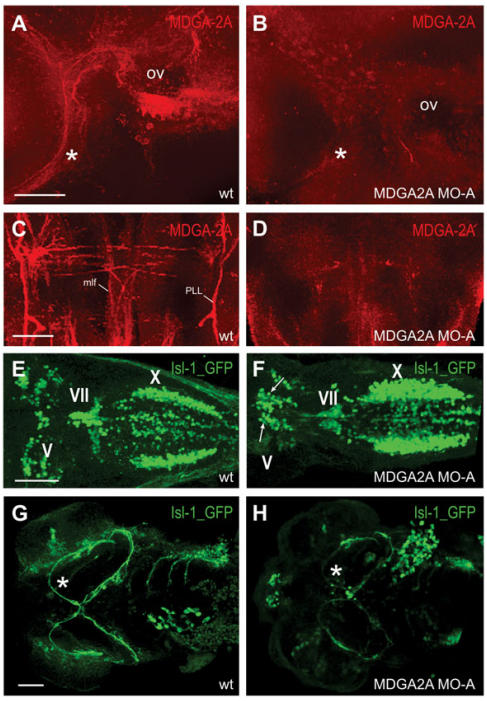

Fig. 3. MDGA2A knockdown causes migration and guidance errors of trigeminal motoneurons. (A–D) MDGA2A staining in wt and MDGA2A knockdown zebrafish at 3dpf. Lateral views of MDGA2A labeled zebrafish demonstrate that antisense morpholino injections against MDGA2A efficiently downregulates the expression of MDGA2A. Neither MDGA2A positive hair cells along the otic vesicle (oc) nor the trigeminal nerve (asterisk) are stained in MDGA2A morphants (A,B). Also staining in the mlf and PLL is clearly downregulated (C,D). (E–H) Migration and axon outgrowth pattern of branchiomotoneurons in wt and MDGA2A knockdown zebrafish at 3dpf. In wt fish branchiomotoneurons occupy characteristic locations, with the trigeminal cluster being located in r2/r3 and the facial cluster lying adjacent to the midline (E). In MDGA2A morphants, trigeminal neurons settle at ectopic locations (arrow) (F). Moreover, staining intensity in the trigeminal (asterisk) and facial (arrowhead) nerve is strongly reduced in MDGA2A knockdown larva, suggesting that fewer axons are present in these nerve bundles. Abbreviations: ov otic vesicle; mlf medial longitudinal fascicle; PLL posterior lateral line fascicle; V trigeminal motoneurons; VII facial motoneurons; X vagal motoneurons. Scale bars in A,B, and E–H equal 50 μm, in C,D 25 μm.

that covered the region of the nV, nVI and nVII axons were recorded every 16 min (supplementary material Movie 1). In wt control embryos trigeminal neurons formed compact clusters and stayed together throughout the period of observation (24–36 hpf; Fig. 4A, w1–w5; supplementary material Movie 2). Interestingly, in MDGA2A morpholino treated embryos, single trigeminal neurons started to move along the axon bundle instead of remaining in a stable cell cluster (Fig. 4A, m1–m5; supplementary material Movie 2). To quantify this phenotype we measured the fluorescence intensity along the trigeminal nerve. At 28 hpf the fluorescence intensity along the axons started to increase in MDGA2A knockdown animals compared to control embryos and remained higher than control values during the rest of the observation period. During this period continuous ectopic migration takes place in morpholino injected animals

RESEARCH ARTICLE Biology Open (2015) 4, 146–154 doi:10.1242/bio.20148482

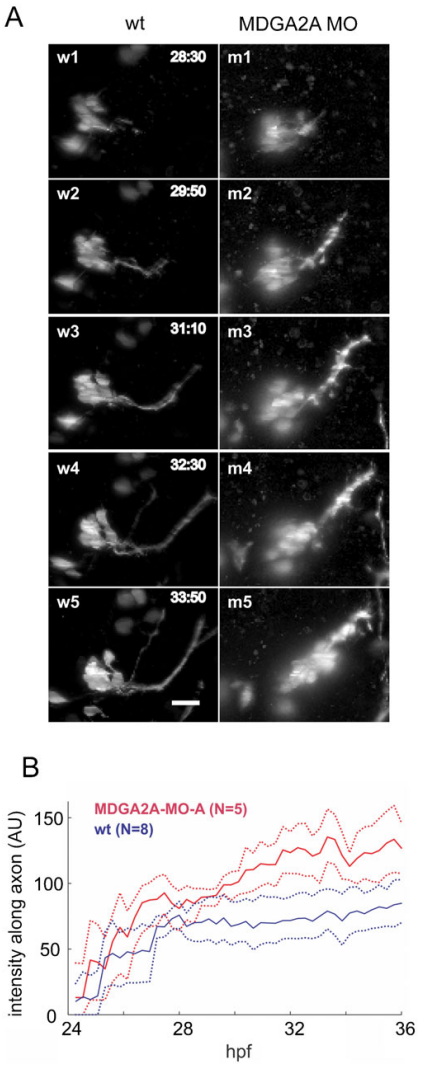

Fig. 4. MDGA2A knockdown increases mobility of trigeminal (V) neurons. (A) Living isl-1 embryos were imaged by digital scanned laser light sheet microscopy from 24–36 hpf at 16 min intervals. For analysis the images were deconvolved and the stacks were compressed into maximum projections. Representative images from control and MDGA2A morpholino treated embryos are shown. During the experimental period trigeminal neurons send out axons along a well-defined path, with no movement of the trigeminal neurons (w1–w5). In MDGA2A knockdown animals the compactness of the trigeminal cell cluster is impaired. Trigeminal neurons migrate along their axon bundles leaving their place of origin (bright dots along the axon bundle; m1–m5). (B) To quantify this migration phenotype, the time course of the fluorescence intensity along the trigeminal axon bundle was quantified in 8 control embryos and 5 MDGA2A morpholino treated embryos. Shown are the mean and bootstrap confidence intervals (as dotted lines, $\alpha=0.05$). Note that the fluorescence intensity along the trigeminal nerve in MDGA2A knockdown animals increases significantly past 30 hpf, representing the aberrant migration of trigeminal neurons. For more details see supplementary material Fig. S3A–C for individual intensity traces. The timestamp is hours post fertilization (h: min), N is the number of analyzed embryos, the scale bar is 20 μm.

(supplementary material Figs S4B, S3; Movie 2). Regular confocal pictures taken from 34 hpf zebrafish embryos treated with 3 different MDGA2A morpholino oligonucleotides, confirmed that cohesion between trigeminal neurons is weakened in MDGA2A knockdown fish and that some cells undergo ectopic migration (supplementary material Fig. S4A,D). While in confocal stacks of wt and control morpholino injected embryos an average of 12.35 ± 0.21 neurons can be seen in the trigeminal nerve cluster, MDGA2A knockdown fish have a significantly reduced number (9.66 ± 0.27; $p<0.005$). These missing cells can be found at ectopic positions often along the trigeminal nerve (arrows in supplementary material Fig. S4A), a situation never observed in wt embryos.

Axonal outgrowth of nVII axons started around 28 hpf and 3 h later a characteristic 60° turn could be observed, as previously reported by Higashijima et al. (Higashijima et al., 2000) (Fig. 5, w2–w4, asterisks; supplementary material Movie 1). At the turning point continuous outgrowth of short protrusions were observed, but they readily retracted and the main axon bundle stayed fasciculated (Fig. 5, w2–w4; supplementary material Movie 1). By 34 hpf, a stable bundle of axons all showing the 60° turn was established. However, upon morpholino mediated knockdown of MDGA2A, the turn of the axon was less pronounced and the turning angle was decreased (Fig. 5, mA2-4, mB2-4; supplementary material Movie 3). As for control embryos, axons in the region of the turning point started to protrude in random directions, but in MDGA2A knockdown

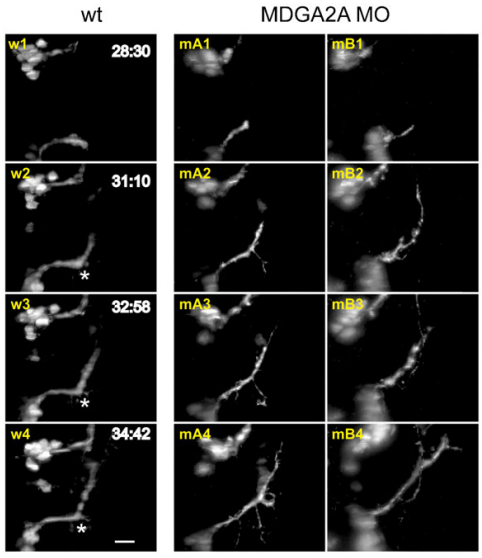

Fig. 5. MDGA2A knockdown decreases nVII axon bundling. Representative images from control (w) and MDGA2A morpholino treated (mA and mB) embryos are shown. 28 to 34 h post fertilization facial neurons in wt embryos project axons along a predetermined path, displaying a well-documented 60° turn (asterisks). In MDGA2A morphants this turning angle is absent or strongly reduced and defasciculation events occur much more frequently. Analyzing fluorescence intensity below the main axon bundle of the facial nerve indicates that fluorescence in MDGA2A knockdown embryos is slightly increased, supporting the finding of increased defasciculation and axon branching of facial neurons (see supplementary material Fig. S3D–F). The scale bar represents 20 μm.

RESEARCH ARTICLE Biology Open (2015) 4, 146–154 doi:10.1242/bio.20148482

animals these axons did less frequently retract, and some even continued growing. In addition, the axon bundles in MDGA2A morpholino treated embryos were less organized and often highly defasciculated compared to control embryos (supplementary material Movie 3). To quantify this axon outgrowth phenotype, we measured the fluorescence intensity in an area below the axon in the DSLM images (supplementary material Fig. S3). In animals older than 30 hpf the total fluorescence intensity in this area was slightly higher for MDGA2A morpholino treated embryos compared to control. Confocal pictures of embryos treated with 3 different MDGA2A morpholinos showed extensive protrusions at the choice point and a significantly reduced turning angle (32.75±1.53°) compared to control fish (58.15±1.11, $p<0.005$; supplementary material Fig. S4B,D).

In summary, in MDGA2A morpholino treated embryos several subpopulations of branchiomotoneurons display errors in the predetermined migration pattern and/or their axons show increased collateral branch formation and less intense bundling.

DISCUSSION

MDGA proteins have been studied in humans (De Juan et al., 2002; Díaz-López et al., 2005), rats (Litwack et al., 2004), mice (Takeuchi et al., 2007), chickens (Fujimura et al., 2006) and medaka (Sano et al., 2009). Here we identified and cloned three MDGA orthologs in zebrafish, MDGA1, MDGA2A and MDGA2B. We found MDGA2A to be expressed in a subset of motoneurons, especially in the ones of the cranial, trigeminal and facial nerves. Morpholino mediated knockdown of MDGA2A led to aberrant cell migration of trigeminal neurons and to defasciculation and increased branch formation of the trigeminal as well as facial nerve. These results demonstrate that MDGA2A interactions are necessary for proper migration, axon outgrowth and bundling in cranial motoneurons.

In agreement with our current findings, MDGAs in other species have already been implicated in neuronal migration and axon guidance. In rats, MDGA positive cells were found in the pontine migratory stream, suggesting that these circumferentially migrating neurons may rely on this cell adhesion molecule for proper neuronal migration (Litwack et al., 2004). In addition, in MDGA1 loss of function mice proper radial migration of superficial layer cortical neurons is blocked (Takeuchi and O'Leary, 2006), and MDGA-2 knockdown in chicken by RNA interference induced strong axon outgrowth phenotypes in MDGA expressing commissural interneurons (Joset et al., 2011). Instead of turning rostral after crossing the ventral midline, commissural axons in MDGA2A knockdown animals stall at the contralateral side, unable to follow ipsilateral-projecting axon fascicles (Joset et al., 2011).

In zebrafish embryos MDGA2A is expressed in motoneurons of the oculomotor (nIII) and trochlear (nIV) cranial nerve in the midbrain, and the branchiomotoneurons of the trigeminal, facial and vagal nerve in the hindbrain. In support of a role in axon outgrowth, MDGA2 is expressed in the spinal cord during neuronal migration and axon path finding in various species.

Only few MDGA binding partners have been discovered so far. We found earlier that chicken MDGA2 formed homophilic trans-interactions in multiple assays, while heterophilic interactions between MDGA2 and MDGA1 were not detected (Joset et al., 2011). MDGA1 in contrast, did not form homophilic interactions but soluble recombinant protein was shown to bind to axon rich regions in chicken and this interaction was MAM domain dependent (Fujimura et al., 2006; Joset et al., 2011). More recently, it was reported by two independent groups that both MDGAs interact via their Ig-repeats with neuroligin-2 in cis (Lee et al., 2013; Pettem et al., 2013). The affinity of MDGA1 for neuroligin-2 was in the low nanomolar range, while MDGA2 binding was weaker (Pettem et al., 2013). Taken together, these results suggest that MDGA1 and MDGA2 binding preferences clearly differ. MDGA1 may undergo strong heterophilic interactions in cis thereby regulating the function of its binding partners, while MDGA2 may preferentially form homophilic interactions in trans serving as an adhesion factor. Depending on the concentration of MDGA2 in trans and the presence of binding partners such as neuroligin-2 in cis, MDGA2s regulatory or adhesive function may dominate.

Recently, it has been shown that neuron to neuron as well as neuron to extracellular matrix contacts are important for facial motoneuron migration (Wanner et al., 2013). While contact to a specific pioneer neuron seems to be required to lead following facial neurons in the early phase of migration, interaction with axons of the medial longitudinal fascicle is required in a subsequent phase of migration (Wanner and Prince, 2013). In the case of facial branchiomotoneuron migration, cdh2 and Tag1 seem to play a crucial role (Wanner and Prince, 2013; Sittaramane et al., 2009); however, these molecules have no influence on trigeminal neuronal migration. In our case the knockdown of MDGA2A has no effect on neuron migration but enhances the mobility of trigeminal neurons, which relocated from their original place to settle at ectopic positions. This increased mobility might be due to the lack of MDGA2A mediated homophilic interactions in trans, weakening the cohesion of trigeminal neurons enabling them to migrate along their axonal fascicle. Interestingly, even though facial neuronal migration is unaffected in MDGA2A knockdown animals, axonal outgrowth of facial neurons is clearly impaired. In line with the fact that MDGA-2 is a homophilic cell adhesion molecule, the MDGA2A positive facial nerve is less compact and seems to contain fewer axons in MDGA2A morphants. In addition, increased axon defasciculation along the facial nerve can be seen and the entire nerve path deviates from patterns seen in wild type embryos, again suggesting that MDGA2A mediated homophilic adhesion is keeping the facial nerve compact. Moreover, at a well-defined choice point, where trigeminal axons in wild type animals make a characteristic 60° turn (Higashijima et al., 2000), axons in MDGA2A knockdown animals display many collaterals and large protrusions, as being unable to make the correct pathway decision. Consequently, the angle at which axons in MDGA2A knockdown animals are leaving this choice point is dramatically reduced, suggesting that some aspects of proper guidance are missing. A similar phenotype has already been observed in MDGA2 knockdown chicken embryos, where turning of commissural interneurons after midline crossing is impaired. Instead of turning rostral, commissural axons in MDGA2A deficient embryos stall after midline crossing being unable to interconnect with MDGA2A positive tracts on the contralateral site (Joset et al., 2011). This similarity between the chicken and our zebrafish phenotype suggests that MDGA2A might confer adhesive interactions between different axonal tracts, thereby enabling follower tracts to use pioneer tracts as predetermined highways.

Interestingly, rare deletions in the MDGA2 gene were recently correlated with autism spectrum disorders (ASD) (Bucan et al., 2009). This puts MDGA2 in line with other neuronal cell adhesion molecules of the immunoglobulin family, such as

RESEARCH ARTICLE Biology Open (2015) 4, 146–154 doi:10.1242/bio.20148482

contactins, NRCAM, CADM1 and LRFN5 that are implicated in axon migration and guidance and were associated with autism (Berglund et al., 1999; Fernandez et al., 2004; Glessner et al., 2009; Roohi et al., 2009; Cottrell et al., 2011; Morrow et al., 2008; van Daalen et al., 2011; Bonora et al., 2005; Marui et al., 2009; Zhiling et al., 2008; de Bruijn et al., 2010). In summary, the association of truncated MDGA2 variants with ASD, and the notion that a number of neuronal cell adhesion factors are implicated in ASD, supports also a role of human MDGA2 as a cell adhesion molecule important in neuronal positioning and axon guidance.

MATERIALS AND METHODS

Fish maintenance and breeding

Wild-type fish from the inbred WIK and Tübingen strain as well as fish from the Islet1-GFP transgenic line were bred and maintained under standard conditions. Embryos were raised at 28℃ in E3 medium. Morphological features characteristic for developmental stages were used to determine the stages of the embryos in hours post fertilization (hpf), according to Kimmel et al. (Kimmel et al., 1995). All experiments were performed according to the European Communities Council Directive for animal use in science (2010/63/EU) and in accordance with Swiss laws.

Identification and cloning of zebrafish MDGAs

Through comparative database searches with the corresponding rat and chicken MDGA sequences we identified and subsequently cloned cDNA sequences of three zebrafish MDGA orthologs, MDGA1, MDGA2A and MDGA2B, respectively. Oligo dT primed cDNA, serving as template for MDGA PCRs, was done using the first strand cDNA kit (Invitrogen, Carlsbad, CA). Total RNA used for reverse transcription was isolated from 5 day old wt fish using the QIAShredder and the RNeasy kit (Qiagen, Hombrechtikon, Switzerland). For polymerase chain reaction (PCR) Taq polymerase (Taq Gold; Applied Biosystems) and sequence-specific oligonucleotide primers were used. Amplified DNA pieces were subcloned into the TOPO pCRII vector (TA Cloning Kit Dual Promoter, Invitrogen, Carlsbad, CA) and subsequently sequenced.

Whole mount in situ hybridization

Linearized MDGA containing plasmids were purified using the QIAquick PCR Purification Kit (Qiagen). *In vitro* transcription of DNA probes using the SP6 and T7 RNA polymerases was performed using the Roche DIG-RNA Labeling Kit (Roche Diagnostics, Rotkreuz, Switzerland). Probes longer than 1000 bp were hydrolyzed prior to hybridization. Embryos predetermined for in situ hybridization were treated with 3 µM PTU [1- phenyl-2-hiourea (Sigma)] to suppress pigmentation. PTU-treated embryos were collected at different stages of development and staged by morphology. The embryos were dechorionated, fixed in paraformaldehyde (4% in PBS, pH 7.25) and incubated at 4℃ overnight or at room temperature (RT) for 1–2 h. Subsequently, the embryos were dehydrated in a PBT/methanol series and stored in methanol at −20℃. For in situ hybridization, embryos were rehydrated stepwise in methanol/PBT. To enhance penetration of the antisense RNA probe, embryos older than 24 hpf were treated with 10 µl/ml Proteinase K (Roche) at different durations, depending on their developmental stage. The reaction was stopped by rinsing in PBT (PBS pH 7.25, 0.1% Tween-20). Then, the embryos were post-fixed in paraformaldehyde (4% in PBS, pH 7.25) for 20 min and washed in PBT 5 times for 5 min. Embryos were prehybridized for 2–5 h between 62 to 68℃ in hybridization buffer (50% formamide, 5×SSC, 5 mg/ml torula yeast RNA (typeVI, Sigma), 50 µg/ml heparin (Sigma), 125 µg/ml fish sperm DNA (Roche), 0.1% Tween-20). Afterwards, the prehybridization buffer was replaced by pre-warmed hybridization buffer containing 1–2 ng/µl of Dig labeled antisense RNA. Hybridization occurred at 62℃–68℃ overnight. The embryos were washed in a series of hybridization buffer/SSC steps for 15 min at 62 to 68℃. Embryos were subsequently washed in MABT (100 mM Maleic acid, 150 mM NaCl, 0.1% Tween-20, pH 7.5) for 5 min at RT and blocked for 2 h in blocking solution (2% Boehringer Blocking reagent in MABT). Antibody solution (anti-Digoxigenin-AP, Fab fragments from Roche diluted 1:4000 in blocking solution) was incubated ON at 4℃, followed by 3×15 min washes in blocking solution and 3×15 min in NTMT (0.1 M Tris-HCl pH 9.5, 0.1 M NaCl, 0.05 M MgCl, 1 mM Levamisol, 0.1% Tween-20). Staining solution (0.5 mg/ml NBT, 0.175 mg/ml BCIP (both from Roche) in NTMT) was applied for 1–4 h in darkness, and was replaced by PBT. Embryos were post-fixed in 4% PFA for 20 min, washed in PBT and brought into Glycerol for imaging and storage. For obtaining optimal pictures, larvae were mounted on an adapted glass slide in 100% glycerol (Sigma-Aldrich) and the DIC modus of a light microscope (Olympus BX61) and a colour camera (ColorView IIIu, Soft Imaging System, Olympus) were used.

Immunohistochemistry

Embryos were fixed in 4% PFA for 2 h at RT and brought into Methanol at −20℃ via dilution series, for at least 1 h or for long term storage. Embryos were rehydrated in a Methanol series and washed 5× in PBT (PBS pH 7.25, 0.1% TritonX-100) before permeabilization in Collagenase A solution (3 mg/ml in Ringer solution) for 150 min at RT. Embryos were than washed twice in PBT, fixed in 4% PFA for 20 min, washed 5× in PBT and blocked at RT for several hours in blocking solution (1% BSA, 1% DMSO, 0.5% TritonX-100, 2.5% Normal goat serum, in PBS). Antibodies (rabbit anti-MDGA2A 1:300, mouse anti-GFP (Roche) 1:200 in blocking solution) were applied and incubated ON at 4℃. Embryos were then washed 4×15 min in PBT, 3×15 min in blocking solution and incubated in secondary antibody solution (Alexa goat anti-rabbit 568 1:500, Alexa goat anti-mouse 488 1:1000 in blocking solution) for 1 h at RT. After 4×15 min washes in PBT, embryos were brought into Glycerol for imaging and storage (at 4℃). To demonstrate the effectiveness of MDGA2A morpholino protein knockdown, wt and morphants were stained and imaged under identical conditions (e.g identical exposure times).

Antisense morpholino oligonucleotide injections

Antisense morpholino oligonucleotides were synthesized by Gene Tools (Gene Tools, LLC, Philomath, OR). The targeting sequence for MDGA2A-MO-A was 5′- ACAGGAGAGCCCAGATAATATCCAT-3′ covering the first 25 nucleotides of the coding sequence (1–25). Targeting sequences of MO-B and MO-C were 5′-CGTTAGTCT-GCACATATCCAGCTCC-3′ (−31 to −6) and 5′-TCTTCACGTTA-GTCTGCACATATCC-3′ (−24 to 1) respectively. Standard control morpholinos 5′- CCTCTTACCTCAGTTACAATTTATA-3′ were used as control to monitor unspecific developmental defects. 4.5 ng (MO-A) to 6 ng (MO-B,C, control) of antisense morpholino oligonucleotides were injected into one- to four-cell stage of Islet1-GFP embryos. After injections, 250 µl Penicillin per dish was added. Dechorionated fish were fixed in paraformaldehyde (4% in PBS, pH 7.25) at different stages followed by dehydration in a PBT/methanol series and stored in methanol at −20℃. The fish were analyzed by immunohistochemistry and light sheet microscopy.

Production of anti-MDGA2A peptide antibodies

For the generation of MDGA2A specific antibodies, a short peptide covering the amino acids 276–289 (LSWVRNTEELPKKS) of MDGA2A was synthesized (Eurogentec, Belgium). The used sequences were checked for intrafamiliar sequence homology using the MegAlign program. Prior to immunization, pre-sera were tested for cross-reactivity by western blot analysis. Two rabbits were injected with the synthesized peptide. Rabbits were boosted after 14 days and 28 days, respectively. A first blood sample was taken at day 38, followed by an additional injection on day 56 and a second blood sample that was taken at day 66. The final bleeding was done after 87 days. Antibodies were delivered as sera and IgGs affinity purified against the corresponding MDGA2A peptide.

Confocal analysis

Fluorescent samples were mounted in GG1 Glycerol Gelatin (Sigma) and viewed with a Leica SP2/SP8 Confocal Microscope. 20× and 63×

RESEARCH ARTICLE Biology Open (2015) 4, 146–154 doi:10.1242/bio.20148482

Glycerin objectives were used to picture confocal sections every approximate 0.6 µm with an average number of 150 steps.

Light sheet microscopy

We employed Digital Scanned Laser Light Sheet Microscopy (DSLM) for three-dimensional imaging, as previously described (Keller et al., 2008). The central thickness of the light sheet was set to 4 µm (FWHM). An Achroplan W 40×/0.8 water-dipping objective (Carl Zeiss) was used for fluorescence detection. Three-dimensional image stacks were recorded in 16 min time intervals with a Coolsnap 4K CCD camera (12 bit, 7.4 µm pixel pitch, 2048 × 2048 pixels; Roper Scientific). The spacing between single images in the three-dimensional stack was set to 2.2 µm and a total of 600 images were recorded per stack, covering a specimen volume of 379 × 379 × 1320 µm.

Image processing

Images were deconvolved with the Lucy-Richardson algorithm and specimen drift was corrected by custom software developed in Matlab, as previously described (Keller et al., 2008). For visualization of the three-dimensional image data as a function of time, maximum-intensity projections were generated.

Intensity measurement

To measure the intensity of axons, a line was drawn manually along the axon, a region in a certain radius around that line was selected and the pixel intensities of that region in the maximum projection were averaged. An area at the edge of the image was used for background subtraction. This procedure was repeated for every maximum projection of a movie to obtain the time course of fluorescence intensity. The values from multiple embryos were averaged and plotted together with the standard error of the mean.

Statistical analysis

Significance of fluorescent intensity along the facial nerve was calculated by bootstrapping. For each time point the mean and confidence intervals at an alpha value at 0.05 were calculated from 1000 repeats. For determining the number of cells in nV clusters wt (n=11), control morpholino injected (n=6) and MDGA2A morphant (n=28) zebrafish in 3D reconstructions of confocal stacks using Bitplane Imaris software were analyzed. Statistical analysis was performed using two-tailed homoscedastic Student's t-test. For the analysis of migrating cells a two-tailed heteroscedastic Student's t-test was done because no migrating cells have been observed in wt zebrafish. The angle of nVII projections (wt n=9, control morpholino injected n=6, and MDGA2A morphants n=26) were measured using Image J's angle tool on maximum intensity projections. Statistical significance was calculated by two-tailed homoscedastic Student's t-test.

Acknowledgements

We thank Kara Dannenhauer for excellent technical assistance and Dr Chiara Cianciolo for critically reading the manuscript.

Competing interests

The authors have no competing interests to declare.

Author contributions

MG conceived the study. EI, CMM, CJB, AL and PR designed and performed experiments. PJK and EHS designed and built the DSLM microscope. EI, CMM, CJB and MG wrote the manuscript. UFG was involved in setting up the DSLM microscope and gave suggestions about the manuscript. CFN gave conceptual input to the project and provided fish and other important resources. All authors have read and approved the final manuscript.

Funding

CJB was supported by the Novartis Research Foundation and fellowships from the Swiss National Science Foundation. This work was supported by ETH Zurich research grants.

References

Berglund, E. O., Murai, K. K., Fredette, B., Sekerková, G., Marturano, B., Weber, L., Mugnaini, E. and Ranscht, B. (1999). Ataxia and abnormal cerebellar microorganization in mice with ablated contactin gene expression. *Neuron* **24**, 739-750.

Bingham, S., Higashijima, S., Okamoto, H. and Chandrasekhar, A. (2002). The Zebrafish trilobite gene is essential for tangential migration of branchiomotor neurons. *Dev. Biol.* **242**, 149-160.

Bingham, S. M., Sittaramane, V., Mapp, O., Patil, S., Prince, V. E. and Chandrasekhar, A. (2010). Multiple mechanisms mediate motor neuron migration in the zebrafish hindbrain. *Dev. Neurobiol.* **70**, 87-99.

Bonora, E., Lamb, J. A., Barnby, G., Sykes, N., Moberly, T., Beyer, K. S., Klauck, S. M., Poustka, F., Bacchelli, E., Blasi, F. et al.; International Molecular Genetic Study of Austism Consortium (2005). Mutation screening and association analysis of six candidate genes for autism on chromosome 7q. *Eur. J. Hum. Genet.* **13**, 198-207.

Bucan, M., Abrahams, B. S., Wang, K., Glessner, J. T., Herman, E. I., Sonnenblick, L. I., Alvarez Retuerto, A. I., Imielinski, M., Hadley, D., Bradfield, J. P. et al. (2009). Genome-wide analyses of exonic copy number variants in a family-based study point to novel autism susceptibility genes. *PLoS Genet.* **5**, e1000536.

Carreira-Barbosa, F., Concha, M. L., Takeuchi, M., Ueno, N., Wilson, S. W. and Tada, M. (2003). Prickle 1 regulates cell movements during gastrulation and neuronal migration in zebrafish. *Development* **130**, 4037-4046.

Chandrasekhar, A. (2004). Turning heads: development of vertebrate branchiomotor neurons. *Dev. Dyn.* **229**, 143-161.

Cottrell, C. E., Bir, N., Varga, E., Alvarez, C. E., Bouyain, S., Zernzach, R., Thrush, D. L., Evans, J., Trimarchi, M., Butter, E. M. et al. (2011). Contactin 4 as an autism susceptibility locus. *Autism Res.* **4**, 189-199.

Cox, J. A., Lamora, A., Johnson, S. L. and Voigt, M. M. (2011). Diverse mechanisms for assembly of branchiomeric nerves. *Dev. Biol.* **357**, 305-317.

de Bruijn, D. R. H., van Dijk, A. H. A., Pfundt, R., Hoischen, A., Merkx, G. F. M., Gradek, G. A., Lybæk, H., Stray-Pedersen, A., Brunner, H. G. and Houge, G. (2010). Severe progressive autism associated with two de novo changes: A 2.6-Mb 2q31.1 deletion and a balanced t(14;21)(q21.1;p11.2) translocation with long-range epigenetic silencing of LRFN5 expression. *Mol Syndromol* **1**, 46-57.

De Juan, C., Iniesta, P., González-Quevedo, R., Morán, A., Sánchez-Pernaute, A., Torres, A. J., Balibrea, J. L., Díaz-Rubio, E., Cruces, J. and Benito, M. (2002). Genomic organization of a novel glycosylphosphatidylinositol MAM gene expressed in human tissues and tumors. *Oncogene* **21**, 3089-3094.

Díaz-López, A., Rivas, C., Iniesta, P., Morán, A., García-Aranda, C., Megías, D., Sánchez-Pernaute, A., Torres, A., Díaz-Rubio, E., Benito, M. et al. (2005). Characterization of MDGA1, a novel human glycosylphosphatidylinositol-anchored protein localized in lipid rafts. *Exp. Cell Res.* **307**, 91-99.

Drapeau, P., Saint-Amant, L., Buss, R. R., Chong, M., McDearmid, J. R. and Brustein, E. (2002). Development of the locomotor network in zebrafish. *Prog. Neurobiol.* **68**, 85-111.

Fernandez, T., Morgan, T., Davis, N., Klin, A., Morris, A., Farhi, A., Lifton, R. P. and State, M. W. (2004). Disruption of contactin 4 (CNTN4) results in developmental delay and other features of 3p deletion syndrome. *Am. J. Hum. Genet.* **74**, 1286-1293.

Fujimura, Y., Iwashita, M., Matsuzaki, F. and Yamamoto, T. (2006). MDGA1, an IgSF molecule containing a MAM domain, heterophilically associates with axon- and muscle-associated binding partners through distinct structural domains. *Brain Res.* **1101**, 12-19.

Gesemann, M., Litwack, E. D., Yee, K. T., Christen, U. and O'Leary, D. D. (2001). Identification of candidate genes for controlling development of the basilar pons by differential display PCR. *Mol. Cell. Neurosci.* **18**, 1-12.

Gilland, E. and Baker, R. (1993). Conservation of neuroepithelial and mesodermal segments in the embryonic vertebrate head. *Acta Anat. (Basel)* **148**, 110-123.

Gilland, E. and Baker, R. (2005). Evolutionary patterns of cranial nerve efferent nuclei in vertebrates. *Brain Behav. Evol.* **66**, 234-254.

Glessner, J. T., Wang, K., Cai, G., Korvatska, O., Kim, C. E., Wood, S., Zhang, H., Estes, A., Brune, C. W., Bradfield, J. P. et al. (2009). Autism genome-wide copy number variation reveals ubiquitin and neuronal genes. *Nature* **459**, 569-573.

Grant, P. K. and Moens, C. B. (2010). The neuroepithelial basement membrane serves as a boundary and a substrate for neuron migration in the zebrafish hindbrain. *Neural Dev.* **5**, 9.

Higashijima, S., Hotta, Y. and Okamoto, H. (2000). Visualization of cranial motor neurons in live transgenic zebrafish expressing green fluorescent protein under the control of the islet-1 promoter/enhancer. *J. Neurosci.* **20**, 206-218.

Ishikawa, T., Gotoh, N., Murayama, C., Abe, T., Iwashita, M., Matsuzaki, F., Suzuki, T. and Yamamoto, T. (2011). IgSF molecule MDGA1 is involved in radial migration and positioning of a subset of cortical upper-layer neurons. *Dev. Dyn.* **240**, 96-107.

Jessen, J. R., Topczewski, J., Bingham, S., Sepich, D. S., Marlow, F., Chandrasekhar, A. and Solnica-Krezel, L. (2002). Zebrafish trilobite identifies new roles for Strabismus in gastrulation and neuronal movements. *Nat. Cell Biol.* **4**, 610-615.

Joset, P., Wacker, A., Babey, R., Ingold, E. A., Andermatt, I., Stoeckli, E. T. and Gesemann, M. (2011). Rostral growth of commissural axons requires the cell adhesion molecule MDGA2. *Neural Dev.* **6**, 22.

Keller, P. J., Schmidt, A. D., Wittbrodt, J. and Stelzer, E. H. K. (2008). Reconstruction of zebrafish early embryonic development by scanned light sheet microscopy. *Science* **322**, 1065-1069.

RESEARCH ARTICLE Biology Open (2015) 4, 146–154 doi:10.1242/bio.20148482

Kimmel, C. B., Ballard, W. W., Kimmel, S. R., Ullmann, B. and Schilling, T. F. (1995). Stages of embryonic development of the zebrafish. *Dev. Dyn.* **203**, 253-310.

Lee, K., Kim, Y., Lee, S.-J., Qiang, Y., Lee, D., Lee, H. W., Kim, H., Je, H. S., Südhof, T. C. and Ko, J. (2013). MDGAs interact selectively with neuroligin-2 but not other neuroligins to regulate inhibitory synapse development. *Proc. Natl. Acad. Sci. USA* **110**, 336-341.

Litwack, E. D., Babey, R., Buser, R., Gesemann, M. and O'Leary, D. D. M. (2004). Identification and characterization of two novel brain-derived immunoglobulin superfamily members with a unique structural organization. *Mol. Cell. Neurosci.* **25**, 263-274.

Maness, P. F. and Schachner, M. (2007). Neural recognition molecules of the immunoglobulin superfamily: signaling transducers of axon guidance and neuronal migration. *Nat. Neurosci.* **10**, 19-26.

Marui, T., Funatogawa, I., Koishi, S., Yamamoto, K., Matsumoto, H., Hashimoto, O., Nanba, E., Nishida, H., Sugiyama, T., Kasai, K. et al. (2009). Association of the neuronal cell adhesion molecule (NRCAM) gene variants with autism. *Int. J. Neuropsychopharmacol.* **12**, 1-10.

Moens, C. B. and Prince, V. E. (2002). Constructing the hindbrain: insights from the zebrafish. *Dev. Dyn.* **224**, 1-17.

Moens, C. B., Cordes, S. P., Giorgianni, M. W., Barsh, G. S. and Kimmel, C. B. (1998). Equivalence in the genetic control of hindbrain segmentation in fish and mouse. *Development* **125**, 381-391.

Morrow, E. M., Yoo, S.-Y., Flavell, S. W., Kim, T.-K., Lin, Y., Hill, R. S., Mukaddes, N. M., Balkhy, S., Gascon, G., Hashmi, A. et al. (2008). Identifying autism loci and genes by tracing recent shared ancestry. *Science* **321**, 218-223.

Nambiar, R. M., Ignatius, M. S. and Henion, P. D. (2007). Zebrafish colgate/hdac1 functions in the non-canonical Wnt pathway during axial extension and in Wnt-independent branchiomotor neuron migration. *Mech. Dev.* **124**, 682-698.

Ohata, S., Kinoshita, S., Aoki, R., Tanaka, H., Wada, H., Tsuruoka-Kinoshita, S., Tsuboi, T., Watabe, S. and Okamoto, H. (2009). Neuroepithelial cells require fucosylated glycans to guide the migration of vagus motor neuron progenitors in the developing zebrafish hindbrain. *Development* **136**, 1653-1663.

Ohata, S., Aoki, R., Kinoshita, S., Yamaguchi, M., Tsuruoka-Kinoshita, S., Tanaka, H., Wada, H., Watabe, S., Tsuboi, T., Masai, I. et al. (2011). Dual roles of Notch in regulation of apically restricted mitosis and apicobasal polarity of neuroepithelial cells. *Neuron* **69**, 215-230.

Pettem, K. L., Yokomaku, D., Takahashi, H., Ge, Y. and Craig, A. M. (2013). Interaction between autism-linked MDGAs and neuroligins suppresses inhibitory synapse development. *J. Cell Biol.* **200**, 321-336.

Rohrschneider, M. R., Elsen, G. E. and Prince, V. E. (2007). Zebrafish Hoxb1a regulates multiple downstream genes including prickle1b. *Dev. Biol.* **309**, 358-372.

Roohi, J., Montagna, C., Tegay, D. H., Palmer, L. E., DeVincent, C., Pomeroy, J. C., Christian, S. L., Nowak, N. and Hatchwell, E. (2009). Disruption of contactin 4 in three subjects with autism spectrum disorder. *J. Med. Genet.* **46**, 176-182.

Sano, S., Takashima, S., Niwa, H., Yokoi, H., Shimada, A., Arenz, A., Wittbrodt, J. and Takeda, H. (2009). Characterization of teleost Mdga1 using a gene-trap approach in medaka (Oryzias latipes). *Genesis* **47**, 505-513.

Schilling, T. F. and Kimmel, C. B. (1997). Musculoskeletal patterning in the pharyngeal segments of the zebrafish embryo. *Development* **124**, 2945-2960.

Sittaramane, V., Sawant, A., Wolman, M. A., Maves, L., Halloran, M. C. and Chandrasekhar, A. (2009). The cell adhesion molecule Tag1, transmembrane protein Stbm/Vangl2, and Lamininalpha1 exhibit genetic interactions during migration of facial branchiomotor neurons in zebrafish. *Dev. Biol.* **325**, 363-373.

Song, M.-R. (2007). Moving cell bodies: understanding the migratory mechanism of facial motor neurons. *Arch. Pharm. Res.* **30**, 1273-1282.

Stockinger, P., Maître, J.-L. and Heisenberg, C.-P. (2011). Defective neuroepithelial cell cohesion affects tangential branchiomotor neuron migration in the zebrafish neural tube. *Development* **138**, 4673-4683.

Takeuchi, A. and O'Leary, D. D. M. (2006). Radial migration of superficial layer cortical neurons controlled by novel Ig cell adhesion molecule MDGA1. *J. Neurosci.* **26**, 4460-4464.

Takeuchi, A., Hamasaki, T., Litwack, E. D. and O'Leary, D. D. M. (2007). Novel IgCAM, MDGA1, expressed in unique cortical area- and layer-specific patterns and transiently by distinct forebrain populations of Cajal-Retzius neurons. *Cereb. Cortex* **17**, 1531-1541.

van Daalen, E., Kemner, C., Verbeek, N. E., van der Zwaag, B., Dijkhuizen, T., Rump, P., Houben, R., van 't Slot, R., de Jonge, M. V., Staal, W. G. et al. (2011). Social Responsiveness Scale-aided analysis of the clinical impact of copy number variations in autism. *Neurogenetics* **12**, 315-323.

Wada, H., Iwasaki, M., Sato, T., Masai, I., Nishiwaki, Y., Tanaka, H., Sato, A., Nojima, Y. and Okamoto, H. (2005). Dual roles of zygotic and maternal Scribble1 in neural migration and convergent extension movements in zebrafish embryos. *Development* **132**, 2273-2285.

Wada, H., Tanaka, H., Nakayama, S., Iwasaki, M. and Okamoto, H. (2006). Frizzled3a and Celsr2 function in the neuroepithelium to regulate migration of facial motor neurons in the developing zebrafish hindbrain. *Development* **133**, 4749-4759.

Walsh, G. S., Grant, P. K., Morgan, J. A. and Moens, C. B. (2011). Planar polarity pathway and Nance-Horan syndrome-like 1b have essential cell-autonomous functions in neuronal migration. *Development* **138**, 3033-3042.

Wanner, S. J. and Prince, V. E. (2013). Axon tracts guide zebrafish facial branchiomotor neuron migration through the hindbrain. *Development* **140**, 906-915.

Wanner, S. J., Saeger, I., Guthrie, S. and Prince, V. E. (2013). Facial motor neuron migration advances. *Curr. Opin. Neurobiol.* **23**, 943-950.

Zhiling, Y., Fujita, E., Tanabe, Y., Yamagata, T., Momoi, T. and Momoi, M. Y. (2008). Mutations in the gene encoding CADM1 are associated with autism spectrum disorder. *Biochem. Biophys. Res. Commun.* **377**, 926-929.

RESEARCH ARTICLE Biology Open (2015) 000, 1–9 doi:10.1242/bio.20148482

Supplementary Material
Esther Ingold et al. doi: 10.1242/bio.20148482

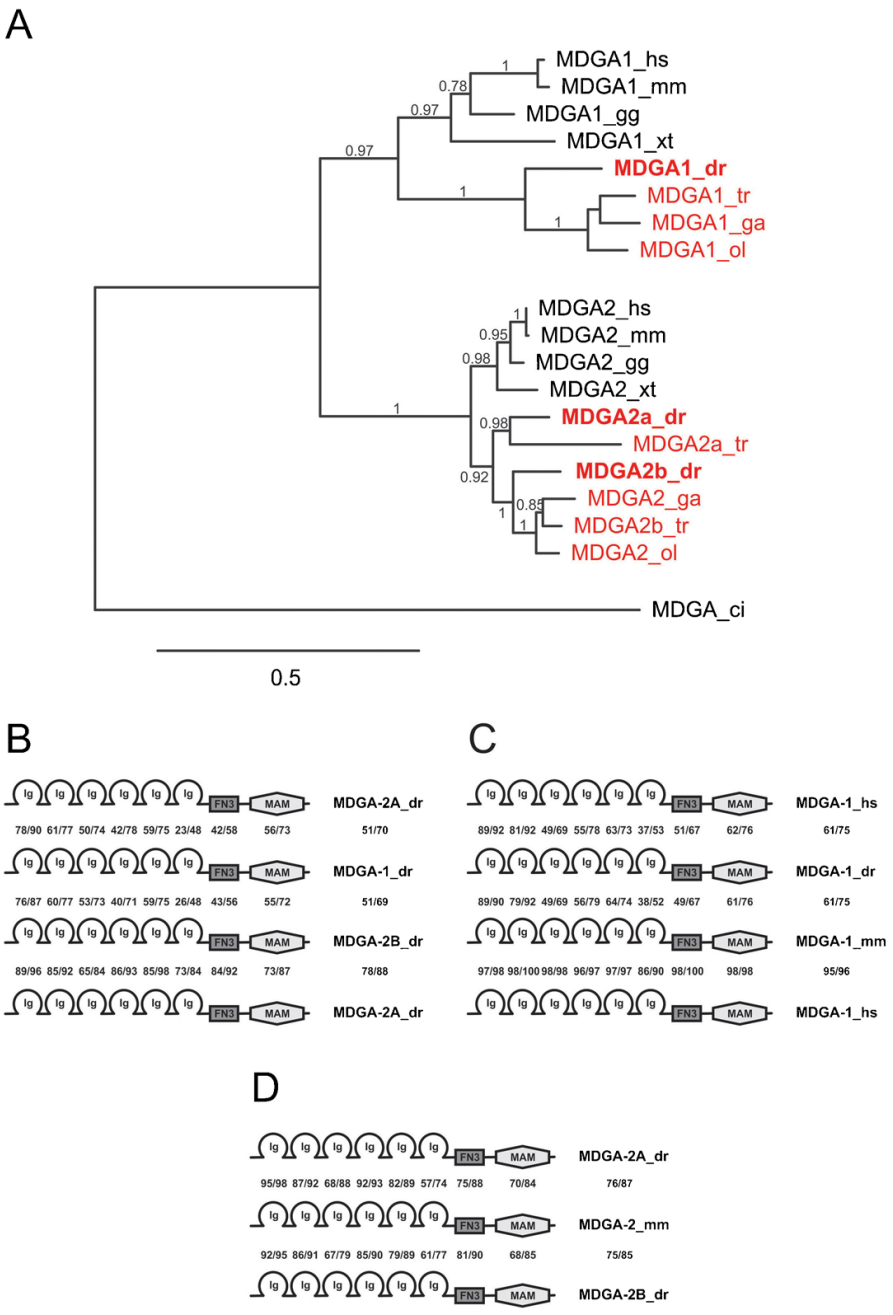

Fig. S1. Phylogenetic relationship and homology between MDGA proteins. (A) Maximum likelihood phylogeny of members of the zebrafish (dr), fugu (tr), medaka (ol), stickleback (ga), mouse (mm), Xenopus (xt), chicken (gg) and human (hs) MDGA family. The phylogenetic tree was build using 722 representative amino acids determined by the program Gblocks after sequence alignment using MUSCLE. Bootstrap values above 50% (0.5) are shown. Fish MDGA proteins are shown in red and zebrafish proteins are highlighted in bold. As an outgroup to root the tree ciona (ci) MDGA was used. Note that in zebrafish and fugu MDGA-2 genes have retained their duplicates after the teleost specific whole genome duplication, resulting in an A and B paralog. The scale bar shows the percentage (0.5 equals 50%) of amino acid substitutions required to generate the corresponding tree. (B) Homology comparison between individual domains of zebrafish MDGAs. Domain boundaries were identified using the smart program (http://smart.embl-heidelberg.de/) and subsequently compared pairwise using BLASTP. While the first number represents the percentage of identical residues, the second number indicates the number of conserved residues (eg. L vs. V; D vs. E; etc.). Note that the amount of conservation varies greatly between the different domains. (C) Conservation between human, mouse and zebrafish MDGA1s. (D) Conservation between mouse and zebrafish MDGA2s. Note that comparison between human and zebrafish MDGA2s gave similar results.

Biology Open

RESEARCH ARTICLE Biology Open (2015) 000, 1–9 doi:10.1242/bio.20148482

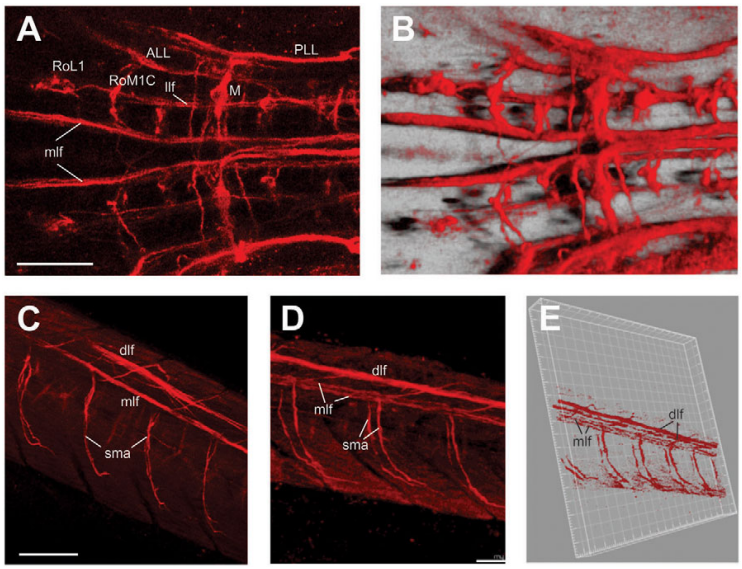

Fig. S2. MDGA-2A antibodies stain multiple tracts in the zebrafish hindbrain and spinal cord. (A) A ladder-like staining of MDGA-2A positive reticulospinal interneurons can be observed. Their MDGA-2A labeled axons project into one of the two major longitudinal fiber pathways through the CNS, the medial longitudinal fascicle (mlf) or the lateral longitudinal fascicle (llf). In the hindbrain, the mlf splits into dorsal and ventral components (mlfD and mlfV, respectively). (B) 3D reconstruction of the area above generated with the Imaris software. (C,D) MDGA-2A positive longitudinal tracts (dlf and mlf) extend into the spinal cord. At each somite segment, the MDGA-2A antibody stains spinal motor axons (sma) emerging from the mlf. (E) A 3D reconstruction of the are depicted in C,D generated with the Imaris software. Scale bars equal 200 μm.

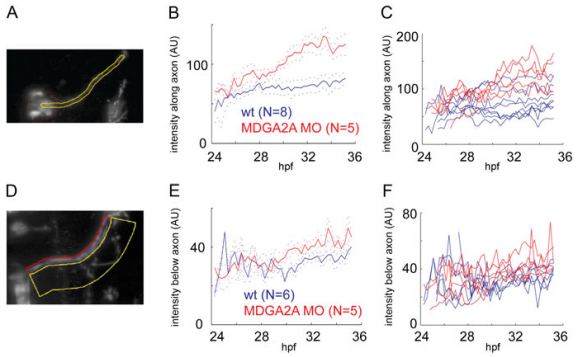

Fig. S3. Detailed quantification of the MDGA-2A phenotypes. (A) Fluorescence intensity in the region along the axon (yellow area) was measured in wt and MDGA-2A knockdown animals. Background fluorescence intensity in an area of identical size but outside the migration path of axons and neurons was subtracted to obtain the net intensity in the area of interest. (B) The fluorescence intensity along the trigeminal axon bundle was quantified in 8 control embryos and 5 MDGA-2A morpholino treated embryos. Shown are the mean and error of the mean (as dotted lines). Due to aberrant neuronal migration along the trigeminal axon bundle staining intensity in this area increases clearly in MDGA-2A knockdown animals. (C) Individual measurements of wt and MDGA-2A knockdown are shown. (D) Fluorescence intensity in an area below the axon bundle of the facial nerve is increased in MDGA-2A knockdown animals. Fluorescence intensity in a region underneath the facial axon bundle (yellow area) was measured in wt and MDGA-2A knockdown animals. Background fluorescence intensity in an area of identical size but outside the projection path of axons was subtracted to obtain the net intensity in the area of interest. (E) In MDGA-2A knockdown animals older than 30 hpf, the mean fluorescence intensity underneath the facial nerve was increased, representing increased branching and defasciculation. Note that in wt animals residual fluorescence intensity can also be detected, as transient branch formations also occur during regular development. (F) Individual measurements of wt and MDGA-2A knockdown are shown.

RESEARCH ARTICLE Biology Open (2015) 000, 1–9 doi:10.1242/bio.2014848

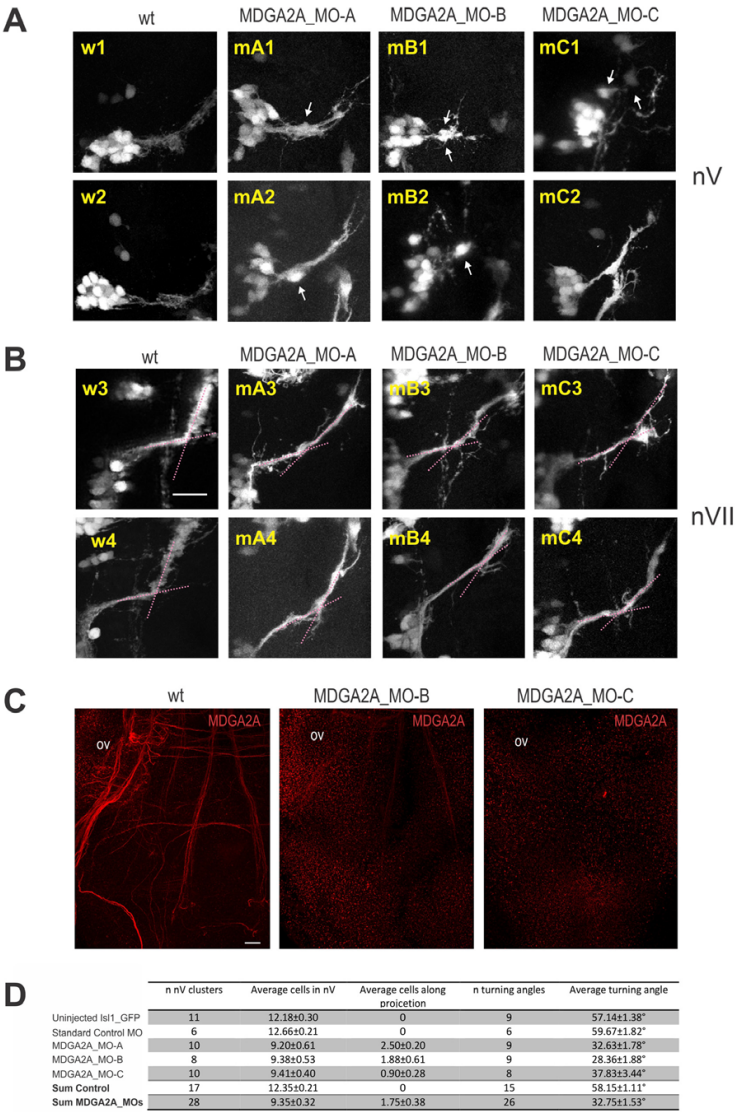

D

	n nV clusters	Average cells in nV	Average cells along proicetion	n turning angles	Average turning angle
Uninjected Isl1_GFP	11	12.18±0.30	0	9	57.14±1.38°
Standard Control MO	6	12.66±0.21	0	6	59.67±1.82°
MDGA2A_MO-A	10	9.20±0.61	2.50±0.20	9	32.63±1.78°
MDGA2A_MO-B	8	9.38±0.53	1.88±0.61	9	28.36±1.88°
MDGA2A_MO-C	10	9.41±0.40	0.90±0.28	8	37.83±3.44°
Sum Control	17	12.35±0.21	0	15	58.15±1.11°
Sum MDGA2A_MOs	28	9.35±0.32	1.75±0.38	26	32.75±1.53°

Fig. S4. Different MDGA2A morpholino oligonucleotides located around the ATG start codor cause identical phenotypes. (A) Morpholino induced MDGA2A knockdown increases mobility of trigeminal neurons. Representative images from wild type and zebrafish embryos treated with different MDGA2A morpholinos are shown. At 34 hpf trigeminal neurons in wild type embryos have formed a dense trigeminal cell cluster and have send out axons towards their targets (w1,w2). In animals treated with different MDGA2A start site morpholinos the compactness of the trigeminal cell cluster is impaired (mA1/2, mB1/2, mC1/2). Trigeminal neurons migrate along their axon bundles leaving their place of origin (arrows). (B) MDGA2A knockdown influences axon turning and bundling of the facial nerve Representative images from control (w3, w4) and MDGA2A morpholino treated embryos (mA3/4, mB3/4, and mC3/4) are shown. 34 h post fertilization facial neurons in wt embryos project axons along a predetermined path, displaying a 60˚ turn (pink dotted lines) at a well-documented turning point. In the differen MDGA2A morphants this turning angle is strongly reduced and the formation of axon collaterals occurs much more frequently around this turning point. The scale bar represents 20 μm. (C) MDGA2A morpholinos efficiently reduce MDGA2A protein expression. wt and MDGA2A morpholinos treated embryos were stained with MDGA2A antibodies to visualize axonal tracts. In w embryos tracts are clearly stained. Under identical staining and recording conditions axonal staining in MDGA2A knockdown animals is absent or very weak, demonstrating that the MDGA2A protein in these animals is strongly downregulated. As a landmark the otic vesicle (ov) is highlighted. The sequence of the morpholinos used (MDGA2A_MO-B/C) is given in the material and methods section. The scale bar represents 20 μm. (D) Statistical analysis of migration and axon guidance defects in MDGA2A knockdown animals. The number o analyzed trigeminal cell clusters and facial nerves for uninjected wild type, standard control and MDGA2A (MO-A, MO-B, MO-C) morpholino injected animals is given. The average cell number in the trigeminal cell cluster as well as the average turning angle of the facia nerve under the different experimental conditions are summarized. Note that the last two lines represent the pooled data of control (wt and standard control morpholino injected embryos) and MDGA2A (MO-A, MO-B, MO-C) morpholino injected animals.

RESEARCH ARTICLE Biology Open (2015) 000, 1–9 doi:10.1242/bio.20148482

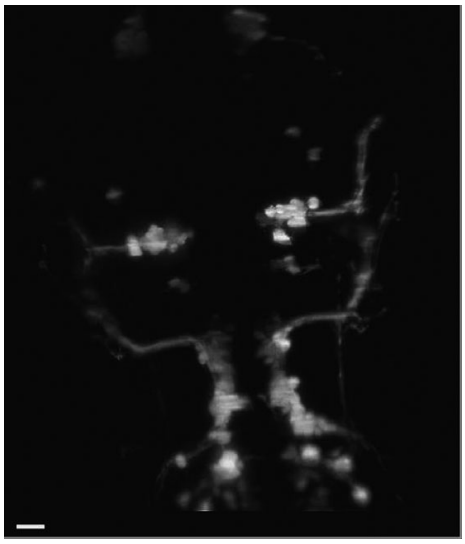

Movie 1. In vivo development of cranial motoneurons observed by light sheet microscopy. Zebrafish islet-GFP wt larva were monitored between 24–36 hpf. Fluorescent images were taken every 16 min and processed as described in material and methods. Scale bare equals 20 μm.

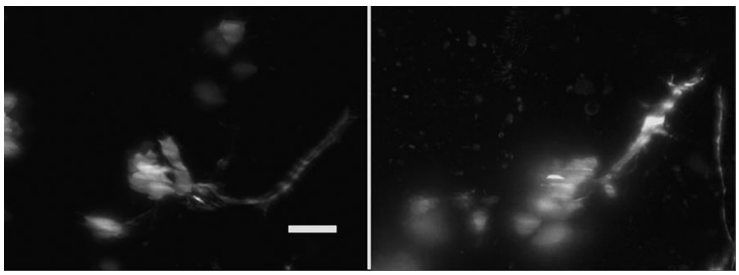

Movie 2. Development and migration of trigeminal motoneurons in wild type and MDGA2A knockdown animals observed by light sheet microscopy. The left panel shows the development of trigeminal neurons during the time between 24 and 36 hpf in islet-GFP fish. Note that neurons within the trigeminal cell cluster remain tightly together, sending out axons into the trigeminal nerve. The right panel depicts the situation in MDGA2A knockdown animals. In the case of MDGA2A knockdown increased mobility and intense migration of trigeminal neurons along the trigeminal nerve can be observed. Scale bar represents 20 μm.

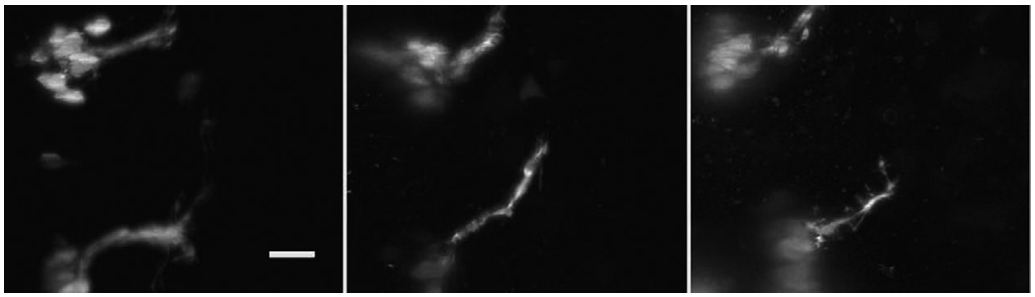

Movie 3. Development of the facial nerve in wild type and MDGA2A knockdown animals. Wild type and MDGA2A knockdown islet-GFP fish were monitored by light sheet microscopy between 24 and 36 hpf. The left panel illustrates the normal development of the facial nerve during this period of development. Around 30 hpf the facial nerve in wt larva displays a characteristic 60˚ turn. At this ''choice point'' temporary stalling and increased transient branching can be observed even in the wild type. However, most branches retract over time and the axon bundle stays fasciculated. The middle and the right panel depict facial nerve growth in MDGA2A knockdown animals. Note that the typically observed 60˚ turn is absent in MDGA2A morphants and that strongly increased branching and defasciculation along the facial nerve is seen in these larva. Scale bar equals 20 μm.

Biology Open

Chapter 6

General Discussion

In the studies presented in this thesis, we investigated the roles of EAAT genes from different vertebrate species not only in glutamate clearance from the synaptic cleft but also in shaping synaptic transmission by a thermodynamically uncoupled anion conductance. We took advantage of the conserved anatomical structure and cell types of the vertebrate retina in order to compare expression patterns and biophysical properties of different EAAT homologues from selected species of the major vertebrate classes. Two EAAT orthologs have been lost in the course of mammalian evolution. Our results present first evidence on why the two orthologs that have been lost in the course of the vertebrate evolution and became redundant.

6.1. Roles of EAAT glutamate transporters in the nervous system and other body parts

The tasks EAAT genes fulfill in the nervous system are as important as diverse. Besides being responsible for glutamate clearance from the synaptic cleft in order to shape and terminate excitatory neurotransmission, they can be directly involved in altering membrane potentials via a anion conductance that was described to be variable between different EAAT subtypes. Furthermore, EAAT3 transports cysteine into neurons and provides a source for glutathione synthesis, which in turn is essential to prevent cells from oxidative stress (Zerangue, Kavanaugh 1996; Himi et al. 2003).

EAAT1 and EAAT2 are predominantly expressed in glia cells but in distinct regions of mammalian brains. While EAAT2 shows expression in glia cells all over the brain, EAAT1 shows more restricted expression in the cerebellum (Rothstein et al. 1994). However, a majority of astrocytes in the brain were reported to express both EAAT homologues (Berger, Hediger 1998). These findings are consistent with our findings in the zebrafish, where EAAT1a, EAAT2a and EAAT2b are expressed in glia cells in the brain (Chapter 2; Niklaus et al. 2017). Knockouts of EAAT1 or EAAT2 in mice resulted in epileptic-like behavior or amygdaloid kindling, emphasizing the importance of the high-affinity glutamate transporter in clearing excitatory neurotransmitter form the synapse (Tanaka et al. 1997; Tsuru et al. 2002).

Neuronal expressed EAAT genes show dual functionality. On one hand, they act as a glutamate sink, clearing glutamate from the synapse, and on the other hand they can modulate synaptic signaling via their chloride conductance (Kanai et al. 2013; Fahlke et al. 2016). EAAT3 is further expressed in the proximal tubules of the kidney, reabsorbing amino acids (Shayakul et al. 1997). Glutamate is then converted to glutamine by glutamine synthetase which in turn is then released again to the blood (Shayakul et al. 1997; Kanai et al. 2013). We observed similar expression patterns of EAAT3 in larval zebrafish (unpublished data). Taken together, EAATs not only play a crucial role in neurotransmission, they also serve a broad range of functions in cell metabolism.

6.2. Neuronal glutamate transporters EAAT3 and EAAT4

Clearly, EAAT3 and EAAT4 serve important functions not only in the nervous system. Remarkably, none of the two orthologs was ever retained as duplicates. The EAAT4 gene was even completely lost from the lizard genome (Gesemann et al. 2010). EAAT3 is expressed in neurons all over the brain of mice and localizes on dendrites and axonal terminals (Rothstein et al. 1994). Knockout of EAAT3 in mice does not lead to severe neurological phenotypes. Brain size and morphology as well as cell number in hippocampus, cerebellum and cortex remain unaffected (Peghini et al. 1997). Consequently, knockout mice did not show epileptic phenotypes or neurodegeneration. Behavioral tests on EAAT3 mutant mice showed decreased

spontaneous locomotion which is related to elevated glutamate levels in synapses, since similar phenotypes have been reported for mice after injection of low doses of NMDA (Lubitz et al. 1993). Nevertheless, reabsorption of glutamate and aspartate in the kidney is decreased and therefore mice lacking EAAT3 develop dicarboxylic aminoaciduria (Peghini et al. 1997).

Expression of EAAT4 is highest in the cerebellum and it was shown to exhibit characteristics of a glutamate-gated chloride channel. More precisely, EAAT4 is expressed by cerebellar Purkinje cells and the transporter localizes to the synapse between climbing fibers and Purkinje cells (Fairman et al. 1995). Huang and co-workers showed that Purkinje cells of EAAT4-deficient mice lack typical glutamate-evoked transport and anion currents (Huang et al. 2004). Further, mice lacking EAAT4 typically show cerebellar dysfunction and subsequent degeneration (Perkins et al. 2016).

6.3. Possible roles of five EAAT homologues in the vertebrate retina

In our studies we found all seven EAAT homologues to be expressed in the retina at least in some of the investigated species (Chapter 2, Chapter 3, Chapter 4 and unpublished observation for EAAT3 and EAAT4). We selected EAAT1, EAAT2, EAAT5, EAAT6 and EAAT7 subgroups that show interesting phylogenetic patterns in order to trace potential adaptations after gene duplication or deletion events.

Our findings of five expressed EAAT orthologs in the *Xenopus* retina is in agreement with previous findings in retinae of tiger salamander, although the authors at that time named EAAT7 as EAAT2b and EAAT6 as EAAT5b (Eliasof et al. 1998). Reported current-voltage relationships as well as exhibited chloride conductance resemble our data as one could expect.

In mice, knockout as well as pharmacological knockdown of EAAT1 leads to a reduced b-wave amplitude due to the lack of a glutamate-clearing mechanism and consequently keeping ON-bipolar cells hyperpolarized (Harada et al. 1998; Tse et al. 2014a). No reduction of the ERG b-wave was observed in EAAT2 knockout or knockdown experiments in mice. We showed that EAAT1 and EAAT2 switched their expression patterns in the retina in the course of mammalian evolution. In lower vertebrates, EAAT1 is expressed in bipolar cells and in photoreceptors, while EAAT2 in turn is expressed in Müller glia cells and photoreceptors. In mice in contrast, EAAT1 shows expression in Müller glia cells and EAAT2 is expressed in photoreceptors and bipolar cells. We showed in our group that knockout and knockdown of EAAT2a, which is predominantly expressed in Müller glia cells in the retina, but not of EAAT2b, which shows expression in photoreceptors, reduces the ON-bipolar cell response (Niklaus et al. 2017). Presumably, functions of EAAT1 and EAAT2 are interchangeable and we provide further support for this hypothesis, since we did not find substantial differences in biophysical properties between these two EAAT orthologs.

Measuring responses of ON-bipolar cells in acute retinal slices indicated a glutamate activated chloride-dependent conductance in teleost retinae (Grant, Dowling 1995, 1996). Later a retina-specific EAAT, namely EAAT5, was discovered and characterized, showing quasi-absent glutamate transport currents but high conductivity for anions (Arriza et al. 1997; Schneider et al. 2014). Further studies showed that EAAT5 acts as a pre- and postsynaptic glutamate receptor on bipolar cells. As a postsynaptic transporter on bipolar cell dendrites, EAAT5 is able to transport chloride against its concentration gradient into the cell at resting membrane potentials, keeping cells hyperpolarized when glutamate is present (Tse et al. 2014b; Wong et al. 2005a; Wong et al. 2005b). Similarly, it was shown that presynaptic expressed EAAT5 in rod bipolar cells acts as an inhibitory presynaptic receptor and as such counteracts depolarizations

of rod bipolar cells (Wersinger et al. 2006).

While only EAAT7 from tiger salamander has been cloned and characterized so far, we report the first expression profiles of EAAT6 and EAAT7 in the retinae of teleost, Amphibia, Reptilia and birds (Arriza et al. 1997). Remarkably, EAAT6 and EAAT7 show expression limited to the retina in zebrafish and *Xenopus*. Immunohistochemical localization of EAAT6a and EAAT6b paralogs in zebrafish revealed unexpected protein localization. EAAT6a is expressed on horizontal cell processes whereas EAAT6b localizes at the outer limiting membrane in photoreceptors (Niklaus 2017). While EAAT6b did not show glutamate evoked currents in TEVC recordings and further Eliasof and co-workers did not report any measurable glutamate induced transport currents in tiger salamander EAAT6, it is highly feasible that EAAT6 does not act as a classical glutamate transporter (Eliasof et al. 1998). We hypothesize that EAAT6 rather transports other amino acids that are involved in metabolic processes.

We showed that EAAT7 of teleost, Amphibia and Reptilia show high anion conductance compared to glutamate transport currents, indicating possible roles in synaptic signal shaping. Other studies in our lab showed that in zebrafish EAAT5b and EAAT7 co-localize on dendritic tips of bipolar cells and that the knockout of either of the genes decreases ERG b-wave amplitude in red-light measurements. Moreover, we found EAAT5b as well to be a glutamate-gated chloride channel with similar properties as EAAT7 and it seems to be very well possible that those genes are functionally redundant.

6.4. How genes disappear

When a gene becomes functionally redundant it is released from selective pressure and therefore mutations in this particular gene are considered to be neutral. In other cases, it might be that selection acts as a driver to eliminate genes from the genome to get an evolutionary advantage. Since light-reception in vertebrates is a highly energy-consuming process, it is thought that loss of the ability to perceive certain wavelengths of light in nocturnal animals could be an evolutionary advantage (for example (Cooper et al. 1993b; Kanai et al. 2013). The loss of green-sensitive RH2 as well as blue-sensitive SWS2 genes during the nocturnal phase of the common ancestor of all placental mammals is an example for such processes (Bowmaker 2008; Lamb 2013). But also more recent adaptations indicate that the loss of opsin genes can lead to a selective advantage. The naked mole rat (*Spalax ehrenbergi*) lives underground and the lack of daylight led to the degeneration of the eye in a way that it lost the ability to form images and only serves to entrain the circadian rhythm (Rado et al. 1992; Cooper et al. 1993a, 1993b). In addition, it was shown that naked mole rats have lost SWS1 and are therefore LWS monochromats (David-Gray et al. 2002). Since only very little light reaches the retina of naked mole rats and photoreceptors are highly metabolic cells, it is assumed that loss of SWS1 was a selective advantage in this specific ecological niche (Cooper et al. 1993b).

Loss of opsin genes during vertebrate evolution led to further adaptations in the retina. Processing of two different wavelengths of light is much simpler than processing four of them. For example, inputs from different cone types are compared via feedback mechanisms in horizontal cells. Thus, it is not surprising that mammals possess two distinct types of horizontal cells, while other vertebrates possess four (Jacobs, Rowe 2004). In the case of the EAATs, where in Amphibia and teleost fish three genes are exclusively expressed in the retina (EAAT5, EAAT6 and EAAT7), we anticipate that the reduction of cone opsins made EAAT6 and EAAT7 become redundant in placental mammals.

Comparison of biophysical properties of all examined EAATs in these studies adds further

evidence to our hypothesis. EAAT7 as well as EAAT5 clearly function as glutamate-gated chloride channel, contributing more to hyperpolarization of the cells rather than to glutamate clearance. In mammals such a function became redundant, as can be seen by the fact that EAAT7 became redundant and was subsequently and neither EAAT1 nor EAAT2 changed their properties towards the properties of EAAT7. Such adaptations would in fact be possible as visible by the zebrafish EAAT2b paralog that exhibits clearly glutamate-gated channel characteristics whereas EAAT2a serves as a glutamate transporter (Figure 1).

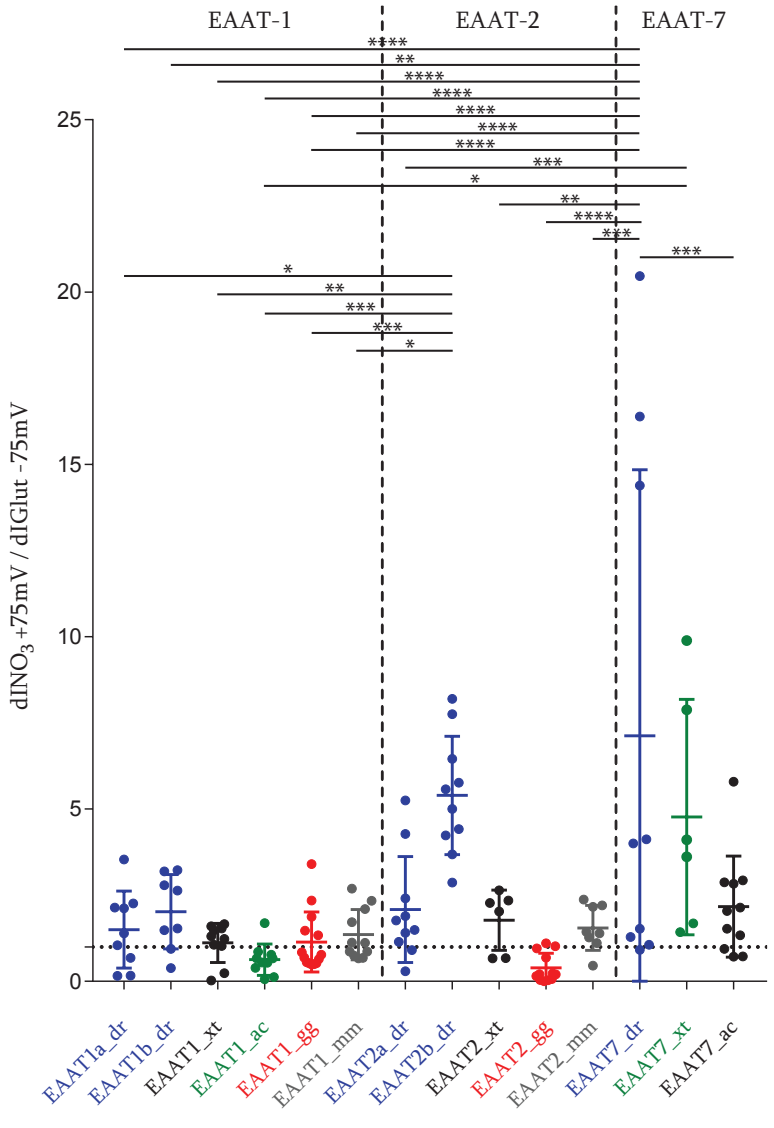

Figure 1: Comparison of anion conductance and glutamate transport currents of all EAAT genes examined in these studies.
EAAT1 and EAAT2 genes show lower ratios of anion currents to glutamate transport currents than EAAT7. EAAT1 and EAAT2 exhibit similar ratios, while duplication of EAAT2 in zebrafish led to the adaptation of the anion conductance in EAAT2b.
For statistics ordinary two-way ANOVA was performed. Asterisks indicate significance levels.

6.5. Outlook

We showed in our studies that glial expressed EAAT1 and EAAT2 show remarkably similar biophysical properties. Thus, the question arose why both transporters have been retained in all investigated species. To elaborate on this question, phenotype of EAAT1 and/or EAAT2 knockout zebrafish could be investigated. EAAT1a deficient fish could be used for studying the role of EAAT1 in sensory hair cells and related sensory organs like the ear or neuromast cells of the lateral line organ. Of special interest would be an EAAT1b mutant fish strain. As EAAT1b is expressed in glia cells in the brain, one could expect excessive glutamate in

glutamatergic synapses and subsequent seizures and neurodegeneration due to excitotoxicity. Similar phenotypes have been observed in our lab for EAAT2a knockout zebrafish (A. Hotz, unpublished data). Further it seems like homozygous EAAT2a mutant fish are dying at early stages during development, indicating the importance of proper glutamate clearing by EAAT2a during zebrafish development (A. Hotz, unpublished data). It is of utmost interest whether such lethal phenotypes or retinal phenotypes that were described could be rescued by expressing an EAAT1 ortholog in those mutant fish (Niklaus et al. 2017). In these studies we have not looked at glutamate affinities for the different EAAT1 and EAAT2 orthologs. Although they have been reported previously to be very similar, measurements in our system and of EAAT orthologs from different vertebrate species could still reveal potential differences that have so far been masked (Jensen, Bräuner-Osborne 2004).

Because EAAT5 and EAAT6 constructs accumulated intracellularly and were not transported to the cellular membrane, we could not elaborate the biophysical properties of them. We found that the zebrafish EAAT5b, EAAT6a and EAAT6b get expressed in the membrane of *Xenopus laevis* oocytes. Thus, this isolated expression system can be used to determine possible functions of these genes. While we could record glutamate induced currents in EAAT5b injected oocytes, no currents could be measured for EAAT6b injected currents. Although it could be that expression levels were low in our case, we speculate that EAAT6 is not a classical glutamate transporter but rather transports other amino acids and is involved in transporting amino acids into the cells that are then used for cellular metabolic processes. This hypothesis is supported by an earlier study that failed to detect glutamate induced anion currents for an EAAT6 ortholog (Eliasof et al. 1998).

Biophysical properties of EAAT5 and EAAT7 are very similar and in our lab it was shown that EAAT5b and EAAT7 co-localize at dendritic tips of bipolar cells in zebrafish (Niklaus 2017). Sharing similar properties and expression sites indicates functional redundancy and gives us hints why EAAT7 is not present anymore in mammalian genomes. Such redundancy could be tested by replacing EAAT5 with EAAT7 in mice for example.

6.6. References

Arriza, J. L.; Eliasof, S.; Kavanaugh, M. P.; Amara, S. G. (1997): Excitatory amino acid transporter 5, a retinal glutamate transporter coupled to a chloride conductance. In *Proceedings of the National Academy of Sciences of the United States of America* 94 (8), pp. 4155–4160.

Berger, U. V.; Hediger, M. A. (1998): Comparative analysis of glutamate transporter expression in rat brain using differential double in situ hybridization. In *Anatomy and Embryology* 198 (1), pp. 13–30. DOI: 10.1007/s004290050161.

Bowmaker, James K. (2008): Evolution of vertebrate visual pigments. In *Vision research* 48 (20), pp. 2022–2041. DOI: 10.1016/j.visres.2008.03.025.

Cooper, H. M.; Herbin, M.; Nevo, E. (1993a): Ocular regression conceals adaptive progression of the visual system in a blind subterranean mammal. In *Nature* 361 (6408), pp. 156–159. DOI: 10.1038/361156a0.

Cooper, H. M.; Herbin, M.; Nevo, E. (1993b): Visual system of a naturally microphthalmic mammal. The blind mole rat, Spalax ehrenbergi. In *The Journal of comparative neurology* 328 (3), pp. 313–350. DOI: 10.1002/cne.903280302.

David-Gray, Z. K.; Bellingham, J.; Munoz, M.; Avivi, A.; Nevo, E.; Foster, R. G. (2002): Adaptive loss of ultraviolet-sensitive/violet-sensitive (UVS/VS) cone opsin in the blind mole rat (Spalax ehrenbergi). In *The European journal of neuroscience* 16 (7), pp. 1186–1194.

Eliasof, S.; Arriza, J. L.; Leighton, B. H.; Kavanaugh, M. P.; Amara, S. G. (1998): Excitatory amino acid transporters of the salamander retina: identification, localization, and function. In *The Journal of neuroscience : the official journal of the Society for Neuroscience* 18 (2), pp. 698–712.

Fahlke, Christoph; Kortzak, Daniel; Machtens, Jan-Philipp (2016): Molecular physiology of EAAT anion channels. In *Pflugers Archiv : European journal of physiology* 468 (3), pp. 491–502. DOI: 10.1007/s00424-015-1768-3.

Fairman, W. A.; Vandenberg, R. J.; Arriza, J. L.; Kavanaugh, M. P.; Amara, S. G. (1995): An excitatory amino-acid transporter with properties of a ligand-gated chloride channel. In *Nature* 375 (6532), pp. 599–603. DOI: 10.1038/375599a0.

Gesemann, Matthias; Lesslauer, Annegret; Maurer, Colette M.; Schönthaler, Helia B.; Neuhauss, Stephan C. F. (2010): Phylogenetic analysis of the vertebrate excitatory/neutral amino acid transporter (SLC1/EAAT) family reveals lineage specific subfamilies. In *BMC evolutionary biology* 10, p. 117. DOI: 10.1186/1471-2148-10-117.

Grant, G. B.; Dowling, J. E. (1995): A glutamate-activated chloride current in cone-driven ON bipolar cells of the white perch retina. In *The Journal of neuroscience : the official journal of the Society for Neuroscience* 15 (5 Pt 2), pp. 3852–3862.

Grant, G. B.; Dowling, J. E. (1996): On bipolar cell responses in the teleost retina are generated by two distinct mechanisms. In *Journal of neurophysiology* 76 (6), pp. 3842–3849.

Harada, T.; Harada, C.; Watanabe, M.; Inoue, Y.; Sakagawa, T.; Nakayama, N. et al. (1998): Functions of the two glutamate transporters GLAST and GLT-1 in the retina. In *Proceedings of the National Academy of Sciences of the United States of America* 95 (8), pp. 4663–4666.

Himi, T.; Ikeda, M.; Yasuhara, T.; Nishida, M.; Morita, I. (2003): Role of neuronal glutamate transporter in the cysteine uptake and intracellular glutathione levels in cultured cortical neurons. In *Journal of neural transmission (Vienna, Austria : 1996)* 110 (12), pp. 1337–1348. DOI: 10.1007/s00702-003-0049-z.

Huang, Yanhua H.; Dykes-Hoberg, Margaret; Tanaka, Kohichi; Rothstein, Jeffrey D.; Bergles, Dwight E. (2004): Climbing fiber activation of EAAT4 transporters and kainate receptors in cerebellar Purkinje cells. In *The Journal of neuroscience : the official journal of the Society for Neuroscience* 24 (1), pp. 103–111. DOI: 10.1523/JNEUROSCI.4473-03.2004.

Jacobs, Gerald H.; Rowe, Mickey P. (2004): Evolution of vertebrate colour vision. In *Clinical and Experimental Optometry* 87 (4-5), pp. 206–216.

Jensen, Anders A.; Bräuner-Osborne, Hans (2004): Pharmacological characterization of human excitatory amino acid transporters EAAT1, EAAT2 and EAAT3 in a fluorescence-based membrane potential assay. In *Biochemical pharmacology* 67 (11), pp. 2115–2127. DOI: 10.1016/j.bcp.2004.02.013.

Kanai, Yoshikatsu; Clémençon, Benjamin; Simonin, Alexandre; Leuenberger, Michele; Lochner, Martin; Weisstanner, Martin; Hediger, Matthias A. (2013): The SLC1 high-affinity glutamate and neutral amino acid transporter family. In *Molecular aspects of medicine* 34 (2-3), pp. 108–120. DOI: 10.1016/j.mam.2013.01.001.

Lamb, Trevor D. (2013): Evolution of phototransduction, vertebrate photoreceptors and retina. In *Progress in retinal and eye research* 36, pp. 52–119. DOI: 10.1016/j.preteyeres.2013.06.001.

Lubitz, D. K. von; Paul, I. A.; Carter, M.; Jacobson, K. A. (1993): Effects of N6-cyclopentyl adenosine and 8-cyclopentyl-1,3-dipropylxanthine on N-methyl-D-aspartate induced seizures in mice. In *European journal of pharmacology* 249 (3), pp. 265–270.

Niklaus, Stephanie (2017): Glutamate Homeostasis in the Zebrafish outer Retina. Diss. Univ. Zürich. - Ref.: Stephan C.F. Neuhauss; Korref.: Christian Grimm, Martin Müller. Zürich.

Niklaus, Stephanie; Cadetti, Lucia; Vom Berg-Maurer, Colette M.; Lehnherr, André; Hotz, Adriana L.; Forster, Ian C. et al. (2017): Shaping of Signal Transmission at the Photoreceptor Synapse by EAAT2 Glutamate Transporters. In *eNeuro* 4 (3). DOI: 10.1523/ENEURO.0339-16.2017.

Peghini, P.; Janzen, J.; Stoffel, W. (1997): Glutamate transporter EAAC-1-deficient mice develop dicarboxylic aminoaciduria and behavioral abnormalities but no neurodegeneration. In *The EMBO journal* 16 (13), pp. 3822–3832. DOI: 10.1093/emboj/16.13.3822.

Perkins, Emma; Suminaite, Daumante; Jackson, Mandy (2016): Cerebellar ataxias: β-III spectrin's interactions suggest common pathogenic pathways. In *The Journal of physiology* 594 (16), pp. 4661–4676. DOI: 10.1113/JP271195.

Rado, R.; Bronchti, G.; Wollberg, Z.; Terkel, J. (1992): Sensitivity to light of the blind mole rat. Behavioral and neuroanatomical study. In *Israel Journal of Zoology* 38 (3-4), pp. 323–331.

Rothstein, Jeffrey D.; Martin, Lee; Levey, Allan I.; Dykes-Hoberg, Margaret; Jin, Lin; Wu, David et al. (1994): Localization of neuronal and glial glutamate transporters. In *Neuron* 13 (3), pp. 713–725. DOI: 10.1016/0896-6273(94)90038-8.

Schneider, Nicole; Cordeiro, Sönke; Machtens, Jan-Philipp; Braams, Simona; Rauen, Thom-

as; Fahlke, Christoph (2014): Functional properties of the retinal glutamate transporters GLT-1c and EAAT5. In *The Journal of biological chemistry* 289 (3), pp. 1815–1824. DOI: 10.1074/jbc.M113.517177.

Shayakul, C.; Kanai, Y.; Lee, W. S.; Brown, D.; Rothstein, J. D.; Hediger, M. A. (1997): Localization of the high-affinity glutamate transporter EAAC1 in rat kidney. In *The American journal of physiology* 273 (6 Pt 2), F1023-9.

Tanaka, K.; Watase, K.; Manabe, T.; Yamada, K.; Watanabe, M.; Takahashi, K. et al. (1997): Epilepsy and exacerbation of brain injury in mice lacking the glutamate transporter GLT-1. In *Science (New York, N.Y.)* 276 (5319), pp. 1699–1702.

Tse, Dennis Y.; Chung, Inyoung; Wu, Samuel M. (2014a): Pharmacological inhibitions of glutamate transporters EAAT1 and EAAT2 compromise glutamate transport in photoreceptor to ON-bipolar cell synapses. In *Vision research* 103, pp. 49–62. DOI: 10.1016/j.visres.2014.07.020.

Tse, Dennis Y.; Chung, Inyoung; Wu, Samuel M. (2014b): Possible roles of glutamate transporter EAAT5 in mouse cone depolarizing bipolar cell light responses. In *Vision research* 103, pp. 63–74. DOI: 10.1016/j.visres.2014.06.005.

Tsuru, Noriko; Ueda, Yuto; Doi, Taku (2002): Amygdaloid kindling in glutamate transporter (GLAST) knockout mice. In *Epilepsia* 43 (8), pp. 805–811.

Wersinger, Eric; Schwab, Yannick; Sahel, José-Alain; Rendon, Alvaro; Pow, David V.; Picaud, Serge; Roux, Michel J. (2006): The glutamate transporter EAAT5 works as a presynaptic receptor in mouse rod bipolar cells. In *The Journal of physiology* 577 (Pt 1), pp. 221–234. DOI: 10.1113/jphysiol.2006.118281.

Wong, Kwoon Y.; Adolph, Alan R.; Dowling, John E. (2005a): Retinal bipolar cell input mechanisms in giant danio. I. Electroretinographic analysis. In *Journal of neurophysiology* 93 (1), pp. 84–93. DOI: 10.1152/jn.00259.2004.

Wong, Kwoon Y.; Cohen, Ethan D.; Dowling, John E. (2005b): Retinal bipolar cell input mechanisms in giant danio. II. Patch-clamp analysis of on bipolar cells. In *Journal of neurophysiology* 93 (1), pp. 94–107. DOI: 10.1152/jn.00270.2004.

Zerangue, N.; Kavanaugh, M. P. (1996): Interaction of L-cysteine with a human excitatory amino acid transporter. In *The Journal of physiology* 493 (Pt 2), pp. 419–423.

Curriculum Vitae

Personal Information

Name:	André LEHNHERR
Address:	Seestrasse 139 8707 Uetikon am See
Place of origin	Spiez BE and Uetikon am See
Date of Birth:	21. June 1988
Citizenship:	Swiss
Mobile:	+41 79 339 58 33
E-Mail:	andre.lehnherr@uzh.ch

Academic Education

2001 – 2007	High School (Matura) Typus N, Literargymnasium Rämibühl, Zurich Switzerland
2007 – 2011:	Undergraduate Studies, Bachelor of Science in Biology, University of Zurich, Switzerland
2012 – 2013:	Graduate Studies in Neuroscience Master of Science in Neuroscience UZH supervised by Prof. Dr. Stephan Neuhauss, Institute of Molecular Life Sciences, University of Zurich, Switzerland **Thesis**: From Past Till Present – Tracing the Solute Carrier Family 1 Genes Throughout Time
2013 – present:	PhD thesis in Neuroscience, University of Zurich, Switzerland, supervised by Prof. Dr. Stephan Neuhauss, Institute of Molecular Life Sciences University of Zurich, Switzerland **Thesis**: Tracing the Evolution of the SLC1 Gene Family Member of the ZNZ International PhD Program in Neuroscience

Professional Experience

09/2013 – 12/2013:	Supervision of a Master Research Project of Colette Steinegger.
	Title of the Project: Comparative Expression Analysis of the SLC1 Gene Family in Adult Retina of Different Vertebrate Species
03/2014	Supervision of Blockcourse Students Bio328 Neurobiology
	Title of the Project: Comparative RNA Expression Patterns of SLC1A Gene Family Member in Xenopus and Zebrafish
02/2015	Teaching Assistant in the practical part of Bio143 Neurobiologie
03/2015	Supervision of Blockcourse Students Bio328 Neurobiology
	Title of the Project: The Role of MDGA2A in Zebrafish Trigeminal and Facial Nerve Development
02/2016	Teaching Assistant in the practical part of Bio143 Neurobiologie
03/2016	Supervision of Blockcourse Students Bio328 Neurobiology
	Title of the Pfoject: Modelling Excitotoxicity in Zebrafish
10/2015 – 10/2016	Co-supervision of the Master Thesis of Adriana Hotz
	Title: Glutamate Homeostasis and Modeling Epilepsy in the Larval Zebrafish Brain
02-03/2017	Guest Scientist at the ICS-4, Forschungszentrum Jülich, Jülich, Germany
	Hosted by Prof. Dr. Christoph Fahlke and Dr. Peter Kovermann

Publications

Ingold, Esther*; Vom Berg-Maurer, Colette M*; Burckhardt, Christoph J.*; Lehnherr, André*; Rieder, Philip; Keller, Philip J. et al. (2015): Proper migration and axon outgrowth of zebrafish cranial motoneuron subpopulations require the cell adhesion molecule MDGA2A. In Biology open 4 (2), pp. 146–154. DOI: 10.1242/bio.20148482.

*These authors contributed equally to this work.

Niklaus, Stephanie; Cadetti, Lucia; Vom Berg-Maurer, Colette M.; Lehnherr, André; Hotz, Adriana L.; Forster, Ian C. et al. (2017): Shaping of Signal Transmission at the Photoreceptor Synapse by EAAT2 Glutamate Transporters. In eNeuro 4 (3). DOI: 10.1523/ENEURO.0339-16.2017.

Presentations at Meetings

2012	IMLS Scientific Retreat, Emmetten, Switzerland **Poster**: Tracing the Evolution of the SLC1 Gene Family
2014	IMLS Scientific Retreat, Emmetten, Switzerland **Poster**: Tracing the Evolution of the SLC1 Gene Family
2015	SMBE 2015, Vienna, Austria **Poster**: Tracing the Evolution of the SLC1 Gene Family
	IMLS Scientific Retreat, Morschach, Switzerland **Poster**: Tracing the Evolution of the SLC1 Gene Family
2016	Models of Diversity Conference, Zurich, Switzerland **Talk**: Tracing the Evolutionary History of a Gene Family in the Retina
	TAGC 2016, Orlando, Florida, USA **Poster**: Tracing the Evolution of the SLC1 Gene Family
	ZNZ Annual Symposium, Zurich, Switzerland **Poster**: Tracing the Evolution of the SLC1 Gene Family
2017	IMLS Scientific Retreat, Emmetten, Switzerland **Talk**: Tracing the Evolution of the SLC1 Gene Family
	ZNZ PhD Retreat, Valens, Switzerland **Poster**: Tracing the Evolution of the SLC1 Gene Family

Acknowledgements

First of all, I want to thank Stephan Neuhauss for giving me the opportunity to do my PhD in his lab and for entrusting this interesting project to me. Further I want to thank you Stephan for always having an open door for scientific and non-scientific discussions, for giving advice when needed, for letting me work independently, for birthday parties and Thanksgiving dinners and of course for sharing passion about Whiskeys, beers and muscle pump.

Next I want to express my gratitude to Matthias Gesemann for starting with this project and for always believing in it as well as in me. Thanks for all the fruitful discussions, all the mentoring and of course for the introduction into the world of ice hockey.

The members of my PhD thesis committee Andreas Wagner and Christian von Mering I want to thank for all the helpful discussions and valuable inputs.

Many thanks go to Christoph Fahlke and Peter Kovermann and the whole ICS-4 at the Forschungszentrum Jülich for hosting me in this very friendly way and introducing me into electrophysiology and for sharing enthusiasm about the project.

A big thank goes to our technicians Kara, Martin, Claudia and Manuela for keeping good care of the fishes and the lab and for making our lab-life so much easier and pleasant. Irene Hofmann I want to thank for the administrative support.

Further I want to acknowledge all the present and former lab members of the Neuhauss lab that made working here a real joy. Especially I want to acknowledge my fellow PhD students Stella, Irene, Steffi, Adriana, Domino, Tamara and Yuya. Stella for being the best long-term office-neighbor and for all good advice, discussions and fun we had – I did not mind that you were so loud ;-). Irene I want to thank for being a great person, for a memorable wedding, for game-nights and for delicious Spanish food. Steffi for trips to mountains, Wasen or diving in Florida – and of course delicious Capuns. Adriana, thank you for your great work during your Master, for sharing passion about Fasnacht and Guggemusig and for all the fun we had inside and outside the lab. Thank you, Domino, for being a reliable partner in sports as well as in having beers. Tamara I want to thank you for teaching me the history of my home.

Big thanks go to Marion for all inputs and discussions about scientific and non-scientific topics, for organizing the lab bootcamp and for inviting us to winetasting, Turnerchränzli and Turnfäscht. Further I want to thank Anja, Michelle and Selin for the company in the office and all the laughers we shared and for enduring my company in the office. The former Master students Tanja, David and Jenny and Anja I want to acknowledge for the good times and all the fun we shared.

Last but not least I want to thank my friends and my family. Adi, Claudi, Marcel, Angi, Meli and Ladina, I want to thank you for all the good times we had and will have and for being true friends. Sabrina thank you for all your caring support and distraction when I needed it the most during the last phase of my PhD.

I want to express my deepest gratitude to my family, of course including Franzi and Lori, for all the love and support you provided me. I would not have been able to do this without you! Thanks for the interest you showed in my work and for always believing in me. The past years were not at all easy for us, I am extremely proud of all of you!